FRAGILITY RELATIONSHIPS FOR POPULATIONS OF BUILDINGS BASED ON INELASTIC RESPONSE

by

Bora Gencturk, Amr S. Elnashai, and Junho Song

Department of Civil and Environmental Engineering
University of Illinois at Urbana-Champaign
Urbana, Illinois

August 2007

Amr S. Elnashai, Ph.D., Director

ABSTRACT

In the absence of comprehensive and statistically viable observational damage data, there is a pressing need for simulation-based fragility relationships for populations of structures so as to improve the reliability of earthquake loss assessment studies. In this report, improved fragility relationships for populations of buildings are developed based on inelastic response analysis. Special focus is placed on the class of woodframe buildings which constitutes the majority of exposed stock in many regions of the USA. The capacity curves are retrieved from the available finite element based pushover analysis in the relevant literature. Extension to other building types is performed using the available capacity diagrams from the FEMA-developed loss assessment software HAZUS. Demand is simulated by synthetically-generated ground motions representing a probable earthquake in the Central USA. Structural assessment is carried out using an advanced Capacity Spectrum Method (CSM) which is developed and presented in the report. Thus, all the required components of fragility analysis – namely capacity, demand, and structural response – are based on rigorous analysis. Using the building classification of the HAZUS loss assessment software, both HAZUS-compatible and conventional fragility relationships are derived for two different soil conditions. Comparisons with HAZUS fragility curves as well as with those from other studies are undertaken. The parameters of the improved fragility relationships are provided for reliable use in loss assessment software.

ACKNOWLEDGMENTS

This research was funded by the Mid-America Earthquake (MAE) Center, award No. EEC-9701785. The MAE Center is an Engineering Research Center funded by the National Science Foundation. The authors acknowledge the support of Professors Andre Filiatrault, David Rosowsky, and Bruce Ellingwood for providing the pushover data included in the database and the support of Prof. Glenn Rix and Dr. Alfredo Fernandez in providing the synthetically generated earthquake records. Mr. Jon A. Heintz, Director of Projects, at the Applied Technology Council kindly sought approval from FEMA to release the results from the ATC-63 study constituting the data provided by Professor Andre Filiatrault.

TABLE OF CONTENTS

LIST OF FIGURES

LIST OF TABLES

LIST OF SYMBOLS

a	Constant used in the force reduction factors
a_1, a_2	Constants of the linear regression analysis
A_x	Center of ellipse
A_y	Yield point acceleration
A_u	Ultimate point acceleration
b	Constants used in the force reduction factors
B	Semiminor axis of ellipse
c	Constant used in the force reduction factors
c^*	Equivalent viscous damping of the SDOF system
C	Base shear coefficient (or semimajor axis of ellipse)
$\boldsymbol{C}$	Damping matrix
C_0, C_1 C_2 C_3	Modification factors for DCM
C_S	Design strength coefficient
D_y	Yield point displacement
D_u	Ultimate point displacement
E_D	Energy dissipated in the inelastic system
E_S	Strain energy of the elastic system
f_y	Yield force
F^*	Force of the SDOF system
g	Gravitational acceleration
k_e, K_i	Elastic stiffness
k_{sec}	Secant stiffness
K_S	Post-elastic stiffness
LS_i	Threshold value for the ith limit state
m_i	Mass of the ith storey
m^*	Equivalent mass of the SDOF system
$\boldsymbol{M}$	Diagonal mass matrix
n	Number of data points
p	Magnitude of lateral loads
$P(\cdot)$	Probability
$\boldsymbol{P}$	Vector of lateral loads
R, R_μ	Force reduction factor
$\boldsymbol{R}$	Vector of internal forces
S_a	Spectral acceleration
S_d	Spectral displacement
S_v	Spectral velocity
$T_a, T_b,$ $T_c, T_{c'},$ T_d, T_f	Periods defining elastic design spectra
T_e, T_i T_n	Elastic fundamental period (and period defining elastic design spectra)
T_{eff}	Effective fundamental period
T_{eq}	Equivalent period
T_g	Predominant period of the ground motion
T_0	Period used in DCM (or in force reduction factors)
u_{go}	Peak ground displacement
$\dot{u}_{go}$	Peak ground velocity

$\ddot{u}_{go}$	Peak ground acceleration
u_y	Yield deformation
u_m	Ultimate deformation
$\boldsymbol{U}$	Displacement vector
V_b	Base shear
V_y	Yield base shear
w_i	Weight of the ith storey
W	Total weight
$\ddot{x}_g$	Ground acceleration
X	Lognormal random variable
z_i	Realizations of the standard normal random variable
Z	Standard normal random variable
α	Post-yield stiffness ratio
α_A	Amplification factor for constant acceleration region
α_D	Amplification factor for constant displacement region
α_V	Amplification factor for constant velocity region
α_1	Fraction of building weight effective in pushover mode
β_C	Uncertainty in capacity of building
β_{CL}	Uncertainty in the limit state threshold value
β_D	Uncertainty in earthquake demand
$\beta_{D/GM}$	Square root of the standard error
β_M	Modeling uncertainty
β_{tot}	Total uncertainty
δ_t	Target displacement
Δ_{roof}	Roof displacement
Δ_{y}	Yield displacement
Δ_{u}	Ultimate displacement
$\boldsymbol{\eta}$	Displacement vector in modal coordinates
η^*	Displacement of the SDOF system
$\Phi[\cdot]$	Standard normal cumulative distribution function (and function used in the force reduction factors)
$\boldsymbol{\Phi}$	Assumed displacement shape
γ	Overstrength factor, true yield strength to design strength
Γ	Modal participation factor
κ	Damping modification factor
λ	Overstrength factor, ultimate strength to yield strength
λ_{CL}^i	Natural logarithm of the ith limit state threshold value
$\lambda_{D/GM}$	Mean of the natural logarithm of the response quantity
μ	Ductility factor
$\boldsymbol{\Psi}$	Distribution of lateral loads
ω_n	Natural frequency of the SDOF system
ζ^*	Viscous damping ratio of the equivalent SDOF system
ζ	Viscous damping ratio
ζ_{eff}	Effective viscous damping ratio

LIST OF ABBREVIATIONS

AD	Acceleration-Displacement
ASCE	American Society of Civil Engineers
ASE	Average Stiffness and Energy
ATC	Applied Technology Council
CASHEW	Cyclic Analysis of Shear Walls
CEUS	Central and Eastern United States
COES	California Office of Emergency Services
COLA	City of Los Angeles
CP	Collapse Prevention
CRM	Consequence-Based Risk Management
CSM	Capacity Spectrum Method
CUREE	Consortium of Universities for Research in Earthquake Engineering
DCM	Displacement Coefficient Method
EP	Elasto-Plastic
FEMA	Federal Emergency Management Agency
GMI	Ground Motion Intensity
IDA	Incremental Dynamic Analysis
IO	Immediate Occupancy
LS	Life Safety
MAE	Mid America Earthquake
MDOF	Multi-Degree-of-Freedom
NEES	Network of Earthquake Engineering Simulation
NEHRP	National Earthquake Hazards Reduction Program
NMSZ	New Madrid Seismic Zone
OSF	Over-Strength Factor
PGA	Peak Ground Acceleration
PGD	Peak Ground Displacement
PGV	Peak Ground Velocity
SAF	Spectral Amplification Factor
SAWS	Seismic Analysis of Woodframe Structures
SDOF	Single-Degree-of-Freedom
SRSS	Square-Root-of-Sum-of-Squares
UBC	Uniform Building Code

CHAPTER 1
INTRODUCTION

1.1. PREAMBLE

Earthquakes have been one of the major challenges that humankind has faced since the dawn of civilizations. As the population increases, along with the need for construction, the importance of engineering in design also increases. The significance of earthquake resistant design is underlined by many recent disasters, such as the 1999 Kocaeli (Turkey) and ChiChi (Taiwan), 2001 Bhuj (India), 2003 Bam (Iran), 2004 Sumatra (Indonesia), 2005 Kashmir (Pakistan), 2006 Jakarta (Indonesia) and 2007 Ica (Peru) Earthquakes. These earthquakes killed hundreds of thousands of people and cost billions of dollars of economic losses, which in most cases constituted a large portion of the affected country's gross national product. The above listed earthquakes are some of the most recent of many others in the last century – 1908 Messina (Italy); 1920 Kansu, 1927 Tsinghai, 1976 Tangshan (China); 1923 Kanto, and 1995 Hyogo-ken Nanbu (Japan) Earthquakes –where the total death toll amounts to almost three quarters of a million. On average earthquakes cause 10,000 deaths and approximately $10 billion in economic losses each year. In addition, among natural disasters earthquakes are the second leading cause of death. This summary indicates how serious the consequences of earthquakes are, and suggests the necessity of investigating and planning in order to reduce the potential loss in future events.

The New Madrid Seismic Zone (NMSZ), also known as the Reelfoot Rift or the New Madrid Fault Line is a major seismic zone in the Central and Eastern United States (CEUS) stretching to southwest from New Madrid, Missouri. In 1811 and 1812 four earthquakes occurred on the New Madrid Fault. The first two earthquakes occurred in the northeast Arkansas on December 16, 1811 with estimated magnitudes of 7.7 and 7. Months later, on January 23 and February 7, 1812, two more earthquakes with magnitudes estimated as 7.6 and 7.9 occurred in southern Missouri. The earthquake occurring on February 7 is the largest earthquake ever recorded in the contiguous United States. Due to the soil profile of CEUS having slow attenuation properties, the earthquakes were felt as far as New York City, Boston, and Washington, D.C. At the time

of these earthquakes this region of the U.S. was not largely populated except St. Louis, Missouri, where a majority of homes and small businesses (mostly made of wood) suffered substantial damage or collapsed entirely. Other than these, landslides, mangled trees and large depressions and uplift due to ground failure were reported. Since the 1970's thousands of earthquakes have been recorded in the region. To conclude, NMSZ is an active, low-probability-high-consequence earthquake region having the potential to produce destructive earthquakes every 300 to 500 years.

The main objective of the Mid America Earthquake (MAE) Center is to minimize the consequences of future earthquakes across hazard-prone regions, including but not limited to CEUS. Consequence-based risk management (CRM), a concept developed and applied by the MAE Center, is a powerful tool for addressing issues of earthquake impact assessment, mitigation, response, and recovery that increasingly affect vulnerable communities. These studies aim to estimate the possible consequences of earthquakes such as deaths and injuries, property losses, earthquake induced homelessness, collateral hazards such as fault ruptures and liquefaction, damage and/or functional losses to industries, lifelines, and emergency care facilities, and indirect losses such as earthquake induced fire, damage from the release of hazardous materials, and the impact on the economic well-being of the urban area or region. Within the context of CRM, loss assessment studies are being carried out by the MAE Center for different cities around the world such as Istanbul, Muzaffarabad, and Jakarta, in addition to those for CEUS.

The three fundamental components of the above mentioned loss assessment studies can be listed as hazard, inventory, and fragility. Hazard is defined as an event which threatens to cause injury, damage, or loss, such as the ground shaking in the case of earthquake loss assessment. Hazard is generally described as either being deterministic or probabilistic, and it should reflect the characteristics of the expected event in the region under consideration. Inventory includes the required information (for the assessment study) on the infrastructure of the subject region. And finally, the fragility component relates the hazard (or exposure) to exceedance probabilities of certain damage states (or losses) linking the inputs (hazard and inventory) to the outputs of the study (e.g. fatalities,

economic losses). The exceedance probabilities are in turn used to obtain social and economic consequences through damage factors and socio-economic impact models.

This report addresses fragility relationships – specifically, those that relate ground motion intensity to structural damage probabilities – and it proposes a new framework for improved fragility analysis of populations of buildings. For further investigation, the fragility relationships are naturally divided into four components: the capacity of buildings, earthquake demand, methodology for structural assessment, and methodology for fragility curve generation. These four components form the structure of this document and whenever possible explanations are gathered under them.

1.2. DEFINITION OF THE PROBLEM

Uniformly-derived and analytically-based fragility relationships for populations of buildings are one of the major requirements of a reliable loss assessment study. However, until now little if any research is devoted to this topic. What follows is a description of the challenges such research presents, with particular attention paid to the previously listed four components of the framework.

The inventory of a loss assessment study includes buildings from various construction materials, heights, aspect ratios, irregular features, and seismic design levels. To be able to accommodate the large variation in building capacity, a certain number of categories (herein building type seismic design level pairs are referred to as building categories) are defined so as to classify the building stock of inventory. Nevertheless, due to vast number of structural configurations, the variation in capacity of building for each category still remains significantly high. Since even a small modification in geometry or in material properties can totally alter the overall response of a structure, representing a building category requires inclusion of several structural configurations in the data set used to derive a representative model. It is impractical to design hundreds of structures for inelastic analyses and develop advanced models to represent all of them. Furthermore, fragility analysis entails assessment of each configuration under varying ground motion that renders the latter option infeasible in terms of computational effort as well as analysis time. Another option is the statistical analysis of post-earthquake observational

data. However this might be even more challenging than the previous option due to the scarcity of observational data and the requirements of having statistically viable samples of structures at similar damage states when subjected to different levels of ground shaking. Due to the above mentioned difficulties, many loss assessment studies rely on expert opinions for representing capacity, and uncertainty associated with this quantity, which can have an adverse impact on the analytical basis of fragility relationships. Therefore, the categories considered in a fragility analysis for populations of buildings should be comprehensive in order to cover the exposed stock and representation of the capacity of building for each category should characterize the real behavior to the required extent while being practical for a large number analysis.

In a loss assessment study, earthquake demand can be established by deterministic (or scenario based) ground motion analysis or using probabilistic ground motion maps. In the former ground motion intensity (GMI) parameter, e.g. peak ground acceleration (PGA) or spectral acceleration, is calculated based on attenuation relationships for a given event while the latter utilizes spectral contour maps which provide the desired GMI parameter for the region of interest. Whichever method is chosen, the earthquake demand used in the derivation of the fragility relationships should be representative of the hazard. One possibility is to use the standardized code spectrum, formed of distinct parts, i.e. constant spectral acceleration, velocity, and displacement. Although this representation provides simplicity due to being based on a reasonable number of parameters, such as the magnitude, PGA, and amplification factors which are functions of the soil profile, the code spectrum is developed for design purposes and it has an inherent conservatism which is not fruitful to fragility analysis. More importantly design (or code) spectrum falls short in terms of characterizing the different features of the earthquake ground motion, e.g. site condition, distance, depth, fault rupture and frequency content among others. In addition, in this type of representation of earthquake demand, describing the variation (or uncertainty) associated with the code spectrum and scaling to satisfy different damage state levels involves several assumptions and simplifications. Another possibility is utilizing acceleration time histories as the demand component which allows better quantification of the variability (in terms of frequency content, duration, time varying amplitude, and site conditions, among others) in ground motion. Besides, the

aforementioned features of earthquakes can be accounted for with appropriate selection of the time histories.

There exist several established methodologies for assessment of structures subjected to lateral loading. Detailed information on the available structural assessment techniques can be found in Chapter 2. However, since the objective here is to discuss the challenges of deriving fragility relationships for populations of buildings, the most important requirements on the methodology for structural assessment can be stated as its ability to predict displacement demands imposed on structures with acceptable accuracy and its feasibility in terms of the involved computational effort. With regard to the latter, fragility analysis of even one structural configuration requires considerable amount of computation time leading to the fact that this might be impractically high when a certain number of building categories each of which including different structural configurations are considered. Hence a feasible estimation method that still satisfies the accuracy criteria should be developed and adopted. Such a method should also be capable of incorporating the representations for the capacity of building and the earthquake demand.

The methodology for fragility curve generation deals with the statistical evaluation of the structural response data. Since the outcome, i.e. the fragility relationships, will be used in earthquake loss assessment studies, they should conform to the input requirements of the latter. A case in point is that, HAZUS (National Institute of Building Sciences, 2003), one of the most widely used loss assessment software in USA, has a different format of fragility relationships than other commonly used ones in literature. Therefore, the outcome of the fragility analysis study should be provided such that it can be utilized by different earthquake loss assessment studies employing different software. Additionally, uncertainties such as those originating from modeling and limit state threshold determination should be incorporated into the methodology for fragility curve generation.

One final remark is that the use of available fragility relationships in literature for different building configurations can be considered as an option for loss assessment studies, yet these studies do not include the uncertainty associated with the capacity of building that exists due to building categories including different structural

configurations. Moreover, it is very unlikely that similar structures will exist in the building stock, in which case representing a building type will require several relationships, deteriorating the uniformity of the analysis.

1.3. OBJECTIVES AND SCOPE

The aim of this study is to provide a new framework for developing fragility relationships for populations of buildings to be used in earthquake loss assessment studies.

This report considers 36 building types with different structural configurations of wood, steel, concrete, and masonry structures, including mobile homes, which cover the vast majority of the building stock in the USA and elsewhere. These building types, which are based on National Earthquake Hazards Reduction Program (NEHRP - Federal Emergency Management Agency, 1998) classification come from HAZUS. Special focus is placed on woodframe building types. Rigorous, synthetically generated ground motion records that conform to seismo-tectonic environment of the NMSZ provide the demand measure.

Emphasis on woodframe buildings reflects two key elements of the study. First, the majority of the building inventory in CEUS is woodframe. Indeed, according at a MAE Center inventory 94% of all the buildings in Memphis area are of woodframe construction (French, 2007). Table 1.1 gives the statistics for the eight states in CEUS based on the default building inventory of HAZUS, which comes from publicly available data from several sources aggregated by the census tract (Technical Manual Chapter 3). Similar patterns exist in other regions in USA; for instance 96% of all buildings in Los Angeles County, 99% of all residences in California, and 80 to 90% of buildings stock in general are woodframe (Malik, 1995).

Earthquake damage to woodframe structures and their consequences also highlight the importance of this building type. In 1994 Northridge Earthquake, 24 out of 25 fatalities (EQE International and the Governor's Office of Emergency Services, 1995) and more than half of the economic losses – approximately $20 billion – were caused by damage to woodframe buildings (Kircher et al., 1997b; Reitherman, 1998). In addition, 100,000

individuals were in need of shelter (Ellingwood et al., 2007) and 48,000 housing units were rendered uninhabitable (Perkins et al., 1998). Woodframe construction is also prevalent in other countries, Japan being a case in point. The second reason for paying particular attention to woodframe building types is to illustrate how capacity of building is treated within the proposed framework.

Table 1.1. Woodframe building statistics for the eight states in CEUS

State	Number of Woodframe Buildings	Total Number of Buildings	Percentage
Illinois	2,353,485	3,251,213	72.38
Indiana	1,396,677	1,932,058	72.29
Arkansas	835,172	1,143,135	73.06
Alabama	1,264,870	1,679,567	75.31
Mississippi	764,990	1,017,335	75.20
Kentucky	1,060,993	1,473,443	72.01
Tennessee	1,602,852	2,077,209	77.16
Missouri	1,183,306	1,770,544	66.83
Total	10,462,345	14,344,504	72.94

Due to the scarcity of actual records of natural earthquakes, synthetically generated earthquake time histories which reflect the characteristics of seismic hazard in CEUS (Fernandez, 2007). Because the regional characteristics of the ground motions utilized matches that of CEUS, the fragility relationships provided in this study are particularly useful for earthquake impact assessment studies of regions within CEUS. However, the flexibility of the method proposed in this report makes the framework applicable to any region: it can be used with a different set of ground motions for developing fragility relationships in other seismic zones.

As previously mentioned the structure of this document stems from the four components used in developing the framework. Chapter 2 provides a summary of previous studies on earthquake loss assessment, fragility relationships, and particularly on each of the four components. Chapter 3 is divided into two parts. In the first part capacity of building representation is described (first component), for the important group of woodframe buildings, a database of pushover curves is formed and the extension to other building

types is performed using the available set from HAZUS. Limit state definitions and how the variation in capacity is treated are also included. Whereas in the second part, details of the ground motion records are given (second component). Example time histories in addition to spectra in different formats are shown. Chapter 4 also contains two parts. The first part deals with the methodology for structural assessment (third component): the inadequacy of the available capacity spectrum methods (CSM) reveals itself in a test case of woodframe building. This report then proposes an advanced capacity spectrum method and validates it using the same building. The second part of Chapter 4 discusses two methods for fragility curve generation (fourth component). These methods allow providing the parameters of improved fragility relationships in both HAZUS compatible and conventional format. Finally in Chapter 5 all the components are brought together to yield the results of improved fragility relationships; comparisons with those from other studies are provided along with discussions.

Figure 1.1 is an illustration of the developed framework. Pushover curves and time histories constitute the capacity of building and earthquake demand respectively. These first two components can be considered as inputs to the simulation engine which is the third component, i.e. the methodology for structural assessment. Structural response data obtained by analyzing the building capacity under the earthquake demand is processed by the methodology for fragility curve generation (fourth component) to yield the results. Limit states, which are determined from the pushover curves, are required at this step. The first two components are described in Chapter 3, and the last two are in Chapter 4, while the fragility relationships are presented in Chapter 5.

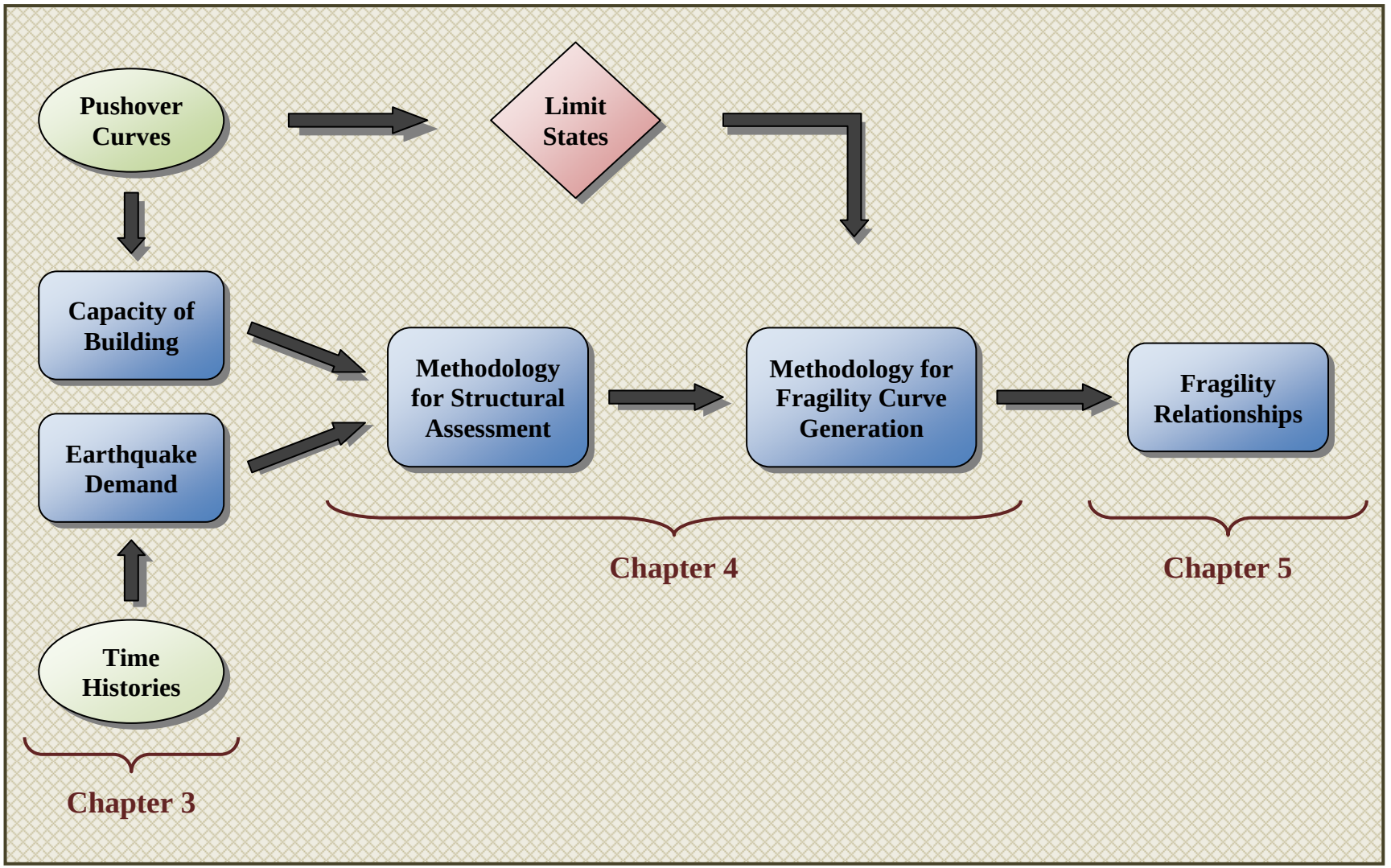

Figure 1.1. Flowchart for the proposed framework of fragility analysis

CHAPTER 2
LITERATURE REVIEW

This chapter provides a summary of previous studies on the related aspects of the report. It first deals with literature on earthquake loss assessment and fragility formulations, and then discusses different approaches to capacity of building modeling and on performing structural assessment.

Due to the increasing vulnerability of the communities particularly susceptible to earthquakes, several earthquake loss assessment studies have been carried out for different regions around the world. Below, in chronological order, are some selected examples on the latter.

Earthquake Planning Scenario for a Magnitude 8.3 Earthquake on the San Andreas Fault in the San Francisco Bay Area (Davis et al., 1982) is one of the oldest studies investigating the possible impacts of earthquakes on communities. The work hypothesizes a repeat of the 1906 San Francisco Earthquake on the northern and 1857 Fort Tejon Earthquake on the southern San Andreas Fault, respectively. The study estimates damage to essential facilities, e.g. highways, airports, and railways for emergency planning efforts.

On account of the fact that that the Hayward fault is capable of producing earthquakes with equivalent or even greater damage potential than San Andreas Fault, Earthquake Planning Scenario for a Magnitude 7.5 Earthquake on the Hayward Fault, in the San Francisco Bay Area is prepared (Steinbrugge et al., 1987), providing a perspective on many of the plausible impacts of the scenario event: from transportation to utility lifelines to critical structures such as hospitals and schools.

The Comprehensive Seismic Risk and Vulnerability Study for the State of South Carolina (URS Corporation et al., 2001) evaluates potential losses from four earthquake scenarios, three from the Charleston seismic source and the other representing an earthquake in Columbia, using HAZUS (National Institute of Building Sciences, 2003). For the scenario with a moment magnitude of 7.3, some of the conclusions are a total of $20 billion (2000 dollars) economic losses, 45,000 casualties, approximately 900 fatalities

(for a day time event), and 60,000 people in need of shelter. The results are proposed as a basis for the state of South Carolina to effectively plan and prepare for future damaging earthquakes.

A study by the New York City Area Consortium for Earthquake Loss Mitigation (Tantala et al., 1999-2003) creates a risk and loss estimation model for the metropolitan New York, New Jersey, and Connecticut region using HAZUS. The study assembles the Tri-State's soil information in addition to compiling a detailed building inventory in order to study three earthquake scenarios with magnitudes 5, 6, and 7 located at the epicenter of 1884 New York City Earthquake (M5.2). The work also estimates different expected losses over a given period of time by studying three probabilistic scenarios with 100, 500, and 2500 return periods. More than 1,000 fatalities, 2,000 hospitalizations, and approximately $39 billion total economic losses are predicted for the M6 scenario.

A similar study aims to estimate the impacts of a 6.7 magnitude event generated by the Seattle Fault on the communities of the Central Puget Sound region (Washington Military Department, 2005). Again HAZUS is utilized for loss assessment purposes. Although default HAZUS building stock is used, special focus is placed on ground motion characterization and site classes. Soil data and shaking maps are provided to the software in addition to information regarding the ground failure hazards such as liquefaction, landslides, and the surface fault rupture. The predicted scenario losses include economic losses of about $33 billion, 1,600 deaths, and 24000 injuries.

For the city of Istanbul a team of four different universities with funding from the Metropolitan Municipality of Istanbul made public a Master Plan on earthquake impact assessment in 2003 (Erdik et al., 2003). Building damage, casualties, financial losses, emergency sheltering needs, road blockage, fire, explosions and hazardous material release are estimated for a deterministic scenario earthquake of M7.5. More than 700,000 buildings are taken under consideration for a population of 9.3 million.

A recent study conducted at the MAE Center undertakes a comprehensive seismic risk assessment, response, and recovery plan for eight states in the NMSZ (Cleveland, 2006). Eight states in CEUS, i.e. Alabama, Arkansas, Illinois, Indiana, Kentucky, Mississippi

and Tennessee are considered for the two levels of analysis. HAZUS is used for two levels of analysis: Level I improves soil maps and utilizes the default building inventory of the software. On the other hand, Level II study improved data on hazards focusing on site characteristics, ground motion attenuations, and new, upgraded inventory data. The study evaluates structural and non-structural damage to building stock and structural damage to essential facilities, utilities and transportation systems in addition to induced damage and direct social and economic losses.

It is not possible to mention all the literature on earthquake loss assessment. However there have been similar studies undertaken for other cities around the world such as Basel (Fah et al., 2001), Lisbon (Dina et al., 1997; Ramos and Lourenco, 2004), Potenza (Dolce et al., 2006), among many others, with different scopes.

Fragility relationships are one of the essential components of earthquake loss assessment studies in terms of relating ground shaking intensity with damage probabilities. Fragility curves can be classified into four categories – empirical, judgmental, analytical, and hybrid – based on the damage data used in constructing the curves. Records from post-earthquake surveys are the main source of information for empirical curves, while judgmental fragility relationships resort to export opinion. As the name indicates, fragilities based on simulations are classified as analytical whereas any combinations of these are considered hybrid relationships.

Observational data from after an earthquake is the most realistic method of deriving fragility relationships because all of the details of the building inventory are included in addition to topography, site, source characteristics, and soil-structure interaction effects. However, post-earthquake surveys do not include all the necessary information such as the building materials and seismic design provisions. They are also only carried out for a limited number of regions generally experiencing low damage from low ground shaking intensity (Orsini, 1999). These limitations necessitate combining earthquake damage data from different sources around the world into new studies that achieve a wider scope of application and minimize the uncertainty in deriving fragility curves. Spence et al. (1992) provides an example study that combines data from different earthquakes around the

world. Nevertheless the available post-earthquake observational data is scarce and the requirement of having statistically viable samples of structures at similar damage states when subjected to different levels of ground shaking renders this option infeasible for deriving fragility relationships for building populations of different composition. Furthermore, vulnerability relationships for buildings with new configurations or materials that are not available in the databases cannot be obtained, precluding the benefits of this approach.

Judgmental fragility curves for populations of buildings are generated based on the opinions of experts in the field of earthquake engineering. These experts are asked to decide the damage distributions as a function of earthquake intensity. Judgment based fragility relationships are not susceptible to the scarcity of data, which means that experts can provide damage estimates for any number of different structural types. Since the Experts also quantify the uncertainty of their estimates, fragility curves for a large number of structural types and building populations can be easily generated. For instance, although experts do not determine the parameters of fragility curves in HAZUS, the capacity diagrams utilized in the derivation of the fragility curves as well as the uncertainty associated with capacity of buildings and earthquake demand are based on judgment. Damage probability matrices and vulnerability curves of Applied Technology Council's documents ATC-13 (1985) and ATC-40 (1996) also have judgmental basis to a certain extent. The reliability of judgment based curves is questionable owing to their dependence on the experience of the individuals consulted and lack of scientific basis. Moreover, it is not viable to determine the degree of conservatism involved in the decisions of these experts and it may be difficult to obtain reliable estimates in the case of new conditions where no experience is available.

Analytical vulnerability relationships obtain statistical data from the simulation of structural models under increasing ground motion intensity. This results in reduced bias and increased reliability when compared to judgment based curves. Analytical fragility relationships are getting more and more popular with the advances in computational structural engineering which speed up the analysis process and render the modeling of complex components, e.g. infill walls or beam-column connections, possible.

Nevertheless, there are still challenges involved with simulation such as the modeling of soil structure interaction and numerical collapse preceding the structural failure. Moreover, the detailed modeling of structural assemblages needs verification from experimental data most of the time. Significant research is devoted to derivation of fragility relationships using simulation of analytical models. Singhal and Kiremidjian (Singhal and Kiremidjian, 1997), and Erberik and Elnashai (Erberik and Elnashai, 2004), utilize 3D models for structural analysis whereas others adopt a simplified approach such as inelastic analysis of equivalent single-degree-of-freedom systems (Jeong and Elnashai, 2007).

Hybrid fragility relationships combine the three other alternatives listed above so as to account for the deficiency inherent to each of them. The subjectivity of judgmental curves is compensated with post-earthquake observational data. For instance, the vulnerability relationships in ATC-13 and ATC-40, even though heavily based on expert opinion, utilize data, to a limited extent, from the 1971 San Fernando and 1994 Northridge Earthquakes, respectively. The previously mentioned HAZUS fragility curves, adopt expert opinion in the determination of building capacity and the uncertainty associated with the latter and the earthquake demand, while the combined uncertainty of capacity and demand is calculated based on analysis. In certain cases experimental test results complement available statistical data. However, due to the impracticality of evaluating every parameter variation in empirical testing, experimental results are mostly used for verification purposes rather than as an additional source to the available statistical damage data. The study by Singhal and Kiremidjian (1997) is an example of hybrid relationships where the results of the analysis is calibrated using observational data from Northridge Earthquake.

Although there have been a limited number of studies on testing of full-scale woodframe houses (Yokel et al., 1973), it was only after 1994 Northridge Earthquake and 1995 Hygo-ken Nanbu (Kobe) Earthquakes, which caused extensive damage in the majority of woodframe structures, that resources were allocated for research in quantifying the dynamic behavior of wood construction. Because of the relative ease in full-scale testing small woodframe houses, several experimental tests have been performed to better

understand their behavior (Kohara and Miyazawa, 1998; Ohashi et al., 1998; Tanaka et al., 1998; Fischer et al., 2001; Paevere, 2002). Since the Consortium of Universities for Research in Earthquake Engineering (CUREE) initiated the Caltech Woodframe Project (http://www.curee.org/projects/woodframe/) woodframe construction has been investigated in detail both with simulations and testing. A summary of recent experimental studies can be found in Lam et al. (2002).

Because shear walls are the main source of lateral resistance and they govern the global response of woodframe structures, significant research has been done on both static and dynamic analysis and testing of wood shear walls (Folz and Filiatrault, 2000; COLA, 2001; Folz and Filiatrault, 2001; Fonseca et al., 2002; Ekiert and Hong, 2006; Ayoub, 2007). Other studies concentrate on computer modeling complete woodframe structures (Kasal et al., 1994; Tarabia and Itani, 1997; Collins et al., 2005a). The software, called Seismic Analysis of Woodframe Structures (SAWS) and developed by Folz and Filiatrault (2004b), has made significant progress in modeling wood buildings (Ellingwood et al., 2007). A summary of modeling approaches for timber buildings can be found in Lam et al. (2004).

With the achievements in the modeling, probabilistic analysis has been performed both on shear walls and complete woodframe structures. Van De Lindt and Walz (2003) developed a new hysteretic model for wood shear walls and conducted a reliability analysis of the latter using existing suites of ground motions. Fragility analysis methodologies are proposed and carried out for complete woodframe buildings (Rosowsky and Ellingwood, 2002) and for their components such as shear walls and connections (Filiatrault and Folz, 2002; Ellingwood et al., 2004; Kim and Rosowsky, 2005; Lee and Rosowsky, 2006; Ellingwood et al., 2007).

Although Porter et al. (2002) made a vulnerability study on a group of index woodframe buildings, fragility relationships are not available in literature for populations of woodframe or for other buildings types. HAZUS includes fragility curves for groups of buildings, however as mentioned earlier, these are derived mainly based on expert opinion.

Due to probabilistic nature of fragility analysis, structures need to be evaluated, depending on the specific objective of the study, for varying material properties and/or structural configurations and increasing severity of input – having stochastic characteristics.

Structural analysis methods are classified into two generic groups – linear and nonlinear – which can each then be subdivided into static and dynamic. Equivalent static analysis is a typical example of linear static procedures; most of the current seismic design codes employ it, and horizontal force distribution is the required input for this method. On the other hand modal and spectral analysis uses superposition and fall under linear dynamic procedures. In both methods, a multi-degree-of-freedom (MDOF) system is decomposed into a series of single-degree-of-freedom (SDOF) systems and elastic response history analysis performed. The former combines the time history of responses while in the latter only the maximum response quantities are superposed to give an upper bound of the maximum response of the MDOF system.

With regard to nonlinear static procedures, CSM, Displacement Coefficient Method (DCM) and the secant method (COLA, 1995) are the most extensively used methodologies. The first two methods utilize pushover curves which are briefly described in section 3.1.1. Depending on whether the lateral force pattern used in the derivation of the curve is kept constant or updated, the pushover method is named as conventional or adaptive, respectively. On the other hand, the secant method uses substitute structure and secant stiffness in its calculations. Inelastic response history and incremental dynamic analysis (IDA) are well established techniques for nonlinear dynamic analysis of structures. The idea of IDA analysis is not new (Bertero, 1977; Nassar and Krawinkler, 1991): it has found wide application in fragility analysis because it can estimate structural capacity under earthquake loading, and because it provides a continuous picture of system response from elasticity to yielding and ultimately to collapse.

Elnashai (2002) examines the available pushover techniques and provides comparisons with IDA. Papanikolaou and Elnashai (2005; 2006) use a set of eight different reinforced

concrete buildings covering various levels of irregularity in plan and elevation, structural ductility, and directional effects to investigate the accuracy and applicability of conventional and adaptive pushover as well as IDA. Their results indicate that, although adaptive pushover analysis is superior to its conventional counterpart, in general it does not provide major advantages over the traditional methodology for pushover analysis. Both techniques are found to be adequate for structural systems free from irregularities in plan and elevation. For other systems, the use of inelastic dynamic analysis is recommended.

Performance levels or limit states for structural systems are defined as the point after which the system is no longer capable of satisfying a desired function. Performance levels can be identified using quantitative or qualitative approaches. Building codes generally adopt qualitative approaches when the objective is to ensure the safety of the occupants and continued serviceability during factored and unfactored loading, respectively. The document by the Federal Emergency Management Agency, FEMA 356 (2000), has detailed information on the qualitative definition of performance levels. The three important limit states corresponding to stiffness, strength, and ductility requirements in design of structures are immediate occupancy (IO), life safety (LS) and collapse prevention (CP). The same document defines IO as the building state where the pre-earthquake design stiffness and strength are retained and occupants are allowed immediate access into the structure following the earthquake, LS as the state where building occupants are protected from loss of life with a significant margin against the onset of partial or total collapse, and CP as the state where the building continues to support gravity loading but retains no margin against collapse.

However, when the previously described structural analysis techniques are concerned, quantitative response limits corresponding to the qualitative code descriptions are required. For this purpose, several researchers adopt the damage index model proposed by Park and Ang (1985) and Park et al. (1987) when inelastic dynamic analysis is performed. In the case of static evaluations, particularly when pushover curves are available, the yield and ultimate limit state definitions by Park (1988) is used for the determination of the above defined performance levels.

Different structural analysis techniques require different representations of earthquake demand. For instance, equivalent linear analysis needs spectral acceleration values at certain periods in order to estimate the lateral forces. On the other hand, as the name indicates, spectral analysis uses spectral representation of the ground motion. Although some of the improved capacity spectrum methods, including the one developed in this report, employ time histories, the demand spectra are essential for evaluation purposes in CSM. Linear and nonlinear response history analyses employ earthquake records, which are preferable in most of the cases due to their more accurate representation of ground motion features such as duration effects and time varying amplitude.

The final step leading to the fragility relationships is the statistical analysis of structural response data. If the system stays within the linear range, the relationship between the response and the intensity measure is also linear. However, under severe seismic excitation the system generally goes into the inelastic range in which case a regression analysis of the responses as a function of the excitation intensity measure is performed. Luco and Cornell (2007) propose a nonlinear regression analysis of the power-law form which allows linear regression analysis by a simple logarithmic transformation. Wen et al. (2004a) use this technique within the proposed vulnerability function framework. The regression constants obtained give the conditional expectation and coefficient of variation of the structural response given the hazard intensity. With the selection of a suitable distribution function and using the latter parameters, the fragility curves can be generated.

A different approach is proposed by Kircher et al. (1997b), for fragility curve generation, where the ground motion intensity is replaced with mean structural response through a process called convolution. This method is also implemented in HAZUS.

CHAPTER 3
CAPACITY OF BUILDINGS AND EARTHQUAKE DEMAND

This chapter investigates the first two components of the proposed framework for fragility analysis, i.e. capacity of buildings and earthquake demand. These two components are inputs to the process which are critically important for the reliability of the developed fragility relationships. In other words, the more representative of the real behavior building capacity and earthquake demand are, the more dependable the end result is. The two major uncertainty constituents contributing to the fragility analysis originate from the two components above and they are characterized by the variation of their ingredients. Therefore the first section of this chapter investigates the capacity of buildings and proposes a new model, the formation of a database composed of pushover curves based on advanced simulation. The second section discusses time histories, selected for the purposes of this study, which are representative of the seismo-tectonic environment in CEUS.

The capacity of buildings and earthquake demand are given as inputs to the methodology for structural assessment (discussed in section 4.1) and the results are processed using the methodology for fragility curve generation (discussed in section 4.2) to obtain the desired fragility relationships.

3.1. CAPACITY OF BUILDINGS

As previously mentioned, there are several ways of representing the capacity of buildings. Because the aim of this study is to obtain fragility relationships for populations of buildings that include various different buildings in terms of construction type, height, design level, among others, a simple representation of lateral force resisting capacity of buildings (here pushover curves are utilized for this purpose) which is still reflective of real behavior, is required.

A pushover curve can be thought of as an envelope for the cyclic response of a structure. It can provide significant insight to the overall behavior of a structure under lateral loading. The main shortcoming of pushover analysis is that it cannot capture the local response, examples being soft storey formation, rebar pullout, buckling, and higher mode

effects. Moreover, using pushover analysis, it is hard to predict the behavior of structures having mass and stiff irregularities in plan and elevation, where torsional effects come into consideration. However, significant research has been devoted to address the above issues and several studies show that pushover analysis can provide reasonable nonlinear force displacement relationships for regular structures with negligible higher mode-effects; refer to Chapter 2.

For the purposes of the current study, which mainly considers building types that conform to the above requirements, pushover curves are adequate to represent the global response under lateral actions. As a consequence building capacity is represented with pushover curves throughout this study. Such representation also suits the requisites of methodology for structural assessment.

3.1.1. Pushover Curves and Capacity Diagrams

An advanced CSM is developed and used in this study for structural response assessment under earthquake ground motion. CSM requires building capacity to be represented in Acceleration-Displacement (AD) format, named by Mahaney et al. (1993). However, most commonly pushover curves are expressed in terms of base shear, V_b, versus roof displacement, Δ_{roof}, which require conversion into AD format.

AD format is obtained by plotting spectral acceleration against spectral displacement, as opposed to period vs. spectral acceleration or period vs. spectral displacement as in the case of commonly used spectra. This type of representation does not explicitly include period (or frequency); however, radial lines drawn from the origin to a point on the curve in AD format define a specific period or frequency (see Figure B.4.). Representation of the capacity curve (or pushover curve for this study) in AD format is referred to as a capacity diagram.

A brief description of how to obtain pushover curves as well as the derivation of the equations used for converting them into capacity diagrams is provided below using the description and notation of Fajfar (2000).

The following description applies a monotonically increasing pattern of lateral forces, representing the inertial forces that the structure would experience when subjected to ground motion, obtaining the characteristic nonlinear force-displacement relationship of the multi-degree of freedom system in terms of base shear and roof displacement, Figure 3.1.

The vector of lateral loads, $\boldsymbol{P}$, used in the pushover analysis is given by:

$$\boldsymbol{P} = p\boldsymbol{\Psi} = p\boldsymbol{M}\boldsymbol{\Phi} \tag{3.1}$$

where $\boldsymbol{M}$, is the diagonal mass matrix and the magnitude of lateral loads is controlled by p. $\boldsymbol{\Psi}$ denotes the distribution of lateral loads and it is related to the assumed displacement shape $\boldsymbol{\Phi}$.

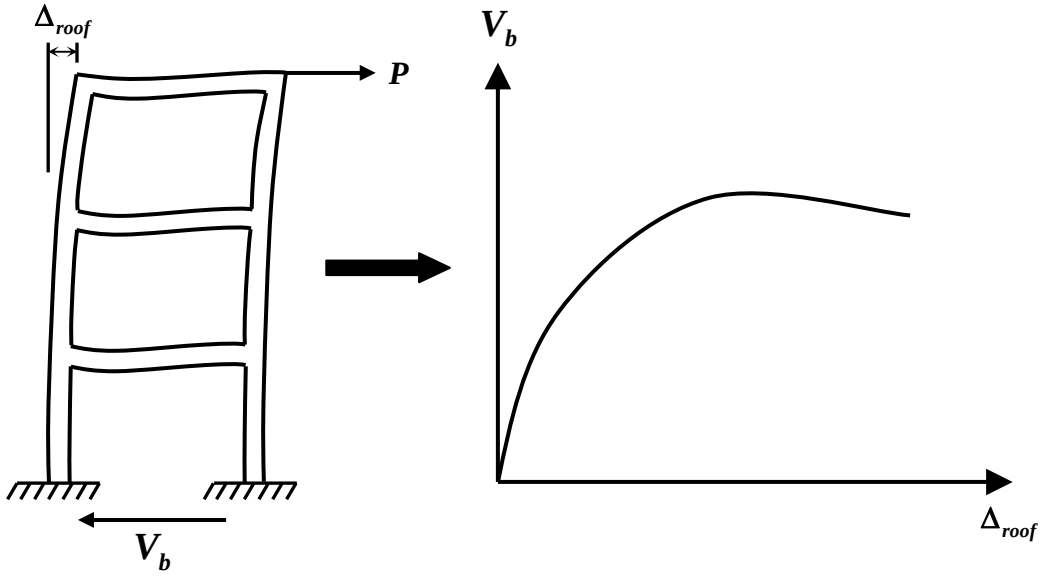

Figure 3.1. Pushover curves

In the conversion from pushover curves to capacity diagrams the multi-degree-of-freedom (MDOF) system is represented as an equivalent single-degree-of-freedom (SDOF) system. The equation of motion for the MDOF system is given by:

$$\boldsymbol{M}\ddot{\boldsymbol{U}} + \boldsymbol{C}\dot{\boldsymbol{U}} + \boldsymbol{R} = -\boldsymbol{M}\boldsymbol{1}\ddot{x}_g \tag{3.2}$$

where $\boldsymbol{U}$ is the displacement vector, $\boldsymbol{C}$ is the damping matrix, $\boldsymbol{R}$ is the vector of internal forces, $\ddot{x}_g$ is the ground acceleration and $\dot{(\ )}$ denotes the time derivative.

Assuming that the displacement shape, $\boldsymbol{\Phi}$, does not change during the structural response to ground motion and knowing that the internal forces, $\boldsymbol{R}$, is equal to externally applied loads, $\boldsymbol{P}$, by defining the displacement vector as in Eq. (3.3); Eq. (3.2) is transformed into Eq. (3.4).

$$\boldsymbol{U} = \boldsymbol{\Phi\eta} \tag{3.3}$$

$$\boldsymbol{\Phi}^{\mathbf{T}}\boldsymbol{M}\boldsymbol{\Phi}\ddot{\boldsymbol{\eta}} + \boldsymbol{\Phi}^{\mathbf{T}}\boldsymbol{C}\boldsymbol{\Phi}\dot{\boldsymbol{\eta}} + \boldsymbol{\Phi}^{\mathbf{T}}\boldsymbol{M}\boldsymbol{\Phi}p = -\boldsymbol{\Phi}^{\mathbf{T}}\boldsymbol{M}\mathbf{1}\ddot{x}_g \tag{3.4}$$

Multiplying and dividing the left hand side of Eq. (3.4) by $\boldsymbol{\Phi}^{\mathbf{T}}\boldsymbol{M}\mathbf{1}$ yields:

$$m^*\ddot{\eta}^* + c^*\dot{\eta}^* + F^* = -m^*\ddot{x}_g \tag{3.5}$$

where m^* and c^* is the equivalent mass and equivalent viscous damping constant of the SDOF system respectively and the latter quantities are given by:

$$m^* = \boldsymbol{\Phi}^{\mathbf{T}}\boldsymbol{M}\mathbf{1} = \sum m_i\Phi_i \tag{3.6}$$

$$c^* = \Gamma\boldsymbol{\Phi}^{\mathbf{T}}\mathbf{C}\boldsymbol{\Phi} \tag{3.7}$$

η^* and F^* are the displacement and force of the SDOF system:

$$\eta^* = \frac{\eta}{\Gamma} \tag{3.8}$$

$$F^* = \frac{V_b}{\Gamma} \tag{3.9}$$

Γ is the modal participation factor and used to convert from the MDOF system to SDOF system and vice-versa. It is given by the below equation where m_i is the storey mass.

$$\Gamma = \frac{\boldsymbol{\Phi}^{\mathbf{T}}\boldsymbol{M}\mathbf{1}}{\boldsymbol{\Phi}^{\mathbf{T}}\boldsymbol{M}\boldsymbol{\Phi}} = \frac{\sum m_i\Phi_i}{\sum m_i\Phi_i^2} \tag{3.10}$$

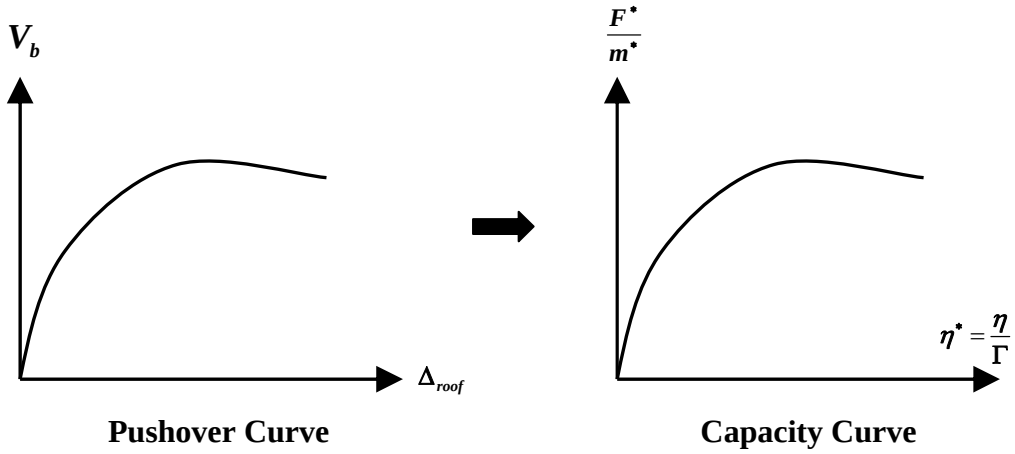

Figure 3.2. Conversion of pushover curves to capacity diagrams

It is important to note that the assumed displacement shape is normalized such that it is equal to unity at the top (roof) of the building.

The spectral acceleration values of the capacity diagram in AD format are obtained by dividing the force, F^*, by the mass of the SDOF system, that is:

$$S_a = \frac{F^*}{m^*} \tag{3.11}$$

For the conversion of pushover curves to capacity diagrams, this study utilizes the same displacement shape, **Φ**, as the one used in obtaining the pushover curve.

3.1.2. Building Types

The outcome of this study will provide an input for future earthquake loss assessment studies. Hence the wide range of building types must be considered so as to achieve uniformity in fragility relationships that future studies can readily apply.

The building types provided in HAZUS (National Institute of Building Sciences, 2003) were first defined in ATC-14 (Applied Technology Council, 1987) and later on they appeared in FEMA 310 (formerly FEMA 178 - 1992), NEHRP Handbook for the Seismic Evaluation of Existing Buildings – A Prestandard (1998) with a number of building types added to cover all common styles of construction.

Table 3.1. Summary of Building Types (National Institute of Building Sciences, 2003)

#	Label	Description	Height Range		Typical		Period (sec)
			Rise	Stories	Stories	Feet	
1	**W1**	Wood, Light Frame		1-2	1	14	0.35
2	**W2**	Wood, Commercial and Industrial		All	2	24	0.40
3	**S1L**	Steel Moment Frame	Low-	1-3	2	24	0.50
4	**S1M**		Mid-	4-7	5	60	1.08
5	**S1H**		High-	8+	13	156	2.21
6	**S2L**	Steel Braced Frame	Low-	1-3	2	24	0.40
7	**S2M**		Mid-	4-7	5	60	0.86
8	**S2H**		High-	8+	13	156	1.77
9	**S3**	Steel Light Frame		All	1	15	0.40
10	**S4L**	Steel Frame with Cast-in-Place Concrete Shear Walls	Low-	1-3	2	24	0.35
11	**S4M**		Mid-	4-7	5	60	0.65
12	**S4H**		High-	8+	13	156	1.32
13	**S5L**	Steel Frame with Unreinforced Masonry Infill Walls	Low-	1-3	2	24	0.35
14	**S5M**		Mid-	4-7	5	60	0.65
15	**S5H**		High-	8+	13	156	1.32
16	**C1L**	Concrete Moment Frame	Low-	1-3	2	20	0.40
17	**C1M**		Mid-	4-7	5	50	0.75
18	**C1H**		High-	8+	12	120	1.45
19	**C2L**	Concrete Shear Walls	Low-	1-3	2	20	0.35
20	**C2M**		Mid	4-7	5	50	0.56
21	**C2H**		High-	8+	12	120	1.09
22	**C3L**	Concrete Frame with Unreinforced Masonry Infill Walls	Low-	1-3	2	20	0.35
23	**C3M**		Mid-	4-7	5	50	0.56
24	**C3H**		High-	8+	12	120	1.09
25	**PC1**	Precast Concrete Tilt-Up Walls		All	1	15	0.35
26	**PC2L**	Precast Concrete Frames with Concrete Shear Walls	Low-	1-3	2	20	0.35
27	**PC2M**		Mid-	4-7	5	50	0.56
28	**PC2H**		High-	8+	12	120	1.09
29	**RM1L**	Reinforced Masonry Bearing Walls with Wood or Metal Deck Diaphragms	Low-	1-3	2	20	0.35
30	**RM1M**		Mid-	4+	5	50	0.56
31	**RM2L**	Unreinforced Masonry Bearing Walls with Precast Concrete Diaphragms	Low-	1-3	2	20	0.35
32	**RM2M**		Mid-	4-7	5	50	0.56
33	**RM2H**		High-	8+	12	120	1.09
34	**URML**	Unreinforced Masonry Bearing Walls	Low-	1-2	1	15	0.35
35	**URMM**		Mid-	3+	3	35	0.50
36	**MH**	Mobile Homes		All	1	10	0.35

HAZUS divides the available building classes in FEMA 310 into height ranges and includes mobile homes. With a total of 36 types, building classification of HAZUS can be considered adequate for most loss assessment studies. Thus this study adopts the same classification system. A summary of these building types is provided in Table 3.1. Further details types can be found in HAZUS Technical Manual Chapter 5.

3.1.3. Database for Woodframe Structures

As an example application of the fragility framework developed here, this study places special focus on woodframe structures. 80 to 90% of all buildings in the USA are of woodframe construction, which is susceptible to damage during hazards such as earthquakes and hurricanes. Similar statistics are also observed for the region of focus of the MAE Center, CEUS; refer to section 1.3.

Table 3.2. Building configurations included in the database

Model #	Source of Data	Related Study	Structural Configuration
1-14	**CUREE Woodframe Project**	Shake Table Tests of a Two Storey Woodframe House	Two Storey Woodframe House
		Seismic Modeling of Index Woodframe Buildings	Small House
			Large House
			Town House
			Apartment Building
14-30	**(Filiatrault, 2007)**	ATC-63 75% Complete Draft	16 Archetype Structures
30-33	**(Rosowsky and WeiChiang, 2007)**	Texas A&M Frames	One Storey Woodframe
			Two Storey Woodframe
			Larger Two Storey Woodframe

In order for the building capacity for this particularly important building group to reflect real behavior, pushover curves for woodframe structures, which are all derived using simulation models, are collected from previous studies to form a database. This allows a more reliable estimation of the uncertainty associated with the building capacity to be achieved. For fragility analysis of the rest of the building groups, this study uses the set of

capacity diagrams defined in HAZUS Technical Manual Chapter 5, which are mainly based on expert opinion.

Three different sources of structural information contribute to the database:

i. CUREE–Caltech Woodframe Project (http://www.curee.org/projects/woodframe)
    a. Shake Table Tests of a Two-Storey Woodframe House (Fischer et al., 2001)
    b. Seismic Modeling of Index Woodframe Buildings (Isoda et al., 2002)
ii. ATC-63 Project – 75% Complete Draft (Filiatrault, 2007)
iii. Texas A&M Woodframe Structures (Rosowsky and WeiChiang, 2007)

The building configurations included in the database are summarized in Table 3.2 and further details are provided below.

3.1.3.1. CUREE-Caltech Woodframe Project

The CUREE-Caltech Woodframe Project (Earthquake Hazard Mitigation of Woodframe Construction) was funded by FEMA through a grant administrated by the California Office of Emergency Service (COES).

The project is composed of five Elements and each element is composed of several different tasks. The following two tasks are taken from Element 1, Testing and Analysis, and from Element 4, Economic Aspects, respectively.

Shake Table Tests of a Two-Storey Woodframe House:

The two storey woodframe house shown in the figure below was built and tested (quasi-static, frequency, damping, and seismic) within the scope of CUREE-Caltech Woodframe Project. Several tests are performed for various stages of completion of the building's lateral force resisting system.

The two-storey building is considered to be complete in phases 9 and 10. The main difference between phase 9 and 10 test structures is the existence of non-structural wall finish materials, i.e. exterior stucco and interior gypsum wallboard.

Figure 3.3. *(Top):* Phase 9 test structure *(Bottom):* Phase 10 test structure (Fischer et al., 2001)

Advanced finite element models are developed for the two test structures using the software Seismic Analysis of Woodframe Structures – SAWS (Folz and Filiatrault, 2002). For details see Appendix A, section A.1.2.1. Pushover curves are obtained using this software and the results are verified against experimental data in the studies by Folz and Filiatrault (2004b).

Seismic Modeling of Index Woodframe Buildings:

The other component of the CUREE-Caltech Woodframe Project that is considered in this study, includes the design of four buildings that are typical of woodframe construction in the U.S. (Reitherman and Cobeen, 2003).

Four index buildings – a small house, a large house, a small townhouse, and an apartment building – are designed according to the codes and practices of their period of construction. Their variants for different construction qualities – poor, typical, and superior – include most of the features observed in woodframe buildings.

The commercially available software RUAUMOKO (Carr, 1998) is used to develop finite element models for these structures and obtain the pushover curves (Isoda et al., 2002; Filiatrault et al., 2003). See Appendix A, section A.1.2.1 for further information.

3.1.3.2. ATC-63 Project

ATC-63 is an ongoing project by Applied Technology Council on the Quantification of Building System Performance and Response Parameters (2007). Pushover curves are obtained for sixteen different woodframe light construction archetype structures. The set of building designs represent different seismic regions and levels of gravity load, and cover the following ranges of three variables: number of stories (one to five), seismic design level (low and high), and building use (residential, and commercial or educational). Further details about these structures can be found in Appendix A, section A.1.2.2.

3.1.3.3. Texas A&M Woodframe Structures

Using SAWS, Rosowsky and WeiChiang (2007) at Texas A&M University developed finite element models and pushover curves for three woodframe structures. These three structures are one-storey, small two-storey, and large two-storey buildings build slab on grade. The small two-storey woodframe structure has the same dimensions and storey weights with those of the phase 9 and 10 variants of the shake table test structure

described in section 3.1.3.1. Further details about these buildings can be found in Appendix A, section A.1.2.3.

3.1.4. Capacity Diagrams and Performance Limit States

This section investigates representation of building capacity and the structural damage limit state definitions. Collection of pushover curves for the building types, with the requirement of these curves being derived using advanced simulation in order to capture real behavior, is a process that requires considerable time and effort. Therefore for the important group of woodframe buildings, this task is carried out while extending the database to cover the rest of the building types is out of the scope of this study, therefore for characterizing the capacity of buildings types other than woodframe, this study uses the capacity diagrams defined in HAZUS.

Regarding the definition of earthquake damage limit states, roof drift values are used as a criterion for all the building types. However, this study adopts different approaches for the determination of the limit state values for woodframe structures and for the rest of the building groups in HAZUS.

In terms of seismic design level, each building type given in Table 3.1, is divided into four categories: pre-code, low code, moderate code, and high code. The latter three are defined according to the Uniform Building Code, UBC (International Conference of Building Officials, 1994) while the first, i.e. pre-code seismic design level, is for structures built before seismic design was required.

3.1.4.1. Woodframe Buildings in the Database

The pushover curves, which come from the sources detailed in the previous sections, are categorized into woodframe building types W1 and W2 using the information pertaining to each of the structural configuration (provided in Appendix A, section A.1.2). The former includes small, single-family, one-to-two storey residential buildings with floor area less than 5,000 ft^2 while the latter comprises large, two-storey or more, multi-family or commercial buildings with floor area greater than 5,000 ft^2. Detailed description of these two building types can be found in Appendix A, section A.1.

Once the available structural configurations are classified under W1 and W2, differentiation in terms of seismic design level is carried out with reference to certain threshold values of base shear coefficient, C, defined for each building category. In other words, a PGA value is determined for each of the low, moderate, and high code design levels that conform to current seismic design codes and practices. Then using Eq. (3.12) which gives the relation between PGA and seismic base shear coefficient C, the limits for each design level is established. The spectral amplification factor (SAF) is assumed to be 2.6, consistent with the relations by Newmark and Hall (1982) and given in Appendix B, Table B.1. The demand reduction factor R that accounts for the inelastic response of the structure is taken for each of the design levels as shown in Table 3.3.

$$C = \frac{PGA \times SAF}{R} \tag{3.12}$$

Overstrength factors (OSF) of 4 and 2 are applied for W1 and W2 building types respectively. A higher OSF is assumed for the W1 building type since these are relatively small structures whose overstrength is solely due to stronger design of members. Whereas in the case of large structures with several members, those falling into the W2 building type, redistribution of forces and sequential yielding are observed, therefore the strength related overstrength factor is reduced to 2 in this case. Base shear coefficients describing low, moderate and high code structures are given in Table 3.3. The base shear values of the pushover curves are normalized by the respective weights of the structures giving the base shear coefficient, V_b/W, and classification is performed based on a comparison between the maximum base shear coefficient value of the curve and the threshold values, $C \times OSF$ defined in Table 3.3.

Structures having a maximum base shear coefficient less than the low code threshold value are classified as pre-code, the ones between low and moderate as low code, those between moderate and high code as moderate, and those having greater than high code threshold value are put into high code seismic design level. The categorization of each of the structural configurations defined in Table 3.2 is given in Table A.20 of Appendix A.

Table 3.3. Threshold values defining the seismic design levels

				W1		W2	
Design Level	$PGA\ (g)$	R	SAF	OSF	$C \times OSF$	OSF	$C \times OSF$
Low	0.1	2.5	2.6	4	0.42	2	0.21
Moderate	0.25	3.5	2.6	4	0.74	2	0.37
High	0.4	4	2.6	4	1.04	2	0.52

Just like in HAZUS, four structural damage (performance) limit states are determined for woodframe structures, i.e. slight, moderate, extensive, and complete. For this purpose the yield and ultimate point definitions by Park (1988) are utilized. The slight damage limit state threshold value is based on the deformations at first yield, the moderate on the yield point of equivalent elasto-plastic system with the same energy absorption as the real system, the extensive on the peak of the load displacement relation, and the complete damage limit state threshold value is taken as the post-peak displacement when the load carrying capacity has undergone a small reduction. Illustrations on how the four damage state levels are determined, using the definitions by Park, are provided in Appendix, section A.1.3.1.

Table 3.4. Limit state threshold values for woodframe building categories; spectral displacements are in inches, spectral accelerations are in g and elastic fundamental periods in seconds

		Limit States							
		Slight		**Moderate**		**Extensive**		**Complete**	
Building Category	T_e	S_d	S_a	S_d	S_a	S_d	S_a	S_d	S_a
W1 – Pre-Code	0.20	0.41	0.16	1.79	0.23	3.48	0.28	5.26	0.27
W1 – Low Code	0.26	0.50	0.33	1.61	0.47	3.19	0.57	4.51	0.54
W1 – Moderate Code	0.46	0.24	0.49	0.81	0.81	2.29	0.93	5.20	0.93
W1 – High Code	0.52	0.29	0.76	0.93	1.15	2.23	1.36	5.19	1.33
W2 – Pre-Code	0.07	1.50	0.08	4.84	0.14	8.58	0.17	9.70	0.16
W2 – Low Code	0.14	0.55	0.10	3.12	0.24	5.68	0.29	7.79	0.27
W2 – Moderate Code	0.15	0.92	0.21	4.35	0.41	8.02	0.49	10.13	0.47
W2 – High Code	0.31	0.57	0.54	2.14	0.67	5.87	0.70	13.17	0.70

The four performance levels are determined on each of the capacity diagrams falling into one building category; the threshold values for each damage state level are obtained by

averaging these. Figure 3.4 provides an example of the capacity diagrams for the W2 pre-code structure together with limit states and the HAZUS median curve.

The four damage state threshold values for all the seismic design levels of the W1 and W2 building types are obtained using the procedure described above and tabulated in Table 3.1. The elastic fundamental period, T_e, values shown in the same table are calculated using the slight damage state threshold value as a measure.

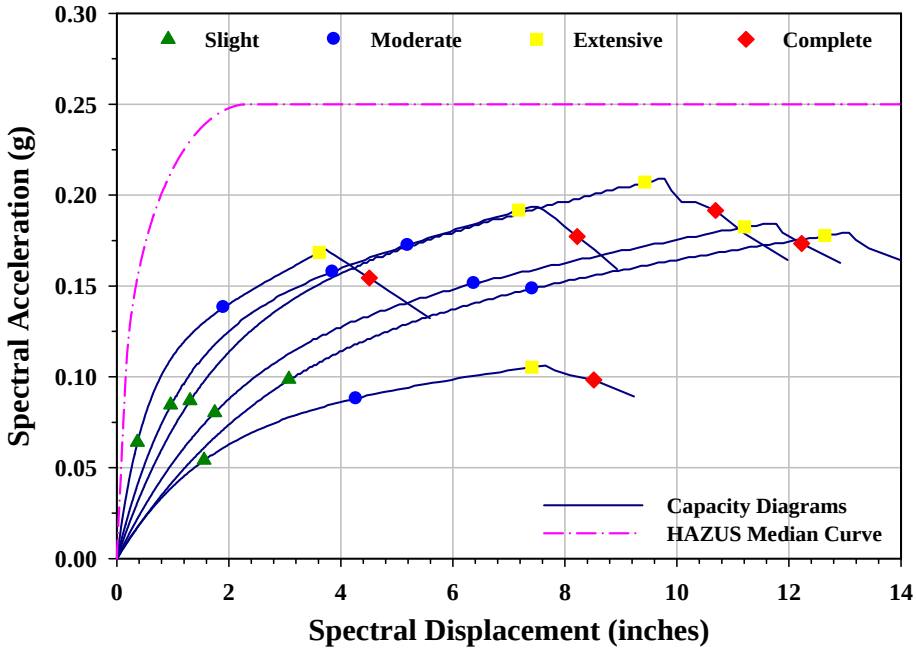

Figure 3.4. Capacity diagrams and limit states for W2 pre-code building category

The most important advantage of using the newly-assembled database is the conclusions drawn regarding the relationship between different design levels of W1 and W2 building groups and their limit states. Contrary to HAZUS approach, high code structures do not necessarily possess higher ductility; on the other hand, their lateral load resistance comes from their strength. This observation is also reflected in the limit state threshold values given in Table 3.4. Although the threshold values seem to increase from high code to pre-code design level for a given building group, which is counterintuitive, the earthquake intensity required to satisfy a given damage limit state of high code design level will be considerably higher than that which is required to satisfy the same damage limit state of the pre-code design level. The significant difference between the strength levels of the

two groups explains this. To further clarify the latter important issue, for a given earthquake intensity, the response obtained from the high code structure will be much lower than that obtained from the pre- and low code counterpart, meaning that the same GMI will satisfy a higher damage limit state level of the structure with inferior seismic design.

To sum up, the uncertainty representation in capacity is achieved through the variation of capacity diagrams under each building category. This study proposes that the assembled database is a more reliable representation of actual behavior than judgmental expert opinion, on which the HAZUS capacity diagrams are based (discussed in the following section, 3.1.4.2). In addition, this study determines the limit states on well established engineering criteria with equivalents in real behavior.

3.1.4.2. Other Building Types Based on HAZUS

For fragility analysis of the building types other than woodframe, this study uses available capacity diagrams from HAZUS. Besides, in order to investigate the effect of representing building capacity with pushover curves which are derived using advanced simulation, HAZUS capacity diagrams for woodframe building types are also embedded into the proposed framework, allowing comparison between the two fragility relationships.

As discussed in section 1.2 in detail, it is a considerably difficult task to represent the capacity for populations of building that reflects the actual behavior of structures under earthquake ground motion. This study overcomes this challenge by using a database of pushover curves based on advanced simulation. Nevertheless, due to falling out of the scope of the work here, the proposed framework is extended to the building groups other than woodframe, using the available set of capacity diagrams from the HAZUS Technical Manual, Chapter 5.

The above mentioned capacity diagrams are defined using two points, i.e. yield and ultimate. The former represents the deformation where transition from elastic to inelastic behavior occurs. The capacity diagram is assumed to be linear up to this point, and a

nonlinear regime, which is described with a segment of an elliptic curve (Cao and Petersen, 2006), exists between the yield and the ultimate points. As the ultimate deformation is attained, a plateau of constant load is maintained (Figure 3.5).

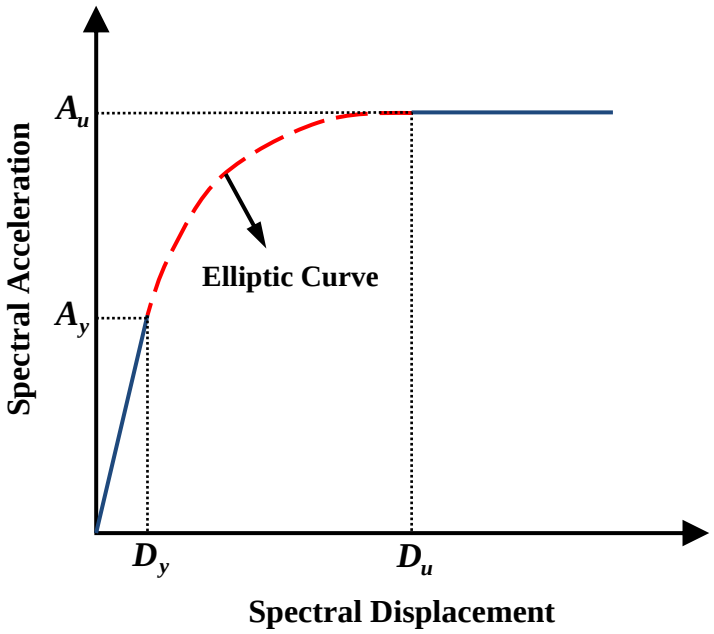

Figure 3.5. Capacity diagrams defined in HAZUS

Determination of the parameters defining the elliptic curve segment is described in Appendix, section A.1.3.2. In addition, yield and ultimate points as well as the parameters of the elliptic region are provided for the four seismic design levels.

D_y, A_y, D_u and A_u are calculated using the following equations:

$$D_y = 9.8 A_y T_e^2 \tag{3.13}$$

$$A_y = C_S \frac{\gamma}{\alpha_1} \tag{3.14}$$

$$D_u = \lambda \mu D_y \tag{3.15}$$

$$A_u = \lambda A_y \tag{3.16}$$

where C_S is the design strength coefficient, T_e is the elastic fundamental mode period of the building, α_1 is the fraction of building weight effective in pushover mode, γ is the

overstrength factor relating the true yield strength to design strength, λ is the overstrength factor relating the ultimate strength to yield strength and μ is the ductility factor relating ultimate displacement to λ times the yield displacement. The fundamental period of the building, T_e, pushover mode parameter, α_1, the ratio of yield to design strength, γ, and the ratio of ultimate to yield strength, λ, are assumed to be independent of seismic design level. However, ductility factor, μ, changes depending on the design level. The values of these parameters can be found in HAZUS Technical Manual Chapter 5, Table 5.4, Table 5.5 and Table 5.6.

The parameters stated in the preceding paragraph are determined based on expert opinion. Similarly, limit states are determined using personal judgment, and they are given in terms of drift ratio (HAZUS Technical Manual Chapter 5).

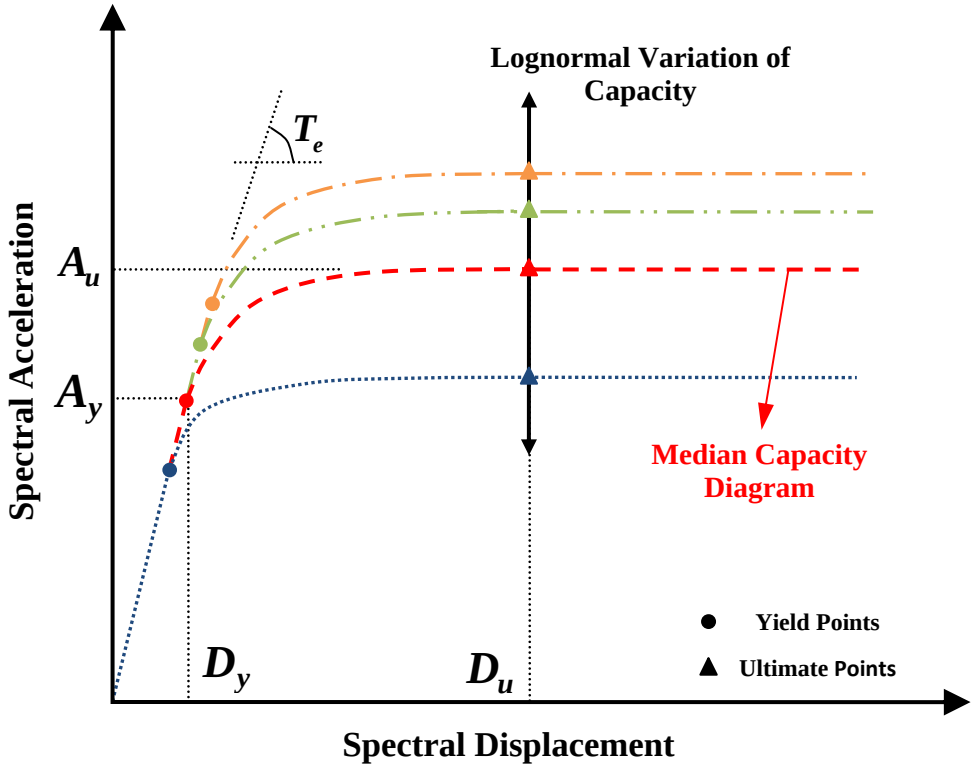

Figure 3.6. Variation in capacity for building types based on HAZUS

To achieve the required variation in building capacity for the purposes of fragility analysis, this study adopts the proposed procedure in HAZUS Technical Manual Chapter 5. The building capacity diagrams are assumed to be lognormally distributed as a

function of the acceleration at the ultimate point. D_y, A_y, D_u, and A_u values given in Appendix A, Table A.21 through Table A.24 are the median values for these parameters. The standard deviation of the lognormal distribution, β_C, is assumed to be 0.25 for code designed buildings, i.e. high code, moderate code, and low code and 0.3 for pre-code buildings.

In order to obtain a finite number of capacity diagrams from the median curve to represent each building category, the importance sampling technique is used. First lognormal distribution with a median value of $ln(A_u)$ and a standard deviation value of β_C is converted to normal distribution having a mean value equal to the median value of the lognormal distribution and having the same standard deviation value. Then, the normal distribution is mapped to a standard normal distribution using a change of variables as:

$$Z = \frac{\ln X - \ln A_u}{\beta_C} \tag{3.17}$$

where X represents the lognormal random variable, lnX is the normal random variable and Z is the desired standard normal random variable. The area under the probability density function of standard normal random variable between -3 and 3, which amount to 99.73% of the total probability, is divided into five equal areas, Figure 3.7. Each area is shown by α in the same figure. Five sampling points, z_i, are obtained by calculating the x coordinate of the centroid of the corresponding area. These values are substituted in to Eq. (3.17) to get corresponding X values which are equal to ultimate acceleration of the variations of the capacity diagram, note that the point with $z_3 = 0$ gives the median curve.

Once the A_u values for the variations of the capacity diagram are obtained, corresponding A_y then D_y values can respectively be calculated first using Eq. (3.16) and then using Eq. (3.13). Where λ and T_e remains constant. Knowing that D_u is also kept constant, the variations of the capacity diagrams can be constructed using the same methodology used to construct the median curve. This procedure gets repeated for the four seismic design

levels of 36 building types (or for each building category) to represent the variation in capacity using five diagrams based on the importance sampling technique.

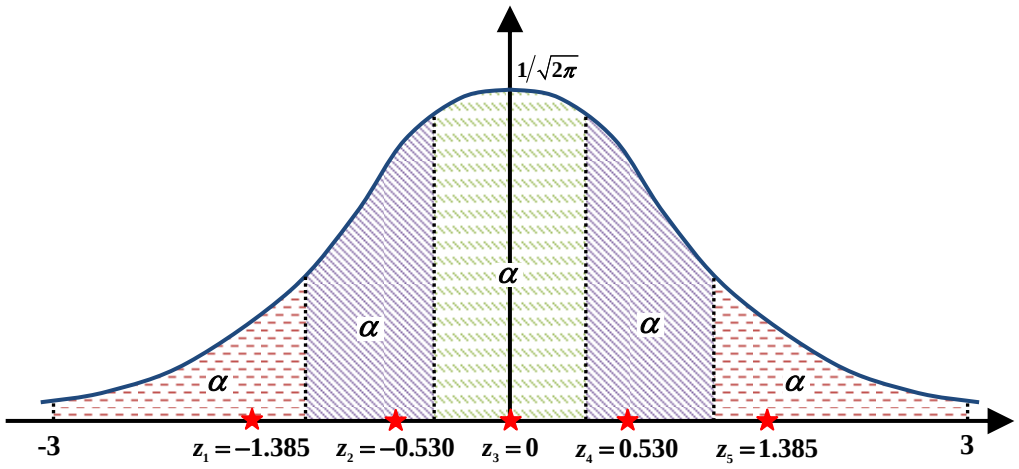

Figure 3.7. Calculation of sampling points from the standard normal distribution (figure not to scale)

Importance sampling technique represents the desired percentage of the total probability (99.73% in this case) using a reasonable number of points (giving it a practical computational time) while precluding the bias that would be introduced by randomly choosing those points.

3.2. EARTHQUAKE DEMAND

Part two of this chapter investigates the second component of the new fragility analysis framework: the earthquake induced demand on structures. Several ways of representing the lateral forces imposed on structures due to earthquake ground motion exist. The present study pursues the most rigorous way, i.e. using ground motion time histories (accelerograms). Use of accelerograms allows the most flexibility for ground motion simulation, in that several different features of earthquakes, e.g. site condition, distance, depth, fault rupture type and many others, can be reflected into earthquake demand by selecting a fair number of records with the desired requirements.

Amongst the list of uncertainties in fragility analysis, such as capacity variation and modeling, the great portion of the total uncertainty is due to ground motion variability. Therefore, selection of the record set to be used is key to the outcome of the fragility

analysis. In view of this the more representative the record set is of the expected event, the higher the reliability of the fragility analysis.

The regional differences in ground motion characteristics are small in seismically active areas, therefore natural time histories selected from one high seismicity zone can be carried to other high seismicity regions as long as the consistency in the required features, i.e. magnitude, depth, fault mechanism and site conditions, is achieved. However, strong motion characteristics in inter-plate and intra-plate regions exhibit significant differences. As a matter of fact, attenuation is much faster in more fragmented inter-plate regions than in intra-plate regions, of which CEUS is an example.

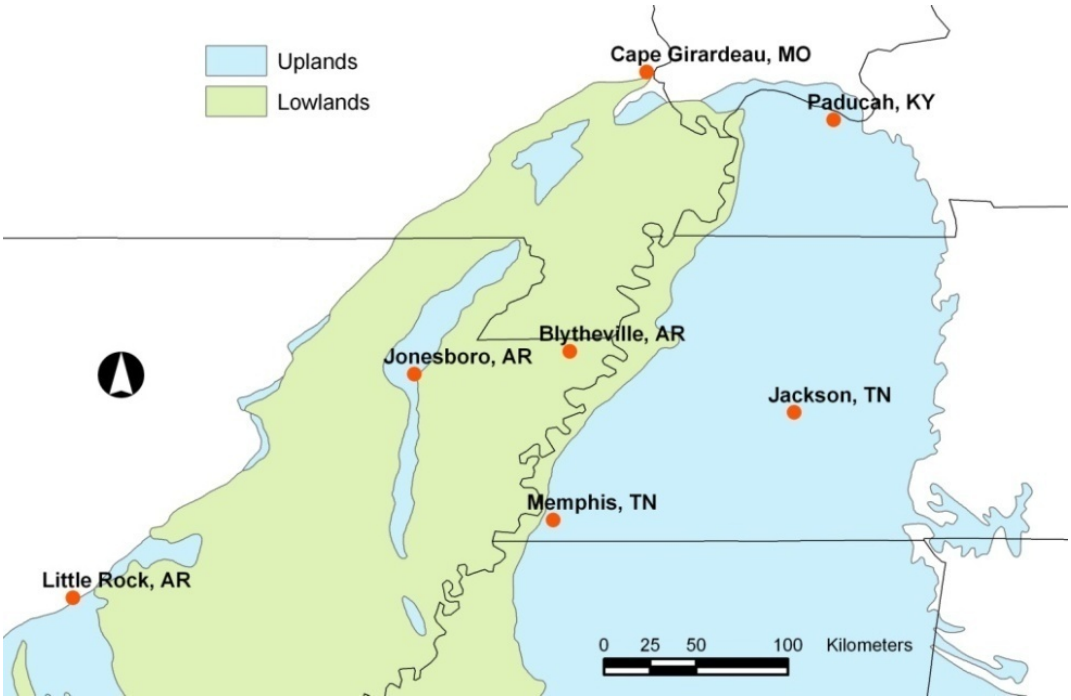

Figure 3.8. Soil profiles for the Upper Mississippi Embayment and cities for which synthetically generated ground motion records are developed (Fernandez, 2007)

As noted before, CEUS is a low probability earthquake region, and the available natural earthquake records are sparse. In addition, none of the records that do exist correspond to a large magnitude event. Stemming from this fact, this study uses synthetically derived accelerograms developed by Fernandez (2007) based on the stochastic method (Boore, 2003). In the study by Fernandez, probabilistic ground motion records have been generated for seven cities within the Upper Mississippi Embayment, including Memphis,

TN (Figure 3.8), which this study uses. Ground motion records for two different site conditions – "lowlands" and "uplands" – are developed for the city of Memphis. Lowlands represents soft soils while uplands are delineated for competent or rock sites.

The aforementioned records are compatible with the uniform hazard spectra previously developed by Fernandez and Rix (2006). In this study Fernandez and Rix incorporate the effects of epistemic (arising from a lack of knowledge, ignorance or modeling) and aleatory uncertainties (stemming from factors that are inherently random) in source, path, and site processes. They also incorporate the effect of nonlinear soil behavior into ground motion attenuation relationships which, in turn, were derived by regression analysis of spectral accelerations from a stochastic ground-motion model based on point-source. The derivation process includes the weighted average of three attenuation relationships, i.e. Atkins and Boore (1995), Frankel et al. (2000) and Silva et al. (2003). But the directivity effects are not accounted for.

The Upper Mississippi Embayment has peculiar ground motion attenuations due to being formed of soft soil sediments with thickness varying between a few feet up to 4,000 feet. And the use of these attenuation relationships, developed for the Upper Mississippi Embayment in the derivation of uniform hazard spectra for the Memphis region and others, has a significant impact on better accommodating the variability of the earthquake process in the site-specific ground motions.

A set of probabilistic ground motions consistent with hazard levels of 10%, 5%, and 2% probability of exceedance in 50 years (with corresponding return periods of 475, 975 and 2475 years) are developed. Each set includes ten acceleration time histories for uplands and lowlands This study uses the set with the 975 years return period. Example time histories for lowlands and uplands soil profiles are shown in Figure 3.9 and Figure 3.10, respectively. And the time histories for the rest of the records in each set can be found in Appendix A, section A.2.

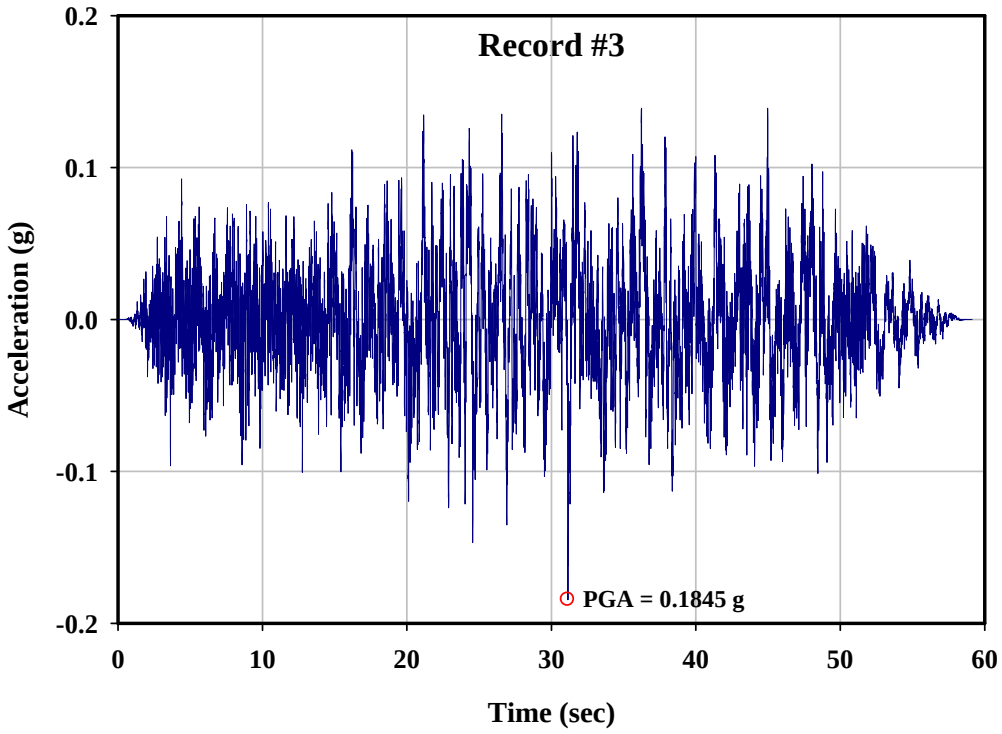

Figure 3.9. Example acceleration time history for lowlands soil profile

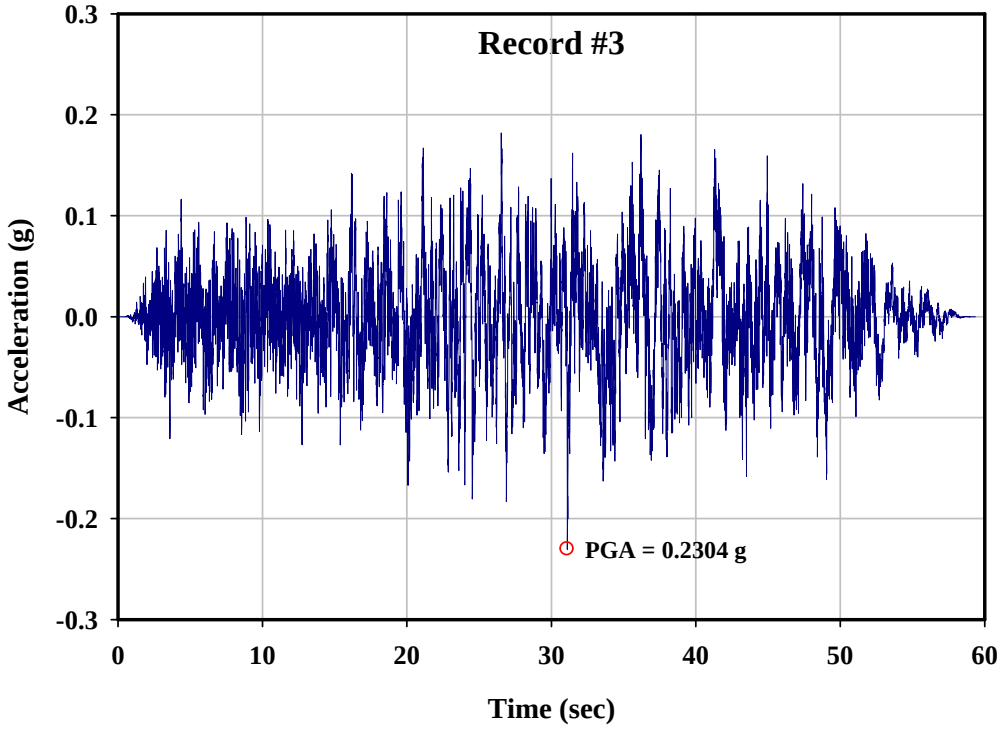

Figure 3.10. Example acceleration time history for uplands soil profile

The PGA, peak ground velocity (PGV), and peak ground displacement (PGD) of the ten earthquake records for each set along with the mean and standard deviation values are given in Table 3.5.

Table 3.5. Single value representations of the earthquake record sets

Record #	Lowlands			Uplands		
	PGA (g)	**PGV (in/sec)**	**PGD (in)**	**PGA (g)**	**PGV (in/sec)**	**PGD (in)**
1	0.204	13.580	6.938	0.201	9.007	3.851
2	0.212	10.733	5.884	0.224	12.048	7.554
3	0.185	8.785	6.902	0.230	17.364	11.546
4	0.207	10.870	7.034	0.226	11.240	6.176
5	0.198	9.821	11.615	0.198	9.808	12.338
6	0.237	17.385	18.182	0.239	13.772	23.945
7	0.192	7.812	6.120	0.275	9.737	8.396
8	0.208	9.511	10.684	0.223	13.614	14.424
9	0.178	17.592	7.321	0.213	13.490	5.489
10	0.213	16.352	6.444	0.250	15.601	13.397
Mean	0.203	12.244	8.712	0.228	12.568	10.712
Standard Deviation	0.017	3.694	3.845	0.023	2.707	5.866

The 5% damped elastic spectra, in different formats, for these records are provided in the figures below. The figures show absolute true spectral acceleration, relative true velocity, and relative true displacement.

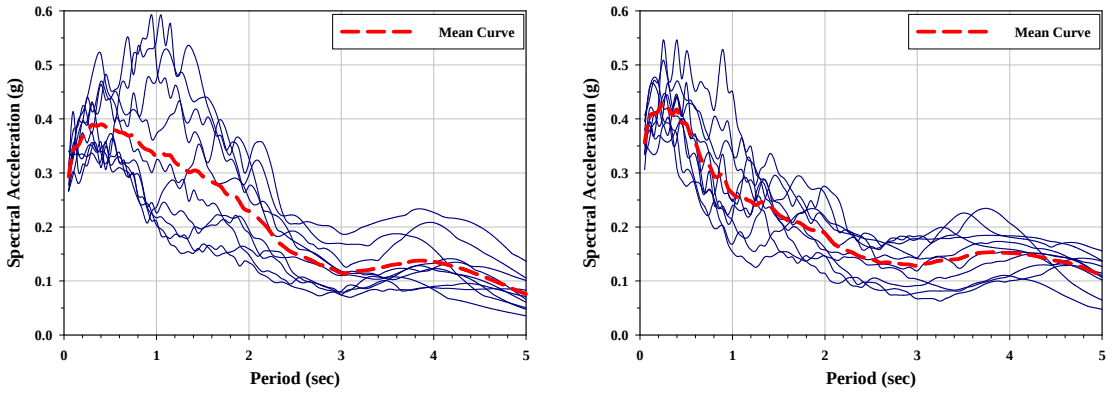

Figure 3.11. 5% damped elastic spectra, period vs. spectral acceleration. *(Left):* Lowlands; *(Right):* Uplands

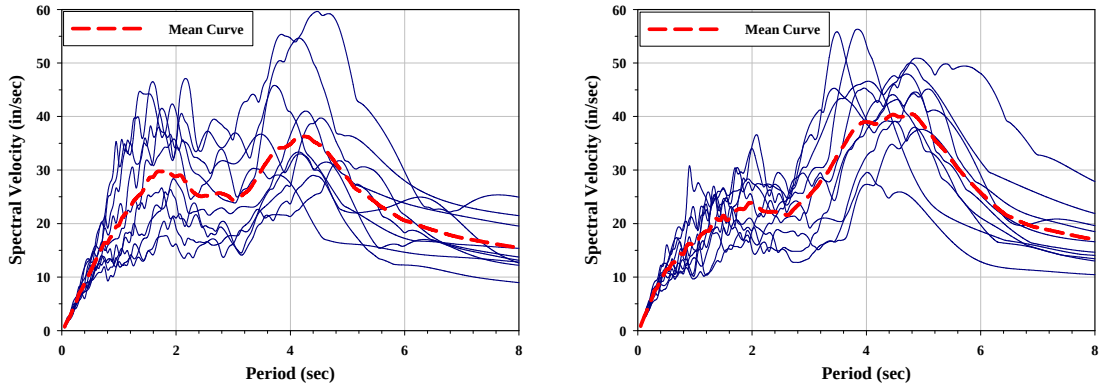

Figure 3.12. 5% damped elastic spectra, period vs. spectral velocity. *(Left):* Lowlands; *(Right):* Uplands

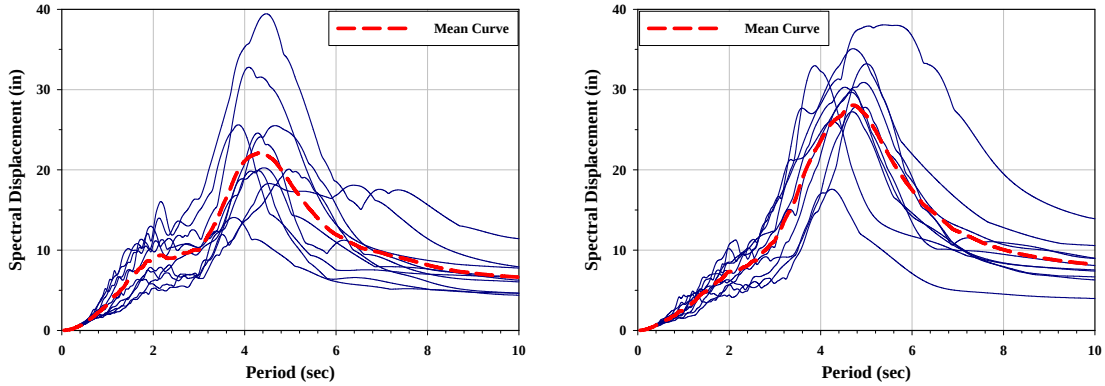

Figure 3.13. 5% damped elastic spectra, period vs. spectral displacement. *(Left):* Lowlands; *(Right):* Uplands

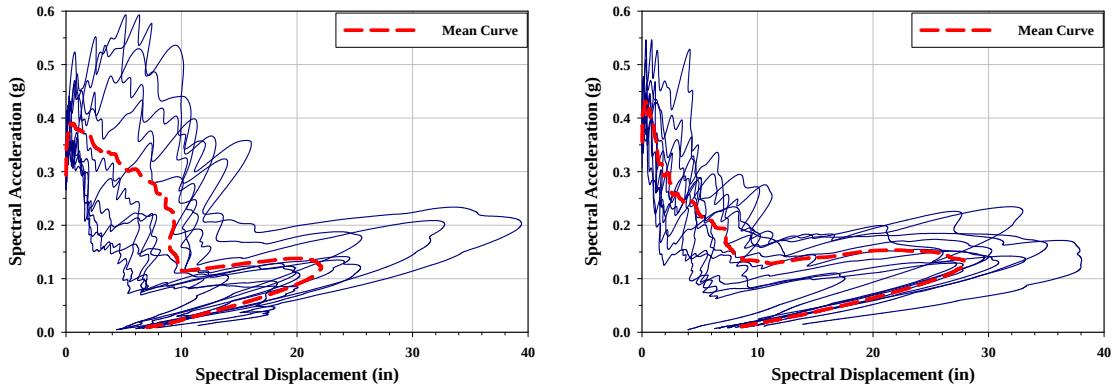

Figure 3.14. 5% damped elastic composite spectra. *(Left):* Lowlands; *(Right):* Uplands

Spectral representation is important for providing insight into different characteristics of the earthquake demand. A case in point is the distance from the source which affects the frequency content of the motion, while distant (or "far field") events have broadband

spectra, close (or "near-field") earthquakes have narrowband, pulse-like input motions. These phenomena, which can be discerned from spectral representations, have an impact on the resonant behavior structures – especially at low periods. Other factors influencing the shape of response spectra are earthquake magnitude, source mechanism characteristics, local geology and site conditions, wave travel paths, and rupture directivity. Nonetheless, magnitude, distance, and site conditions are more influential than others. Site conditions affect the acceleration amplifications which are extended to a larger period range for soft soils and the peak of the spectrum shifts towards higher periods since the predominant vibration of the site is greater for soft soils than it is for rock sites. This can be observed from Figure 3.11, where the peak of the spectra occurs at a lower period for uplands soil profile than that of lowlands and the amplifications are spread to a wider period range in the latter. Therefore use of site or record specific spectra provides an advantage over design spectra where incorporating the aforesaid features of ground motions is limited.

Moreover, representation in spectral displacement vs. period domain and acceleration displacement domain are fundamental for the displacement based design and the capacity spectrum assessment, respectively. Use of design spectra for the displacement based design approaches is debatable in that design spectra estimates unrealistic displacement demands imposed on structures having significantly large periods. The composite spectra (similar to one shown in Figure 3.14) where spectral acceleration values are plotted against spectral displacements is key in graphical CSM procedures where structural capacity and earthquake demand are plotted together and the structural response is obtained through iterations (discussed in detail in section 4.1).

Earthquake records for the city of Memphis are selected for two reasons: first they are capable of representing the required characteristics of earthquakes nucleating in the NMSZ and different sets are provided for the two soil profiles, lowlands and uplands. The rationale for choosing the records with 5% probability of exceedance in 50 years is to minimize the possible alterations in characteristics of ground motions, introduced by scaling, based on PGA, between 0.1 g and 2.0 g, to satisfy the limit states.

It is known that short period structures (fundamental periods less than 0.5 sec) are sensitive to PGA whilst moderately long period structures (0.5-3.0 sec) are affected mostly by the peak ground velocity, and the peak ground displacement is the main influencing factor on long period structures (greater than 3.0 sec). The structures that are subject of this study are buildings mostly having limited irregularity in plan and elevation with short and moderate heights. Most of the buildings in the capacity diagram set by HAZUS (Table 3.1) and the woodframe structures from the database (Table 3.4) have fundamental periods that fall into short period range. On account of this and due it is simplicity in application, scaling by PGA is adopted here through which the degree of spectral dispersion is minimized in the low period range.

The aleatoric uncertainty in earthquake demand is characterized by the variability (in terms of frequency content, duration, time varying amplitude, PGA, PGV, PGD, and site conditions) of ground motion records presented in this chapter.

To conclude, in this study the demand is represented by synthetically generated ground motion records compatible with the seismo-tectonic and geotechnical characteristics of the NMSZ. The ground motions used reflect the magnitude, distance, and site conditions that contribute to seismic hazard in the CEUS. For further details reference is made to Rix and Fernandez (2006; 2007).

CHAPTER 4
METHODOLOGY FOR STRUCTURAL ASSESSMENT AND FRAGILITY CURVE GENERATION

This chapter investigates the methodology for structural assessment and fragility curve generation and presents the selected approaches. The capacity of buildings and earthquake demand are used together by the methodology for structural assessment proposed below to obtain the response data. Thereafter the analysis results are statistically evaluated to derive the fragility relationships. Therefore these last two components can be considered as the analytical evaluation of the capacity and demand inputs.

The methodology for structural assessment is of considerable importance inasmuch as it should yield an accurate prediction of displacement response of a structure under the given ground motion. Furthermore, the methodology for fragility curve generation is essential and should be capable of providing fragility relationships which can be used as an input to related future studies.

4.1. METHODOLOGY FOR STRUCTURAL ASSESSMENT

On the grounds that this study considers populations of buildings, it represents building capacity using pushover curves (or equivalently capacity diagrams) which entail the adoption of a procedure similar to CSM for structural response assessment. The following sections first provide a critical review on the available variants of the CSM and then illustrate their inapplicability or inaccuracy for the requirements of the structural response assessment considered in the present study. For this purpose, one of the woodframe buildings from the database, with available experimental data, is used as a test case. Next this study develops an "Advanced Capacity Spectrum Method," which yields the most reliable displacement predictions when applied to the same structure.

4.1.1. Review of the Available Variants of the Capacity Spectrum Method

As discussed in detail in Chapter 2, CSM was first proposed by Freeman et al. (1975) and Freeman (1978), and after it had appeared in ATC-40 (Applied Technology Council,

1996) it became the subject of several studies and various revisions for improvement. This section summarizes previously developed versions of the CSM under three headings: CSM in ATC-40, CSM with Inelastic Design Spectra, and CSM with Equivalent Elastic Spectra from Damping Models.

All the CSM procedures considered here, including the proposed advanced method, require bilinear representation of the capacity diagram. Bilinear representation based on the equal energy principle is adopted (a description on how to obtain it is provided in Appendix B, section B.1.1). Demand representation in the first two variants – namely, CSM in ATC-40 and CSM with Inelastic Design Spectra – is achieved using elastic design spectra developed from peak ground motion parameters. This study uses the procedure by Newmark and Hall (1982), described in Appendix B, section B.1.1.

4.1.1.1. CSM in ATC-40

The original CSM (Applied Technology Council, 1996) proposes three analogous but different procedures, namely, Procedure A, B, and C. Procedure C being purely graphical and not lending itself to programming, is not considered here. Procedure A provides the most direct application of CSM, and it updates the bilinear representation of capacity diagram depending on the performance point chosen. Procedure B does not include this feature. Procedures A and B not only differ in updating the bilinear representation but they also utilize different procedures to determine structural performance. Procedure A reduces the demand diagram depending on the equivalent damping obtained from the trial performance point until convergence is satisfied. Procedure B obtains the performance point from the intersection of the capacity diagram and the "constant period curve" which is constructed by joining points obtained for different values of ductility for a given SDOF system with prefixed period and hardening values (or bilinear representation).

Since Procedure A is reported to fail satisfying convergence in certain cases (Chopra and Goel, 1999, 2000; Lin et al., 2004b) and Procedure B lacks updating of the bilinear representation of capacity diagram, the forthcoming test case will use combined procedure for assessment using this version of CSM. In other words, different bilinear representations will be developed depending on the trial performance point and the

displacement demand will be determined using the technique of Procedure B. A match between the trial performance point, which in turn determines the bilinear representation, and the displacement demand obtained using that bilinear representation will be the ultimate result of CSM. The impact of updating the bilinear representation depending on the trial performance point will become apparent as the results from CSM in ATC-40 and CSM with inelastic design spectra are compared in the following sections.

Three structural behavior types are defined in ATC-40: types A, B, and C. They are characterized by the hysteretic behavior of systems, from stable to severely pinched loops (A to C in that order), and they are also used to determine the so-called parameter "damping modification factor." The Damping modification factor is defined so as to account for the imperfect hysteretic loops that might occur due to duration effects and poor ductility detailing of structures.

Because CSM in ATC-40 utilizes spectral reduction factors, and because they are not applicable to spectra from specific records, this method is only suitable for evaluating structures under code-conforming demand diagrams; that is, those having distinct regions of constant acceleration, velocity, and displacement.

Details on how to implement this variant of the CSM are provided in Appendix B, section B.1.1.1.

4.1.1.2. CSM with Inelastic Design Spectra

First Bertero (1995) and Reinhorn (1997), and later Fajfar (1999) and Chopra and Goel (1999; 2000) proposed direct use of inelastic design spectra instead of utilizing equivalent linear systems. They suggested obtaining inelastic design spectra from their elastic counterparts by using the force reduction factors. Chopra and Goel (1999; 2000) used reduction factors from different studies (Newmark and Hall, 1982; Krawinkler and Nassar, 1992; Vidic et al., 1994) and showed that up to 50 percent difference, on the non-conservative side, can be obtained between the results of CSM in ATC-40 and those of CSM with inelastic design spectra.

Since force reduction factors can only be used for reducing design (or code conforming) spectra, similar to CSM in ATC-40, this version of CSM is not suitable for assessment of structures under specific earthquake records.

The most important limitation that comes with employing force reduction factors is that they are derived for systems with elasto-plastic (EP) force-deformation relationships (or for systems with small strain hardening values). However, the following sections show that during the process of updating the bilinear representation of the capacity diagram strain hardening values up to 25% or more is observed. Rahnama and Krawinkler (1993), showed that if the strain hardening is increased from 0 to 10%, a difference of about 20% is observed in force reduction factors. The structures in this study have strain hardening values of 25% or more, which would result in 20% error or more if updating the bilinear representation was used in this version of CSM. Such a level of error is not acceptable.

Therefore, in the light of above discussion, it can be concluded that certain types of capacity diagrams, i.e. those that cannot be idealized with bilinear representations having small strain hardening values, are not amenable for evaluation with this version of CSM. To overcome this incompatibility occurring between the capacity and the demand diagrams, a single EP representation, again making use of the equal energy principle, needs to be developed (see details provided in Appendix B, section B.1.1). Lack of updating the bilinear representation resulted in significant reduction in accuracy, as will be seen as the results are presented.

For the assessment of the example woodframe structure with this version of CSM, this study uses force reduction factors from ATC-40 (Applied Technology Council, 1996), Newmark and Hall (1982), Krawinkler and Nassar (1992), Vidic et al. (1994) and Miranda and Bertero (1994). The relationships from ATC-40 are given in Appendix B, section B.1.1.1 and the rest are provided in section B.1.1.2. For the force reduction factors derived by Borzi and Elnashai (2000), whilst using an extensive list of earthquake records that are uniformly processed and a number of hysteretic models, the application is restricted to ductility factor, μ, greater than 2. Since several of examples considered here

have ductility less than 2, the expressions by Borzi and Elnashai are not employed in this study.

The criterion to obtain the performance point is akin to the one in CSM in ATC-40, though here the ductility ratio replaces effective damping. Agreement of the effective damping from the capacity diagram and the same quantity associated with inelastic design spectra yields the structural response.

4.1.1.3. CSM with Equivalent Elastic Spectra from Damping Models

As an alternative improvement to CSM in ATC-40, using equivalent viscous damping models from different studies is proposed (Reinhorn, 1997; Lin and Chang, 2003; Lin et al., 2004a; Kim et al., 2005). Lin and Chang (2003) used damping models from Iwan and Gates (1979), WJE (1996), and Kowalsky et al. (1994b) to show that the deviation in the results of Chopra and Goel (1999; 2000) from the exact solution can be further reduced. Although Lin and Chang had demonstrated that the actual peak absolute acceleration should be used instead of the pseudo-acceleration in order to improve the accuracy of the original CSM, Kim et al. argued that the effectiveness of using actual peak absolute acceleration for constructing demand spectra should be verified through additional analyses. A rigorous review of available equivalent viscous damping models, including but not limited with those provided in Appendix B, section B.1.1.3, can be found in Kim et al. and Xue (2001). Kim et al. also presented results obtained using the empirical equivalent period equation of Iwan and Gates.

In contrast to the versions of CSM described up to this point, CSM with equivalent elastic spectra is proper for predicting displacement demands under specific earthquake records. Damping and period of the equivalent linear system are calculated from the properties of the inelastic system. These two parameters are used to derive the over-damped elastic demand diagram; and the performance point is obtained, through iterations, as the intersection point of demand and capacity diagrams. Similar to the ATC-40 methodology and unlike the CSM with inelastic design spectra, bilinear representation of the capacity diagram is updated depending on the trial performance point in this version of CSM.

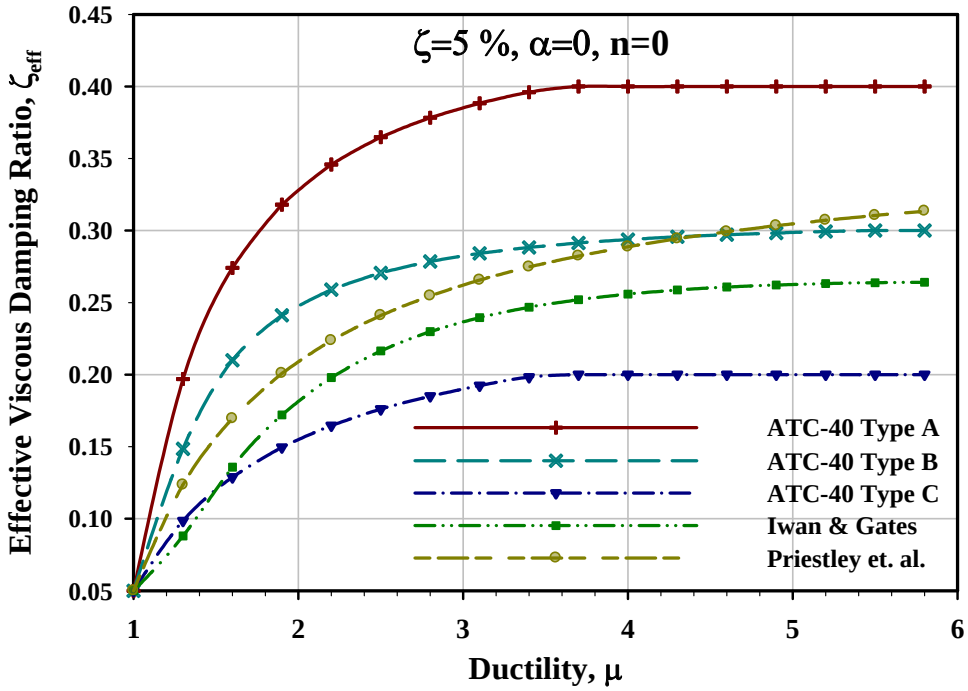

Figure 4.1. Ductility damping relationships from different studies

Damping models from ATC-40, Iwan and Gates (1979), and Priestley et al. (1996) are considered in this study. Damping models from WJE (1996) and Kowalsky et al. (1994b) are not included because the former starts at an elastic damping value of 5% which is higher than the required value for the evaluation of example structure, and the latter is reported to yield negative damping values for high strain hardening ratios (Kim et al., 2005). Details of all the above stated damping models can be found in Appendix B, section B.1.1.3.

A Comparison of different ductility damping relationships used in the test case is shown in Figure 4.1.

4.1.2. The Woodframe Structure as a Test Case

The woodframe structure from the study by Fischer et al. (2001) is used for the purposes of evaluating the available variants of the CSM whose details are provided in the preceding section. This woodframe structure is one of the many others whose pushover curve is included in the database, section 3.1.3.1.

Available shake table test data (roof displacement) from two records – Canoga and Rinaldi Park from 1994 Northridge Earthquake – is the primary reason for selecting this structure for the evaluation of the analytical methods. Moreover, previous studies used neither full scale nor woodframe structures for CSM assessment.

Both variations of the structure are studied; namely, Phase 9 and Phase 10. Properties for this woodframe structure are given in Appendix A, Table A.1. For convenience they are repeated here:

Table 4.1. Properties of the woodframe structures used in the test case

Storey Number	Storey Height from Ground (in)	Storey Weight (kips)	$\boldsymbol{\phi_i}$	$\boldsymbol{w_i\phi_i}$	$\boldsymbol{w_i\phi_i^2}$	Viscous Damping Ratio* (%)
1	108	13.8	0.64	8.82	5.63	1
2	216	10.8	1	10.8	10.8	1
	SUM	24.6	-	19.62	16.43	-
Conversion Factors						
	$\boldsymbol{\Gamma}$	1.194				
	$\frac{\boldsymbol{\Gamma m^* g}}{\boldsymbol{W}}$	0.952				

***** The viscous damping ratio in each of the modes is taken as one percent of the critical as stated in Folz et al. (2002).

As an example application of the conversion procedure from pushover curve to capacity diagram, the required constants are calculated as:

$$\Gamma = \frac{\sum w_i \Phi_i}{\sum w_i \Phi_i^2} = \frac{19.62}{16.43} = 1.194 \tag{4.1}$$

The equivalent mass and damping ratio of the SDOF system are found in Eq. (4.2) and Eq. (4.3), respectively.

$$m^* = \sum \frac{w_i}{g} \Phi_i = 609.81 \quad slugs \tag{4.2}$$

$$\zeta^* = \Gamma \Phi^T \zeta \Phi = 1.194 \begin{bmatrix} 0.639 & 1 \end{bmatrix} \begin{bmatrix} 0.01 & 0 \\ 0 & 0.01 \end{bmatrix} \begin{bmatrix} 0.639 \\ 1 \end{bmatrix} = 0.0168 \qquad (4.3)$$

Folz and Filiatrault (2002) derived three different pushover curves (using triangular and uniform distribution, as well as adaptive pushover technique) for each variation of the woodframe structure employing the computer program, SAWS, developed by the same authors, and verified these curves against experimental data (Folz and Filiatrault, 2004b). In order to be consistent with the conversion factors calculated above, pushover curves from triangular distribution are used here. Pushover curves together with the capacity diagrams are shown in Figure 4.2.

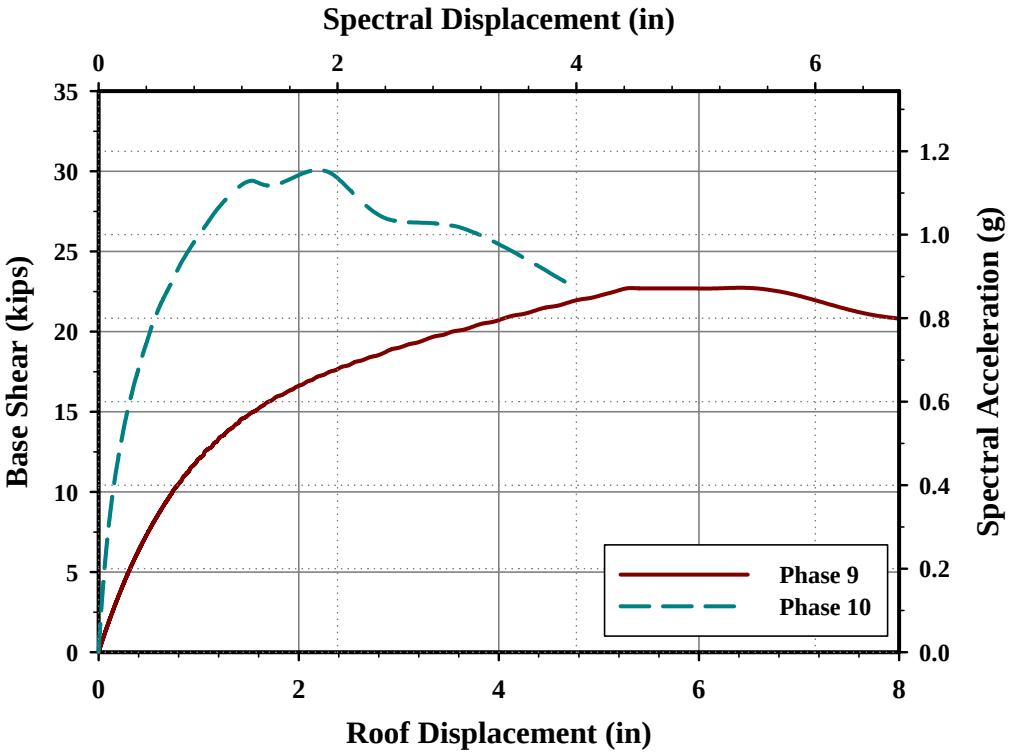

Figure 4.2. Pushover curves (axes on left and bottom) and capacity diagrams (axes on top and right) for the two variations of the woodframe structure

The properties of the ground motions used are provided in Table 4.2. Accelerograms and elastic spectra (actual and design) are shown in Figure 4.3. Newmark and Hall (1982) methodology, described in Appendix B, section B.1.1, is used to obtain elastic design spectra (Chopra, 2000 - Section 6.6).

Table 4.2. Characteristics of the ground motions used in seismic tests

Ground Motion	Amplitude Scaling Factor	PGA (g)	PGV (in/s)	PGD (in)
Canoga Park	1.2	0.50	28.43	9.49
Rinaldi Park	1.0	0.89	70.24	11.91

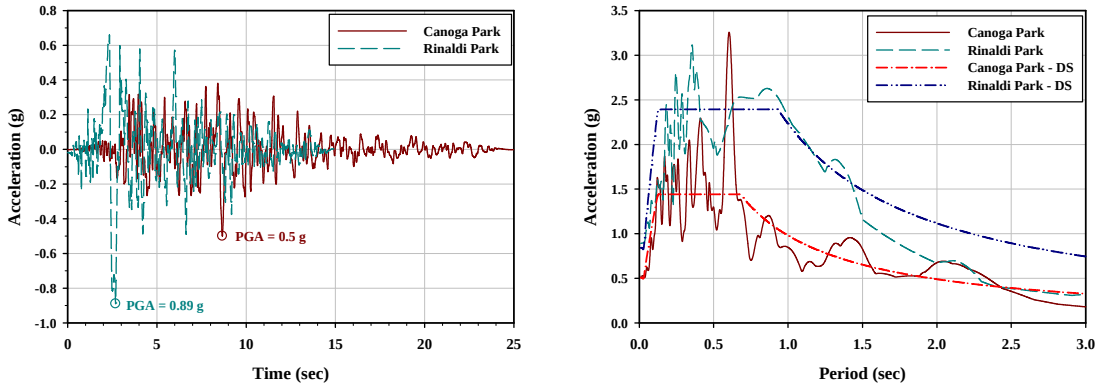

Figure 4.3. *(Left):* Accelerograms; *(Right):* Elastic actual and design spectra for Canoga and Rinaldi Park records from 1994 Northridge Earthquake

The maximum roof displacements observed for each variation of woodframe structure under Canoga and Rinaldi Park records are used as benchmark values for comparison against results from available versions of CSM and the developed advanced method. Table 4.3 shows experimental results.

Table 4.3. Seismic test results

Woodframe Structure	Max. Roof Displacement (in)	
	Canoga Park	Rinaldi Park
Phase 9	2.74	4.31
Phase 10	0.62	0.99

Finally, Figure 4.4 shows the bilinear representations of the capacity diagrams at experimental data points (note that the figure is in AD format). These representations are important in that they shed light on the degree of plastic deformation the structure has undergone. Under the Canoga Park record, the Phase 9 structure yields moderately while under the Rinaldi Park record it undergoes a considerable amount of yielding. The Phase 10 structure remains fairly elastic under both ground motions. Parameters defining each of the four bilinear representations are provided in Table 4.4.

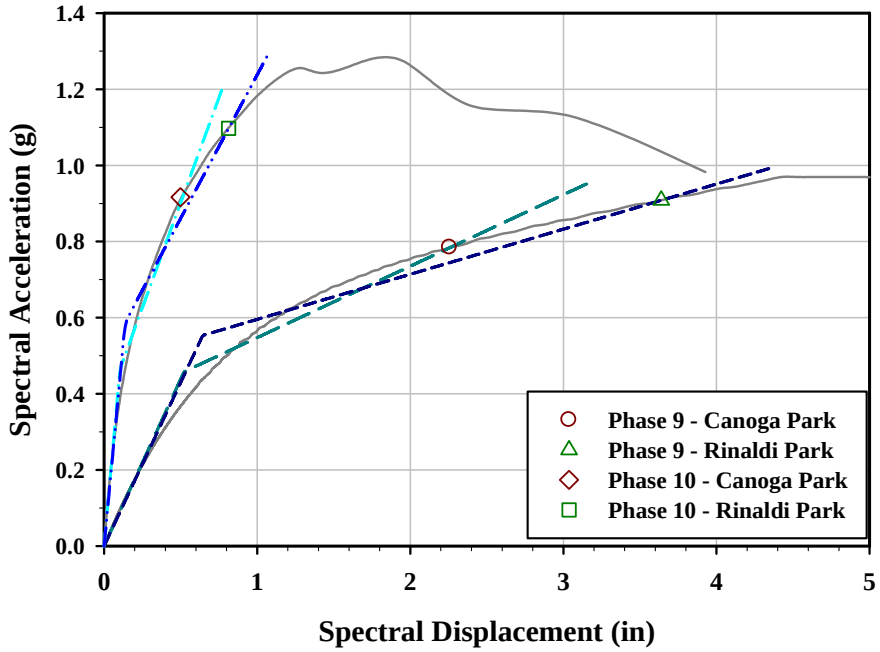

Figure 4.4. Bilinear representations at displacement demands obtained from experimental tests

Table 4.4. Parameters of the bilinear representation at structural performance points obtained from shake table tests

Structure & Ground Motion	Elastic Period, T_e (sec)	Yield Displacement, D_y (in)	Post- to Elastic Stiffness Ratio, α	Ductility Ratio, μ
Phase 9 - Canoga P.	0.342	0.522	0.214	4.23
Phase 9 – Rinaldi P.	0.345	0.645	0.138	5.61
Phase 10 – Canoga P.	0.151	0.104	0.247	4.97
Phase 10 – Rinaldi P.	0.155	0.139	0.178	5.96

4.1.3. Results from Available Capacity Spectrum Methods

This section presents results from available versions of CSM. The Displacement Coefficient Method is also used to evaluate the example woodframe structure (see Appendix B, section B.1.1.4 and section B.1.2.2 for an explanation). Further details can be found in FEMA 273 (Federal Emergency Management Agency, 1997) and ATC-40 (Applied Technology Council, 1996). All the results are tabulated in Table 4.5. Values shown in parenthesis are percentage differences from experimental results and the given

ductility values are calculated as the ratio of the displacement demand to yield displacement, which are obtained from the bilinear representations.

4.1.3.1. CSM in ATC-40

Although both variations of the woodframe structure can be classified as Type B according ATC-40, results from all three structural behavior types are presented to form a basis for further discussion. Results for Type B classification are shown in Figure 4.5 and the rest of the results are tabulated in Table 4.5. Because this figure is in AD format, the results are multiplied with the conversion factor Γ before comparing them with experimental results in Table 4.5.

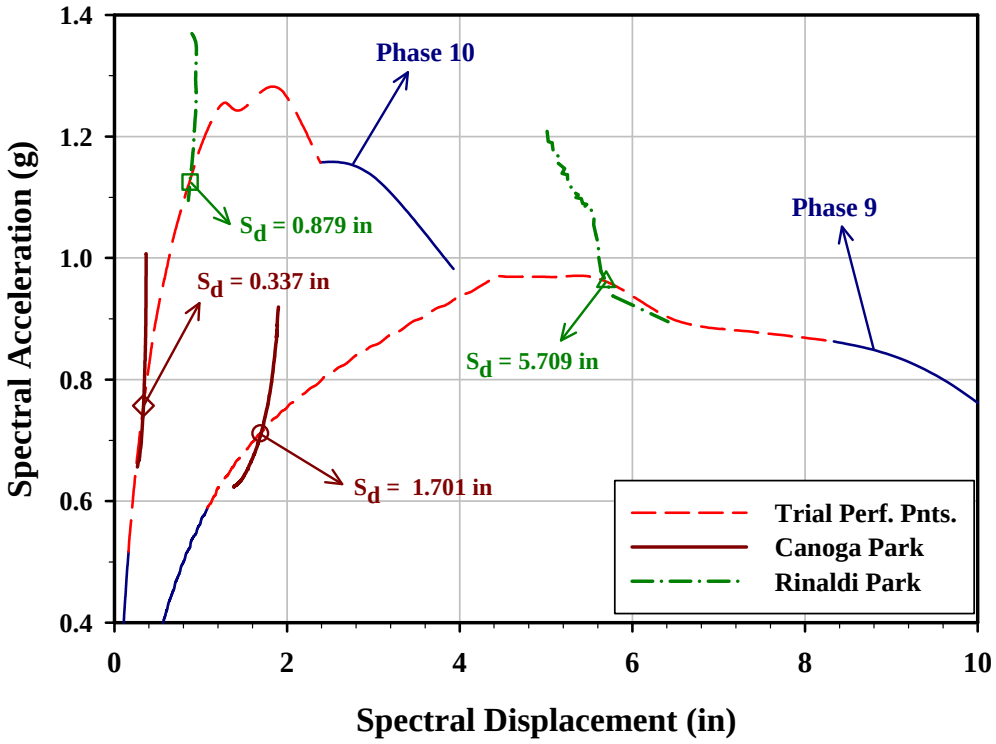

Figure 4.5. Results from CSM in ATC-40, Type B classification of the example woodframe structure

One observation is that CSM in ATC-40 underestimates the displacement demand for most of the cases considered. Several other studies support this observation (Chopra and Goel, 1999, 2000; Kim et al., 2005; Fragiacomo et al., 2006). Another observation is that this version fails to converge under Rinaldi Park record for the Phase 9 variation. It is

worth noting here that the combined procedure used in this study is capable of yielding the displacement demand for each bilinear representation. However the non-convergence is due to disagreement between the trial performance point chosen for developing that bilinear representation and the displacement demand thus obtained. The reason for the non-convergence will be further discussed in section 4.1.3.3.

CSM in ATC-40 seems to provide fairly good predictions of the displacement demand when compared with the experimental results, yet it will become evident as the results from CSM with inelastic demand spectra and the developed advanced method are presented that this success is due to significant underestimations involved with this version of CSM.

Another important conclusion is made concerning the selection of structural behavior types. More than 100% difference is observed between Types A and C. Since ATC-40 does not provide rigorous definitions for the structural behavior types, in cases when there is no experimental data to compare them against, selecting the correct type might significantly influence the reliability of the results.

4.1.3.2. CSM with Inelastic Design Spectra

As pointed out earlier, when inelastic design spectra are used in CSM, updating the bilinear representation of the capacity diagram depending on the trial performance point is not justifiable due to the incompatibility of the capacity and demand diagrams. For this reason, in order to apply the inelastic design spectra concept along with CSM to the woodframe structure, this study develops a single elasto-plastic (EP) representation for each of the capacity diagrams. Figure 4.6 lists them and their properties. This EP representation is not updated and used as it is during the entire procedure of performance point determination.

As examples, graphical results for Phase 9 structure under Canoga Park record and Phase 10 structure under Rinaldi Park record are shown in Figure 4.7. The other two cases are included in Appendix B, section B.1.2.1. In the test cases, this version of CSM considerably overestimates the displacement demand imposed on the woodframe

structure (up to 100% or more in some of the cases considered). This is mainly attributed to the lack of the possibility of updating the bilinear representation and using single elasto-plastic representations, confirming the importance of this feature of CSM. The results from nonlinear time history analysis of EP systems for the used ground motions are also provided in Table 4.5. Essentially, nonlinear time history analysis of EP systems yields the exact results for the considered SDOF systems. Therefore the deviation of the results from nonlinear time history analysis predicted by force reduction relationships can be used as a measure to assess the accuracy of this version of CSM. Furthermore, when compared against results from the nonlinear time history analysis of EP systems, ATC-40 gives the worst approximations for displacement demands in comparison to those achieved from force reduction relationships. The same issue is raised by Chopra and Goel (1999; 2000). Hence the results that were close to the experimental ones obtained using CSM in ATC-40 can be related to the underestimations and updating of the bilinear representation.

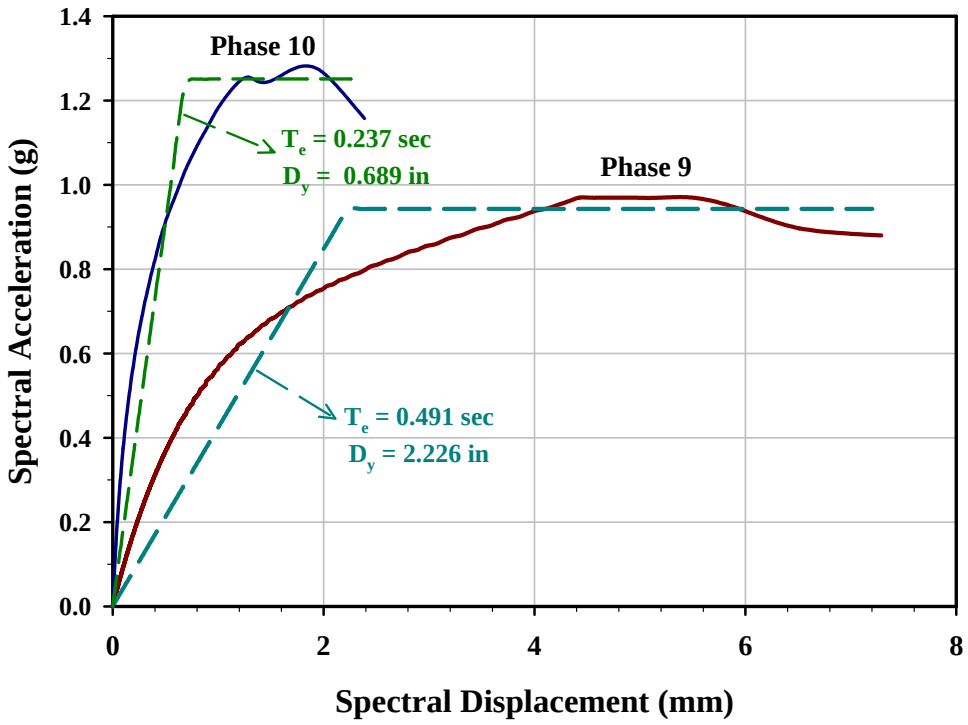

Figure 4.6. CSM with inelastic design spectra; elasto-plastic representations for capacity diagrams of Phase 9 and Phase 10 variations of the woodframe structure

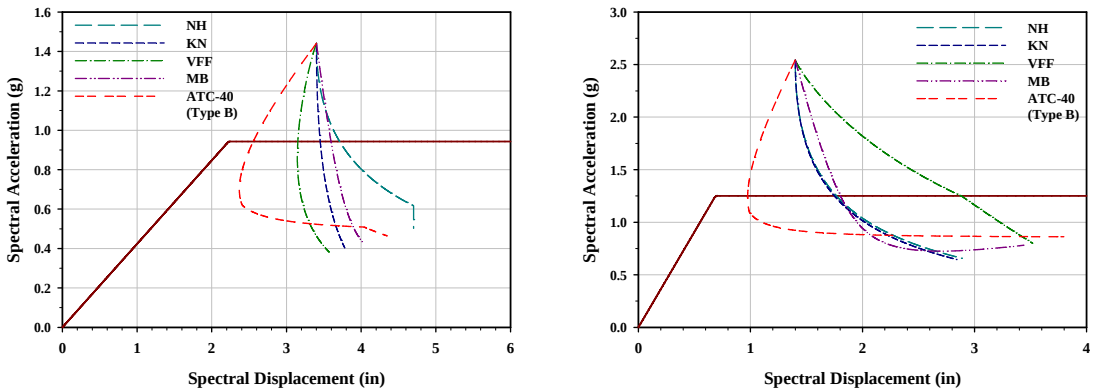

Figure 4.7. Results from CSM with inelastic design spectra for the cases *(Left):* Phase 9 under Canoga Park record; *(Right):* Phase 10 under Rinaldi Park record

In the light of the above discussions this version of the CSM is found to be inappropriate for assessment of structures with force-deformation relationships that cannot be idealized using bilinear representation(s) with small strain hardening values and under actual demand spectra (from specific records). Unfortunately this is the case for most of the structures that one may come across in practice.

4.1.3.3. CSM with Equivalent Elastic Spectra from Damping Models

It can be concluded from Table 4.5 that for moderate yielding, i.e. the Phase 9 test structure under Canoga Park record, this variant of the CSM provides the best estimates for the displacement demand among other versions of CSM considered up to this point. On the other hand, it underestimates structural response for Phase 10 test structure under the Canoga Park record and the method fails to converge for both variations of the woodframe structure under Rinaldi Park record. The former is due to the elastic behavior of the woodframe structure, as can be observed from Figure 4.2. At the experimental displacement value of $0.618\ in$ (or at a spectral displacement value of $0.618/1.194 = 0.518\ in$) Phase 10 test structure is still within the elastic range. And the latter is a result of the ductility damping relations. As the severity of ground motion increases, the level of nonlinearity associated with the structural response increases and more ductility is expected from the structure. But the ductility damping relationships converge to a constant value of damping as ductility increases (Figure 4.1). Thus, the versions of CSM utilizing equivalent linear systems suffer from the latter problem and yield poor

approximations for displacement response under severe ground motions such as the Rinaldi Park record. This observation is also reported by Shinozuka et al. (2000), Lin and Miranda (2004) and Kim et al. (2005).

Figure 4.8 shows graphical solution for converging cases of this version of CSM.

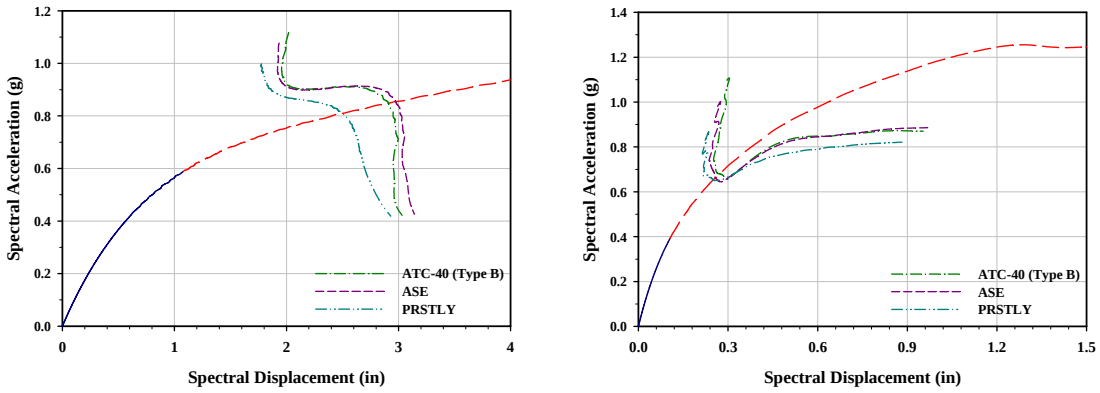

Figure 4.8. Graphical solution from CSM with equivalent elastic spectra from damping models *(Left):* Phase 9 under Canoga Park record; *(Right):* Phase 10 under Rinaldi Park record

If updating of the bilinear representation is abandoned for this version of CSM and a single EP force deformation relationship is used, as in the case of CSM with inelastic design spectra, a convergent solution for any ground motion can be obtained. Although not reported on here, this possibility was investigated and it was found that, like the results of CSM with inelastic design spectra, the method consistently and intolerably overestimated the displacement demand.

4.1.3.4. Displacement Coefficient Method (DCM)

DCM, an alternative for static inelastic assessment, is used to evaluate the woodframe structure (for calculations see Appendix B, section B.1.2.2). It also substantially overestimates the structural response for all the cases considered (Table 4.5). Lin et al. (2004a) reports the same problem.

4.1.4. An Advanced Capacity Spectrum Method

The advanced CSM proposed in this section aims to overcome the difficulties encountered in nonlinear static analysis and provide better estimates of structural

response. The underlying idea is to utilize inelastic dynamic analysis of SDOF systems represented by bilinear force deformation relationships. Even though it might seem contradictory with the original CSM, where only static procedures and equivalent linear systems are used, with today's computing technology, nonlinear time history analysis of SDOF systems is a matter of fractions of a second on an average personal computer. In addition, this method eliminates approximations and hence errors introduced into the solution with use of equivalent linear systems, design spectra (in lieu of actual spectra), and force reduction factors.

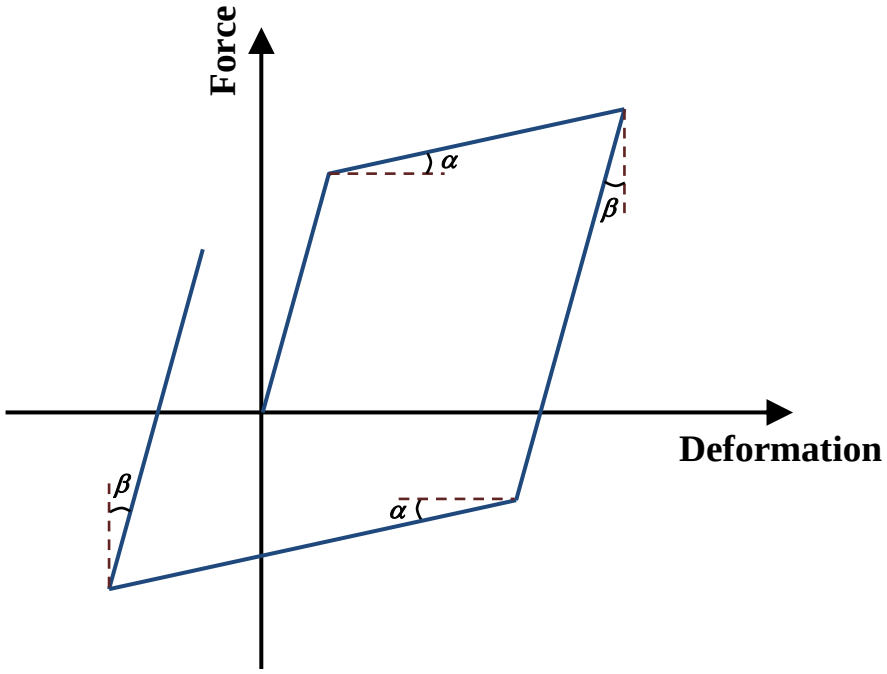

Figure 4.9. Force-deformation relationship for kinematic hardening behavior

The step by step procedure to determine the displacement demand with the advanced method is given below:

i. Choose a set of trial performance points along the capacity diagram.
ii. Like other versions of CSM (except CSM with inelastic design spectra), develop a bilinear representation for each of the trial performance points.

iii. Obtain peak responses of SDOF systems, whose force deformation relation are defined by the bilinear representations, using nonlinear time history analysis. Kinematic hardening behavior is assumed for hysteretic response (Figure 4.9).

iv. The intersection of the curve constructed by joining the points found in Step 3 with the capacity diagram gives the displacement demand imposed on the structure.

A somewhat similar approach was proposed for vulnerability analysis of RC structures by Rossetto and Elnashai (2005) using adaptive pushover analysis that is sensitive to specific input motion record. The current method is however distinct in its direct use of inelastic response history analysis of bilinear systems. Moreover, the assessment of an advanced inelastic response-based CMS approach for full-scale structures using experimental data has not been undertaken before.

4.1.5. Results for the Assessment of the Test Case Using the Advanced CSM

Figure 4.10 shows the graphical interpretation of solution using the proposed method.

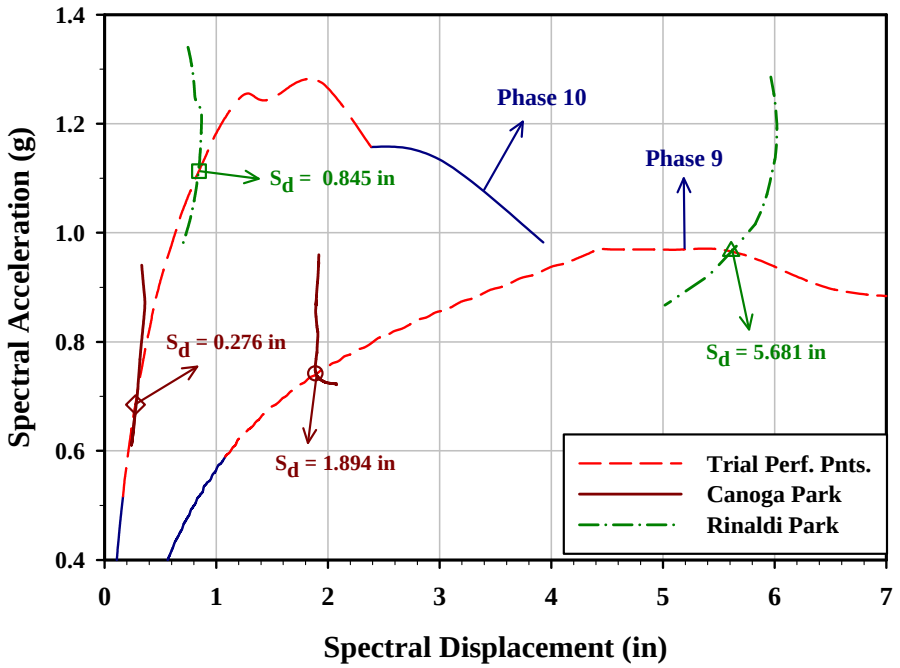

Figure 4.10. Results from the Advanced Capacity Spectrum Method

Using the advanced capacity spectrum method, a convergent solution is obtained for all the cases considered. It yields the least overall error for the assessment of both variations of the woodframe structure under both ground motions considered. As described before, the deviation from experimental result for analysis of Phase 10 test structure under Canoga Park record should be ascribed to the elastic behavior. This is justified by the analysis of an elastic system with 1.68% damping and secant stiffness – calculated at the point on the pushover curve having a displacement of 0.618 in. The elastic structural response of 0.614 in is obtained from this analysis under the Canoga Park record which is very close to the experimental result. Although the advanced method predicts the structural response with 57% error for the Phase 9 test structure under Rinaldi Park record, still it yields the most reliable results. For this case, CSM with inelastic design spectra unacceptably overestimates the experimental results (approximately 100% - average of the considered force reduction factors) and CSM with equivalent elastic spectra from damping models fails to converge. Recognizing the fact that the selection of structural behavior types considerably affects the results in ATC-40 (e.g. with Type A, structural response is predicted with 6.1% error, while Type C does not converge) the advanced CSM remains the most dependable option for inelastic assessment of the woodframe structure.

Yielding convergent solutions even under very severe ground motions, the proposed advanced method can be utilized for analyzing structures, whose pushover curves are available, under any desired ground motion. Thus, computationally expensive inelastic dynamic analysis of structural models with several degrees of freedom can be avoided.

The limitations to the proposed method are due to inherent assumptions of CSM; one is the deficiency in representing MDOF structures as SDOF systems. This might introduce a significant amount of error in cases where torsional effects due to asymmetry of mass and stiffness in plan and elevation are present and where the structure responds as a combination of the first and the higher modes. Gupta and Krawinkler (2000) provide a discussion of this issue.

One other drawback of the CSM is that it relies on the pushover curves which might not include all features of a building, such as soft stories and higher mode effects as pointed out above. In addition, pushover curves might be significantly different in push and pull directions and they might be in two orthogonal directions. Therefore, the more regular the structure is, the more accurate the results are.

When the above limitations are satisfied to the required extent (which is the case for the building groups considered in this study), the proposed version of CSM provides reliable and accurate results for estimating displacement demands imposed on structures behaving beyond their elastic limits.

4.1.6. Conclusions on the Methodology for Structural Assessment

An advanced procedure for CSM, incorporating nonlinear time history analysis, and other available versions of CSM are assessed using the experimental test data of a full-scale woodframe structure.

Updating of bilinear representations along the capacity diagram is adopted in order to increase the accuracy. In addition, for the determination of performance point, a procedure analogous to Procedure B in ATC-40 is utilized to guarantee convergence. It is found that the original CSM in ATC-40 yields significantly different results for different structural behavior types; a wrong classification might result in misleading and non-conservative demand estimates that are too inaccurate to be used for design or retrofit purposes. Updating of bilinear representation could not be used in the version of CSM with inelastic design spectra due to the incompatibility of the capacity and demand diagrams. This entailed a significant inaccuracy in the results and a substantial overestimation of the displacement demands. Moreover, the significance of updating bilinear representations for capacity diagrams that are not suitable for characterization with single elasto-plastic or for bilinear force-deformation relationships is demonstrated. CSM with equivalent elastic spectra from damping models predicted displacement demand with reasonable accuracy for the Canoga Park record. However, it failed to converge for the Rinaldi Park record (PGA equal to 0.89 g) and is inadequate for severe ground motions. The application of the proposed advanced method on the woodframe

structure, on the other hand, revealed that convergence under any record can be satisfied with reasonable accuracy.

The method proposed in this study can be further verified using analytical and experimental results of structures from different construction types such as RC, steel, etc. Furthermore the kinematic hardening behavior assumption with the bilinear force-deformation relationship can be relaxed, and more complicated models – such as a tri-linear model with stiffness and strength degradation – can be employed to obtain the peak responses. Still, the proposed advanced method can be used as an accurate and reliable method for the inelastic assessment of structures.

Table 4.5. Summary of results for nonlinear static analysis of the example woodframe structure[1]

Analysis Method	Results	Phase 9 Test Structure				Phase 10 Test Structure			
		Canoga Park		Rinaldi Park		Canoga Park		Rinaldi Park	
		Disp. (in)	Ductility	Disp. (in)	Ductility	Disp. (in)	Ductility	Disp. (in)	Ductility
Shake Table Tests[2]	**Exp.**	2.744 (0.0)	4.23	4.315 (0.0)	5.61	0.618 (0.0)	4.97	0.988 (0.0)	5.96
CSM in ATC-40	**Type A**	1.606 (-41.5)	3.59	4.050 (-6.1)	5.49	0.320 (-48.2)	3.96	0.757 (-23.4)	5.47
	Type B	2.031 (-26.0)	3.91	6.816 (57.9)	6.93	0.402 (-34.9)	4.21	1.049 (6.2)	6.28
	Type C	3.223 (17.4)	4.76	---	---	0.591 (-4.4)	4.71	2.010 (103.4)	8.24
CSM with Inelastic Design Spectra	**NH**	4.434 (61.6)	1.67	10.995 (154.8)	4.14	0.956 (54.7)	1.16	2.112 (113.7)	2.57
	KN	4.121 (50.2)	1.55	7.678 (77.9)	2.89	0.956 (54.7)	1.16	2.088 (111.3)	2.54
	VFF	3.763 (37.1)	1.42	8.989 (108.3)	3.38	1.013 (64.0)	1.23	3.437 (247.8)	4.18
	MB	4.294 (56.5)	1.62	8.139 (88.6)	3.06	1.005 (62.6)	1.22	2.153 (117.9)	2.62
	ATC-40 (Type B)	3.045 (10.9)	1.15	6.562 (52.1)	2.47	0.846 (36.9)	1.03	1.164 (17.8)	1.42
	EP-Exact	3.659 (33.3)	1.15	10.553 (144.6)	3.33	1.375 (122.5)	1.40	1.459 (47.7)	1.49
CSM with Equivalent Elastic Spectra from Damping Models	**ASE**	3.505 (27.7)	5.62	---	---	0.305 (-50.7)	4.50	---	---
	PRSTLY	2.853 (3.97)	4.86	---	---	0.297 (-52.0)	4.38	---	---
	ATC-40 (Type B)	3.436 (25.2)	5.51	---	---	0.308 (-50.2)	4.55	---	---
Displacement Coefficient Method	**DCM**	4.076 (48.5)	6.39	6.764 (56.8)	8.18	0.958 (55.0)	9.31	1.589 (36.5)	11.61
Advanced CSM	**Nonlinear Time History**	2.261 (-17.6)	4.60	6.783 (57.2)	8.45	0.329 (-46.8)	4.62	1.009 (2.1)	8.13

1 Results shown by "---" are not available due to non-convergence.

2 Ductility values are obtained from bilinear representations of capacity diagrams.

4.2. METHODOLOGY FOR FRAGILITY CURVE GENERATION

This second section of Chapter 4 investigates the methodology for fragility curve generation. Fragility curve generation is basically statistical analysis of the results obtained from the structural response assessment -– that is, of the variations of capacity of buildings under various ground motions using the methodology for structural response assessment described in the preceding section. This final component of the proposed framework for fragility analysis yields the desired relationships and completes the procedure.

The objective of this study is to provide parameters of the improved fragility relationships for populations of buildings in a format that can be directly utilized by future studies on earthquake loss assessment. In the field of earthquake engineering the most commonly accepted convention for the fragility relationships is to express the exceedance probabilities as a function of the hazard parameters, e.g. PGA, PGV, spectral displacement at certain period. This format herein is referred to as "conventional fragility relationships" and the methodology used for this purpose is described in section 4.2.1. The other, less established format considered here is from HAZUS (National Institute of Building Sciences, 2003), where exceedance probabilities are functions of structural response. The latter here is called "HAZUS compatible fragility relationships" and how to derive the fragility relationships in this format from the available analysis data is explained in section 4.2.2.

4.2.1. Conventional Fragility Relationships

As stated, conventional fragility relationships relate the ground motion parameters to the exceedance probabilities. In this study, the ground motion records are scaled based on PGA, and are therefore chosen as the representative parameter of the hazard. Nonetheless, any other convenient counterpart can be substituted with PGA via simply repeating the linear regression analysis described below.

The methodology by Wen et al. (2004b) is adopted for deriving fragility relationships in conventional format. Wen et al. proposes the use of Eq. (4.4).

$$P\left(LS_i/GMI\right)=1-\Phi\left(\frac{\lambda_{CL}^{i}-\lambda_{D/GMI}}{\sqrt{\beta_{D/GMI}{}^{2}+\beta_{CL}{}^{2}+\beta_{M}{}^{2}}}\right) \tag{4.4}$$

where $P(LS_i/GMI)$ is the probability of exceeding a particular limit state given the ground motion intensity (GMI), $\Phi[\cdot]$ is the standard normal cumulative distribution function, $\lambda_{CL}^{i}$is the natural logarithm of the limit state threshold value for the selected limit state, β_{CL} is the uncertainty associated with limit state threshold values (taken as 0.3 in this study), β_M is the uncertainty associated with the modeling of the structure (taken as 0.3 in this study), finally $\lambda_{D/GMI}$ and $\beta_{D/GMI}$ are given by Eq. (4.5) and Eq. (4.6), respectively.

$$\lambda_{D/GMI}=\ln a_1+a_2\ln\left(GMI\right) \tag{4.5}$$

$$\beta_{D/GMI}=\sqrt{\frac{\sum_{k=1}^{n}\left[\ln\left(GMI_k\right)-\lambda_{D/GMI}\left(GMI_k\right)\right]^2}{n-2}} \tag{4.6}$$

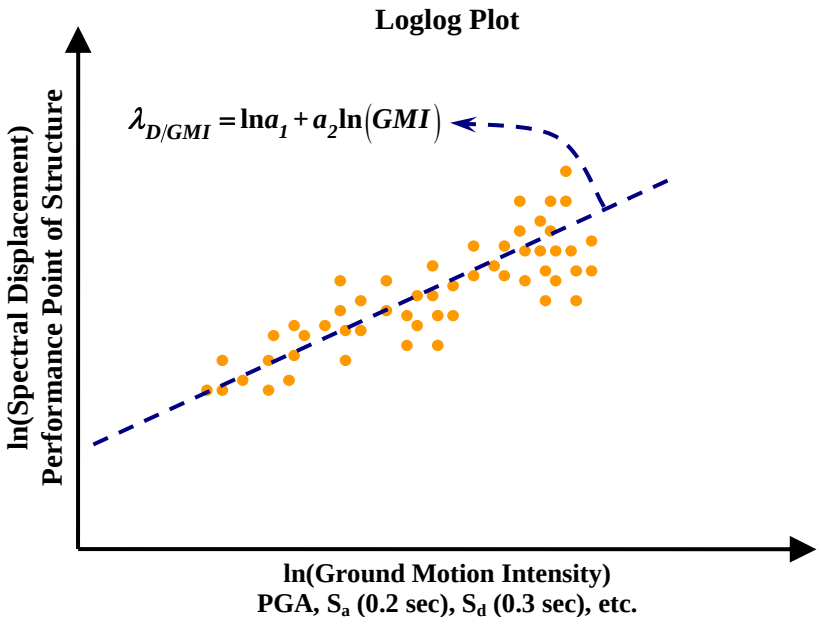

Figure 4.11. Linear regression analysis of structural response data

The constants a_1 and a_2 are calculated through a linear regression analysis, illustrated in Figure 4.11. $\beta_{D/GMI}$ is called as the square root of the standard error and n in the given expression is the number of data points.

It is important to note that in general three limit states are used for conventional fragility relationships (as opposed to four in HAZUS compatible fragility relationships) due to the fact that three limit states can be associated directly with the socio-economic consequences of continued operation, limited economic loss, and life loss prevention. As a consequence the three appropriate limit states out of the four can be simply selected, should it become necessary. The MAE Center impact assessment software platform MAEviz utilizes the above limit states that lead to 4 damage states; i.e. minor, moderate, severe, and collapse.

4.2.2. HAZUS Compatible Fragility Relationships

HAZUS is the most widely used loss assessment software in USA. As opposed to conventional fragility relationships where the horizontal axis is the GMI, HAZUS fragility relationships associate structural response with the exceedance probabilities. Therefore, in order to be able to make comparisons and provide the parameters of the improved relationships, HAZUS-compatible fragility relationships are derived alongside the conventional ones as used in other applications.

The HAZUS fragility relationships are given by the following equation:

$$P\left(Exceedence_i \mid S_d\right) = \Phi\left[\frac{1}{\left(\beta_{tot}\right)_i}\ln\left(\frac{S_d}{LS_i}\right)\right] \tag{4.7}$$

where, S_d is structural response (variable), LS_i is the threshold value for the i[th] limit state and $(\beta_{tot})_i$ is given by:

$$\left(\beta_{tot}\right)_i = \sqrt{\left[\left(CONV\left[\beta_C, \beta_D\right]\right)_i\right]^2 + \left[\left(\beta_{LS}\right)_i\right]^2} \tag{4.8}$$

in which $(\beta_{LS})_i$ is the uncertainty associated with the limit state threshold values (taken to be 0.4 in HAZUS), β_D is uncertainty in earthquake demand, while $(CONV[\beta_C, \beta_D])_i$ is the combined uncertainty of capacity and demand. This uncertainty is obtained as a result of the convolution process (Kircher et al., 1997a; Whitman et al., 1997), which is described in what follows. These two terms are assumed to be independent and the total uncertainty is calculated by the square-root-of-sum-of-squares (SRSS).

As stated, in HAZUS exceedance probabilities are expressed in terms of the structural response and the only required information to be able to draw the HAZUS compatible fragility curves is the combined uncertainty of capacity and demand which is shown by the term $(CONV[\beta_C, \beta_D])_i$ in Eq. (4.8) and obtained through the so called "convolution" process. Here this method is explained in a format which is suitable for application using the data of structural response results that would be obtained from analysis of the variations of the capacity under the variations of the demand.

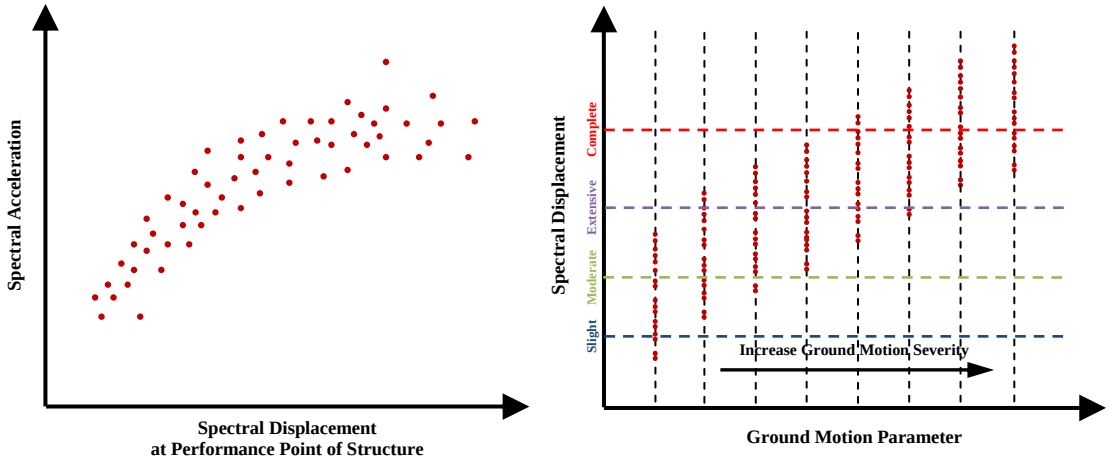

Figure 4.12. Derivation of HAZUS compatible fragility relationships *(Left):* Results in AD format; *(Right):* Results for spectral displacement plotted against GMI

If the structural responses from the above defined data are plotted, Figure 4.12 – (Left) is obtained. Each of the dots shown in this figure has a GMI value associated with it, Figure 4.12 – (Left) can be converted to Figure 4.12 – (Right) by plotting the spectral displacements against the GMI values. All the spectral displacement values referred to in here correspond to structural performance and should not be confused with spectral displacement at certain period used as a GMI parameter. Figure 4.13 shows a closer look

at the data in Figure 4.12 – (Right) at one of the scaling levels of the ground motion parameter, i.e. the one of the vertical lines.

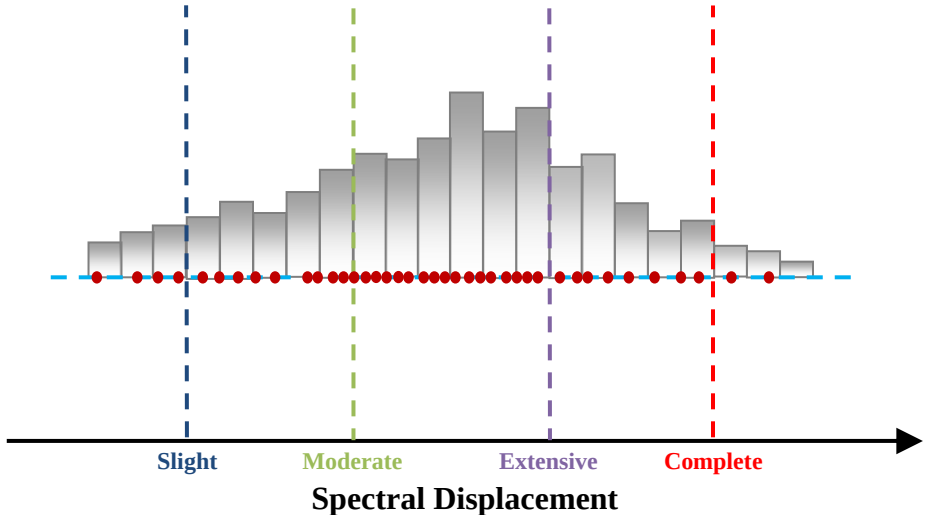

Figure 4.13. Probability distribution at each scaling of GMI

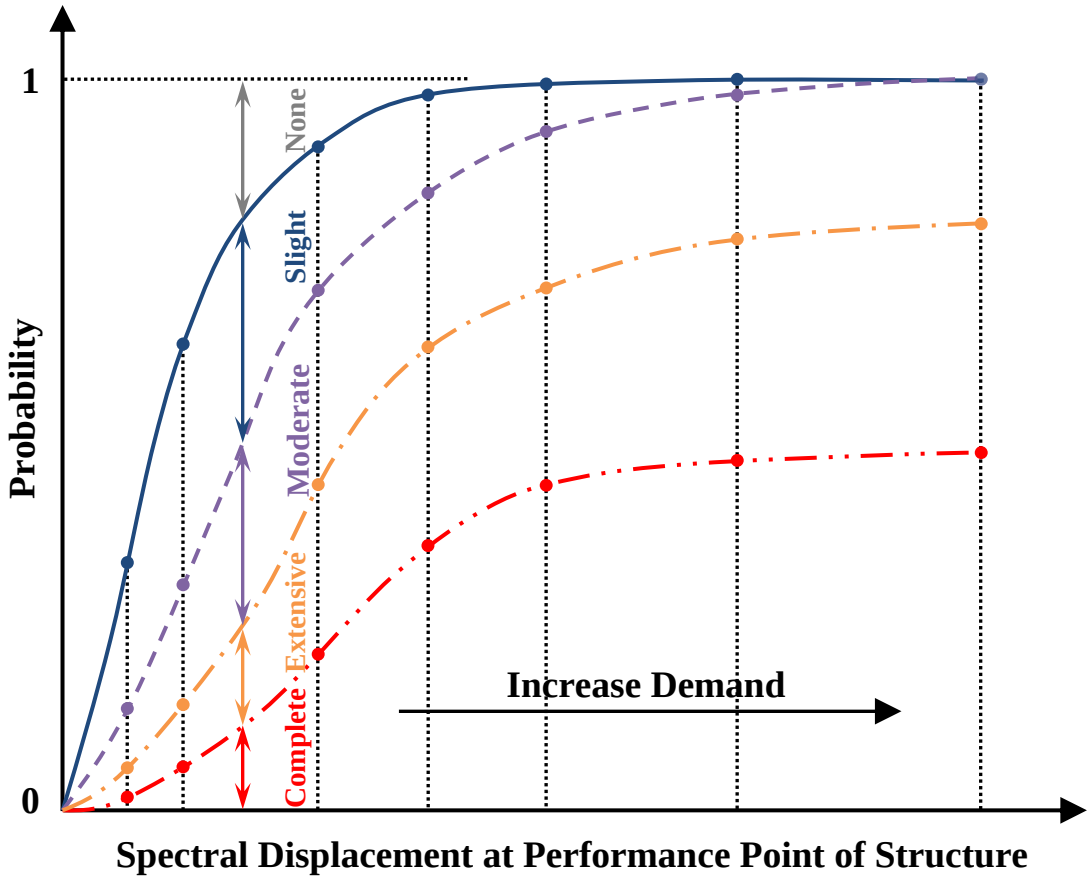

Figure 4.14. Fragility curves giving the combined uncertainty of capacity and demand

The probability of reaching or exceeding each damage state level is simply obtained by counting the number of data points with a spectral displacement value greater than or equal to a particular limit state threshold (this can be performed because limit states are defined in terms of spectral displacement) and dividing by the total number of data points. Thus four probability values are obtained at every scaling of the GMI. These four probability values are placed on a vertical line in the spectral displacement at structural performance vs. probability plot, e.g., Figure 4.14. The spectral displacement value of the vertical line (or the position on horizontal axis) is the mean of the spectral displacement values obtained from analyzing all the capacity diagrams of the building category under consideration under all the ground motions for the selected GMI scaling.

A lognormal distribution is fitted to the data points (shown in Figure 4.14) of each of the four damage states, thus giving the parameters of the distribution, i.e. the median and the standard deviation. Consequently, the obtained standard deviation value is equal to the combined uncertainty of capacity and demand, the term $(CONV[\beta_C, \beta_D])_i$ in Eq. (4.8). Finally the total uncertainty can be obtained using the same equation, and the fragility curves are drawn by utilizing Eq. (4.7).

CHAPTER 5
RESULTS AND DISCUSSION

This chapter integrates the four components of the proposed framework for fragility analysis – building capacity, earthquake demand, methodology for structural assessment, and methodology for fragility curve generation – to yield the results of the improved fragility relationships for populations of buildings.

The chapter is divided into two parts: the results related to woodframe structures and the results for the rest of the building types. On top of the results, discussions and comparisons are included.

5.1. FRAGILITY RELATIONSHIPS FOR WOODFRAME STRUCTURES

Woodframe buildings constitute the majority of the inventory for CEUS, and thus the proposed improvement for the capacity component of fragility analysis is applied to these structures (see section 3.1.3). In other words, the main difference between the fragility relationships for woodframe structures and those for the rest of the building groups is the existence of the database for the former while the latter uses the available capacity diagrams from HAZUS.

Since fragility relationships for woodframe building types, are also derived using associated capacity diagrams from HAZUS, fragility formulations from three different sources exist for these structures: the available curves in HAZUS, the results from this study using HAZUS capacity diagrams, and the results from this study using capacity diagrams from the assembled database. The latter two differ only in terms of building capacity while the HAZUS curves are from an independent source.

5.1.1. Conventional Fragility Relationships

A sample of results are shown in Figure 5.1 depicting conventional fragility curves for a W1 pre-code building category for different damage state levels. Since there are four curves to be compared for each damage state level, each damage state is plotted in a different figure in order to render the comparison as clear as possible. It is important to

note two points here. First, lines shown as lowland and upland in the below figures are obtained by using the capacity diagrams in the database while, as the name indicates, HAZUS Lowland and HAZUS Upland lines are obtained using available capacity diagrams from HAZUS. Second, although all four damage state levels are shown here, as stated in section 4.2.1, some loss assessment software, such as MAEviz, utilizes only three, in which case the appropriate three out of the four can simply be chosen.

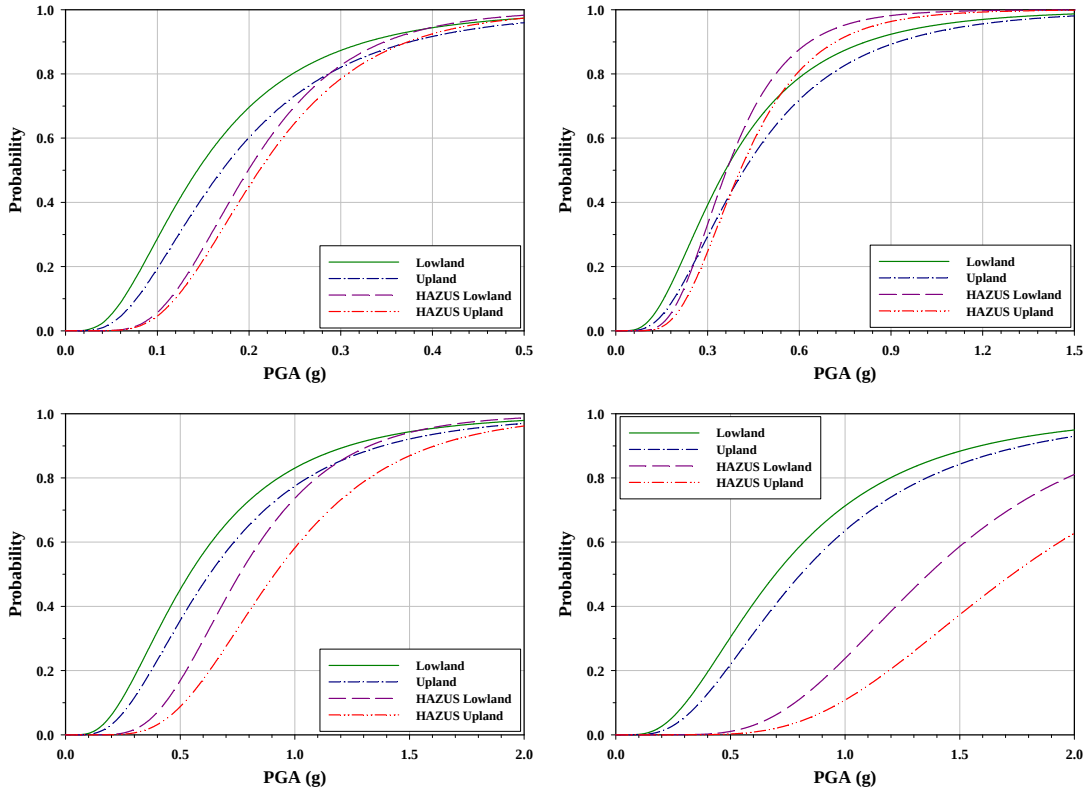

Figure 5.1. Fragility relationships in conventional format for W1 pre-code building category *(Top-Left):* Slight damage limit state; *(Top-Right):* Moderate damage limit state; *(Bottom-Left):* Extensive damage limit state; *(Bottom-Right):* Complete damage limit state

As observed from the above figures, if the capacity diagrams from HAZUS are used, lower damage probabilities are obtained for almost the entire range of the PGA values. This is especially true of the Extensive and Slight damage levels. However, for a moderate damage state level, for low PGA values lower damage probabilities and for high PGA values higher damage probabilities are obtained.

The underestimation of damage probabilities by HAZUS for all limit states can be extended to pre-, low, and moderate code seismic design levels of the W2 building type. On the contrary, for the low, moderate, and high codes of W1 and high code of W2 building types, a higher probability of damage is predicted when capacity diagrams from HAZUS are used. As examples, the fragility relationships for W1 moderate code and W2 high code building categories are shown in Figure 5.2 and Figure 5.3 respectively. It is also important to note that the damage probabilities are significantly low for high code structures of both W1 and W2 building types. Similar results are obtained for high code design levels of woodframe structures in other studies (Ellingwood et al., 2007).

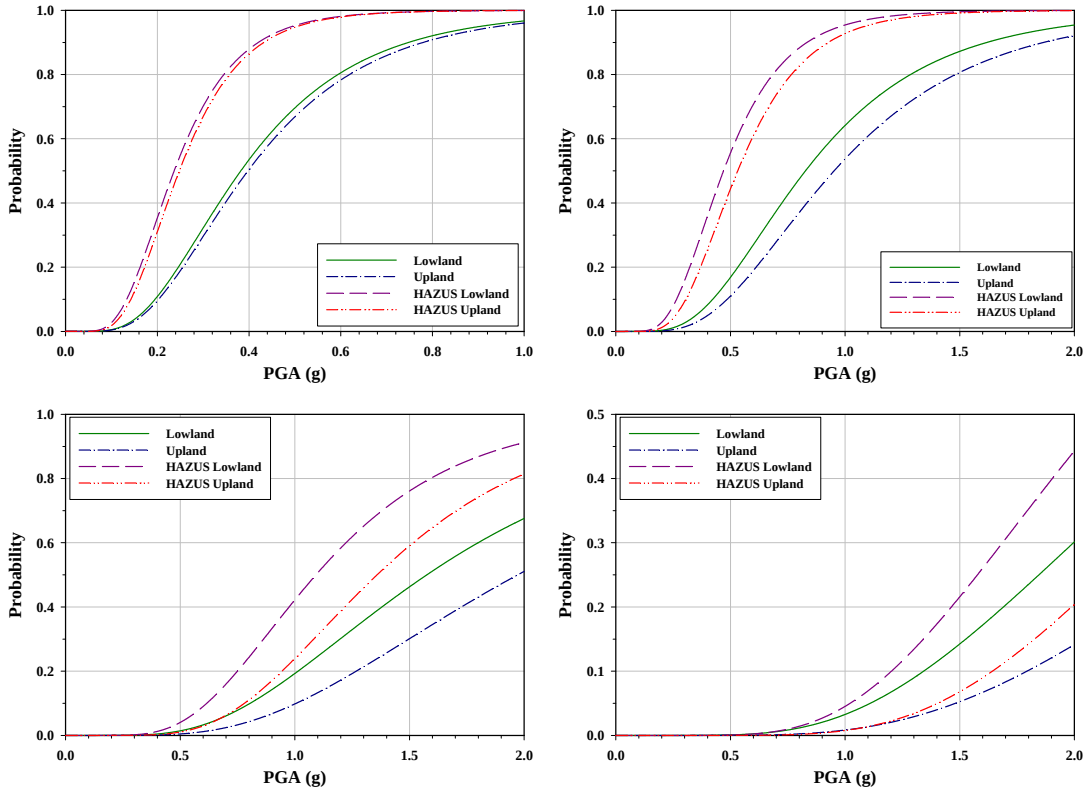

Figure 5.2. Fragility relationships in conventional format for W1 moderate code building category *(Top-Left):* Slight damage limit state; *(Top-Right):* Moderate damage limit state; *(Bottom-Left):* Extensive damage limit state; *(Bottom-Right):* Complete damage limit state

The results presented here show that the effect of capacity representation on the fragility relationships is significant. The results can be considerably different depending on which capacity representation a study uses, and the limit state definitions as well as the capacity diagrams employed have a substantial impact on the consequent fragility relationships.

Here this study proposes that those results obtained by using capacity diagrams from the woodframe database assembled in section 3.1.3 and the limit states determined by using these capacity diagrams are more reliable for two reasons. First because the capacity diagrams in the database are based on advanced simulation, which is capable of capturing real behavior, and second, the relevant limit states are determined using well accepted engineering criteria as opposed to the expert opinion that HAZUS capacity diagrams and limit states rely on.

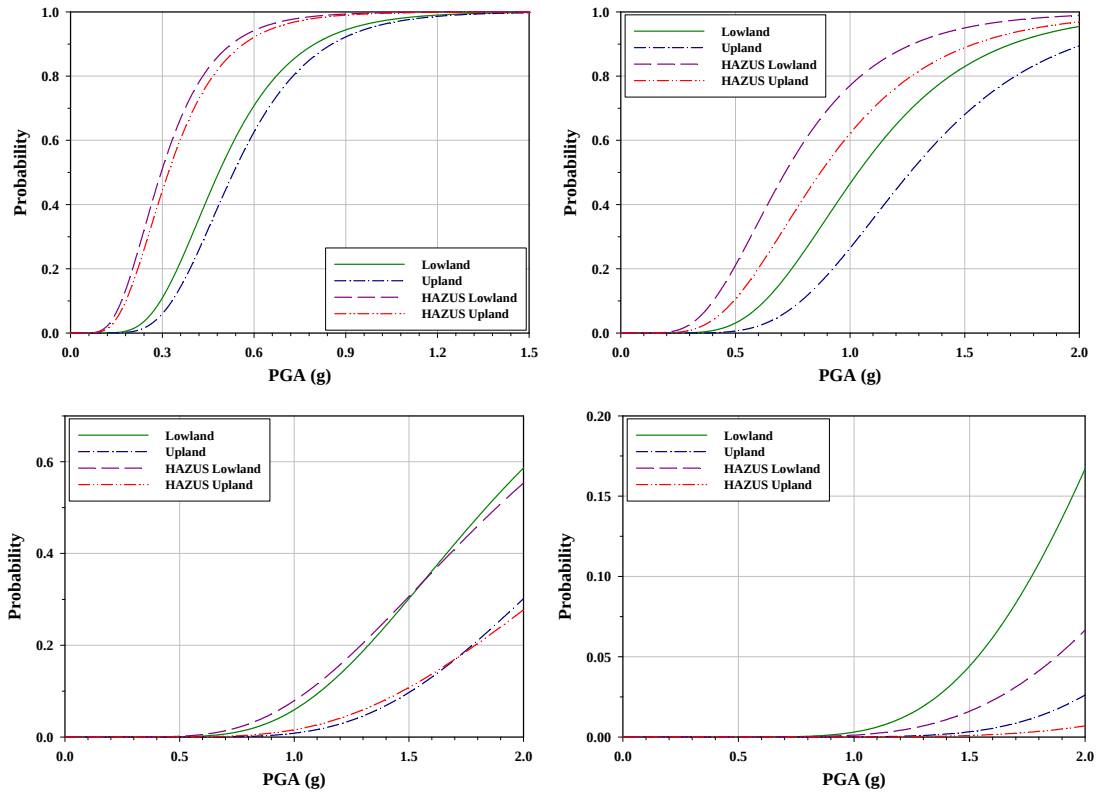

Figure 5.3. Fragility relationships in conventional format for W2 high code building category *(Top-Left):* Slight damage limit state; *(Top-Right):* Moderate damage limit state; *(Bottom-Left):* Extensive damage limit state; *(Bottom-Right):* Complete damage limit state

Up to this point, the effect of using different sources for capacity diagrams has been investigated. Below, the effect of soil profile is studied. Serving this purpose, fragility relationships obtained using the capacity diagrams from the database (HAZUS) for lowlands and uplands soil profiles are plotted for all damage state levels of W1 high code structure (as an example) in Figure 5.4 and Figure 5.5.

It is observed that the source of capacity diagrams and the soil profiles are not correlated and, as expected, lowlands soil profile yields higher damage probabilities than uplands soil profile for all damage state levels and the entire range of PGA values. This is because lowlands soil profile is more demanding when compared to uplands soil profile for the considered woodframe building types.

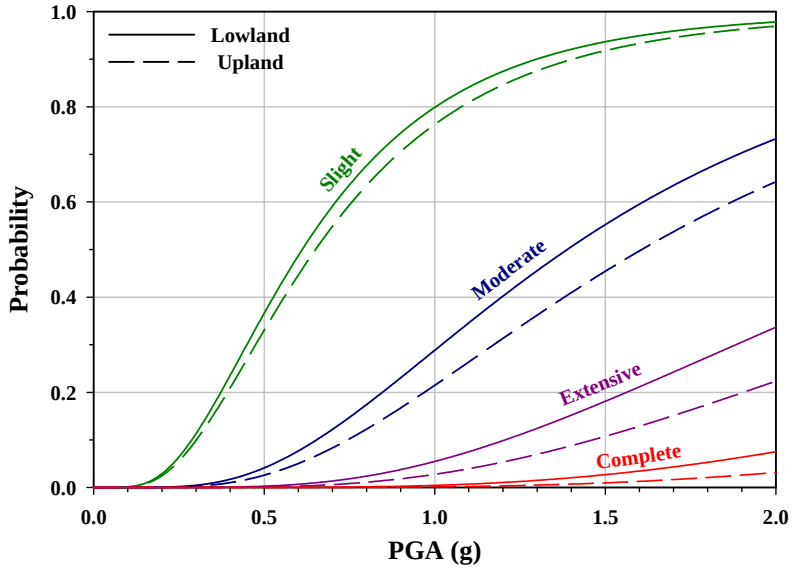

Figure 5.4. The effect of soil profile on the fragility relationships – W1 high code building category; capacity diagrams from the database

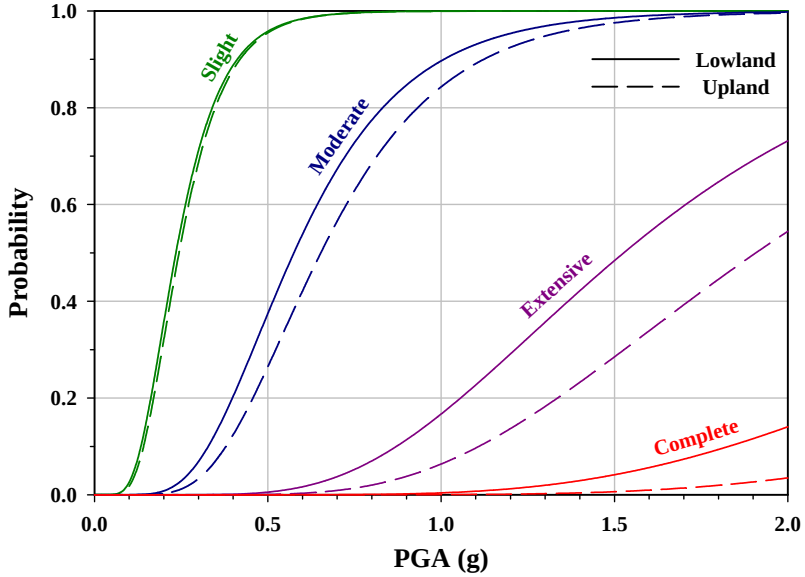

Figure 5.5. The effect of soil profile on the fragility relationships – W1 high code building category; capacity diagrams from HAZUS

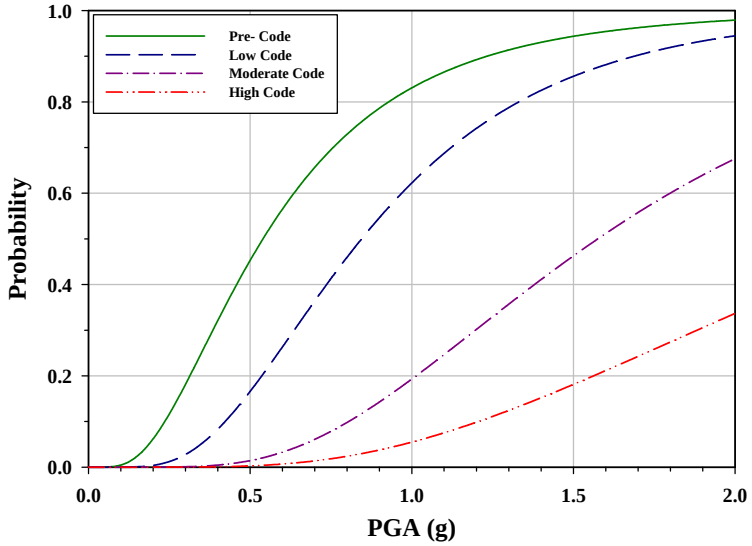

Figure 5.6. Comparison fragility curves for different design levels of W1 building type for lowlands soil profile and moderate damage state level; capacity diagrams from the database

Finally Figure 5.6 is included to support the argument made towards the end of section 3.1.4.1 regarding the limit state threshold values obtained from the mean capacity diagrams in the database. As observed from the above figure, while the threshold values decrease going from high code to pre- and low code, the probability of reaching and exceeding moderate damage state level also decrease.

Table 5.1. Parameters of conventional fragility relationships for woodframe building types W1 and W2 – obtained using capacity diagrams from the database

	Lowland			Upland		
Building Category	$\boldsymbol{lna_1}$	$\boldsymbol{a_2}$	$\boldsymbol{\beta_{tot}}$	$\boldsymbol{lna_1}$	$\boldsymbol{a_2}$	$\boldsymbol{\beta_{tot}}$
W1 – Pre-Code	2.246	1.620	1.044	2.012	1.644	1.013
W1 – Low Code	1.435	1.642	0.887	1.081	1.481	0.813
W1 – Moderate Code	0.098	1.606	0.841	-0.137	1.421	0.746
W1 – High Code	-0.534	1.418	0.833	-0.679	1.286	0.772
W2 – Pre-Code	3.090	1.236	0.643	3.030	1.394	0.615
W2 – Low Code	2.573	1.412	0.657	2.290	1.477	0.562
W2 – Moderate Code	2.110	1.395	0.884	1.756	1.332	0.792
W2 – High Code	0.703	1.753	0.683	0.404	1.543	0.569

Conventional fragility curves may be drawn using the limit states from Table 3.4, the fragility parameters provided in Table 5.1, and utilizing Eq. (4.4). The parameters for

conventional fragility relationships of woodframe structures obtained using HAZUS capacity diagrams are tabulated in Appendix C, section C.2.1.

5.1.2. HAZUS Compatible Fragility Relationships

In the case of HAZUS compatible fragility relationships, in addition to those considered in the previous section – i.e. relationships based on capacity diagrams from the database and relationships based on capacity diagrams from HAZUS – one more source of information exists: available fragility relationships in HAZUS. As examples, fragility relationships for W1 low code building and W1 high code building are provided in Figure 5.7 and Figure 5.8 respectively.

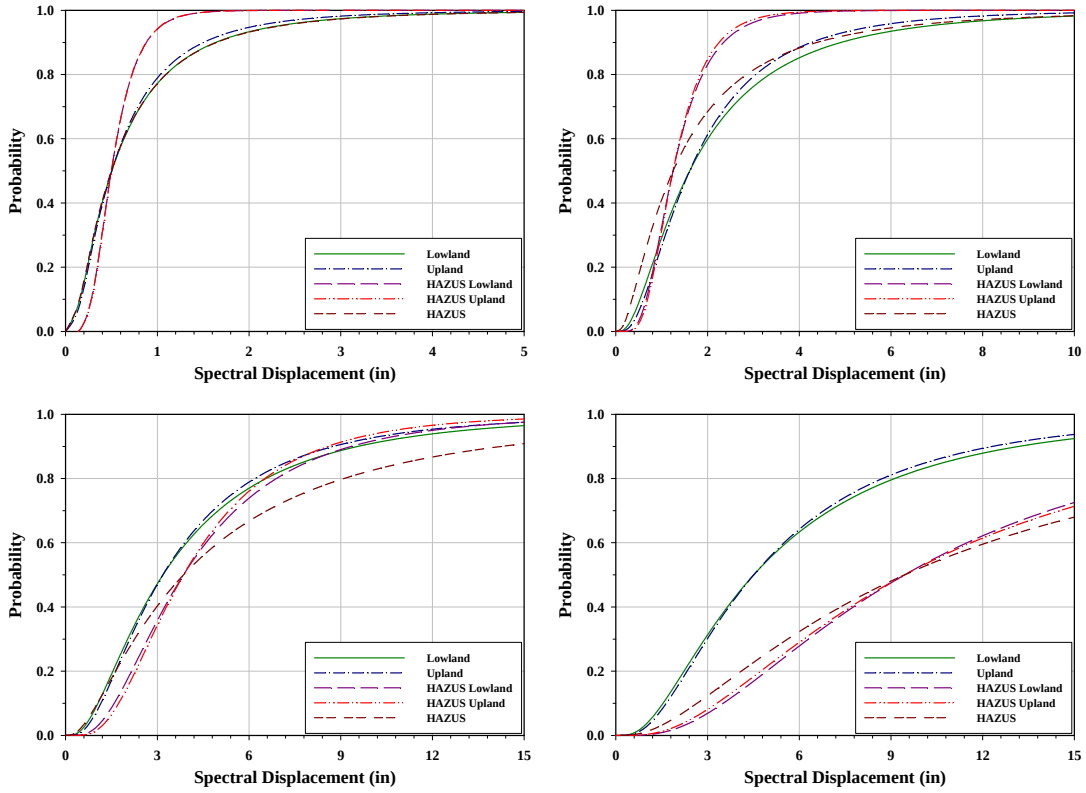

Figure 5.7. HAZUS compatible fragility relationships for W1 low code building category *(Top-Left):* Slight damage limit state; *(Top-Right):* Moderate damage limit state; *(Bottom-Left):* Extensive damage limit state; *(Bottom-Right):* Complete damage limit state

Before going into comparison of fragility relationships, it is worth noting that, having their origins in Eq. (4.7) the HAZUS compatible fragility curves are anchored to the limit state threshold values. In other words, the spectral displacement value corresponding to

50% probability is equal to the damage state threshold value of the considered limit state. This fact can also be observed from the figures provided in this section. The curves having identical limit state threshold values differ only in their standard deviation values which determine the flatness of the curves. As the standard deviation values increase (meaning higher uncertainty) the curves become flatter.

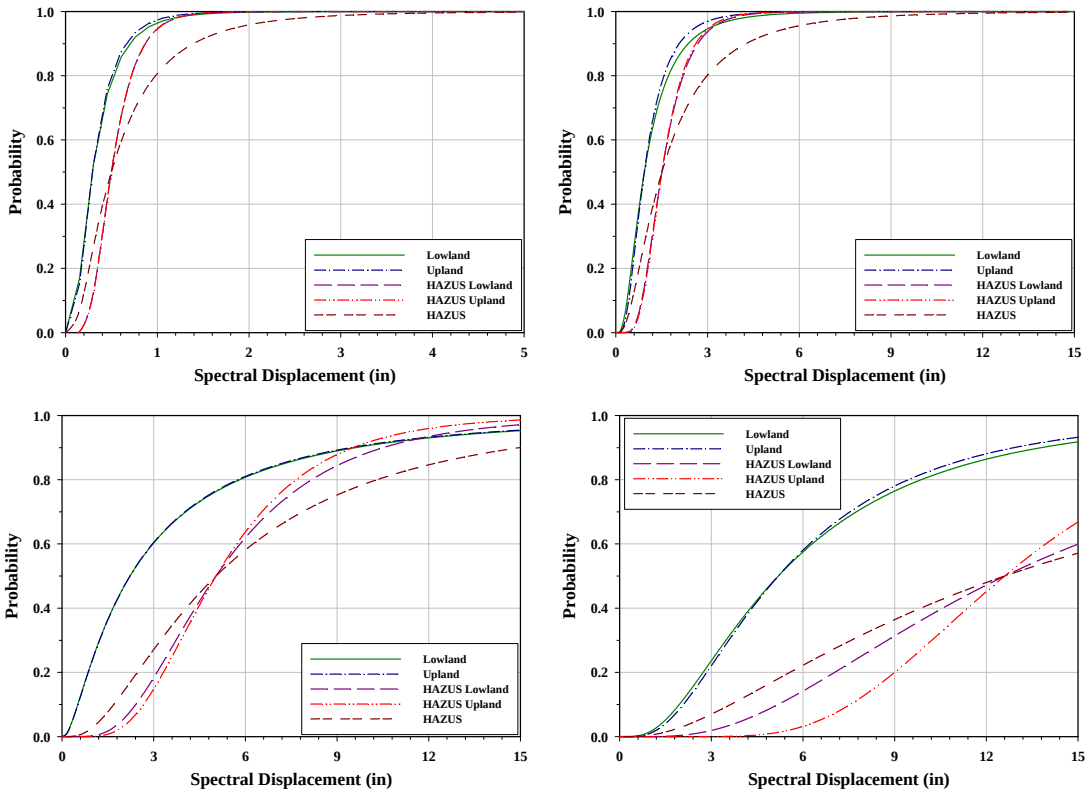

Figure 5.8. HAZUS compatible fragility relationships for W1 high code building category *(Top-Left):* Slight damage limit state; *(Top-Right):* Moderate damage limit state; *(Bottom-Left):* Extensive damage limit state; *(Bottom-Right):* Complete damage limit state

In Figure 5.7 and Figure 5.8 the legends are the same as those in Figure 5.1, Figure 5.2, and Figure 5.3 and as an addition, fragility curves from HAZUS Manual are labeled as HAZUS. An investigation of the these figures indicate that the fragility relationships derived here and those from HAZUS can be comparable in certain cases (Figure 5.7) while they can be significantly different in others (Figure 5.8). Hence it is not possible to make general conclusions. Still, a common observed trend is that HAZUS underestimates damage more as the strength of the structure increases, i.e. moving from pre-code to high code. This is attributed to high limit state threshold values defined in HAZUS.

Table 5.2. Parameters of HAZUS compatible fragility relationships for woodframe building types W1 and W2 – obtained using capacity diagrams from the database

Building Category	Lowland				Upland			
	β_{tot}^{1}	β_{tot}^{2}	β_{tot}^{3}	β_{tot}^{4}	β_{tot}^{1}	β_{tot}^{2}	β_{tot}^{3}	β_{tot}^{4}
W1 – Pre-Code	1.371	1.186	1.117	1.062	1.277	1.174	1.124	1.156
W1 – Low Code	0.919	0.870	0.858	0.837	0.853	0.759	0.790	0.784
W1 – Moderate Code	0.626	0.826	0.848	0.848	0.572	0.697	0.843	0.992
W1 – High Code	0.680	0.728	1.141	0.763	0.633	0.623	1.128	0.711
W2 – Pre-Code	0.822	0.674	0.649	0.660	0.724	0.584	0.594	0.600
W2 – Low Code	0.791	0.596	0.709	0.687	0.654	0.499	0.511	0.517
W2 – Moderate Code	1.141	0.831	0.772	0.809	1.020	0.759	0.668	0.612
W2 – High Code	0.529	0.605	0.816	0.670	0.440	0.521	0.633	0.533

The parameters of the HAZUS compatible fragility relationships for W1 and W2 building types, obtained using the capacity diagrams from the database, are given in Table 5.2. HAZUS compatible fragility curves can be drawn using the limit states from Table 3.4 and utilizing Eq. (4.7). The parameters for HAZUS compatible fragility relationships of woodframe structures obtained using HAZUS capacity diagrams are tabulated in Appendix C, section C.2.2.

5.1.3. Comparisons with Other Studies

In literature, there are a limited number of studies that provide fragility relationships for woodframe buildings. In section 5.1.3, the fragility relationships obtained in this study are compared with the ones developed by Ellingwood et al. (2007) and Porter et al. (2002). It is important to note that the latter are developed for specific buildings rather than building groups and the fragility relationships proposed in this study cover but are not limited to these particular woodframe structures. Therefore, the basis for comparison is not to verify either of the studies but to illustrate the similarities and differences.

5.1.3.1. Fragility Relationships from Ellingwood et al. (2007)

Ellingwood et al. developed fragility relationships for a single storey woodframe house using the same ground motion records employed here. It is assumed that the overall behavior of the structure is governed by the shear wall having the greatest lateral displacement in a static pushover analysis. Ellingwood et al. (2007) modeled the latter

using the previously mentioned software SAWS (section 3.1.3.1). Incremental dynamic analysis (IDS) is used for evaluation of the shear wall and the fragility curves are developed using a similar method to the one described in section 4.2.1.

The GMI parameter that Ellingwood et al. employ is the spectral acceleration value at the fundamental period of the structure, i.e. 0.24 sec. Therefore, in order to be able to make comparisons, the fragility relationships developed here are converted so that they have the same measure of GMI. Since there is more than one structural configuration in each of the building categories considered in this study, the fundamental period is taken as the average of the of all buildings belonging to same category.

Ellingwood et al. (2007) provide the fragility relationships for two different wall configurations: those with and those without seismic hold-downs (or wall anchorage). The one storey woodframe structure falls into the W1 building type, and the two configurations, with and without hold-downs, can be considered as moderate and high code respectively.

Table 5.3. Differences between the present study's proposed fragility relationships and those by Ellingwood et al. (2007)

	Approach	
	Present Study	**Ellingwood et al. (2007)**
Structural Configuration	Building group W1 and W2	One storey woodframe building
Capacity of Building	Pushover curves	Finite element modeling
Limit States	Defined on capacity diagrams	Taken as 1%, 2% and 3% interstorey drifts for IO, LS and CP limit states
Structural Assessment	Advanced CSM technique	IDA
Modeling Uncertainty	Taken as 0.3	Taken as 0.15

Figure 5.9 and Figure 5.10 show the comparisons of the fragility relationships for moderate and high code design levels respectively. As can be observed from these plots, the immediate occupancy and life safety performance levels from Ellingwood et al. fall between slight and moderate, and between extensive and complete limit states

respectively. The collapse performance level is not provided by Ellingwood et al. due to having negligibly small probabilities for the entire range of spectral acceleration values.

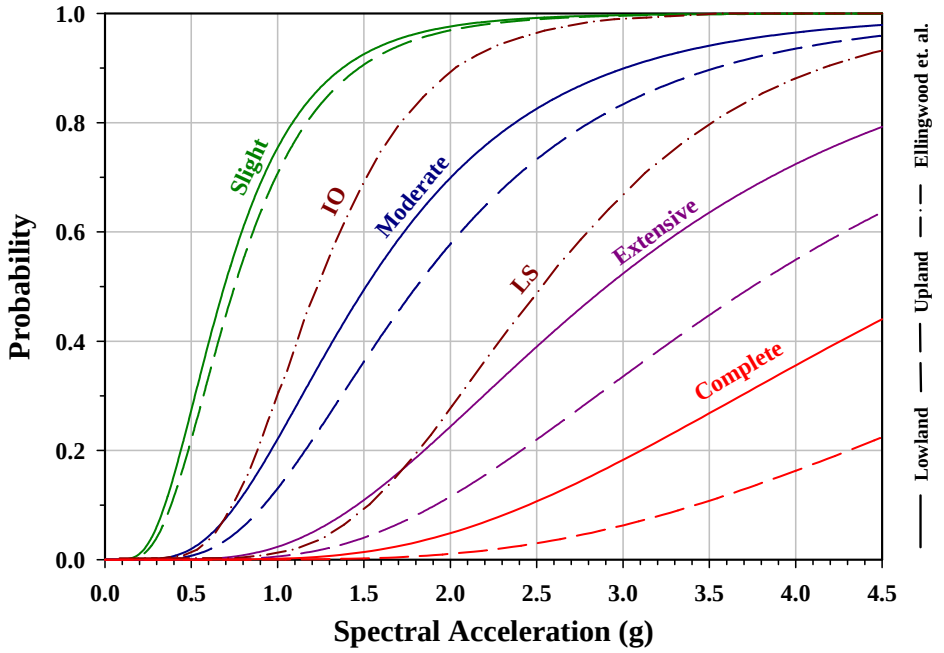

Figure 5.9. Comparison of fragility relationships with those from Ellingwood et al. (2007) – W1 moderate code structure (IO: Immediate Occupancy, LS: Life Safety)

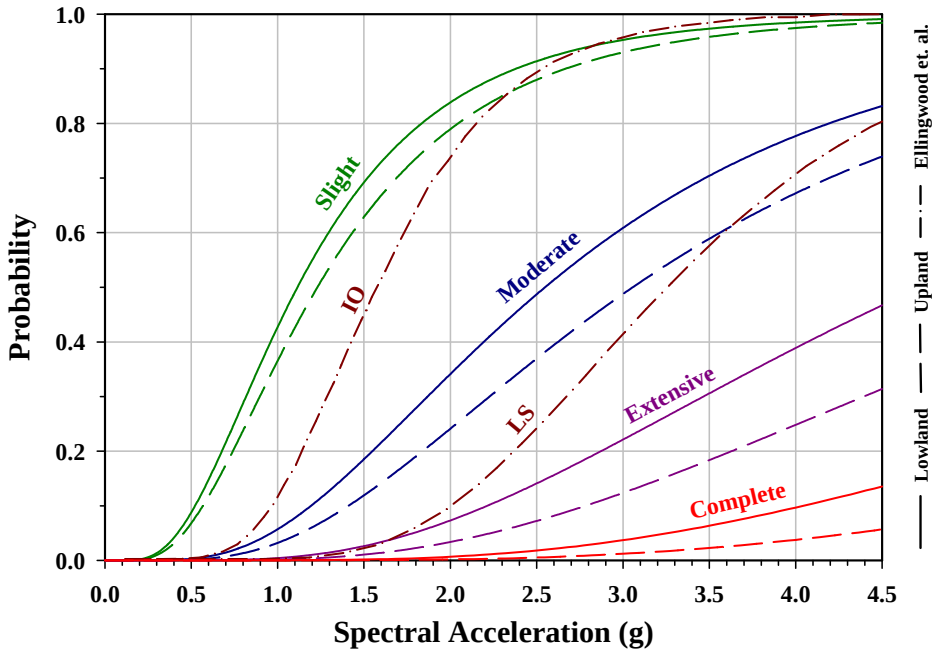

Figure 5.10. Comparison of fragility relationships with those from Ellingwood et al. (2007) – W1 high code structure (IO: Immediate Occupancy, LS: Life Safety)

It can be concluded that the two fragility relationships are in agreement and the discrepancies can be attributed to the differences between the two methodologies described in Table 5.3.

5.1.3.2. Fragility Relationships from Porter et al. (2002)

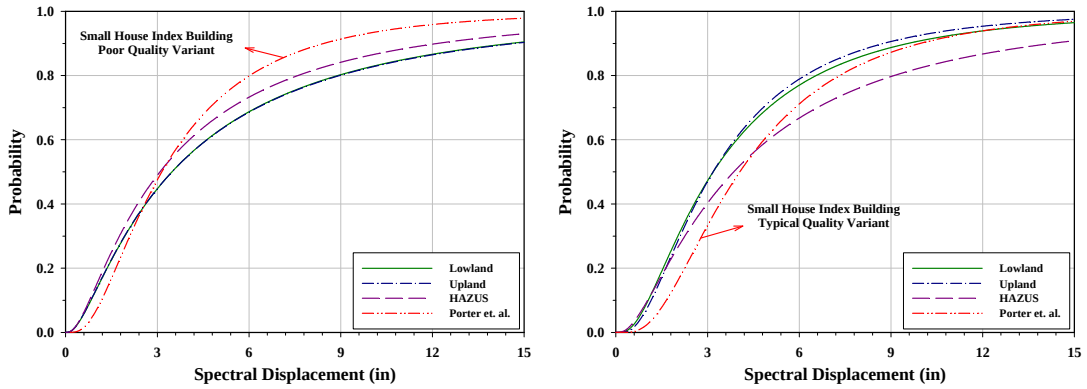

Figure 5.11. Comparison of fragility relationships with those from Porter et al. (2002), W1 building type *(Left):* pre-code seismic design level, extensive damage limit state; *(Right):* low code seismic design level, extensive damage limit state

As a part of CUREE Caltech Woodframe Project, Porter et al. (2002) developed fragility relationships for the index woodframe buildings described in section 3.1.3.1. As detailed in Appendix A, section A.1.2.1, the computer modeling of these structures uses the software RUAUMOKO (Carr, 1998) and the earthquake records from Phase 2 of the SAC Steel Project (Somerville et al., 1997) for ground motion simulation. The latter are scaled based on spectral acceleration at the fundamental period of the structure from 0.1 g to 2.0 g with 0.1 g increments; 20 time histories are chosen randomly from the SAC ground motion set and each of the index buildings are analyzed for every level of scaling to obtain the peak transient interstorey drift ratios. The uncertainties considered in capacity are due to mass and damping only. The limit states are based on damage factors (replacement cost/total cost of building) of 0-5%, 5-20%, 20-50% and 50-100% for slight, moderate, extensive and complete damage states.

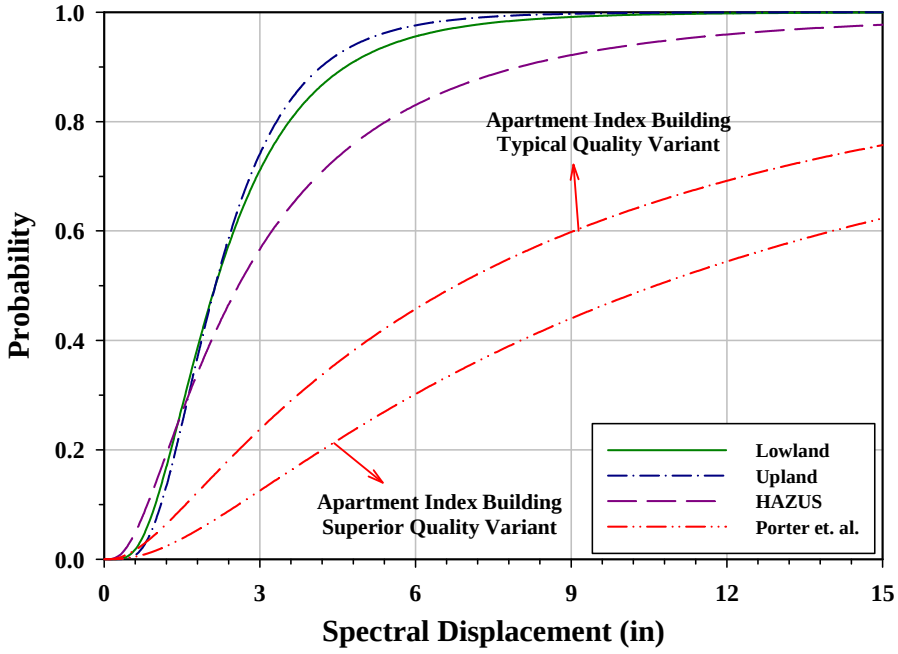

Figure 5.12. Comparison of fragility relationships with those from Porter et al. (2002), W2 building type high code seismic design level, moderate damage limit state

Table 5.4. Differences between proposed the fragility relationships and those by Porter et al. (2002)

	Approach	
	Present Study	**Porter et al. (2002)**
Structural Configuration	Building group W1 and W2	Specific buildings, i.e. index woodframe structures
Capacity of Building	Pushover curves	Finite element modeling
Limit States	Defined on capacity diagrams	Defined in terms of damage factors
Structural Assessment	Advanced CSM technique	Nonlinear time history
Ground Motion Selection and Scaling	Synthetically generated time histories for CEUS (Fernandez, 2007)	SAC Phase 2 time histories (Somerville et al., 1997)

Porter et al. (2002) provided fragility relationships in HAZUS compatible format, so this format is used here for comparison purposes. Fragility parameters for all the index buildings defined in Table 3.2 are provided. However, for most of them the extensive and complete damage fragility curves have negligibly low probabilities. Porter et al. (2002) ascribed this to those limit states not being satisfied for the adopted scaling levels.

The classification of index woodframe buildings in terms of seismic design level based on the criteria used in this study (explained in section 3.1.4.1) are given in Table A.20, of Appendix A. Although results from the two studies are in agreement for a small number of design level damage state pairs (see Figure 5.11), for most of the cases, there are significant differences between the fragility relationships (see Figure 5.12). In addition, as stated above, for most of the extensive and complete damage limit states of the index buildings, results from Porter et al. (2002) have exceedance probabilities very close to zero. Since the highest uncertainty is introduced through ground motion records, the differences between the fragility relationships are mainly due to use of time histories with considerably different characteristics. In addition, Porter et al. (2002) scales the latter the ground motions based on spectral acceleration at the fundamental period of structure by while this study uses PGA for this purpose. Table 5.4 summarizes the different approaches from these two studies providing insight into discrepancies between the fragility relationships.

5.2. FRAGILITY RELATIONSHIPS FOR OTHER BUILDING TYPES

Assembling a database in order to represent the capacity component of the fragility analysis requires considerable time and effort. For the important woodframe building type, this study carries out this task and uses it to demonstrate fully the fragility analysis framework proposed here. Extension of the available database of capacity diagrams to other building types is underway although it is out of the scope of this study. Nonetheless, the current framework is extended to other building types using the available capacity diagrams from HAZUS (HAZUS Technical Manual Chapter 5 - National Institute of Building Sciences, 2003).

As is done for the woodframe building types in the previous sections, the developed fragility relationships for the rest of building types analyzed are presented in two formats i.e. conventional and HAZUS compatible.

5.2.1. Conventional Fragility Relationships

As an example of conventional fragility relationships for other building types, fragility curves for all four seismic design levels of building type S3 (see Table 3.1 for the list of building types) are provided in Figure 5.13. S3 comprises steel, light frame buildings. These are single storey, pre-engineered and prefabricated structures. Further details can be found in HAZUS Technical Manual Chapter 5, page 5-9.

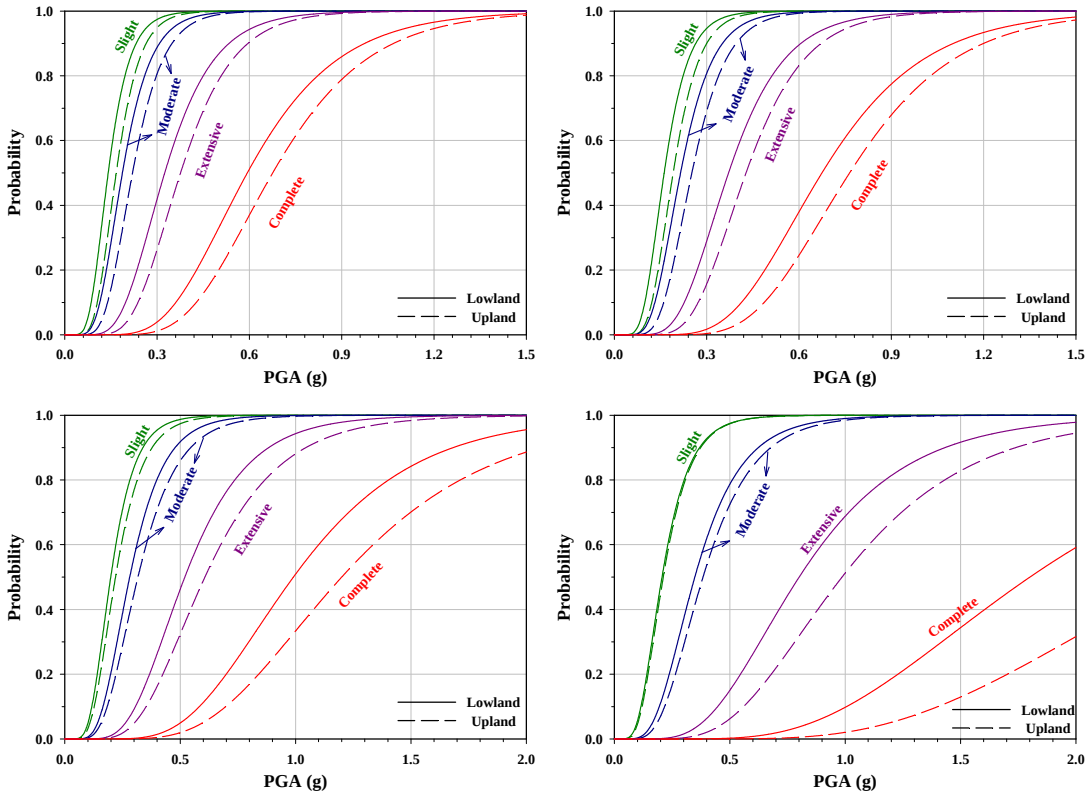

Figure 5.13. Fragility curves for all seismic design levels of S3 building type *(Top-Left):* Pre-code; *(Top-Right):* Low code; *(Bottom-Left):* Moderate code; *(Bottom-Right):* High code seismic design

The improved fragility relationships in conventional format can be utilized using the limit states defined in Table C.1, fragility parameters from Table C.2 or Table C.3 (depending on the soil profile), and Eq. (4.4).

5.2.2. HAZUS Compatible Fragility Relationships

Improved HAZUS compatible relationships are important in that the parameters can be input to the software and advanced, region specific simulations can be carried out. The

improvements for building types other than woodframe are basically in earthquake demand and the methodology for structural assessment owing to the fact that that same building capacity is employed (and assuming that the difference between the convolution process used here, which is modified in order to be able to process the data, and the original one is negligible). As a result, it is possible to investigate the combined effect of improvement in the earthquake demand and methodology for structural assessment (second and the third components of the fragility analysis framework) which is revealed by a comparison between the available HAZUS fragility curves and those derived here by using the HAZUS capacity diagrams.

Since capacity diagrams (and hence the limit states) are taken from HAZUS, the original fragility curves from HAZUS and the improved ones presented here are anchored to the same point. The parameter that changes the shape of the curves is the standard deviation of the lognormal distribution, i.e. β_{tot} in Eq. (4.7). For illustration purposes, the extensive damage limit state of the S3 building type high code seismic design level is used (see Figure 5.14).

As observed from the below figure, there is a slight difference between the results of uplands and lowlands soil profiles while the original HAZUS curve has a significantly higher uncertainty associated with it. This observation is true for all the cases considered – all building types, seismic design, and damage state levels – with a few exceptional cases. Therefore it can be concluded that HAZUS predicts higher uncertainty when compared with the results obtained from the simulations performed in this study. The impact is that HAZUS overestimates the damage for limit states whose threshold value is not exceed while contrariwise, it underestimates the damage. This result can be attributed to the judgmental foundations of the HAZUS curves. In order to render them applicable to a wider region (the whole USA), it is plausible to assign higher uncertainty to fragility relationships.

One can use the above described logical reasoning and the results provided in Figure 5.15 and Figure C.1 through Figure C.3 so as to draw conclusions regarding the difference between the original HAZUS curves and the improved ones provided here.

The improved fragility relationships for the building types defined in Table 3.1, can be input to HAZUS using the original limit state threshold values from Table C.1 and derived standard deviation values from Table C.4 or Table C.5 (depending on the soil type).

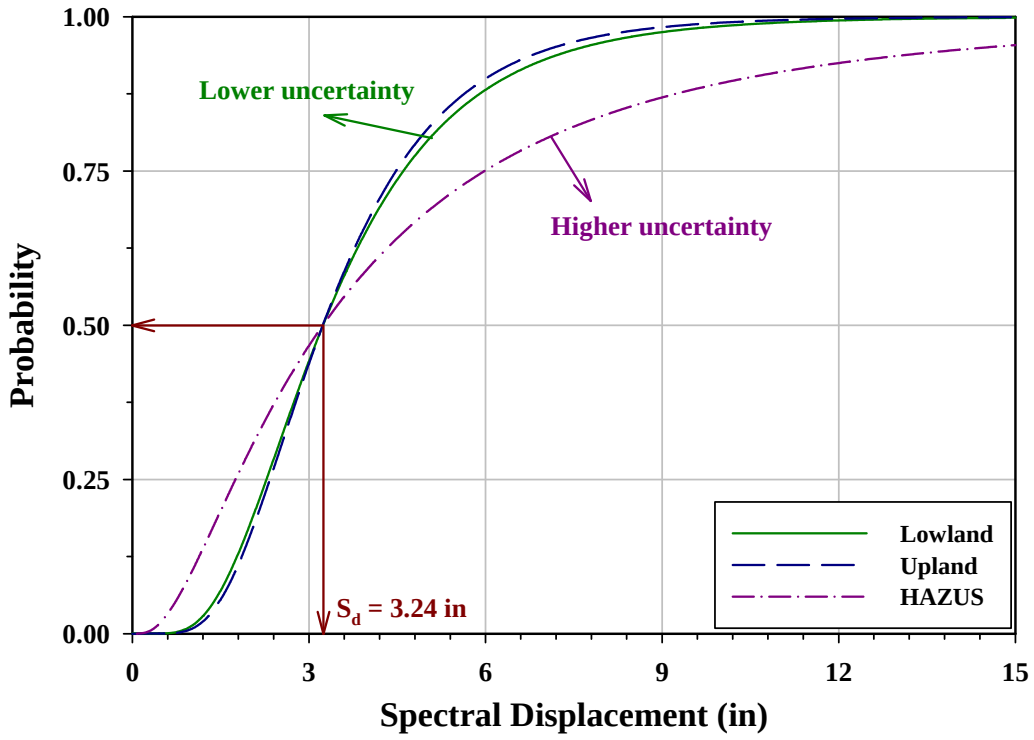

Figure 5.14. Effect of uncertainty (standard deviation of the lognormal distribution) on the fragility curves for the S3 high code building category, extensive damage limit state

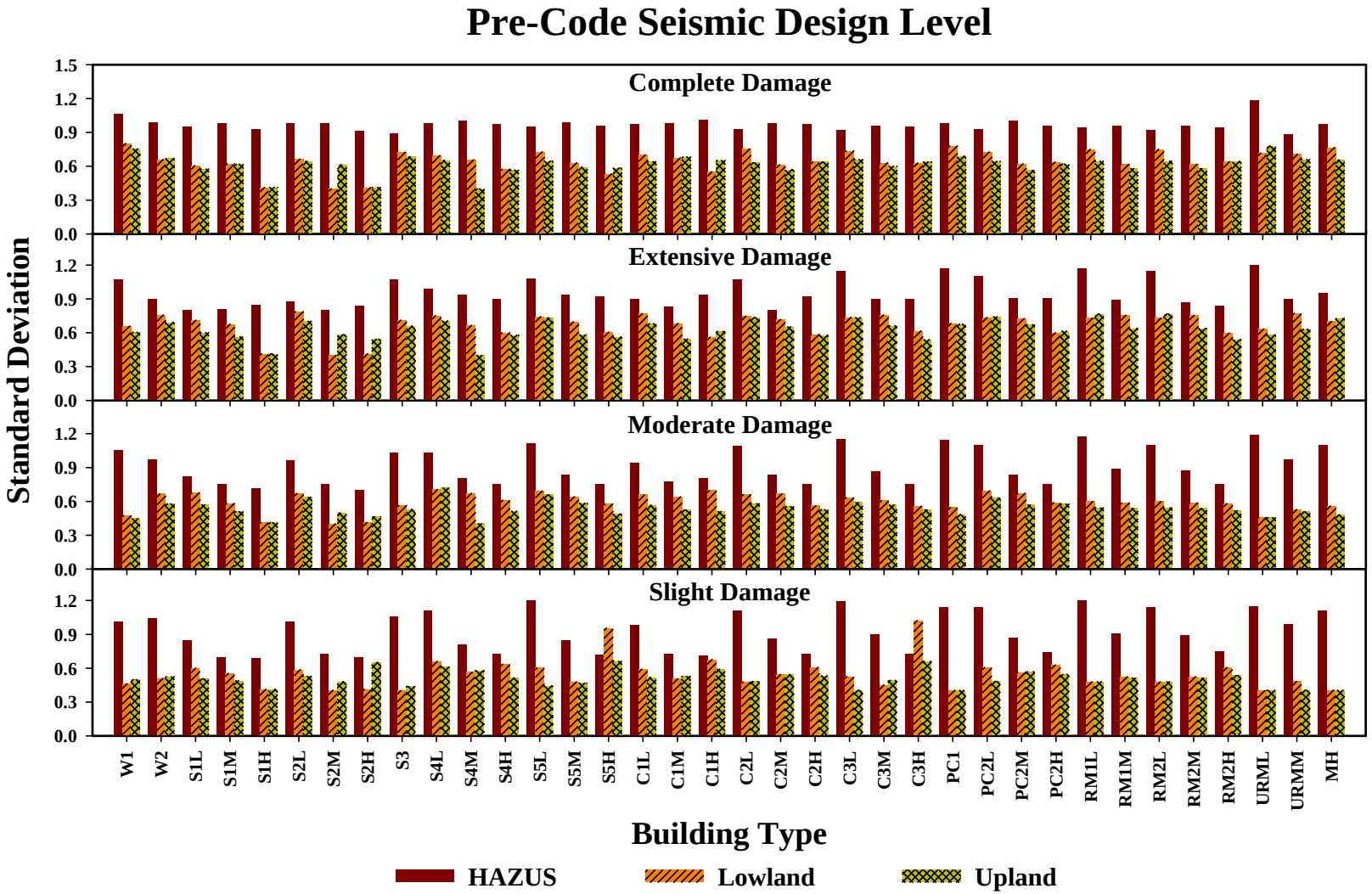

Figure 5.15. Comparison of standard deviation values from HAZUS and improved fragility analysis – pre-code seismic design level

CHAPTER 6
CONCLUSIONS

In this study a new framework is proposed for deriving fragility relationships for populations of buildings. Thirty six building types are considered while particular focus is placed on woodframe structures. Earthquake records specifically developed for the CEUS are used for ground motion characterization. An advanced CSM is developed and implemented for structural response assessment. The proposed fragility relationships are provided in a suitable format for direct implementation in both HAZUS and in other loss assessment software.

Conclusions were drawn in various parts of the report. Below, the main outcomes are reiterated.

- In order to provide a comprehensive set of fragilities for all the main types of building inventory for future loss assessment studies, 36 different building types of wood, steel, concrete, and masonry (as well as mobile homes) are considered in the report. These building types are further refined using four seismic design levels, i.e. pre-, low, moderate, and high seismic code.

- Special attention is focused on woodframe buildings due to the available statistics indicating the prevalence of this type of construction in CEUS and elsewhere in the USA. Indeed, 80-90% of all buildings in many parts of the USA are woodframe.

- The capacity of woodframe buildings is represented by a database of analysis-based pushover curves from available studies in literature. The extension to other buildings is carried out using the set of capacity diagrams from HAZUS.

- The classification of pushover curves into the two considered woodframe building types is based on the floor area and height while differentiation in terms of seismic design levels is based on the observed base shear coefficients.

- For woodframe buildings, pushover curves are converted to capacity diagrams and performance limit states are determined on the latter based on well established engineering criteria. For the remaining building types limit states from HAZUS are utilized.

- Variation in building capacity for woodframe structures is naturally achieved by a employing a number of different capacity diagrams under the same building category. For the remaining building types, the importance sampling technique is applied to median capacity diagrams provided in HAZUS.

- The demand is represented by synthetically-generated ground motion records compatible with the seismo-tectonic environment of the NMSZ in the CEUS (Fernandez, 2007). Two soil profiles are considered, i.e. lowlands (soft soils) and uplands (rock sites) profiles.

- Representing the capacity of buildings using pushover curves entailed the use of a similar procedure to CSM. Through investigations on the available variants of CSM, shortcomings in the prediction of the displacement demands were observed. Therefore an advanced CSM, incorporating inelastic dynamic analysis, is developed and verified using test cases. This new version of CSM is subsequently used for structural assessment.

- Two different techniques are used to obtain the parameters of the improved fragility relationships in order to make their use in future earthquake loss assessment studies utilizing both HAZUS and other software.

- Comparisons between the fragility relationships for woodframe buildings obtained using capacity curves from HAZUS and the analytically-based counterparts confirm that the capacity representation has a significant impact on the final fragility relationships. Indeed, use of the HAZUS capacity curves leads to the underestimation of damage probabilities for pre-code seismic design level of W1 building type and pre-, low, and moderate code seismic design levels of W2 building type. On the contrary, for the low, moderate, and high codes of W1

and the high code of W2 building types, a higher probability of damage is predicted when the HAZUS capacity curves are used.

- Fragility curves based on analytical simulations and their consistent limit states are more reliable than relying on expert opinion as in the case of HAZUS.

- The lowlands soil profile yields higher damage probabilities than uplands soil profile for all damage state levels and the entire range of the GMI parameter.

- The observed common trend in comparing the HAZUS and new fragilities is that HAZUS underestimates damage as the strength of the structure increases. This is mainly attributed to the high limit state threshold values defined in HAZUS.

- Comparisons of the new fragilities with those from other studies indicate that there is a good agreement with the work of Ellingwood et al. (2007) for the one-storey woodframe building. The differences between these two studies are mainly due to capacity of building representation and limit state determination.

- It is further observed that fragility relationships from Porter et al. (2002) are close to the new ones in some cases and significantly different in others. Earthquake demand representation has a great influence on the results and the discrepancies between the two are mainly attributed to use of fundamentally different record sets.

- Since capacity diagrams and limit states from HAZUS are used in the derivation of fragility relationships for buildings other than woodframe, the differences from the original curves in HAZUS are only due to differences in standard deviation values (or uncertainty). It is noted that lower uncertainties are associated with all the building types when the earthquake ground motion set for CEUS are used. The impact of using this set is that HAZUS overestimates the damage for limit states whose threshold value is not exceeded, while it otherwise underestimates damage. This observation is attributed to the judgmental nature of the HAZUS curves.

The framework proposed in this report is amenable to rapid and efficient updating with additional pushover curves and ground motion records. The outcome of the work presented herein is a more reliable set of simulation-based fragility relationships. Owing to the rigorous models, limit states, and input motion used, the relationships are recommended for use in HAZUS and other impact assessment software. The new fragility curves are of interest to researchers because of the new approach in deriving them, and to risk modelers and managers because of the reliability of impact assessments obtained from their use. The importance of the work presented in this study is emphasized by the observation that the overwhelming majority of structures in many regions in the Central USA are woodframe construction, for which advanced analysis-based fragilities are provided.

APPENDIX A

A.1. CAPACITY OF BUILDINGS

A.1.1. Building Types

Detailed description of the building types can be found in (HAZUS Technical Manual Chapter 5 - National Institute of Building Sciences, 2003), here only those of W1 and W2 are given.

A.1.1.1. Wood, Light Frame (W1)

These are typically single-family or small, multiple-family dwellings of not more than 5,000 ft^2 of floor area. The essential structural feature of these buildings is repetitive framing by wood rafters or joists on wood stud walls. Loads are light and spans are small. These buildings may have relatively heavy masonry chimneys and may be partially or fully covered with masonry veneer. Most of these buildings, especially the single-family residences, are not engineered but constructed in accordance with "conventional construction" provisions of building codes. Hence, they usually have the components of a lateral-force-resisting system even though it may be incomplete. Lateral loads are transferred by diaphragms, roof panels and floors that may be sheathed with sawn lumber, plywood or fiber wood sheeting. Shear walls are sheeted with boards, stucco, plaster, plywood, gypsum board, particle board, or fiber board, or interior partition walls sheathed with plaster or gypsum board

A.1.1.2. Wood, Greater than 5,000 ft^2 (W2)

These buildings are typically commercial or industrial buildings, or multi-family residential buildings with a floor area greater than 5,000 ft^2. These buildings include structural systems framed by beams or major horizontally spanning members over columns. These horizontal members may be glue-laminated (glue-lam) wood, solid-sawn wood beams, or steel beams or trusses. Lateral loads usually are resisted by wood diaphragms and exterior walls sheathed with plywood, stucco, plaster, or other paneling. The walls may have diagonal rod bracing. Large openings for stores and garages often require post-and-beam framing. Lateral load resistance on those lines may be achieved with steel rigid frames (moment frames) or diagonal bracing.

A.1.2. Woodframe Structures Database

A.1.2.1. CUREE-Caltech Woodframe Project

Shake Table Tests of a Two Storey Woodframe House:

Definition of the phase 9 test structure is: "Two-stories with roof, east & west sheathed with window openings and small door opening on west wall and large door opening on east wall, north & south sheathed with openings, second floor diaphragm nailed at 100% with no blocking & PL400 adhesive." For the phase 10 structure the definition is the same with the one for phase 9 test structure except the statement: "Finished with exterior stucco and interior gypsum wallboard." (Fischer et al., 2001)

Elevation and plan views of the structure are shown in Figure and Figure A.2, respectively.

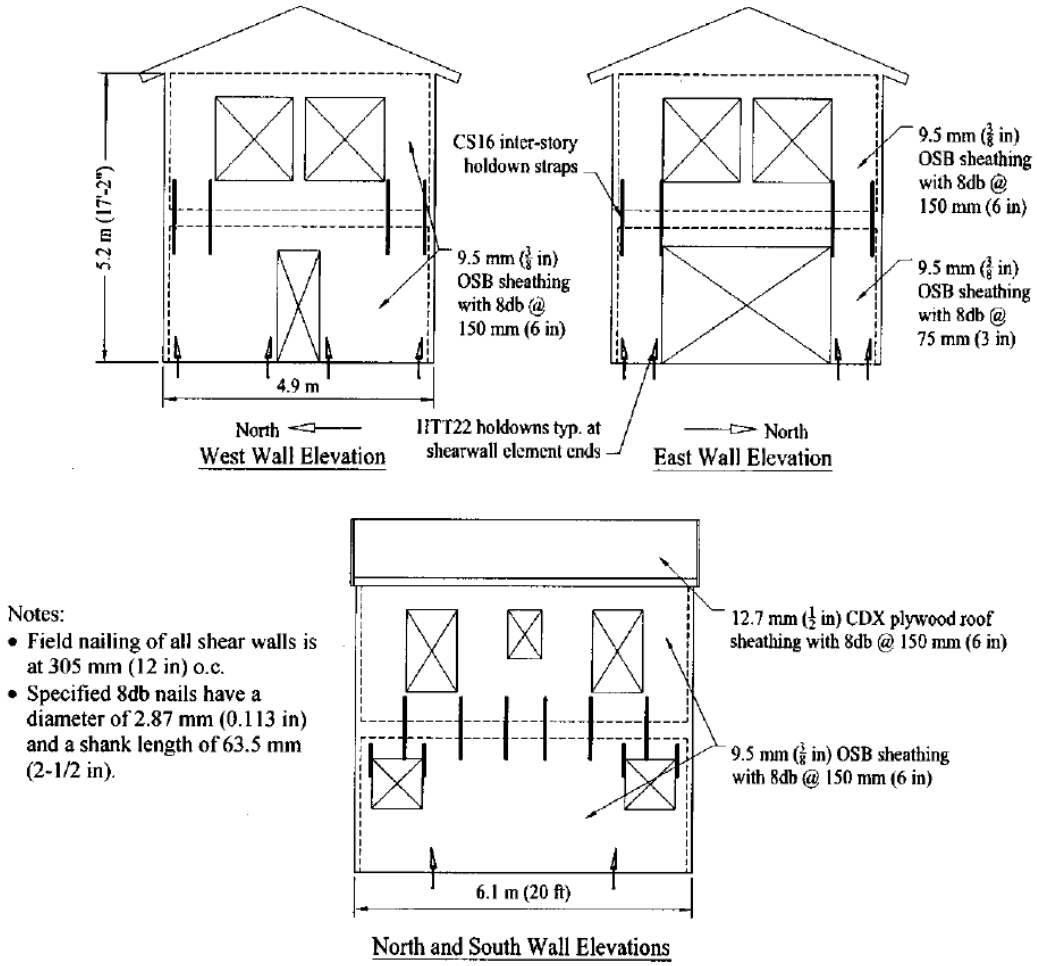

Figure A.1. Elevation views of the test structures (Fischer et al., 2001)

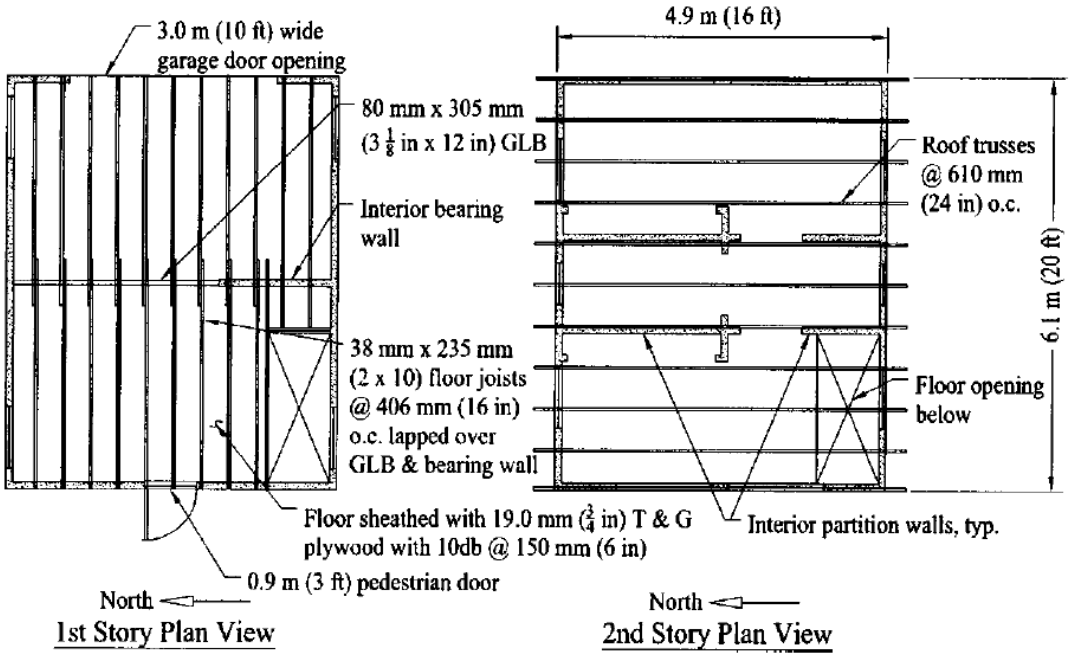

Figure A.2. Plan views of the test structures (Fischer et al., 2001)

Phase 9 and 10 structures are modeled using the software SAWS. The test structure is modeled as a planar pancake system with the floor diaphragm and roof diaphragm superimposed on top of each other. The foundation of the structural model was connected to the floor diaphragm with zero-length non-linear shear springs to the first storey shear walls. Similarly the floor diaphragm was connected to the roof diaphragm with zero-length non-linear springs representing the second storey shear walls. The mass of each storey is assumed to be distributed uniformly in the corresponding floor diaphragm. The modelings of each of the phase 9 and 10 structures are shown in Figure A.3.

Hysteresis behavior developed by Folz and Filiatrault (2001) is used for each of the shear walls present in these models (see Figure A.4). This model includes pinching, stiffness, and strength degradation. The software Cyclic Analysis of Shear Walls – CASHEW (Folz and Filiatrault, 2000) is used to determine the parameters of the hysteresis models mentioned. Data obtained through experimental testing of these shear wall is given as given as input to CASHEW.

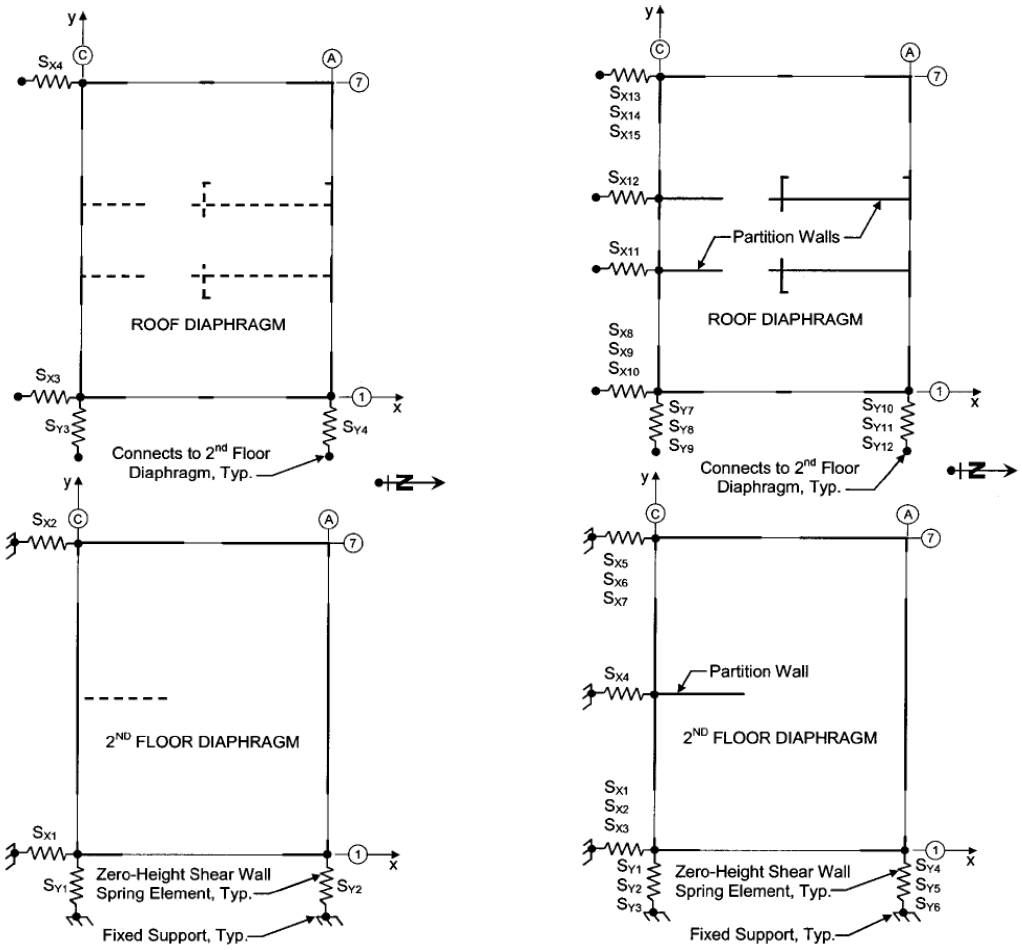

Figure A.3. SAWS model for *(Left)*: Phase 9 test structure; *(Right):* Phase 10 test structure (Folz and Filiatrault, 2002)

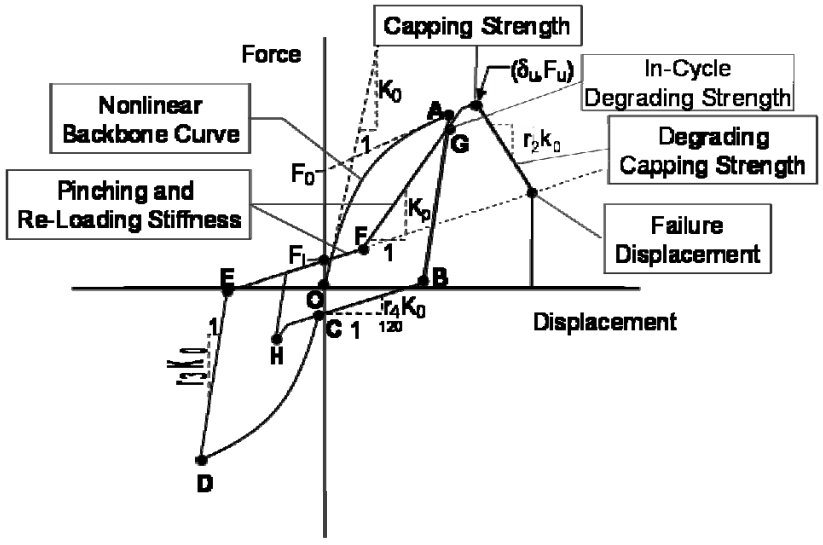

Figure A.4. Hysteresis model developed by Folz and Filiatrault (2001)

The height and weight data as well as the constants for conversion of pushover curves to capacity diagrams for these two structures are given in Table A.1.

Table A.1. Height and weight information and conversion factors from pushover curve to capacity diagram for Phase 9 and Phase 10 test structures

Storey Number	Storey Height from Ground (in)	Storey Weight (kips)	ϕ_i	$w_i\phi_i$	$w_i\phi_i^2$
Base	0	0	0	0	0
1	108	13.8	0.64	8.82	5.63
2	216	10.8	1	10.8	10.8
	SUM	24.6	-	19.62	16.43
Conversion Factors					
Γ		1.194			
$\frac{\Gamma m^* g}{W}$		0.952			

where w_i are the storey weights and W is the total weight of the structure. The conversion factor for base shear is normalized by the total weight of the structure.

It is important to note here that additional weights are used when necessary to keep the total seismic weight of the structure constant during different phases of testing.

Seismic Modeling of Index Woodframe Buildings:

The design of the woodframe index buildings is done by private construction companies. Design drawings and all information regarding the construction materials, nailing patterns, and other details can be found in (Isoda et al., 2002; Reitherman and Cobeen, 2003).

Below, a short description and representative figures for each of these buildings, i.e. small house, large house, small townhouse, and apartment building are provided.

i. Small house:

Description from Reitherman and Cobeen (2003): "A one storey, two bedrooms, one bath house built circa 1950 with a simple 1,200 square foot floor plan on a level lot. Prescriptive construction is assumed. Wood framed floor cripple walls are included in the poor- and typical-quality construction variants."

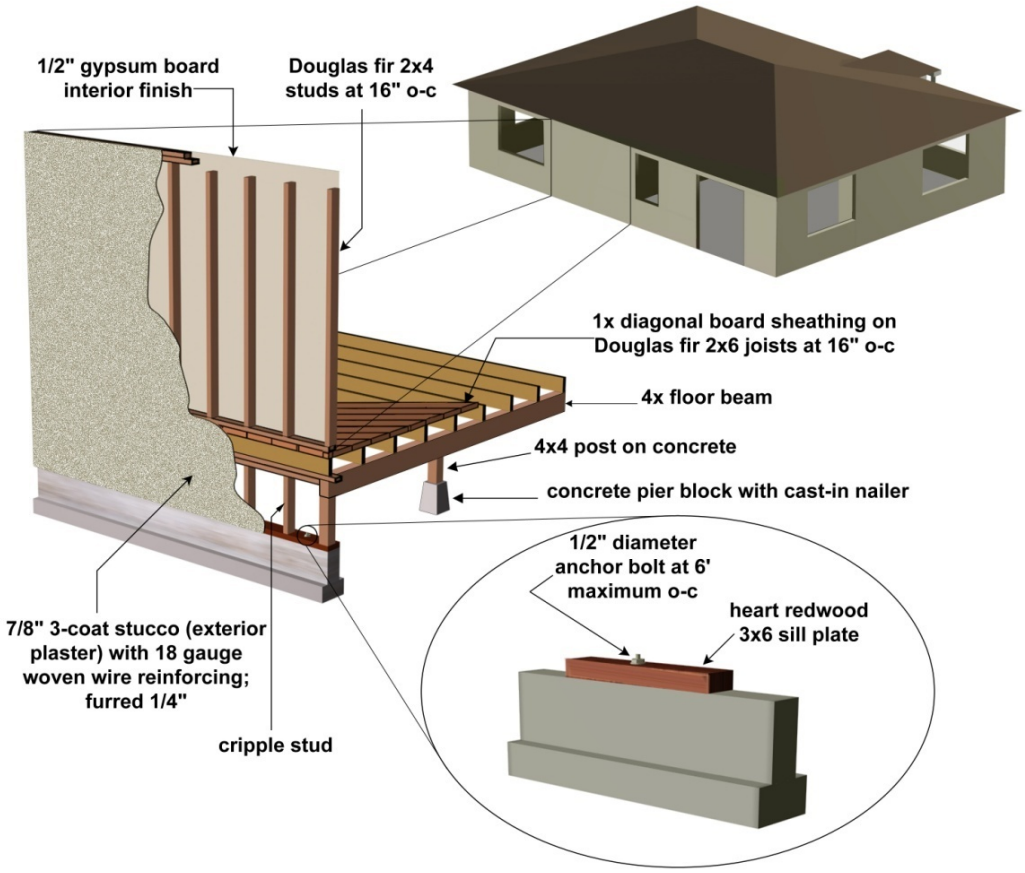

Figure A.5. Illustration of the small house index building (Reitherman and Cobeen, 2003)

Table A.2 summarizes the variants for small house index building. The height and weight data as well as the constants for conversion of pushover curves to capacity diagrams for small house index building are given in Table A.3.

Table A.2. Construction variants for small house index building (Isoda et al., 2002)

Superior Quality	Typical Quality	Poor Quality
Concrete Stem Wall	Unbraced cripple wall with average-quality stucco, 80 % of stiffness and strength from high-quality laboratory tests	Unbraced cripple wall with poor-quality stucco, 55 % of stiffness and strength from high-quality laboratory tests
Good quality stucco, 100 % of stiffness and strength from high-quality laboratory test	Average quality stucco, 90 % of stiffness and strength from high-quality laboratory tests	Poor quality stucco, 70 % of stiffness and strength from high-quality laboratory tests
Superior nailing of interior gypsum wallboard, 100 % of stiffness and strength from high-quality laboratory tests	Good nailing of interior gypsum wallboard, 85 % of stiffness and strength from high-quality laboratory tests	Poor nailing of interior gypsum wallboard, 75 % of stiffness and strength from high-quality laboratory tests

Table A.3. Height and weight information and conversion factors from pushover curve to capacity diagram for small house index building

Storey Number	Storey Height from Ground (in)	Storey Weight (kips)	ϕ_i	$w_i\phi_i$	$w_i\phi_i^2$
Base	0	0	0	0	0
1	24	16.63	0.1	1.74	0.18
2	132	28.94	1	28.94	28.94
	SUM	45.57	-	30.68	29.12
Conversion Factors					
Γ		1.053			
$\frac{\Gamma m^* g}{W}$		0.709			

ii. Large House:

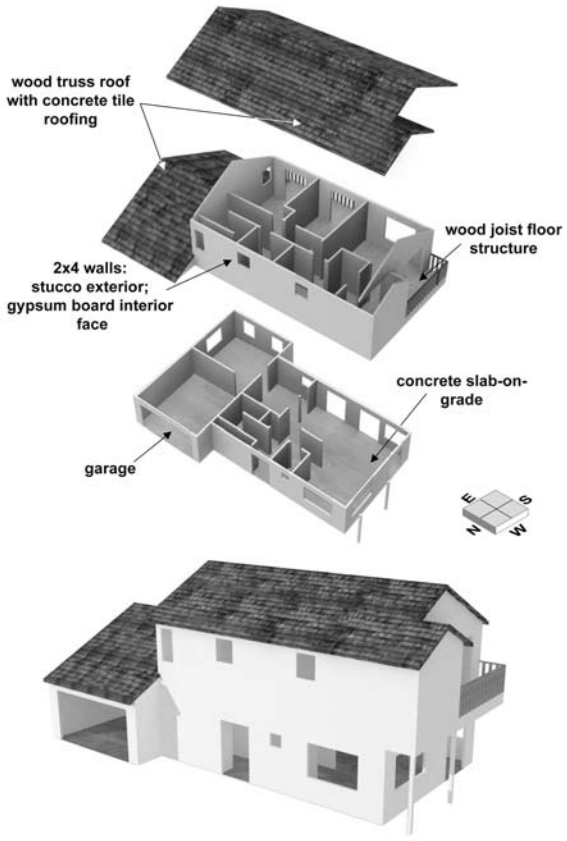

Figure A.6. Illustration of the large house index building (Reitherman and Cobeen, 2003)

Description from Reitherman and Cobeen (2003): "An engineered two storey single family dwelling of approximately 2,400 square feet on a level lot with a slab on grade

and spread footings. This building is assumed to have been built as a housing development, production house, either in the 1980's or 1990's."

Table A.4 summarizes the variants for large house index building. The height and weight data as well as the constants for conversion of pushover curves to capacity diagrams for large house index building are given in Table A.5.

Table A.4. Construction variants for large house index building (Isoda et al., 2002)

Superior Quality	Typical Quality	Poor Quality
Good nailing of diaphragms, 100% of stiffness and strength from high-quality laboratory tests	Average nailing of diaphragms, 90% of stiffness and strength from high-quality laboratory tests	Poor nailing of diaphragms, 80% of stiffness and strength from high-quality laboratory tests
Good nailing of shear walls, 100% of stiffness and strength from high-quality laboratory tests	Average nailing of shear walls, 5% greater of nail spacing	Poor nailing of shear walls, 20% greater of nail spacing, 5% reduction of stiffness and strength due to water damage
Good connections between structural elements, 100% of stiffness and strength from high-quality laboratory tests	Typical connections between structural elements, 10% reduction of stiffness and strength in shear walls from high-quality laboratory tests	Poor connections between structural elements, 20% reduction of stiffness and strength in shear walls from high-quality laboratory tests
Good Quality Stucco, 100% of stiffness and strength from high-quality laboratory tests	Average Quality Stucco, 90% of stiffness and strength from high-quality laboratory tests	Poor-Quality Stucco, 70% of stiffness and strength from high-quality laboratory tests
Superior Nailing of interior gypsum wallboard, 100% of stiffness and strength from high-quality laboratory tests	Good Nailing of interior gypsum wallboard, 85% of stiffness and strength from high-quality laboratory tests	Poor Nailing of interior gypsum wallboard, 75% of stiffness and strength from high-quality laboratory tests

Table A.5. Height and weight information and conversion factors from pushover curve to capacity diagram for large house index building

Storey Number	Storey Height from Ground (in)	Storey Weight (kips)	ϕ_i	$w_i\phi_i$	$w_i\phi_i^2$
Base	0	0	0	0	0
1	108	45.26	0.49	22.38	11.06
2	216	27.93	1	27.93	27.93
	SUM	73.19	-	50.31	38.99
Conversion Factors					
Γ		1.290			
$\frac{\Gamma m^* g}{W}$		0.887			

iii. Small Townhouse:

Description from Reitherman and Cobeen (2003): "A two-storey 1,500 to 1,800 square foot unit with a common wall. Part of the dwelling is over a two-car garage. It is on a level lot with a slab on grade and spread foundations. It is recently built and the seismic design is engineered."

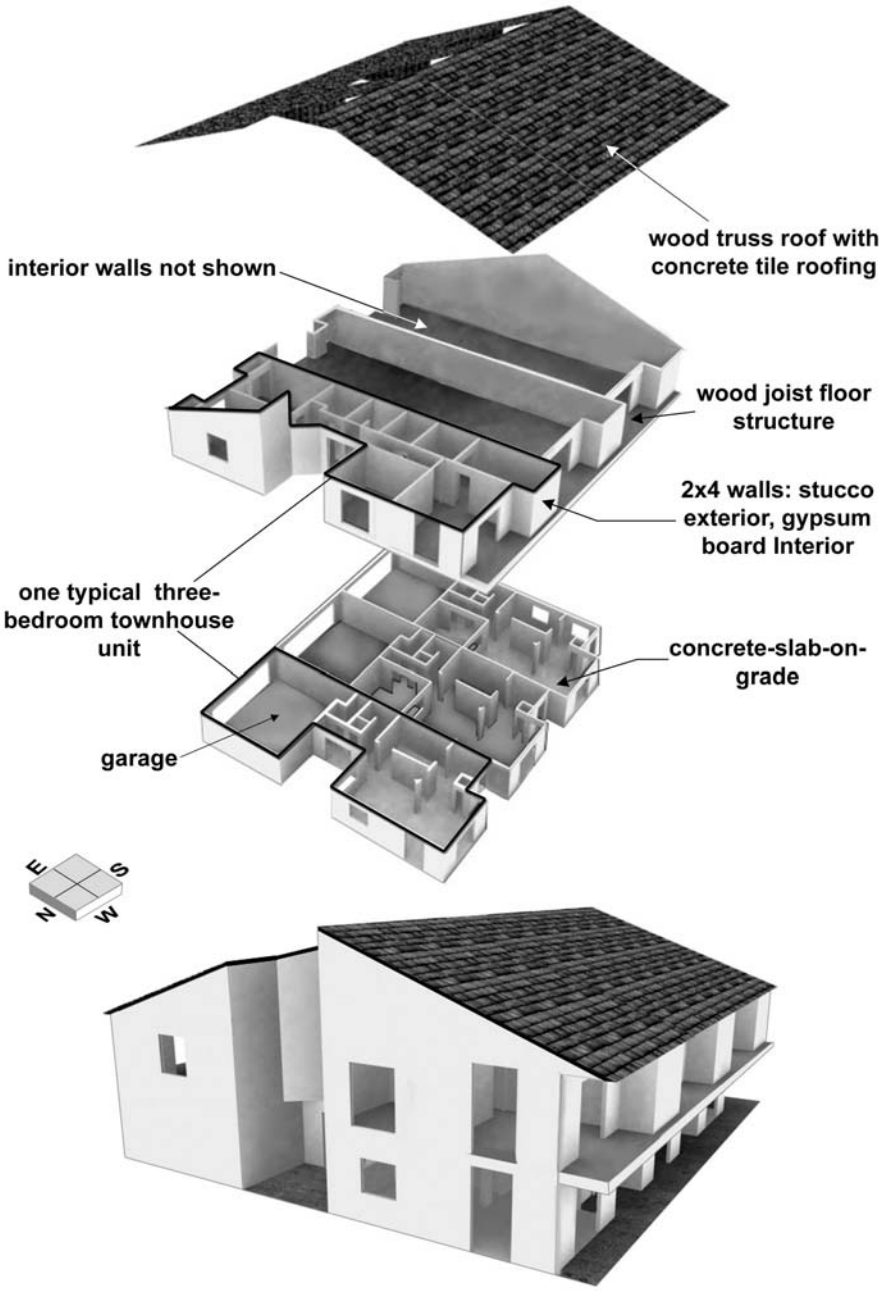

Figure A.7. Illustration of the small townhouse index building (Reitherman and Cobeen, 2003)

The construction variants for small townhouse index building are same as those of the large house index building. The height and weight data as well as the constants for conversion of pushover curves to capacity diagrams for small townhouse index building are given in Table A.6.

Table A.6. Height and weight information and conversion factors from pushover curve to capacity diagram for small townhouse index building

Storey Number	Storey Height from Ground (in)	Storey Weight (kips)	ϕ_i	$w_i\phi_i$	$w_i\phi_i^2$
Base	0	0	0	0	0
1	108	89.25	0.34	30.44	10.38
2	216	99.87	1	99.87	99.87
	SUM	189.12	-	130.31	110.25
Conversion Factors					
	Γ	1.182			
	$\frac{\Gamma m^* g}{W}$	0.814			

iv. Apartment Building:

Description from Reitherman and Cobeen (2003): "A three storey, rectangular building with ten units, each with 800 square feet and space for mechanical and common areas. All walls and elevated floors are woodframe. It has parking on the ground floor. Each unit has two bedrooms, one bath and one parking stall. It would be constructed prior to 1970 and "engineered" to a minimal extent.

Table A.7. Height and weight information and conversion factors from pushover curve to capacity diagram for apartment index building

Storey Number	Storey Height from Ground (in)	Storey Weight (kips)	ϕ_i	$w_i\phi_i$	$w_i\phi_i^2$
Base	0	0	0	0	0
1	108	120.15	0.35	42.23	14.84
2	216	127.60	0.75	95.29	71.15
3	324	100.16	1	100.16	100.16
	SUM	347.91	-	237.678	186.15
Conversion Factors					
	Γ	1.277			
	$\frac{\Gamma m^* g}{W}$	0.872			

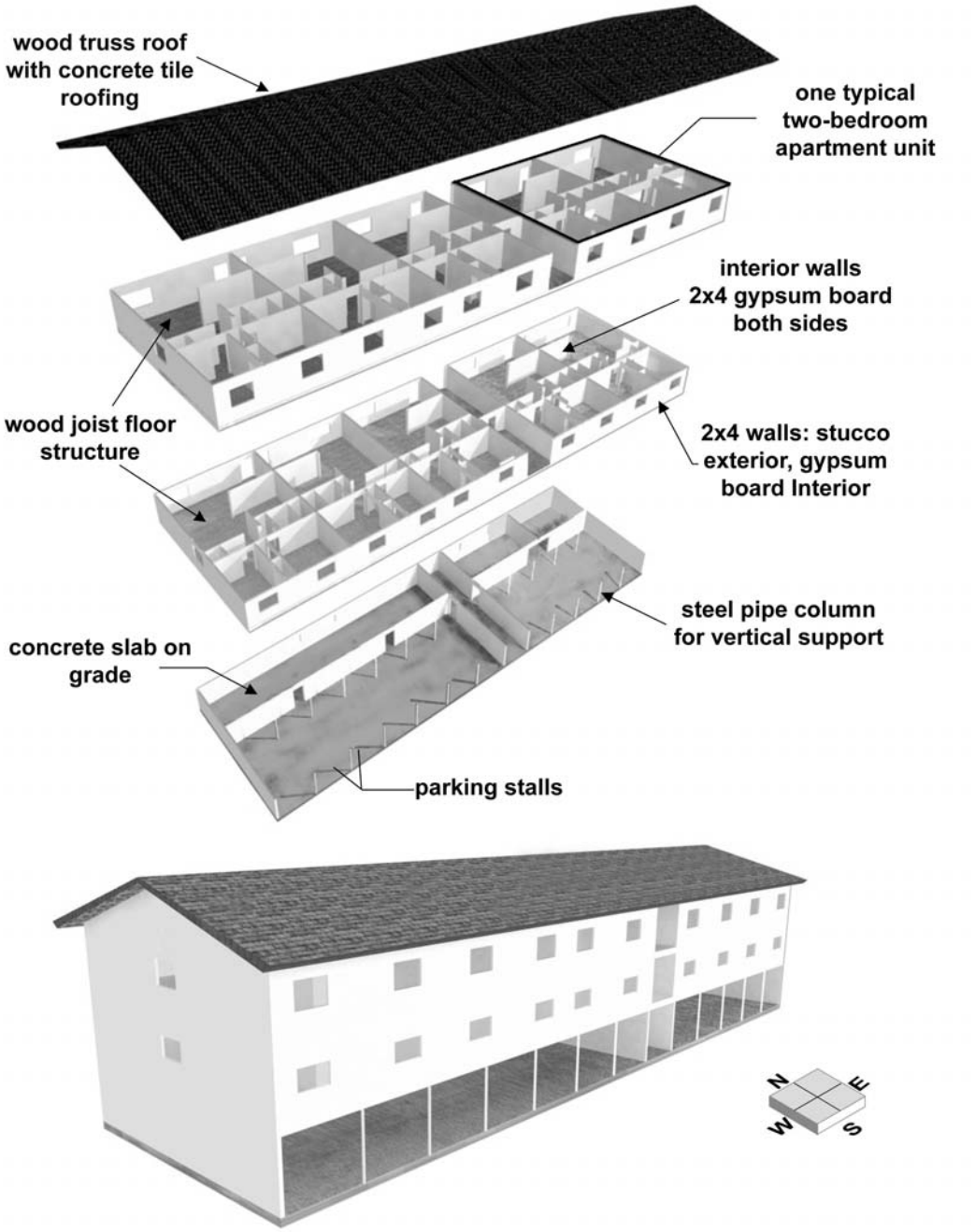

Figure A.8. Illustration of the apartment index building (Reitherman and Cobeen, 2003)

The construction variants for apartment index building are the same as those of the large house index building. The height and weight data as well as the constants for conversion of pushover curves to capacity diagrams for apartment index building are given in Table A.7.

v. Modeling Approach for Index Woodframe Buildings:

As mentioned in the main text, the software RUAUMOKO is used for finite element modeling of the buildings. Similar to the Two-storey Shake Table Test Structures, the index buildings are modeled as a planar "pancake" system with the floor diaphragm and roof diaphragm superimposed on top of each other (Figure A.9). Again zero-length non-linear shear spring elements are used to connect the floor diaphragms. And the floor diaphragms are modeled using plane stress quadrilateral finite elements with very high in-plane stiffness. Frame elements are used along the edges of floor diaphragms to connect the corners of the quadrilateral elements to the shear wall elements. The bending stiffness of the frame elements is assumed to be very small to allow free deformations of the diaphragm. The axial stiffness of the frame elements is assumed to be very high in order to distribute the in-plane forces of the shear elements along the edges of the floor diaphragms.

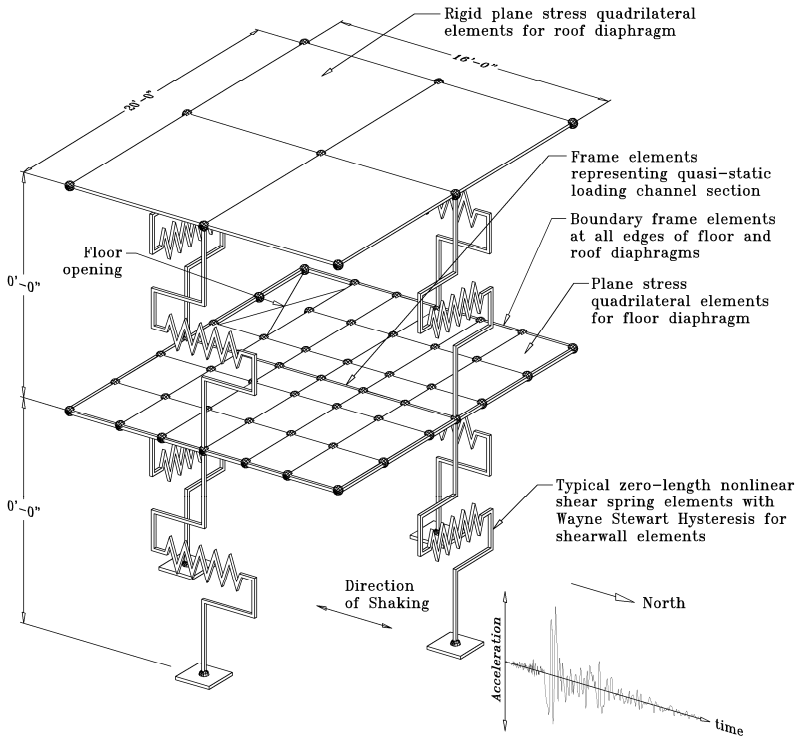

Figure A.9. Pancake model for analysis of index woodframe buildings (Isoda et al., 2002)

Each wall in the structure (shear, cripple and gypsum) is modeled by a single zero-length nonlinear in-plane shear spring using the Wayne Stewart hysteresis rule (Stewart, 1987). Figure A.10 shows this hysteresis rule and the required input parameters for the RUAUMOKO program. Note that this hysteresis rule incorporates stiffness and strength degradations.

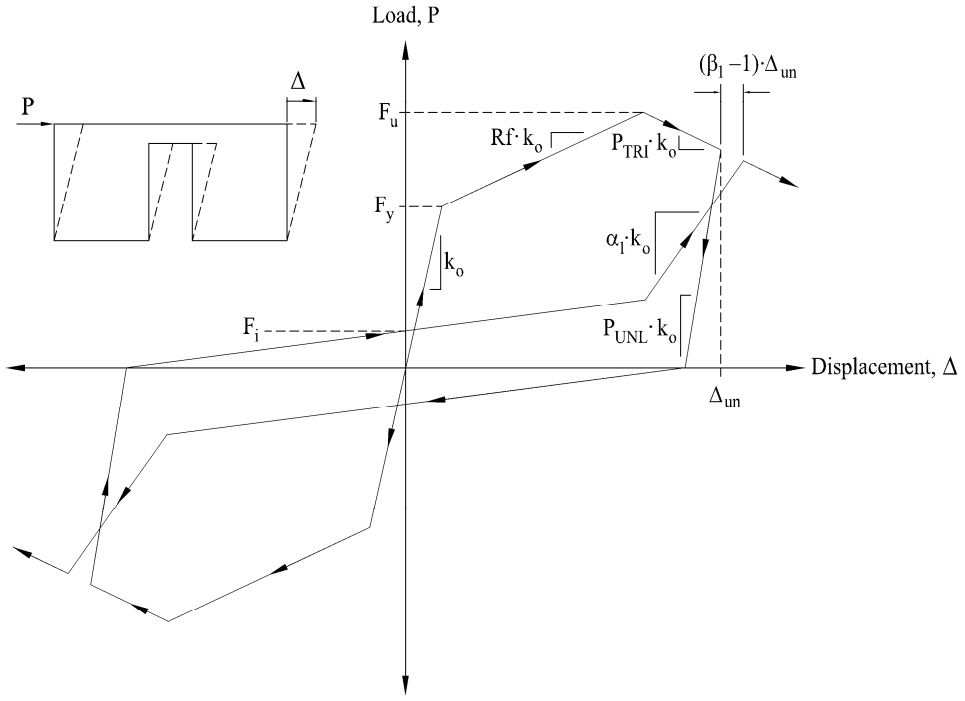

Figure A.10. Wayne Stewart degrading hysteresis model used in RUAUMOKO (Isoda et al., 2002)

The seismic weight of each structure for use in the model is computed using the dead load of all elements. This dead load is distributed as lumped seismic weights at the nodes according to their tributary areas. For each building model, a Rayleigh viscous damping model is considered. This damping model is based on damping ratios of 1% of critical in the first and second elastic modes of vibration.

Again the software CASHEW is utilized to fit experimental data from different sources including The University of California at Irvine for the City of Los Angeles (COLA) Project (Pardoen et al., 2003), The University of California at Davis under CUREE-Caltech Woodframe Project (Chai et al., 2002), to the Wayne-Stewart hysteresis model, obtaining the required parameters.

A.1.2.2. ATC-63 Project

This set of archetype buildings includes designs for:

i. High seismic region, high gravity loading
ii. High seismic region, low gravity loading
iii. Low seismic region, high gravity loading
iv. Low seismic region, low gravity loading

The main assumptions incorporated into the archetype building designs are:

i. Torsional response is not considered, allowing archetypes to be represented as single wall lines in 2-D models
ii. Contribution to strength and stiffness from non-structural finishes and partitions is not considered

Archetype index buildings cover the specified ranges of the shown variables in Table A.8. These are further explained below.

The number of stories ranges from one to five. Woodframe buildings of two to three stories are common across most of the United States. And multi-family woodframe buildings of four to five stories represent a growing trend, especially along the West Coast.

Archetypes are designed for seismic loads in accordance with ASCE 7-05 (American Society of Civil Engineers, 2005). Through an iterative design procedure a reduction factor of $R = 6$ is found to be satisfactory for all sixteen archetype index buildings, resulting in a design base shear coefficient of 1.00 g for high seismic hazard (SDC D) and 0.375g for low seismic hazard (SDC B/C). Design for wind loads is not considered.

The third variable, building use, includes residential use; other uses including commercial. The primary difference between residential and commercial use is the spacing between shear wall lines, which in turn affects the seismic mass tributary to a given wall line. Residential buildings inherently have more walls and therefore closer spacing between shear wall lines. Buildings for other uses are more likely to be a big open box with shear walls at the perimeter or much more widely spaced.

Table A.8. Range of variables considered for the definition of woodframe archetype buildings (Applied Technology Council, 2007)

Variable	Range
Number of Stories	1 to 5
Seismic Design Categories (SDC)	B/C and D
Storey Height	10 ft
Non-structural Wall Finishes	Not Considered
Wood Shear Wall Pier Aspect Ratios	High/Low

The building use variable is also associated with variations in shear wall aspect ratios. Residential archetypes are designed with high aspect ratio shear walls (height/width of

2.7 to 3.3), reflecting the prevalence of these shear walls in residential construction. Other uses are designed with low aspect ratio shear walls (height/width of 1.5 or less), also consistent with prevalent construction. This variation is included to allow evaluation of aspect ratio effects in the analysis. Two exceptions occur where high aspect ratios are used for commercial use in low seismic hazard zones, because the shear wall length required did not justify use of low aspect ratio shear walls.

It is worth including the following recommendations from the ATC-63 committee (Applied Technology Council, 2007) for these archetype index buildings.

"Three recommendations are made when developing seismic design parameters for new building systems intended to be incorporated into wood light-frame buildings. First, a mix of shear wall aspect ratios is likely to be the norm. It is recommended that careful thought be given to whether a condition of all high, all low, or mixed aspect ratios is most critical. This might change with the system being considered. Second, in many cases new bracing elements may be mixed with conventional shear wall bracing, and may be designed to carry a small or large portion of the storey shear. The portion of the storey shear carried by the new system may need to be added as an archetype variable. Third, the effect of finish materials should be reconsidered in the context of the system being proposed; it may be appropriate to include a range of finish material effect as an archetype variable."

The two different building configurations used to define the two-dimensional archetype configurations for woodframe buildings are shown below. The first configuration, Figure A.11, is representative of residential building dimensions, while the second configuration, Figure A.12, is associated with office, retail, educational, and warehouse manufacturing woodframe buildings.

Similar to the Phase 9 and 10 structures in this report, archetype buildings are modeled based on a "pancake" approach. The computer program SAWS is used for analysis purposes. SAWS only allows analysis of 3-D models, therefore degenerated 2-D models are constructed.

As explained before, the building structure is composed of rigid horizontal diaphragms and nonlinear lateral load resisting shear wall elements. The hysteretic behavior of each wall panel is represented by an equivalent nonlinear shear spring element. For wood shear walls the hysteresis model developed by Folz and Filiatrault (2001) is used.

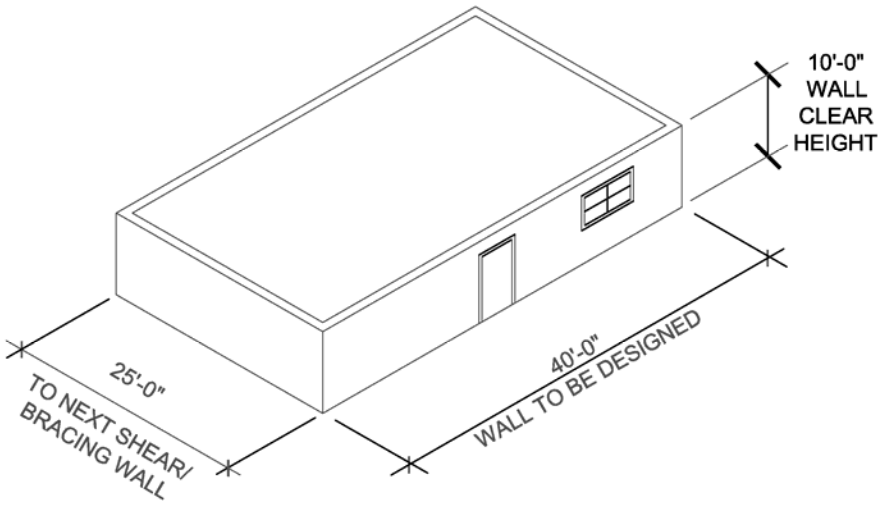

Figure A.11. Residential building configuration (Applied Technology Council, 2007)

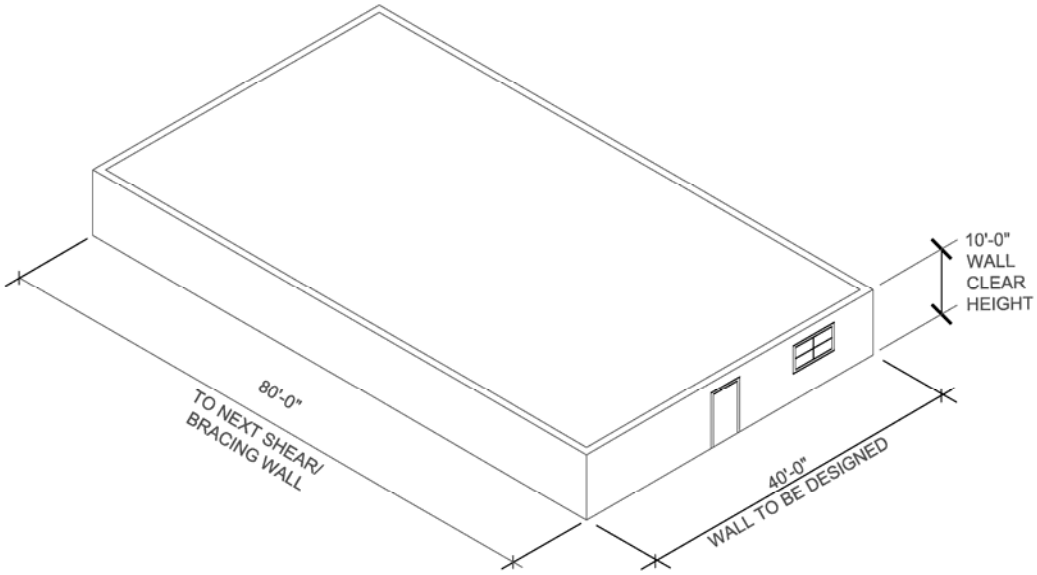

Figure A.12. Commercial building configuration (Applied Technology Council, 2007)

The experimental test data from CUREE-Caltech Woodframe Project (Fonseca et al., 2002), the Network of Earthquake Engineering Simulation's (NEES) NEESWood Project (Ekiert and Hong, 2006), and COLA wood shear wall test program (COLA, 2001) are used to determine the parameters of above mentioned hysteresis model in order to represent the behavior of shear wall in archetype index buildings.

The archetype buildings are summarized in Table A.9.

Table A.9. Summary of woodframe archetype structural design properties (Applied Technology Council, 2007)

Model #	No. of Stories	Building Configuration	Wall Aspect Ratio	Actual Natural Period, T (sec)	V/W
High Seismic Design (SDC D) – $R = 6$					
1	1	Commercial	Low	0.51	0.117
2	1	1&2 Family	High	0.38	0.117
5	2	Commercial	Low	0.52	0.117
6	2	1&2 Family	High	0.46	0.117
9	3	Commercial	Low	0.61	0.117
10	3	Multi-Family	High	0.47	0.117
13	4	Multi-Family	High	0.52	0.117
15	5	Multi-Family	High	0.64	0.117
Low Seismic Design (SDC B/C) – $R = 6$					
3	1	Commercial	High	0.65	0.044
4	1	1&2 Family	High	0.53	0.044
7	2	Commercial	High	0.74	0.044
8	2	1&2 Family	High	0.80	0.044
11	3	Commercial	Low	1.10	0.044
12	3	Multi-Family	High	0.83	0.044
14	4	Multi-Family	High	0.99	0.044
16	5	Multi-Family	High	1.12	0.044

In the tables below the height and weight data as well as the constants for conversion of pushover curves to capacity diagrams for the sixteen archetype buildings are given.

Table A.10. Height and weight information and conversion factors from pushover curve to capacity diagram for archetype buildings with model # 1 and 3

Storey Number	Storey Height from Ground (in)	Storey Weight (kips)	ϕ_i	$w_i\phi_i$	$w_i\phi_i^2$
Base	0	0	0	0	0
1	132	41	1	41	41
	SUM	41	-	41	41
Conversion Factors					
	$\boldsymbol{\Gamma}$		1		
	$\frac{\boldsymbol{\Gamma m^* g}}{\mathbf{W}}$		1		

Table A.11. Height and weight information and conversion factors from pushover curve to capacity diagram for archetype buildings with model # 2 and 4

Storey Number	Storey Height from Ground (in)	Storey Weight (kips)	ϕ_i	$w_i\phi_i$	$w_i\phi_i^2$
Base	0	0	0	0	0
1	132	13.65	1	13.65	13.65
	SUM	13.65	-	13.65	13.65
Conversion Factors					
	Γ		1		
	$\frac{\Gamma m^* g}{W}$		1		

Table A.12. Height and weight information and conversion factors from pushover curve to capacity diagram for archetype buildings with model # 5 and 7

Storey Number	Storey Height from Ground (in)	Storey Weight (kips)	ϕ_i	$w_i\phi_i$	$w_i\phi_i^2$
Base	0	0	0	0	0
1	132	82	1	82	82
2	264	41	1	41	41
	SUM	123	-	123	123
Conversion Factors					
	Γ		1		
	$\frac{\Gamma m^* g}{W}$		1		

Table A.13. Height and weight information and conversion factors from pushover curve to capacity diagram for archetype buildings with model # 6 and 8

Storey Number	Storey Height from Ground (in)	Storey Weight (kips)	ϕ_i	$w_i\phi_i$	$w_i\phi_i^2$
Base	0	0	0	0	0
1	132	17.30	0.63	10.96	6.95
2	264	13.65	1	13.65	13.65
	SUM	30.95	-	24.61	20.60
Conversion Factors					
	Γ		1.195		
	$\frac{\Gamma m^* g}{W}$		0.950		

Table A.14. Height and weight information and conversion factors from pushover curve to capacity diagram for archetype buildings with model # 9 and 11

Storey Number	Storey Height from Ground (in)	Storey Weight (kips)	ϕ_i	$w_i\phi_i$	$w_i\phi_i^2$
Base	0	0	0	0	0
1	132	82	0.67	54.67	36.44
2	264	82	1.33	109.33	145.78
3	396	41	1	41	41
	SUM	205	-	205	232.22
Conversion Factors					
	$\boldsymbol{\Gamma}$		0.918		
	$\frac{\boldsymbol{\Gamma m^* g}}{\mathbf{W}}$		0.918		

Table A.15. Height and weight information and conversion factors from pushover curve to capacity diagram for archetype buildings with model # 10 and 12

Storey Number	Storey Height from Ground (in)	Storey Weight (kips)	ϕ_i	$w_i\phi_i$	$w_i\phi_i^2$
Base	0	0	0	0	0
1	132	27.3	0.67	18.20	12.13
2	264	27.3	1.33	36.40	48.53
3	396	13.65	1	13.65	13.65
	SUM	68.25	-	68.25	74.31
Conversion Factors					
	$\boldsymbol{\Gamma}$		0.918		
	$\frac{\boldsymbol{\Gamma m^* g}}{\mathbf{W}}$		0.918		

Table A.16. Height and weight information and conversion factors from pushover curve to capacity diagram for archetype buildings with model # 13 and 14

Storey Number	Storey Height from Ground (in)	Storey Weight (kips)	ϕ_i	$w_i\phi_i$	$w_i\phi_i^2$
Base	0	0	0	0	0
1	132	27.3	0.5	13.65	6.83
2	264	27.3	1.0	27.3	27.3
3	396	27.3	1.5	40.95	61.43
4	528	13.65	1	13.65	13.65
	SUM	95.55	-	95.55	109.21
Conversion Factors					
	$\boldsymbol{\Gamma}$		0.875		
	$\frac{\boldsymbol{\Gamma m^* g}}{\mathbf{W}}$		0.875		

Table A.17. Height and weight information and conversion factors from pushover curve to capacity diagram for archetype buildings with model # 15 and 16

Storey Number	Storey Height from Ground (in)	Storey Weight (kips)			
Base	0	0	0	0	0
1	132	27.3	0.4	13.92	4.37
2	264	27.3	0.8	21.84	17.47
3	396	27.3	1.2	32.76	39.31
4	528	27.3	1.6	43.68	69.89
5	660	13.65	1	13.65	13.65
	SUM	122.85	-	122.85	144.69
Conversion Factors					
			0.849		
	———		0.849		

Design drawings for each of the archetype buildings are provided in Figure A.13 through Figure A.28.

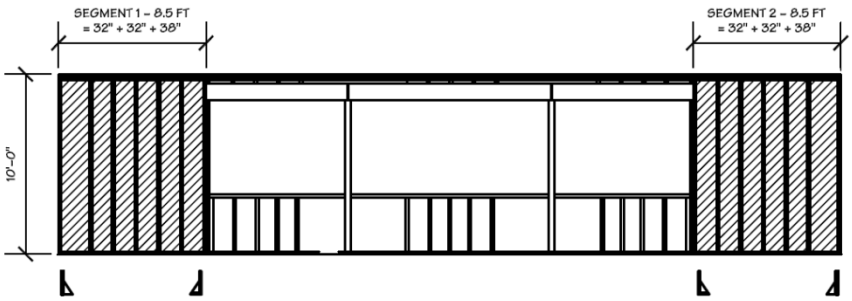

Figure A.13. Design drawings of archetype buildings, model # 1, commercial *2 x 8.5 ft* (Filiatrault, 2007)

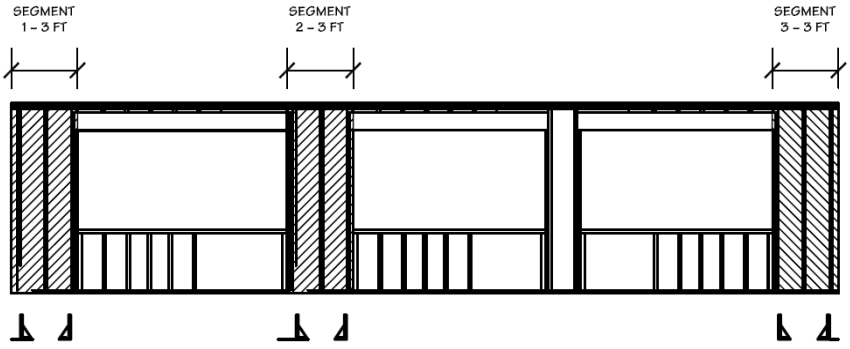

Figure A.14. Design drawings of archetype buildings, model # 2, residential *3 x 3 ft* (Filiatrault, 2007)

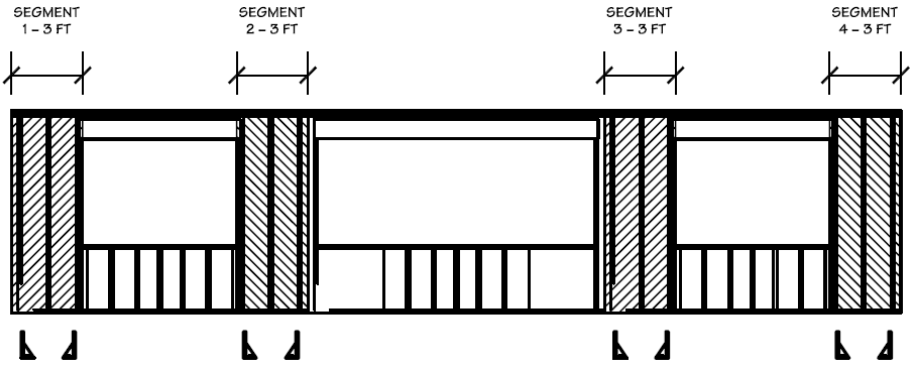

Figure A.15. Design drawings of archetype buildings, model # 3, commercial *4 x 3 ft* (Filiatrault, 2007)

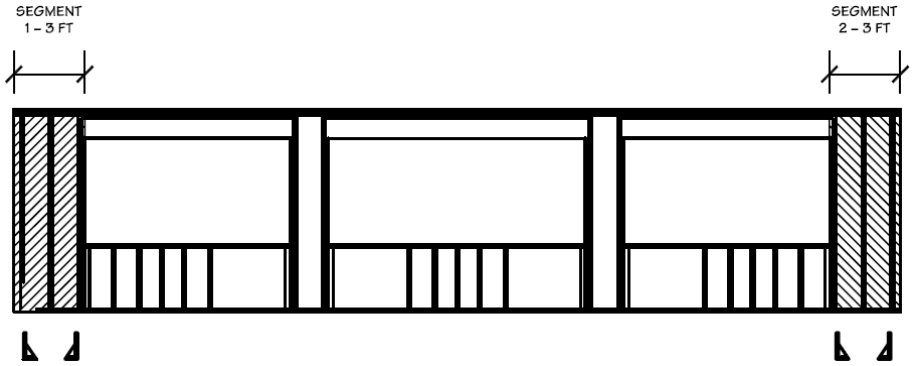

Figure A.16. Design drawings of archetype buildings, model # 4, residential *2 x 3 ft* (Filiatrault, 2007)

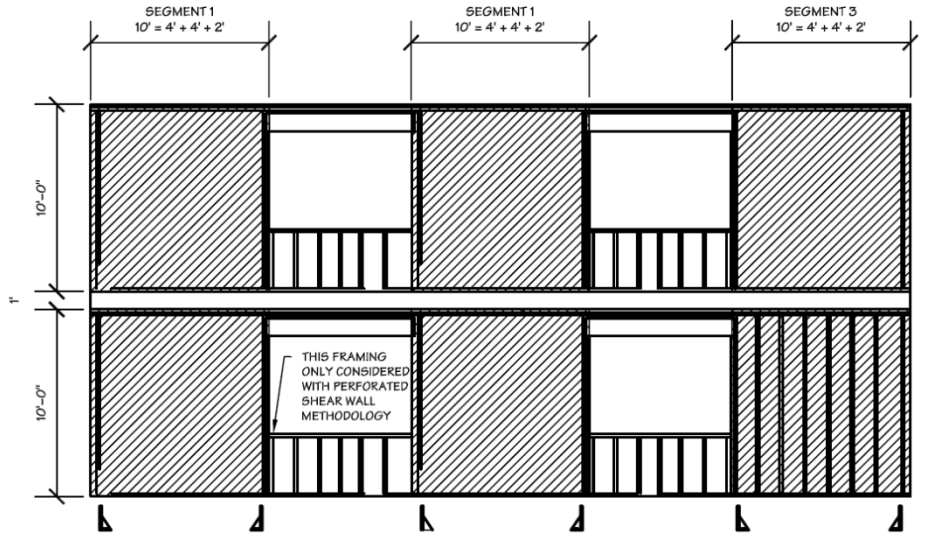

Figure A.17. Design drawings of archetype buildings, model # 5, commercial *3 x 10 ft* (Filiatrault, 2007)

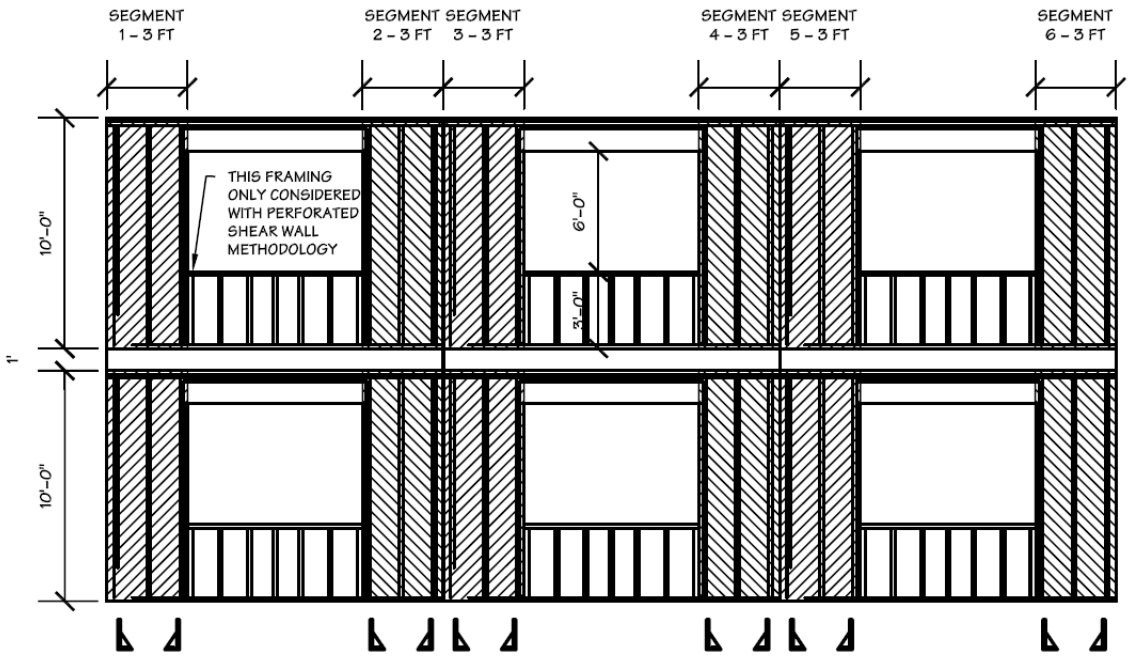

Figure A.18. Design drawings of archetype buildings, model # 6, residential *6 x 3 ft* (Filiatrault, 2007)

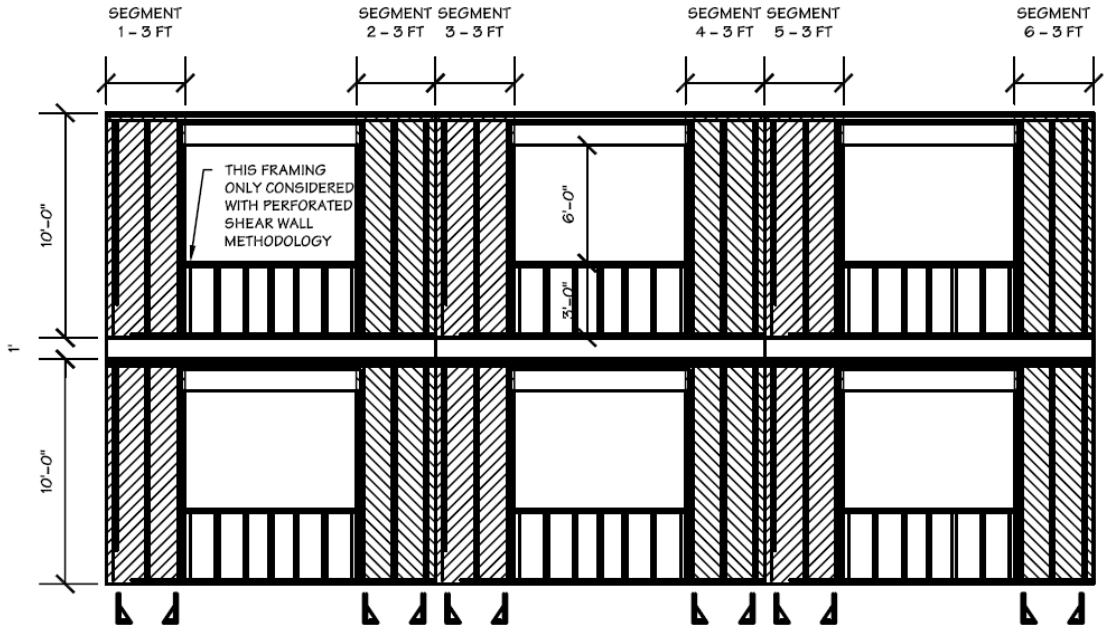

Figure A.19. Design drawings of archetype buildings, model # 7, commercial *6 x 3 ft* – six separate walls (Filiatrault, 2007)

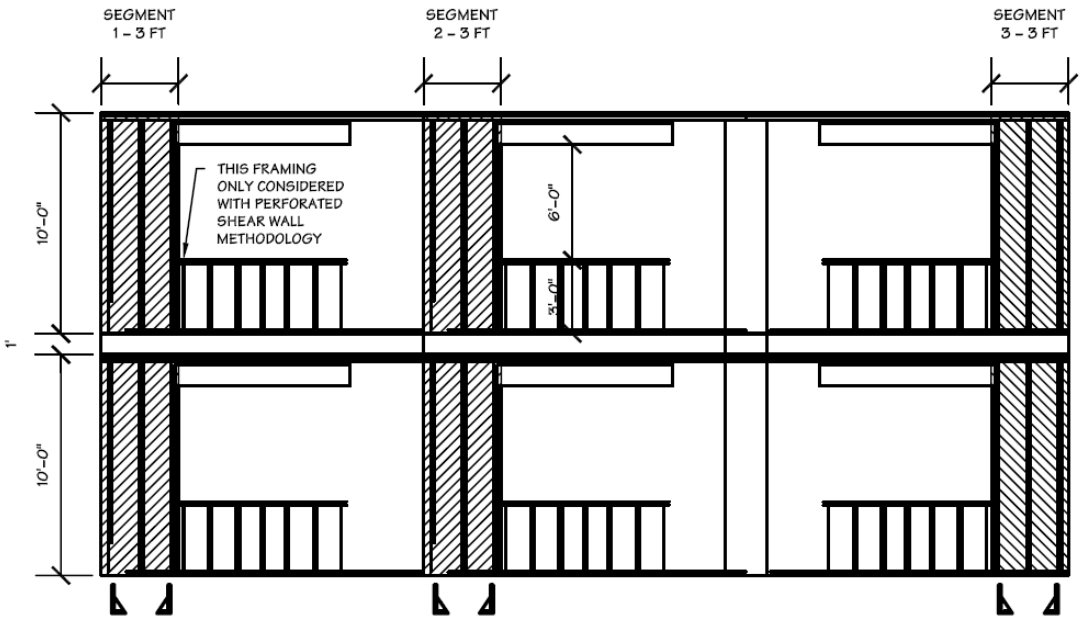

Figure A.20. Design drawings of archetype buildings, model # 8, residential *3 x 3 ft* (Filiatrault, 2007)

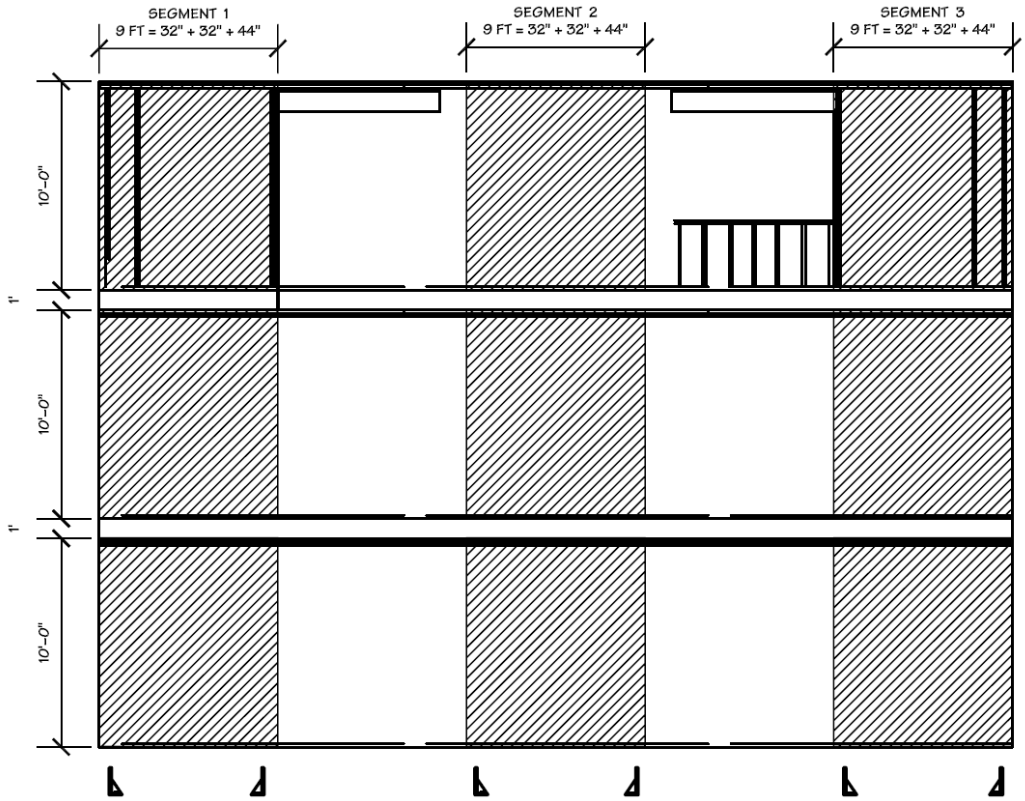

Figure A.21. Design drawings of archetype buildings, model # 9, commercial *3 x 9 ft* (Filiatrault, 2007)

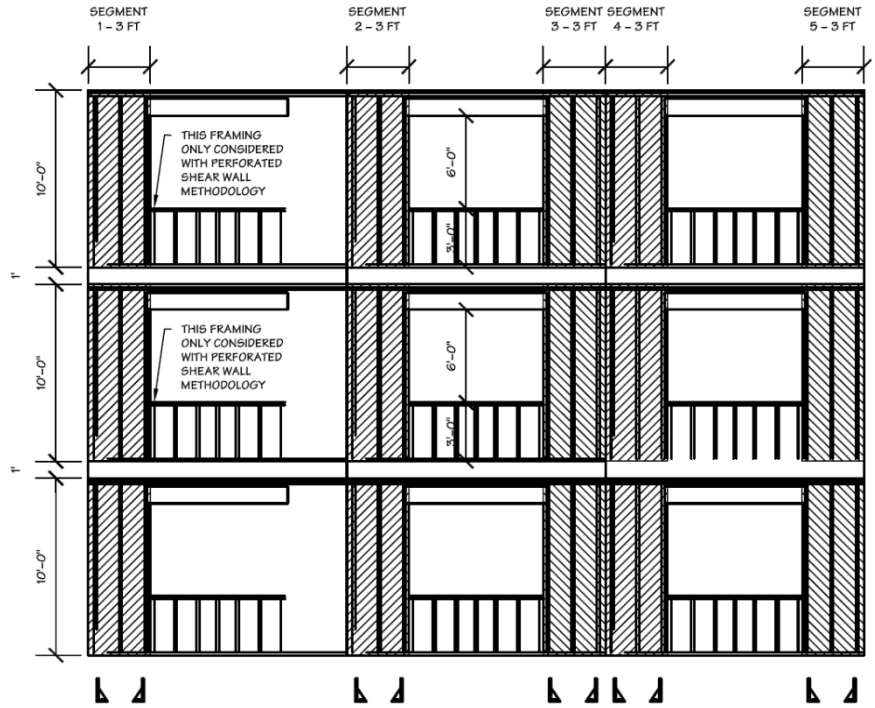

Figure A.22. Design drawings of archetype buildings, model # 10, residential *5 x 3 ft* – five separate walls (Filiatrault, 2007)

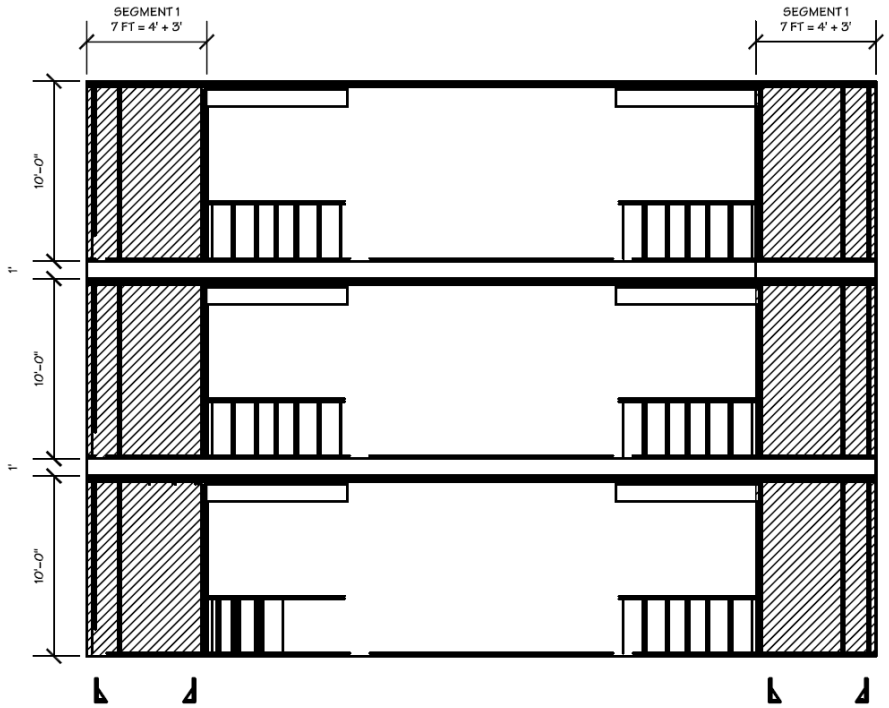

Figure A.23. Design drawings of archetype buildings, model # 11, commercial *2 x 7 ft* (Filiatrault, 2007)

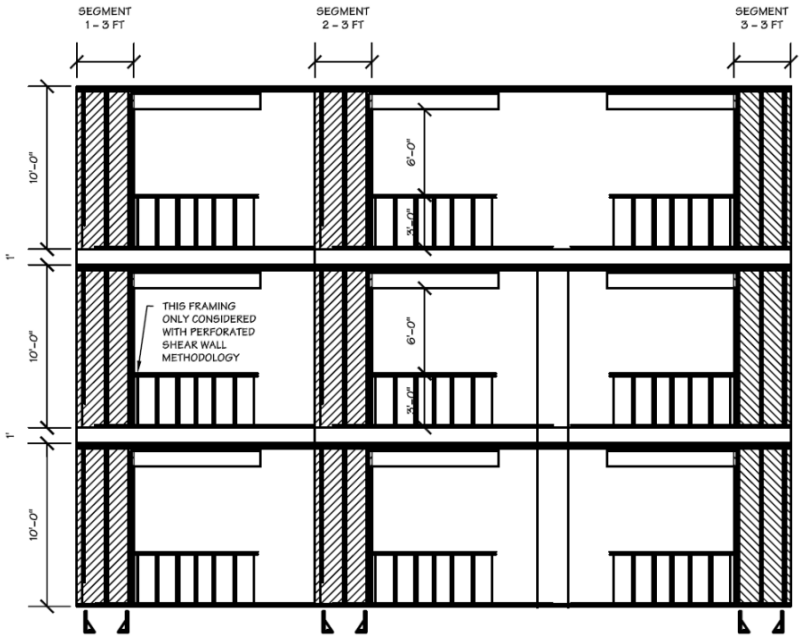

Figure A.24. Design drawings of archetype buildings, model # 12, residential *3 x 3 ft* (Filiatrault, 2007)

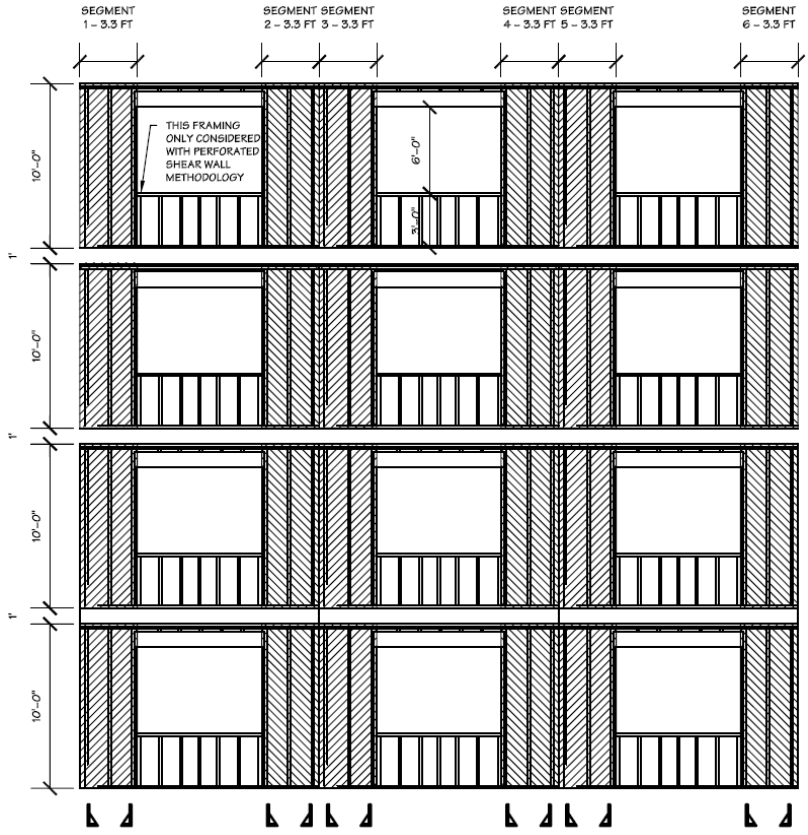

Figure A.25. Design drawings of archetype buildings, model # 13, residential *6 x 3.3 ft* – six separate walls (Filiatrault, 2007)

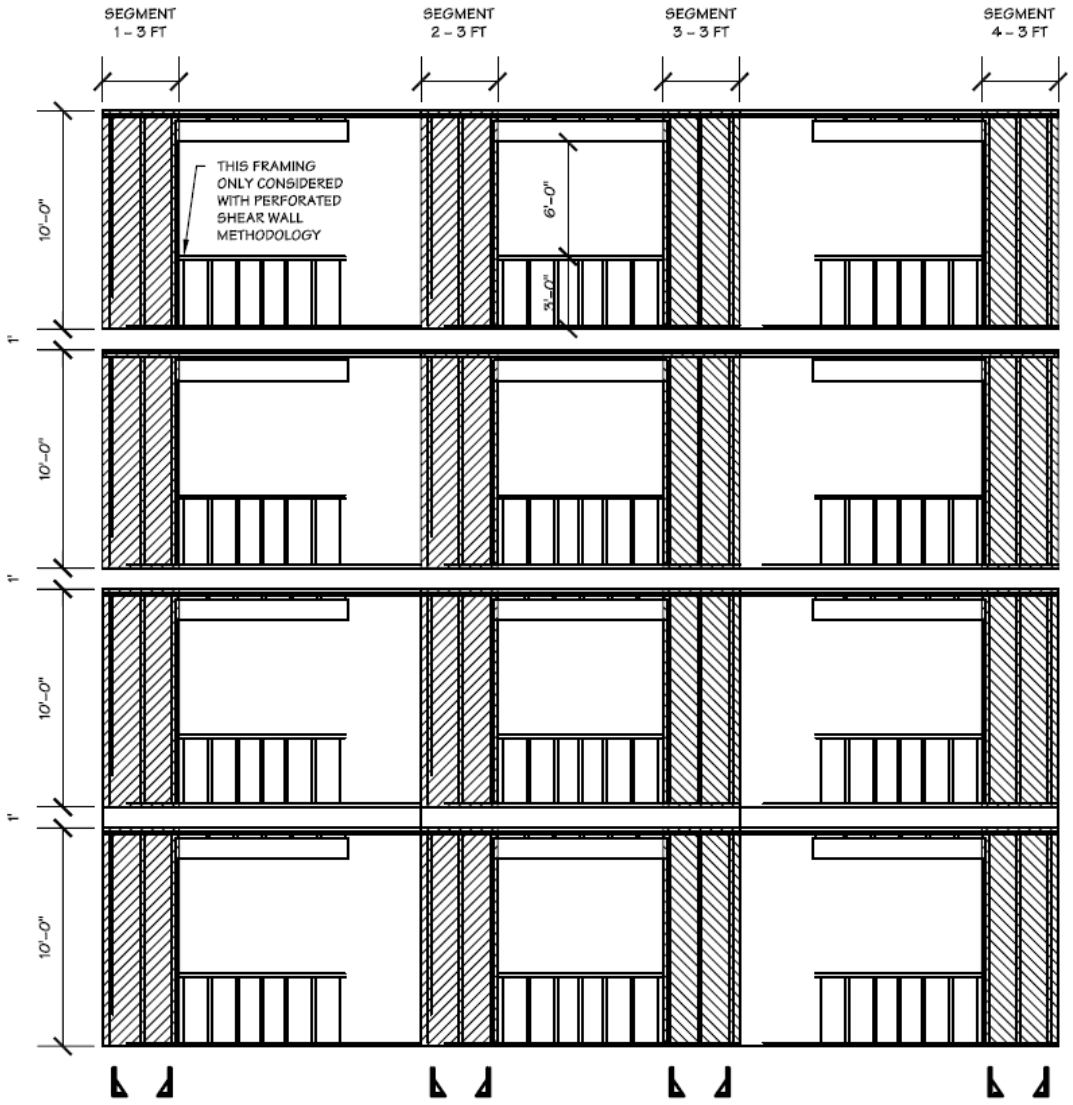

Figure A.26. Design drawings of archetype buildings, model # 14, residential *4 x 3 ft* (Filiatrault, 2007)

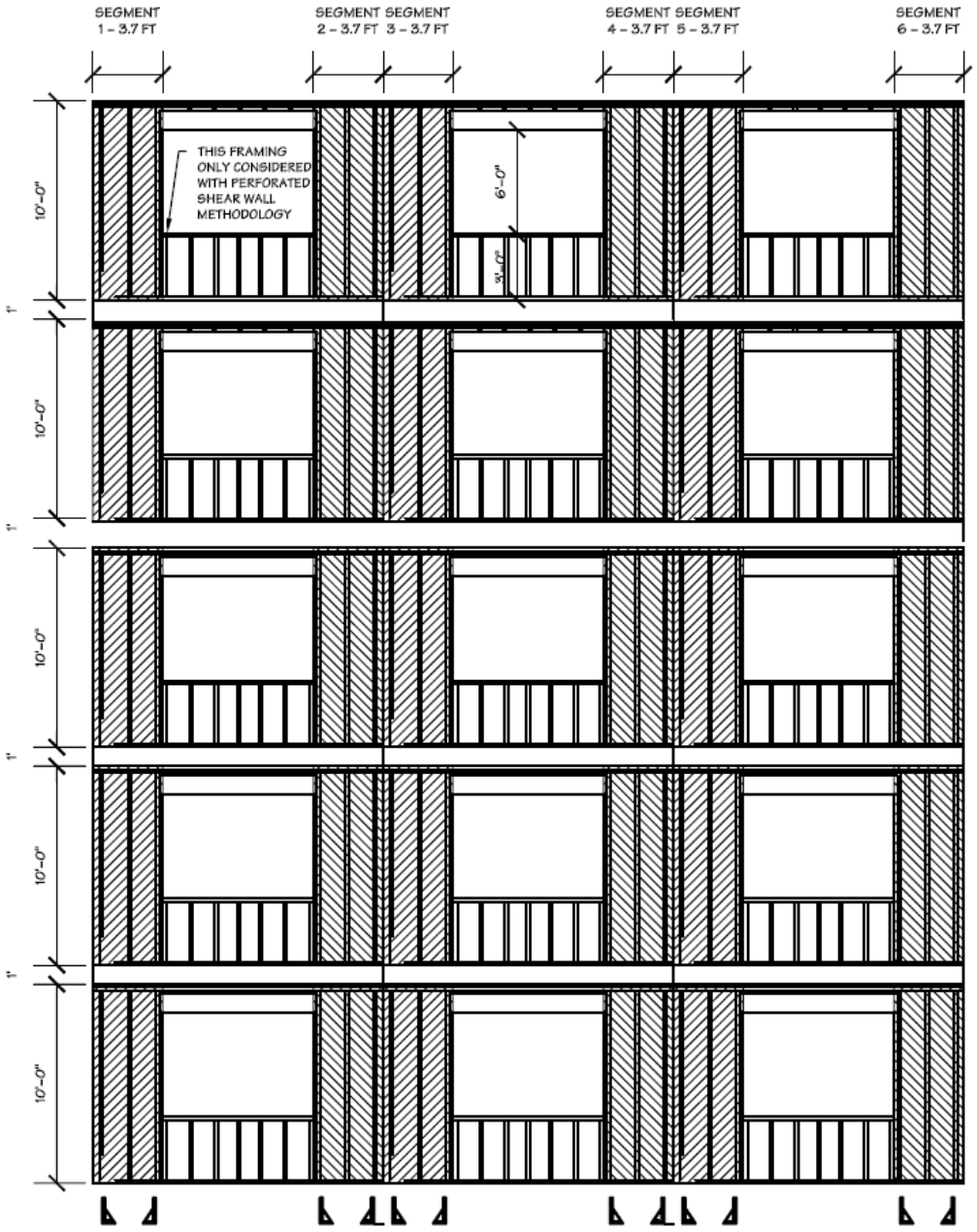

Figure A.27. Design drawings of archetype buildings, model # 15, residential *6 x 3.7 ft* – six separate walls (Filiatrault, 2007)

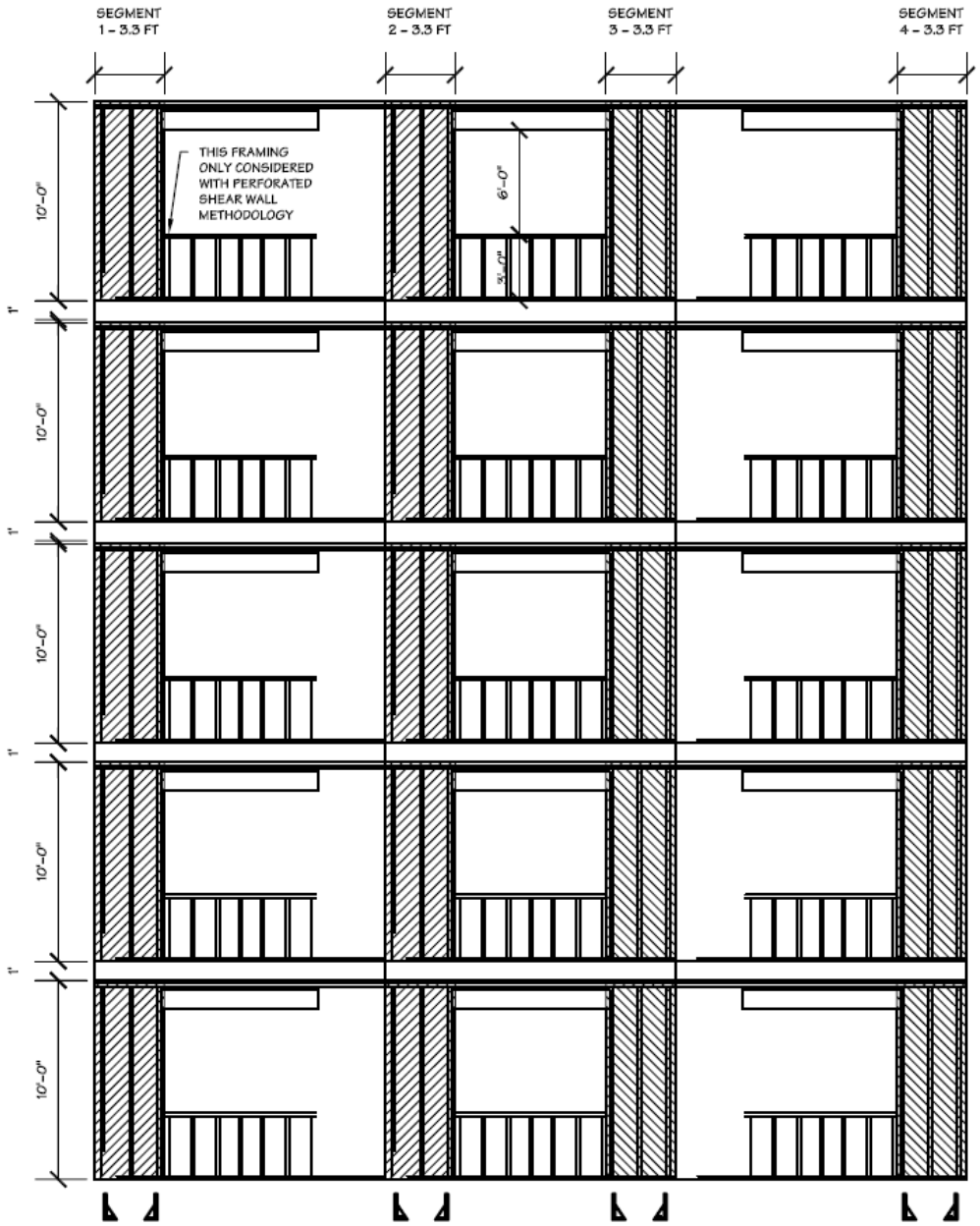

Figure A.28. Design drawings of archetype buildings, model # 16, residential *4 x 3.7 ft* (Filiatrault, 2007)

A.1.2.3. Texas A&M Woodframe Structures

The height and weight data as well as the constants for conversion of pushover curves to capacity diagrams for the three Texas A&M woodframe buildings, i.e. the one-storey, small two-storey, and large two-storey buildings, are given below. The small two-storey woodframe building is omitted since it would include the same parameters shown in Table A.1, as a result of having the same storey heights and weights as the phase 9 and 10 test structures.

Table A.18. Height and weight information and conversion factors from pushover curve to capacity diagram for one-storey woodframe structure

Storey Number	Storey Height from Ground (in)	Storey Weight (kips)	ϕ_i	$w_i\phi_i$	$w_i\phi_i^2$
Base	0	0	0	0	0
1	96	15	1	15	15
	SUM	15	-	15	15
Conversion Factors					
	$\boldsymbol{\Gamma}$		1		
	$\frac{\boldsymbol{\Gamma m^* g}}{\boldsymbol{W}}$		1		

Table A.19. Height and weight information and conversion factors from pushover curve to capacity diagram for large two-storey woodframe structure

Storey Number	Storey Height from Ground (in)	Storey Weight (kips)	ϕ_i	$w_i\phi_i$	$w_i\phi_i^2$
Base	0	0	0	0	0
1	96	37.7	0.65	24.68	16.15
2	192	28.8	1	28.80	28.80
	SUM	66.5	-	53.48	44.95
Conversion Factors					
	$\boldsymbol{\Gamma}$		1.190		
	$\frac{\boldsymbol{\Gamma m^* g}}{\boldsymbol{W}}$		0.957		

The dimensions and elevation views both in X and Y directions for these buildings are shown in Figure A.29 through Figure A.34.

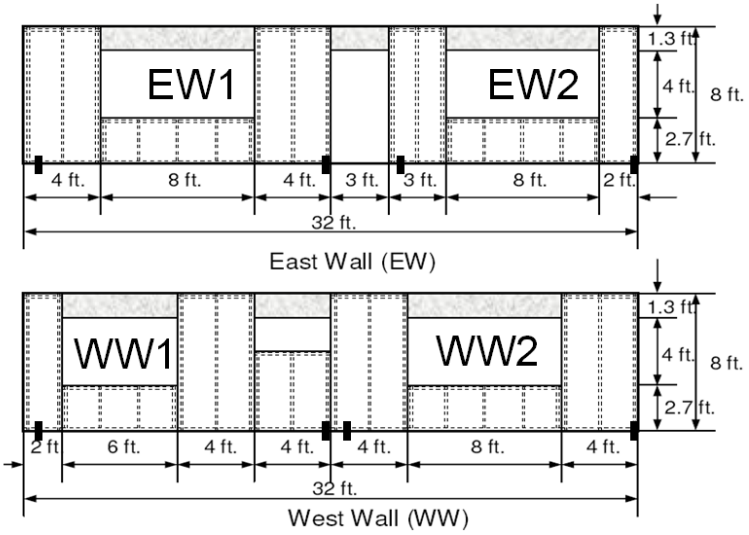

Figure A.29. X – direction elevation view and dimensioning of the one-storey woodframe building (Rosowsky and WeiChiang, 2007)

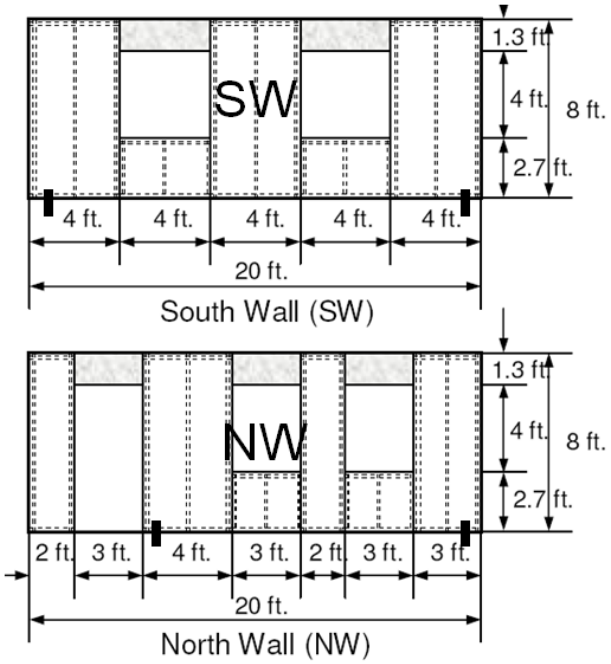

Figure A.30. Y – direction elevation view and dimensioning of the one-storey woodframe building (Rosowsky and WeiChiang, 2007)

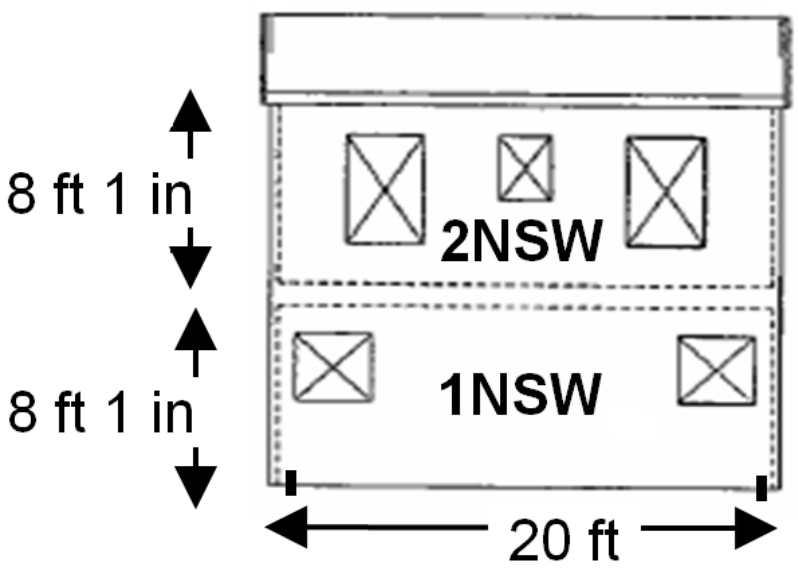

Figure A.31. X – direction elevation view and dimensioning of the small two-storey woodframe building (Rosowsky and WeiChiang, 2007)

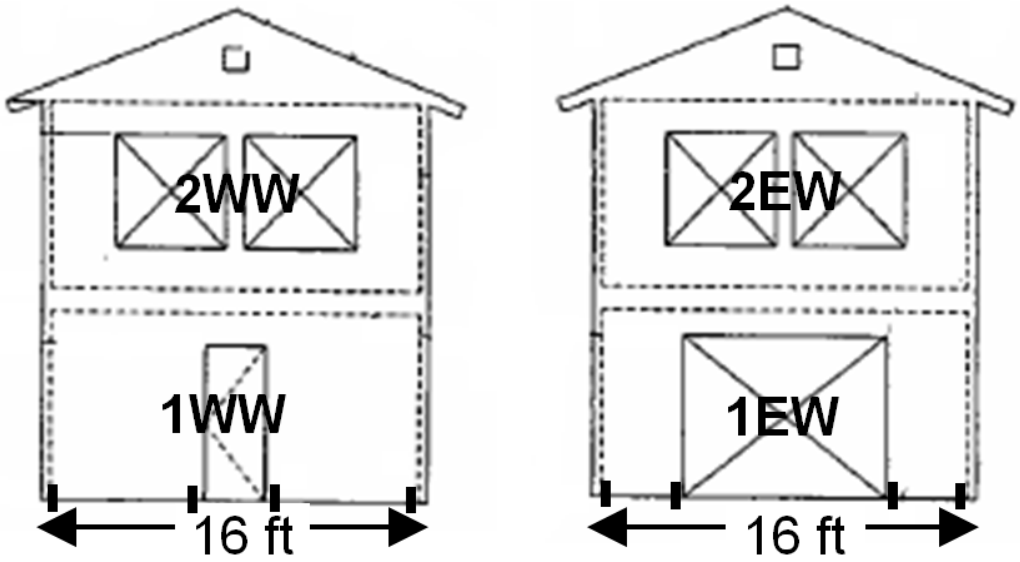

Figure A.32. Y – direction elevation view and dimensioning of the small two-storey woodframe building (Rosowsky and WeiChiang, 2007)

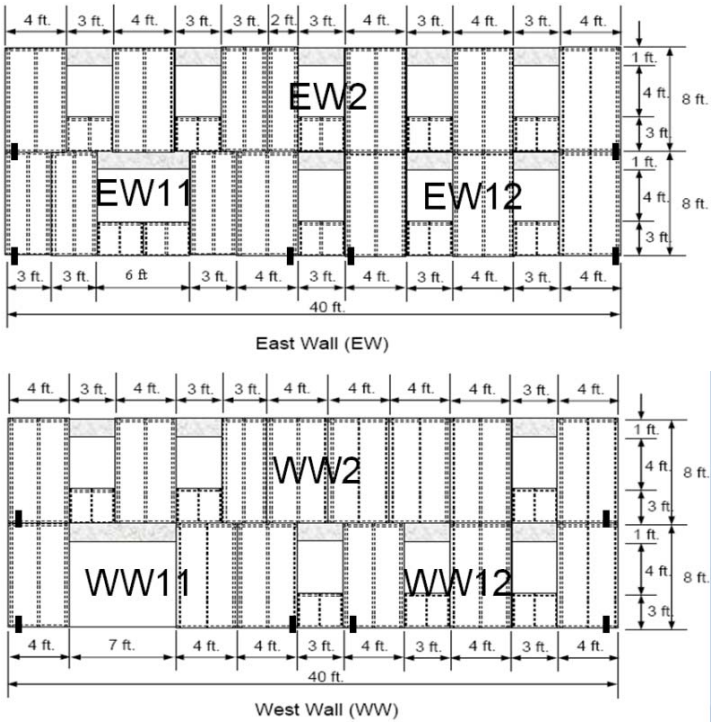

Figure A.33. X – direction elevation view and dimensioning of the large two-storey woodframe building (Rosowsky and WeiChiang, 2007)

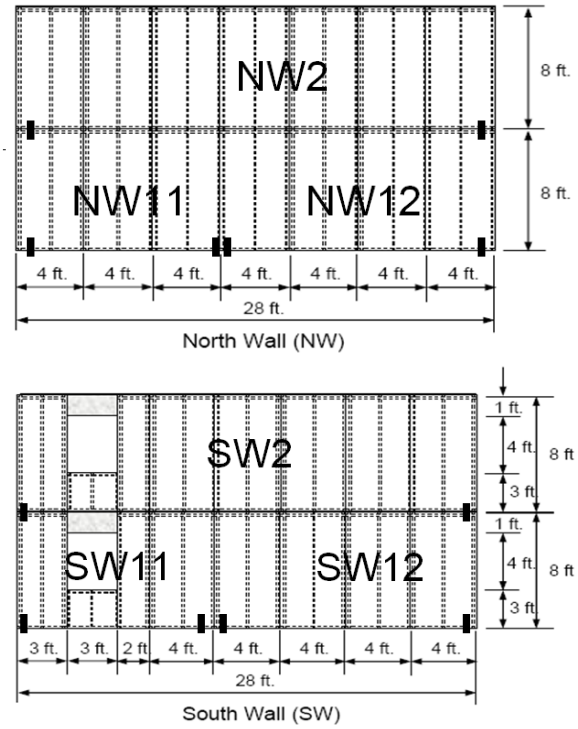

Figure A.34. Y – direction elevation view and dimensioning of the large two-storey woodframe building (Rosowsky and WeiChiang, 2007)

A.1.3. Capacity Diagrams and Performance Limit States

A.1.3.1. Woodframe Buildings in the Database

The categorization of each of the structural configurations included in the database for woodframe buildings is provided in Table A.20.

Table A.20. Classification of structural configurations in the database

Building Category	Structural Configuration
W1 – Pre-Code	Small House – Poor ATC-63 Model # 4 ATC-63 Model # 8
W1 – Low Code	Small House – Typical ATC-63 Model #2 ATC-63 Model #6 Texas A&M Large Two Storey
W1 – Moderate Code	Large House – Poor Small Townhouse – Poor Small Townhouse Typical Texas A&M – Small Two Storey
W1 – High Code	Phase 9 Test Structure Phase 10 Test Structure Small House – Superior Large House – Typical Large House – Superior Small Townhouse – Superior Texas A&M – One Storey
W2 – Pre-Code	ATC-63 Model #3 ATC-63 Model #7 ATC-63 Model #11 ATC-63 Model #12 ATC-63 Model #14 ATC-63 Model #16
W2 – Low Code	ATC-63 Model #1 ATC-63 Model #5 ATC-63 Model #9
W2 – Moderate Code	Apartment Building – Poor ATC-63 Model #10 ATC-63 Model #13 ATC-63 Model #15
W2 – High Code	Apartment Building – Typical Apartment Building – Superior

The threshold values for four limit states for structural damage, i.e. slight, moderate, extensive, and complete, are based on the definitions by Park (1988), shown in the below figures respectively.

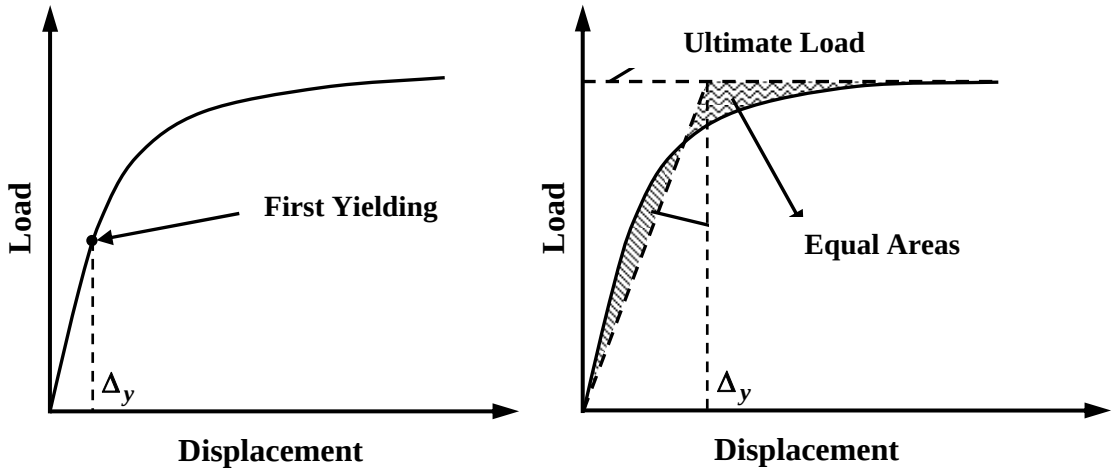

Figure A.35. Yield point definitions by Park (1988) used for determining structural damage states *(Left):* Slight damage; *(Right):* Moderate damage

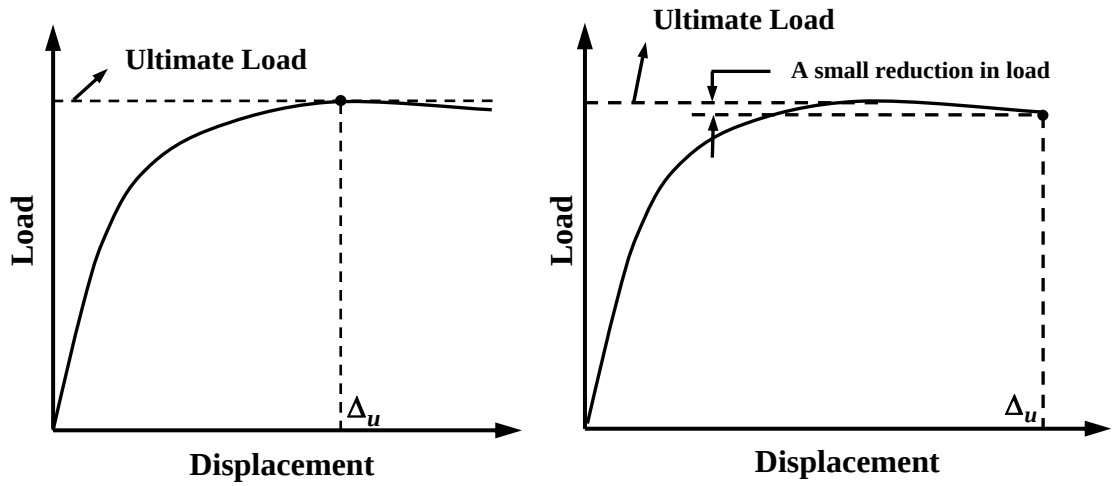

Figure A.36. Ultimate point definitions by Park (1988) used for determining structural damage states *(Left):* Moderate damage; *(Right):* Complete damage

A.1.3.2. Other Building Types Based on HAZUS

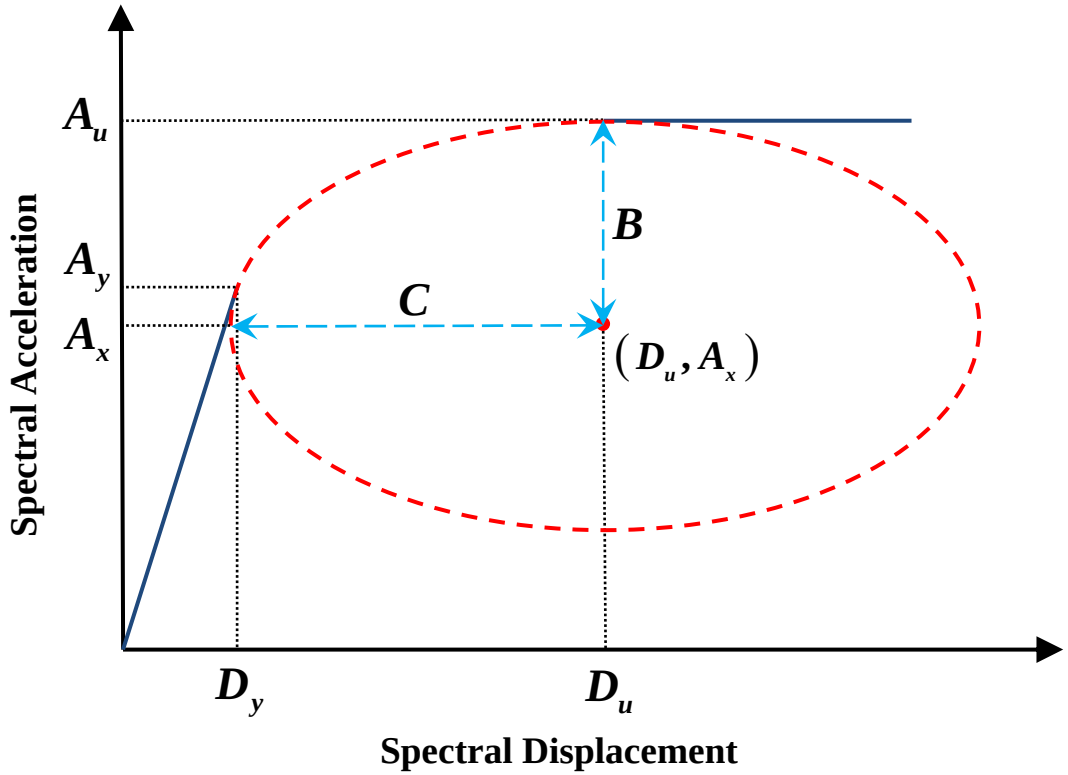

Figure A.37. Parameters of the elliptic curve segment

Based on the yield, (D_y, A_y), and ultimate points, (D_u, A_u), the elliptic curve segment defining the transition region between these two points can be described, using the notation by Cao and Petersen (2006), with the following equation.

$$\left(\frac{S_d - D_u}{C}\right)^2 + \left(\frac{S_a - A_x}{B}\right)^2 = 1 \qquad \text{(A.1)}$$

where S_d and S_a are the spectral displacement and spectral acceleration respectively and the parameters A_x, B and C are shown in Figure A.37. In order to define the ellipse completely the latter three parameters need to be determined. Two equations can be written using the yield and ultimate points (ellipse should pass through these points) and the third equation is obtained by the compatibility of slope at the yield point (for smooth transaction between the linear segment and the elliptic curve):

$$\frac{dS_a}{dS_d} = \frac{A_y}{D_y} - \left(\frac{S_d - D_u}{S_a - A_x}\right)\left(\frac{B}{C}\right)^2 \qquad \text{(A.2)}$$

The three equations can be solved for the three unknowns A_x, B and C allowing the complete definition of Eq. (A.1).

The parameters of the yield and ultimate points, i.e. D_y, A_y, D_u and A_u as well as those of the elliptic curve, i.e. A_x, B, C are provided in the below tables for the for seismic design levels of pre-, low, moderate, and high code. Limit state threshold values are also included in the same tables.

It is important to note that the modal height values given in the below tables are calculated by multiplying building height, given in Table 3.1, by the parameter "fraction of building height at location of pushover-mode displacement" defined in HAZUS (HAZUS Technical Manual Chapter 5 - National Institute of Building Sciences, 2003). The zeros in Table A.23 and Table A.24 are due to those building types being not permitted by the current seismic design codes.

Table A.21. Limit state threshold values and parameters of the capacity diagrams, pre-code seismic design level (B. T.: Building Type; M.H.: Modal Height in inches; S: Slight; M: Moderate; E: Extensive; C: Complete are in terms of roof drift; D_y, D_u, B and C are in inches; A_y, A_u and A_x are in g's)

Pre-Code Seismic Design Level												
		Dmg. Stat. Thrsh. Val.				Cap. Diag. Param.				Ellip. Cur. Param.		
B. T.	**M. H.**	**S**	**M**	**E**	**C**	D_y	A_y	D_u	A_u	A_x	B	C
W1	126	0.0032	0.0079	0.0245	0.0600	0.24	0.20	4.32	0.60	0.14	0.46	4.12
W2	216	0.0032	0.0079	0.0245	0.0600	0.16	0.10	2.35	0.25	0.08	0.17	2.21
S1L	216	0.0048	0.0076	0.0162	0.0400	0.15	0.06	2.75	0.19	0.04	0.14	2.62
S1M	540	0.0032	0.0051	0.0108	0.0267	0.44	0.04	5.33	0.12	0.02	0.10	5.01
S1H	1123	0.0024	0.0038	0.0081	0.0200	1.16	0.02	10.48	0.07	0.00	0.07	9.88
S2L	216	0.0040	0.0064	0.0160	0.0400	0.16	0.10	1.88	0.20	0.09	0.11	1.73
S2M	540	0.0027	0.0043	0.0107	0.0267	0.61	0.08	4.85	0.17	0.07	0.10	4.30
S2H	1123	0.0020	0.0032	0.0080	0.0200	1.94	0.06	11.62	0.13	0.04	0.09	9.99
S3	135	0.0032	0.0051	0.0128	0.0350	0.16	0.10	1.88	0.20	0.09	0.11	1.73
S4L	216	0.0032	0.0051	0.0128	0.0350	0.10	0.08	1.30	0.18	0.07	0.11	1.21
S4M	540	0.0021	0.0034	0.0086	0.0233	0.27	0.07	2.46	0.15	0.05	0.10	2.22
S4H	1123	0.0016	0.0026	0.0064	0.0175	0.87	0.05	5.88	0.11	0.03	0.09	5.22
S5L	216	0.0024	0.0048	0.0120	0.0280	0.12	0.10	1.20	0.20	0.09	0.11	1.09
S5M	540	0.0016	0.0032	0.0080	0.0187	0.34	0.08	2.27	0.17	0.06	0.11	1.97
S5H	1123	0.0012	0.0024	0.0060	0.0140	1.09	0.06	5.45	0.13	0.03	0.09	4.63
C1L	180	0.0040	0.0064	0.0160	0.0400	0.10	0.06	1.76	0.19	0.04	0.14	1.68
C1M	450	0.0027	0.0043	0.0107	0.0267	0.29	0.05	3.46	0.16	0.02	0.13	3.25
C1H	864	0.0020	0.0032	0.0080	0.0200	0.50	0.02	4.52	0.07	0.00	0.07	4.26

Table A.21. (Continued)

Pre-Code Seismic Design Level												
		Dmg. Stat. Thrsh. Val.				Cap. Diag. Param.				Ellip. Cur. Param.		
B. T.	**M. H.**	**S**	**M**	**E**	**C**	D_y	A_y	D_u	A_u	A_x	B	C
C2L	180	0.0032	0.0061	0.0158	0.0400	0.12	0.10	1.80	0.25	0.08	0.17	1.69
C2M	450	0.0021	0.0041	0.0105	0.0267	0.26	0.08	2.60	0.21	0.05	0.16	2.39
C2H	864	0.0016	0.0031	0.0079	0.0200	0.74	0.06	5.51	0.16	0.02	0.14	5.01
C3L	180	0.0024	0.0048	0.0120	0.0280	0.12	0.10	1.35	0.23	0.08	0.15	1.24
C3M	450	0.0016	0.0032	0.0080	0.0187	0.26	0.08	1.95	0.19	0.05	0.14	1.74
C3H	864	0.0012	0.0024	0.0060	0.0140	0.74	0.06	4.13	0.14	0.02	0.13	3.66
PC1	135	0.0032	0.0051	0.0128	0.0350	0.18	0.15	2.16	0.30	0.13	0.17	1.99
PC2L	180	0.0032	0.0051	0.0128	0.0350	0.12	0.10	1.44	0.20	0.09	0.11	1.33
PC2M	450	0.0021	0.0034	0.0086	0.0233	0.26	0.08	2.08	0.17	0.07	0.10	1.85
PC2H	864	0.0016	0.0026	0.0064	0.0175	0.74	0.06	4.41	0.13	0.04	0.08	3.79
RM1L	180	0.0032	0.0051	0.0128	0.0350	0.16	0.13	1.92	0.27	0.12	0.15	1.77
RM1M	450	0.0021	0.0034	0.0086	0.0233	0.35	0.11	2.77	0.22	0.09	0.13	2.46
RM2L	180	0.0032	0.0051	0.0128	0.0350	0.16	0.13	1.92	0.27	0.12	0.15	1.77
RM2M	450	0.0021	0.0034	0.0086	0.0233	0.35	0.11	2.77	0.22	0.09	0.13	2.46
RM2H	864	0.0016	0.0026	0.0064	0.0175	0.98	0.09	5.88	0.17	0.06	0.11	5.06
URML	135	0.0024	0.0048	0.0120	0.0280	0.24	0.20	2.40	0.40	0.17	0.23	2.18
URMM	315	0.0016	0.0032	0.0080	0.0187	0.27	0.11	1.81	0.22	0.08	0.14	1.57
MH	120	0.0032	0.0064	0.0192	0.0560	0.18	0.15	2.16	0.30	0.13	0.17	1.99

Table A.22. Limit state threshold values and parameters of the capacity diagrams, low code seismic design level (B. T.: Building Type; M.H.: Modal Height in inches; S: Slight; M: Moderate; E: Extensive; C: Complete are in terms of roof drift; D_y, D_u, B and C are in inches; A_y, A_u and A_x are in g's)

Low Code Seismic Design Level												
		Dmg. Stat. Thrsh. Val.				Cap. Diag. Param.				Ellip. Cur. Param.		
B. T.	**M. H.**	**S**	**M**	**E**	**C**	D_y	A_y	D_u	A_u	A_x	B	C
W1	126	0.0040	0.0099	0.0306	0.0750	0.24	0.20	4.32	0.60	0.14	0.46	4.12
W2	216	0.0040	0.0099	0.0306	0.0750	0.16	0.10	2.35	0.25	0.08	0.17	2.21
S1L	216	0.0060	0.0096	0.0203	0.0500	0.15	0.06	2.29	0.19	0.04	0.15	2.17
S1M	540	0.0040	0.0064	0.0135	0.0333	0.44	0.04	4.44	0.12	0.01	0.11	4.17
S1H	1123	0.0030	0.0048	0.0101	0.0250	1.16	0.02	8.73	0.07	-0.01	0.09	8.45
S2L	216	0.0050	0.0080	0.0200	0.0500	0.16	0.10	1.57	0.20	0.09	0.11	1.42
S2M	540	0.0033	0.0053	0.0133	0.0333	0.61	0.08	4.04	0.17	0.06	0.11	3.52
S2H	1123	0.0025	0.0040	0.0100	0.0250	1.94	0.06	9.68	0.13	0.03	0.10	8.21
S3	135	0.0040	0.0064	0.0161	0.0438	0.16	0.10	1.57	0.20	0.09	0.11	1.42

Table A.22. (Continued)

		Low Code Seismic Design Level										
		Dmg. Stat. Thrsh. Val.				Cap. Diag. Param.				Ellip. Cur. Param.		
B. T.	**M. H.**	**S**	**M**	**E**	**C**	D_y	A_y	D_u	A_u	A_x	B	C
S4L	216	0.0040	0.0064	0.0161	0.0438	0.10	0.08	1.08	0.18	0.06	0.12	0.99
S4M	540	0.0027	0.0043	0.0107	0.0292	0.27	0.07	2.05	0.15	0.04	0.11	1.83
S4H	1123	0.0020	0.0032	0.0080	0.0219	0.87	0.05	4.90	0.11	0.01	0.10	4.34
S5L	216	0.0030	0.0060	0.0150	0.0350	0.12	0.10	1.20	0.20	0.09	0.11	1.09
S5M	540	0.0020	0.0040	0.0100	0.0233	0.34	0.08	2.27	0.17	0.06	0.11	1.97
S5H	1123	0.0015	0.0030	0.0075	0.0175	1.09	0.06	5.45	0.13	0.03	0.09	4.63
C1L	180	0.0050	0.0080	0.0200	0.0500	0.10	0.06	1.47	0.19	0.04	0.15	1.39
C1M	450	0.0033	0.0053	0.0133	0.0333	0.29	0.05	2.88	0.16	0.01	0.15	2.70
C1H	864	0.0025	0.0040	0.0100	0.0250	0.50	0.02	3.77	0.07	-0.01	0.09	3.65
C2L	180	0.0040	0.0076	0.0197	0.0500	0.12	0.10	1.50	0.25	0.07	0.18	1.40
C2M	450	0.0027	0.0051	0.0132	0.0333	0.26	0.08	2.16	0.21	0.04	0.17	1.97
C2H	864	0.0020	0.0038	0.0099	0.0250	0.74	0.06	4.59	0.16	0.00	0.16	4.21
C3L	180	0.0030	0.0060	0.0150	0.0350	0.12	0.10	1.35	0.23	0.08	0.15	1.24
C3M	450	0.0020	0.0040	0.0100	0.0233	0.26	0.08	1.95	0.19	0.05	0.14	1.74
C3H	864	0.0015	0.0030	0.0075	0.0175	0.74	0.06	4.13	0.14	0.02	0.13	3.66
PC1	135	0.0040	0.0064	0.0161	0.0438	0.18	0.15	1.80	0.30	0.13	0.17	1.63
PC2L	180	0.0040	0.0064	0.0161	0.0438	0.12	0.10	1.20	0.20	0.09	0.11	1.09
PC2M	450	0.0027	0.0043	0.0107	0.0292	0.26	0.08	1.73	0.17	0.06	0.11	1.51
PC2H	864	0.0020	0.0032	0.0080	0.0219	0.74	0.06	3.67	0.13	0.03	0.10	3.11
RM1L	180	0.0040	0.0064	0.0161	0.0438	0.16	0.13	1.60	0.27	0.11	0.15	1.45
RM1M	450	0.0027	0.0043	0.0107	0.0292	0.35	0.11	2.31	0.22	0.08	0.14	2.01
RM2L	180	0.0040	0.0064	0.0161	0.0438	0.16	0.13	1.60	0.27	0.11	0.15	1.45
RM2M	450	0.0027	0.0043	0.0107	0.0292	0.35	0.11	2.31	0.22	0.08	0.14	2.01
RM2H	864	0.0020	0.0032	0.0080	0.0219	0.98	0.09	4.90	0.17	0.04	0.13	4.16
URML	135	0.0030	0.0060	0.0150	0.0350	0.24	0.20	2.40	0.40	0.17	0.23	2.18
URMM	315	0.0020	0.0040	0.0100	0.0233	0.27	0.11	1.81	0.22	0.08	0.14	1.57
MH	120	0.0040	0.0080	0.0240	0.0700	0.18	0.15	2.16	0.30	0.13	0.17	1.99

Table A.23. Limit state threshold values and parameters of the capacity diagrams, moderate code seismic design level (B. T.: Building Type; M.H.: Modal Height in inches; S: Slight; M: Moderate; E: Extensive; C: Complete are in terms of roof drift; D_y, D_u, B and C are in inches; A_y, A_u and A_x are in g's)

Moderate Code Seismic Design Level												
		Dmg. Stat. Thrsh. Val.				Cap. Diag. Param.				Ellip. Cur. Param.		
B. T.	**M. H.**	**S**	**M**	**E**	**C**	D_y	A_y	D_u	A_u	A_x	B	C
W1	126	0.0040	0.0099	0.0306	0.0750	0.36	0.30	6.48	0.90	0.21	0.69	6.17
W2	216	0.0040	0.0099	0.0306	0.0750	0.31	0.20	4.70	0.50	0.16	0.34	4.42
S1L	216	0.0060	0.0104	0.0235	0.0600	0.31	0.13	5.50	0.38	0.09	0.29	5.24
S1M	540	0.0040	0.0069	0.0157	0.0400	0.89	0.08	10.65	0.23	0.03	0.20	10.01
S1H	1123	0.0030	0.0052	0.0118	0.0300	2.33	0.05	20.96	0.15	0.00	0.15	19.77
S2L	216	0.0050	0.0087	0.0233	0.0600	0.31	0.20	3.76	0.40	0.18	0.22	3.46
S2M	540	0.0033	0.0058	0.0156	0.0400	1.21	0.17	9.70	0.33	0.13	0.20	8.61
S2H	1123	0.0025	0.0043	0.0117	0.0300	3.87	0.13	23.24	0.25	0.08	0.17	19.99
S3	135	0.0040	0.0070	0.0187	0.0525	0.31	0.20	3.76	0.40	0.18	0.22	3.46
S4L	216	0.0040	0.0069	0.0187	0.0525	0.19	0.16	2.59	0.36	0.13	0.23	2.41
S4M	540	0.0027	0.0046	0.0125	0.0350	0.55	0.13	4.91	0.30	0.09	0.21	4.44
S4H	1123	0.0020	0.0035	0.0093	0.0262	1.74	0.10	11.76	0.23	0.05	0.17	10.43
S5L	216	0	0	0	0	0	0	0	0	0	0	0
S5M	540	0	0	0	0	0	0	0	0	0	0	0
S5H	1123	0	0	0	0	0	0	0	0	0	0	0
C1L	180	0.0050	0.0087	0.0233	0.0600	0.20	0.13	3.52	0.38	0.09	0.29	3.35
C1M	450	0.0033	0.0058	0.0156	0.0400	0.58	0.10	6.91	0.31	0.04	0.27	6.50
C1H	864	0.0025	0.0043	0.0117	0.0300	1.01	0.05	9.05	0.15	0.00	0.15	8.54
C2L	180	0.0040	0.0084	0.0232	0.0600	0.24	0.20	3.60	0.50	0.16	0.34	3.38
C2M	450	0.0027	0.0056	0.0154	0.0400	0.52	0.17	5.19	0.42	0.11	0.31	4.77
C2H	864	0.0020	0.0042	0.0116	0.0300	1.47	0.13	11.02	0.32	0.04	0.27	10.01
C3L	180	0	0	0	0	0	0	0	0	0	0	0
C3M	450	0	0	0	0	0	0	0	0	0	0	0
C3H	864	0	0	0	0	0	0	0	0	0	0	0
PC1	135	0.0040	0.0070	0.0187	0.0525	0.36	0.30	4.32	0.60	0.27	0.33	3.98
PC2L	180	0.0040	0.0069	0.0187	0.0525	0.24	0.20	2.88	0.40	0.18	0.22	2.65
PC2M	450	0.0027	0.0046	0.0125	0.0350	0.52	0.17	4.15	0.33	0.13	0.20	3.69
PC2H	864	0.0020	0.0035	0.0094	0.0263	1.47	0.13	8.82	0.25	0.08	0.17	7.59
RM1L	180	0.0040	0.0069	0.0187	0.0525	0.32	0.27	3.84	0.53	0.24	0.30	3.54
RM1M	450	0.0027	0.0046	0.0125	0.0350	0.69	0.22	5.54	0.44	0.18	0.27	4.92

Table A.23. (Continued)

Moderate Code Seismic Design Level												
		Dmg. Stat. Thrsh. Val.				Cap. Diag. Param.				Ellip. Cur. Param.		
B. T.	**M. H.**	**S**	**M**	**E**	**C**	D_y	A_y	D_u	A_u	A_x	B	C
RM2L	180	0.0040	0.0069	0.0187	0.0525	0.32	0.27	3.84	0.53	0.24	0.30	3.54
RM2M	450	0.0027	0.0046	0.0125	0.0350	0.69	0.22	5.54	0.44	0.18	0.27	4.92
RM2H	864	0.0020	0.0035	0.0094	0.0263	1.96	0.17	11.76	0.34	0.11	0.23	10.12
URML	135	0	0	0	0	0	0	0	0	0	0	0
URMM	315	0	0	0	0	0	0	0	0	0	0	0
MH	120	0.0040	0.0080	0.0240	0.0700	0.18	0.15	2.16	0.30	0.13	0.17	1.99

Table A.24. Limit state threshold values and parameters of the capacity diagrams, high code seismic design level (B. T.: Building Type; M.H.: Modal Height in inches; S: Slight; M: Moderate; E: Extensive; C: Complete are in terms of roof drift; D_y, D_u, B and C are in inches; A_y, A_u and A_x are in g's)

Moderate Code Seismic Design Level												
		Dmg. Stat. Thrsh. Val.				Cap. Diag. Param.				Ellip. Cur. Param.		
B. T.	**M. H.**	**S**	**M**	**E**	**C**	D_y	A_y	D_u	A_u	A_x	B	C
W1	126	0.0040	0.0120	0.0400	0.1000	0.48	0.40	11.51	1.20	0.32	0.88	11.08
W2	216	0.0040	0.0120	0.0400	0.1000	0.63	0.40	12.53	1.00	0.34	0.66	11.95
S1L	216	0.0060	0.0120	0.0300	0.0800	0.61	0.25	14.67	0.75	0.20	0.55	14.12
S1M	540	0.0040	0.0080	0.0200	0.0533	1.78	0.16	28.40	0.47	0.10	0.37	26.94
S1H	1123	0.0030	0.0060	0.0150	0.0400	4.66	0.10	55.88	0.29	0.04	0.25	52.53
S2L	216	0.0050	0.0100	0.0300	0.0800	0.63	0.40	10.02	0.80	0.37	0.43	9.42
S2M	540	0.0033	0.0067	0.0200	0.0533	2.43	0.33	25.88	0.67	0.29	0.38	23.62
S2H	1123	0.0025	0.0050	0.0150	0.0400	7.75	0.25	61.97	0.51	0.20	0.31	54.95
S3	135	0.0040	0.0080	0.0240	0.0700	0.63	0.40	10.02	0.80	0.37	0.43	9.42
S4L	216	0.0040	0.0080	0.0240	0.0700	0.38	0.32	6.91	0.72	0.29	0.43	6.55
S4M	540	0.0027	0.0053	0.0160	0.0467	1.09	0.27	13.10	0.60	0.22	0.38	12.10
S4H	1123	0.0020	0.0040	0.0120	0.0350	3.49	0.20	31.37	0.46	0.15	0.31	28.38
S5L	216	0	0	0	0	0	0	0	0	0	0	0
S5M	540	0	0	0	0	0	0	0	0	0	0	0
S5H	1123	0	0	0	0	0	0	0	0	0	0	0
C1L	180	0.0050	0.0100	0.0300	0.0800	0.39	0.25	9.39	0.75	0.20	0.55	9.04
C1M	450	0.0033	0.0067	0.0200	0.0533	1.15	0.21	18.44	0.62	0.13	0.49	17.50
C1H	864	0.0025	0.0050	0.0150	0.0400	2.01	0.10	24.13	0.29	0.04	0.25	22.69
C2L	180	0.0040	0.0100	0.0300	0.0800	0.48	0.40	9.59	1.00	0.34	0.66	9.14
C2M	450	0.0027	0.0067	0.0200	0.0533	1.04	0.33	13.84	0.83	0.25	0.58	12.94
C2H	864	0.0020	0.0050	0.0150	0.0400	2.94	0.25	29.39	0.64	0.16	0.48	26.99

Table A.24. (Continued)

		Moderate Code Seismic Design Level										
		Dmg. Stat. Thrsh. Val.				Cap. Diag. Param.				Ellip. Cur. Param.		
B. T.	**M. H.**	**S**	**M**	**E**	**C**	D_y	A_y	D_u	A_u	A_x	B	C
C3L	180	0	0	0	0	0	0	0	0	0	0	0
C3M	450	0	0	0	0	0	0	0	0	0	0	0
C3H	864	0	0	0	0	0	0	0	0	0	0	0
PC1	135	0.0040	0.0080	0.0240	0.0700	0.72	0.60	11.51	1.20	0.55	0.65	10.82
PC2L	180	0.0040	0.0080	0.0240	0.0700	0.48	0.40	7.67	0.80	0.37	0.43	7.21
PC2M	450	0.0027	0.0053	0.0160	0.0467	1.04	0.33	11.07	0.67	0.29	0.38	10.11
PC2H	864	0.0020	0.0040	0.0120	0.0350	2.94	0.25	23.52	0.51	0.20	0.31	20.86
RM1L	180	0.0040	0.0080	0.0240	0.0700	0.64	0.53	10.23	1.07	0.49	0.57	9.61
RM1M	450	0.0027	0.0053	0.0160	0.0467	1.38	0.44	14.76	0.89	0.39	0.50	13.48
RM2L	180	0.0040	0.0080	0.0240	0.0700	0.64	0.53	10.23	1.07	0.49	0.57	9.61
RM2M	450	0.0027	0.0053	0.0160	0.0467	1.38	0.44	14.76	0.89	0.39	0.50	13.48
RM2H	864	0.0020	0.0040	0.0120	0.0350	3.92	0.34	31.35	0.68	0.27	0.41	27.80
URML	135	0	0	0	0	0	0	0	0	0	0	0
URMM	315	0	0	0	0	0	0	0	0	0	0	0
MH	120	0.0040	0.0080	0.0240	0.0700	0.18	0.15	2.16	0.30	0.13	0.17	1.99

A.2. EARTHQUAKE DEMAND

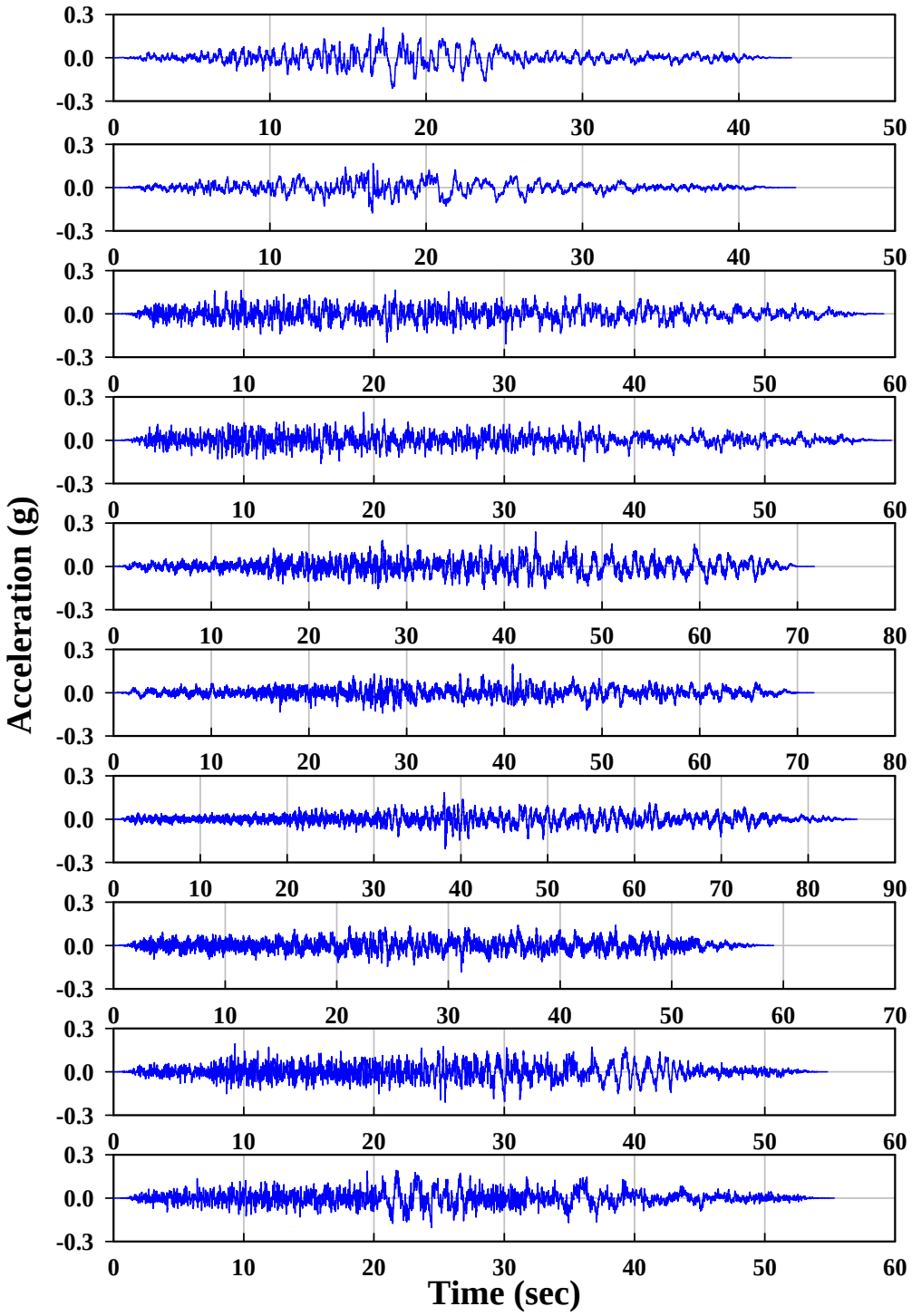

Figure A.38. Ten acceleration time histories for lowlands soil profile, 975 years return period

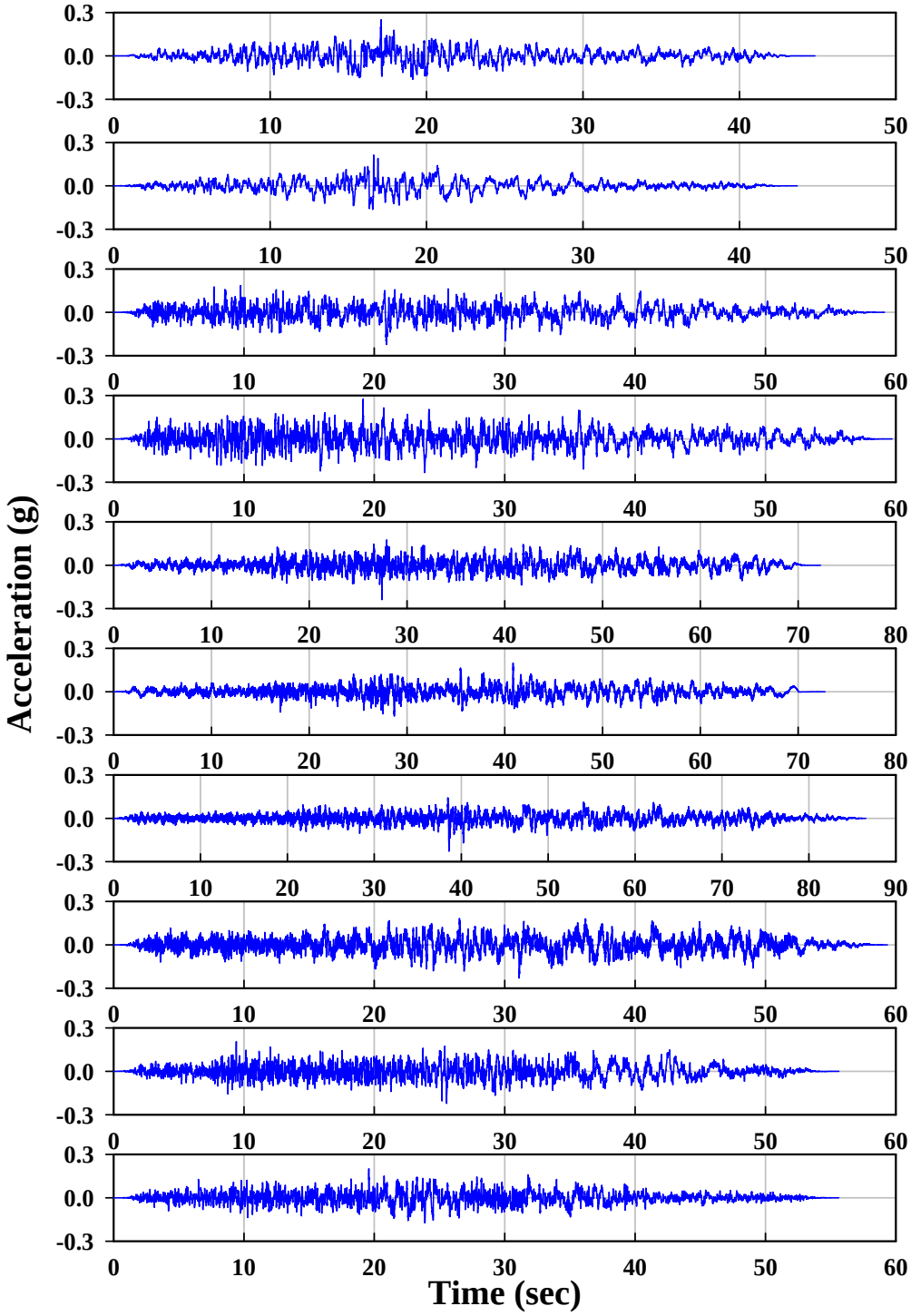

Figure A.39. Ten acceleration time histories for uplands soil profile, 975 years return period

APPENDIX B

B.1. METHODOLOGY FOR STRUCTURAL ASSESSMENT

B.1.1. Review of the Available Variants of the Capacity Spectrum Method

Elasto-Plastic Representation Based on Equal Energy Principle:

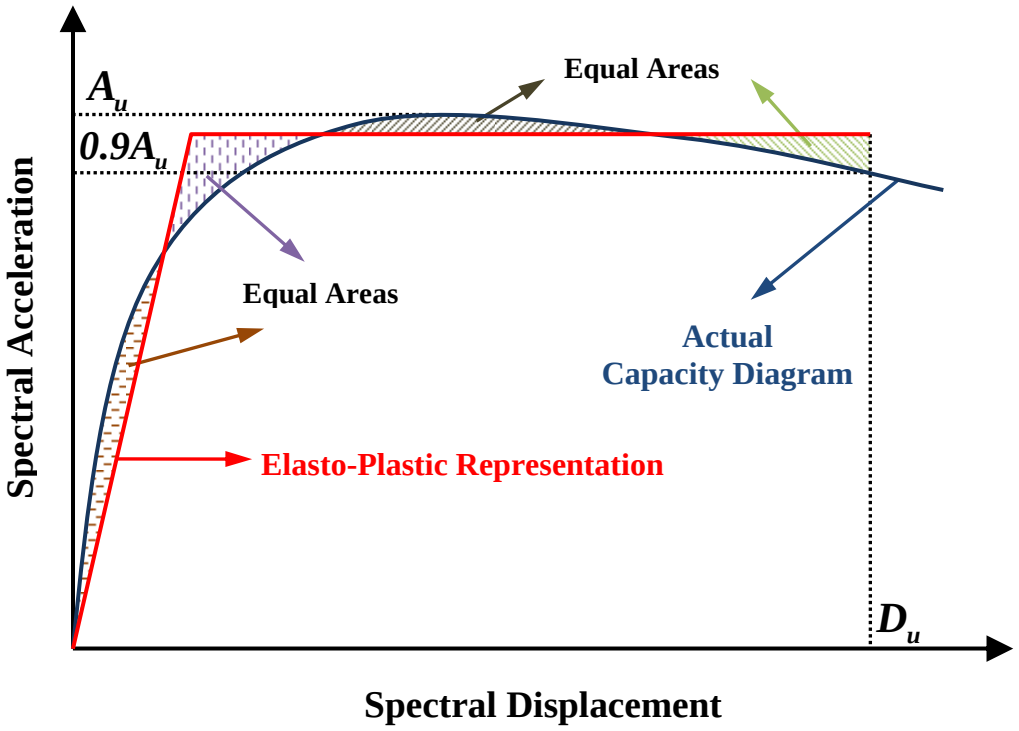

Figure B.1. Elasto-plastic representation of the capacity diagram required in using CSM with inelastic design spectra

The following elasto-plastic representation (with reference to Figure B.1) can be used during the assessment of woodframe structure as a test case using the version of CSM described in section 4.1.1.2:

Determine the ultimate point allowable for the deformation of the structure. In this study it is taken as the acceleration value equal to 90% of the maximum acceleration value of the capacity diagram.

Draw a horizontal line, crossing the descending branch of the capacity diagram such that the area under the horizontal curve from the point of first intersection with the capacity

curve to the ultimate point is equal to the area under the actual capacity curve between the same points.

Extend the horizontal line and draw another line from the origin, such that when the two straight lines intersect, the sum of the areas under the drawn inclined horizontal line and the area under the horizontal line from the intersection point of the two straight lines to the first intersection point of the horizontal line with the actual capacity diagram is equal to area under the actual capacity diagram between origin and the latter point.

The straight lines shown in Figure B.1 are obtained, which give the elasto-plastic representation of the capacity diagram.

Bilinear Representations Based on Equal Energy Principle:

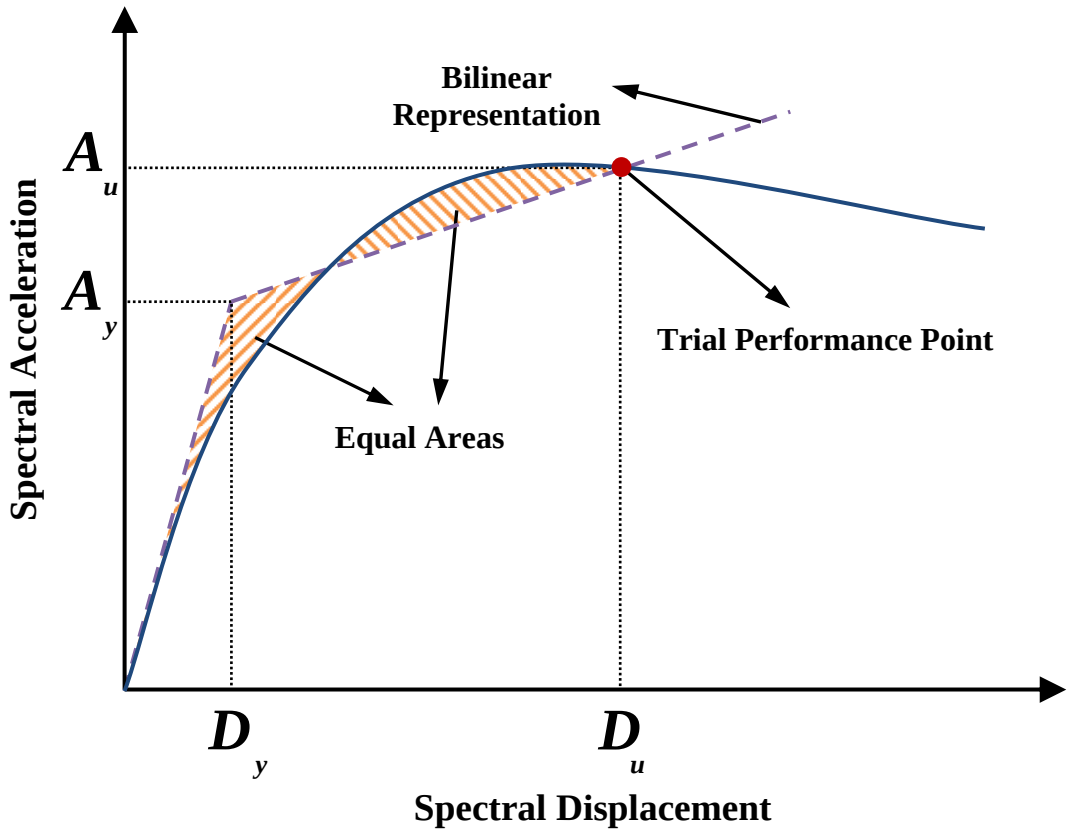

Figure B.2. Bilinear representations based on equal energy principle

To start with, the point on which the bilinear representation will be based should be determined, i.e. D_u, A_u in Figure B.2. Then following the below steps, the parameters of the bilinear representation, i.e. D_y, A_y and α, can be determined (note that equal energy principle is adopted and AD format is used for illustration purposes).

i. Draw a line from the origin at the initial stiffness value of the building.
ii. Draw a second line from the trial performance point such that when it intersects with the first line, at the point D_y, A_y the shaded areas shown in the Figure B.2 figure are equal.

The points, D_y, A_y and D_u, A_u define the bilinear representation of the curve. The slope, α, of the post yield line α, can be obtained using the following relation:

$$\alpha = \frac{A_u - A_y}{D_u - D_y} \tag{B.1}$$

Demand Diagram from Peak Ground Motion Parameters:

A tri-partite plot is utilized for the construction of elastic design spectrum according to Newmark and Hall (1982). A 50th percentile or an 84.1th percentile spectrum can be obtained using this procedure. Explanations below refer to Figure B.3; Chopra's description (2000) provides the basis for what follows.

i. The three dashed lines corresponding to peak values of ground acceleration, $\ddot{u}_{go}$, velocity, $\dot{u}_{go}$, and displacement, u_{go}, are plotted for design ground motion.
ii. According to damping factor, amplification factors are determined using the equations given in Table B.1.
iii. $\ddot{u}_{go}$ is multiplied with the amplification factor α_A to obtain the straight line b-c representing the constant value of pseudo-acceleration, S_a.
iv. $\dot{u}_{go}$ is multiplied with the amplification factor α_V to obtain the straight line c-d representing a constant value of pseudo-velocity, S_v.
v. u_{go} is multiplied with the amplification factor α_D to obtain the straight line e-d representing a constant value of deformation, S_d.
vi. For periods shorter than 1/33 sec, T_a, velocity is equal to the line represented by $\ddot{u}_{go}$ and for periods longer than 33 sec, T_f, velocity is equal to the line represented by u_{go}.
vii. Straight lines are plotted for transitions from T_a to T_b and T_e to T_f.

viii. Once the pseudo-velocity spectrum is obtained, pseudo-acceleration and deformation spectrum can be obtained using the relations given in Eq. (B.2), where ω_n is the natural frequency of the SDOF system and related to elastic period by Eq. (B.3).

$$\frac{S_a}{\omega_n} = S_v = \omega_n S_d \tag{B.2}$$

$$\omega_n = \frac{2\pi}{T_e} \tag{B.3}$$

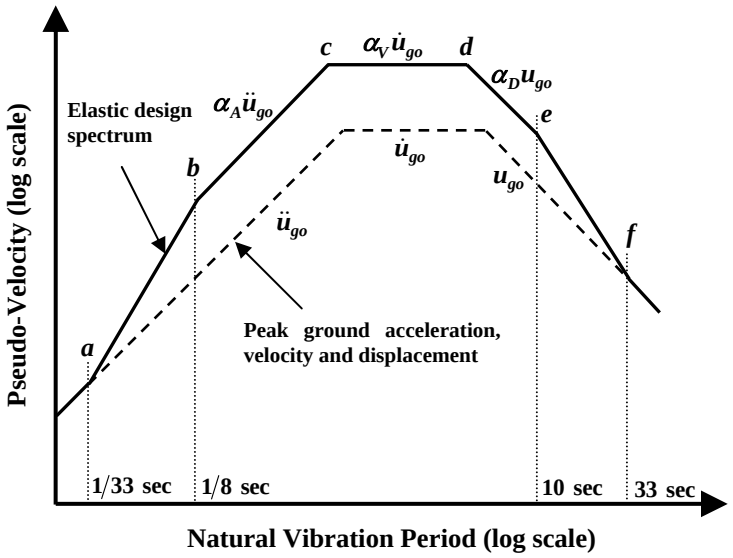

Figure B.3. Newmark and Hall (1982) elastic design spectrum, reproduced from Chopra (2000)

Table B.1. Amplification factors: elastic design spectra, Newmark and Hall (1982)

	Median (50th percentile)	**One Sigma (84.1th percentile)**
$\boldsymbol{\alpha_A}$	$3.21 - 0.68 \ln\zeta$	$4.38 - 1.04 \ln\zeta$
$\boldsymbol{\alpha_V}$	$2.31 - 0.41 \ln\zeta$	$3.38 - 0.67 \ln\zeta$
$\boldsymbol{\alpha_D}$	$1.82 - 0.27 \ln\zeta$	$2.73 - 0.45 \ln\zeta$

If the pseudo-acceleration is plotted against deformation, the demand diagram is obtained in AD format (Figure B.4).

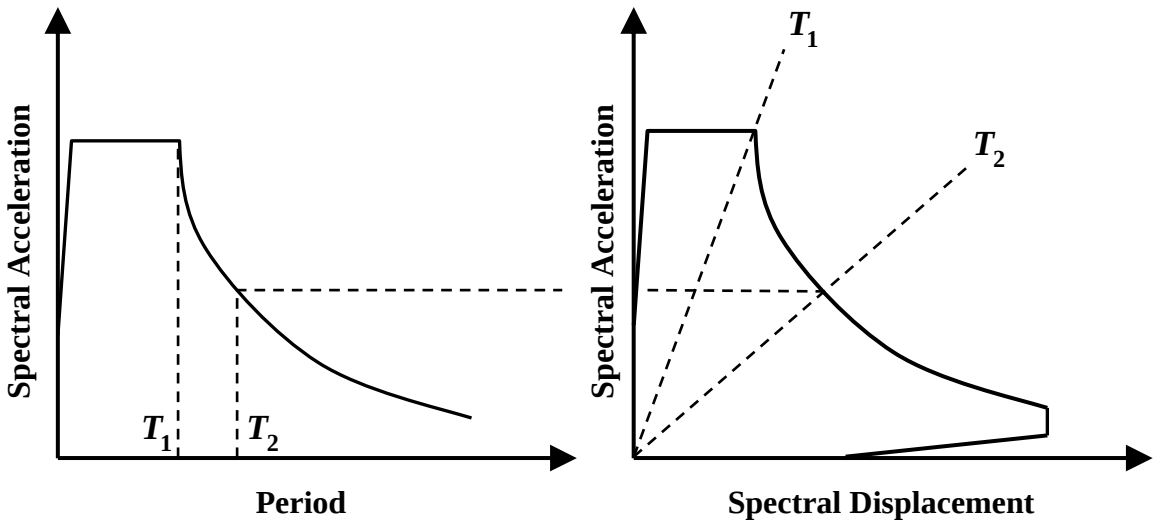

Figure B.4. Demand diagram in *(Left):* Standard format; *(Right):* Acceleration-Displacement Format

B.1.1.1. CSM in ATC-40

The capacity and demand diagrams are superimposed and the intersection point gives the estimate for the performance point (displacement demand). The criteria giving the actual performance point is the agreement between the viscous damping of the demand diagram and the equivalent viscous damping of the structure obtained from the intersection point (Figure B.5). Iterations start with 5 percent damped elastic spectrum. If the structure acts within the elastic range the demand diagram should intersect the capacity diagram at a deformation level less than the yield deformation. If this is not true, it indicates that the structure will deform beyond its elastic limits. Hence the elastic demand diagram should be reduced so as to incorporate the inelastic energy dissipation of the structure.

Effective viscous damping associated with the capacity diagram is obtained from an equivalent linear system described by the bilinear representation of the capacity diagram at the trial performance point. The inherent assumption is that the hysteretic energy dissipated due to the inelastic deformation of the structure can be represented as equivalent viscous damping. Hence, the intersection point of capacity and demand diagrams is used to develop the equivalent linear system based on secant stiffness (Jennings, 1968).

When the force deformation relationship of the SDOF system is represented as a bilinear system with elastic stiffness k_e and yielding branch stiffness of αk_e (Figure B.6), the natural vibration period of the equivalent linear system, T_{eq}, with secant stiffness k_{sec}, is given by:

$$T_{eq} = T_n \sqrt{\frac{\mu}{1+\alpha\mu-\alpha}} \tag{B.4}$$

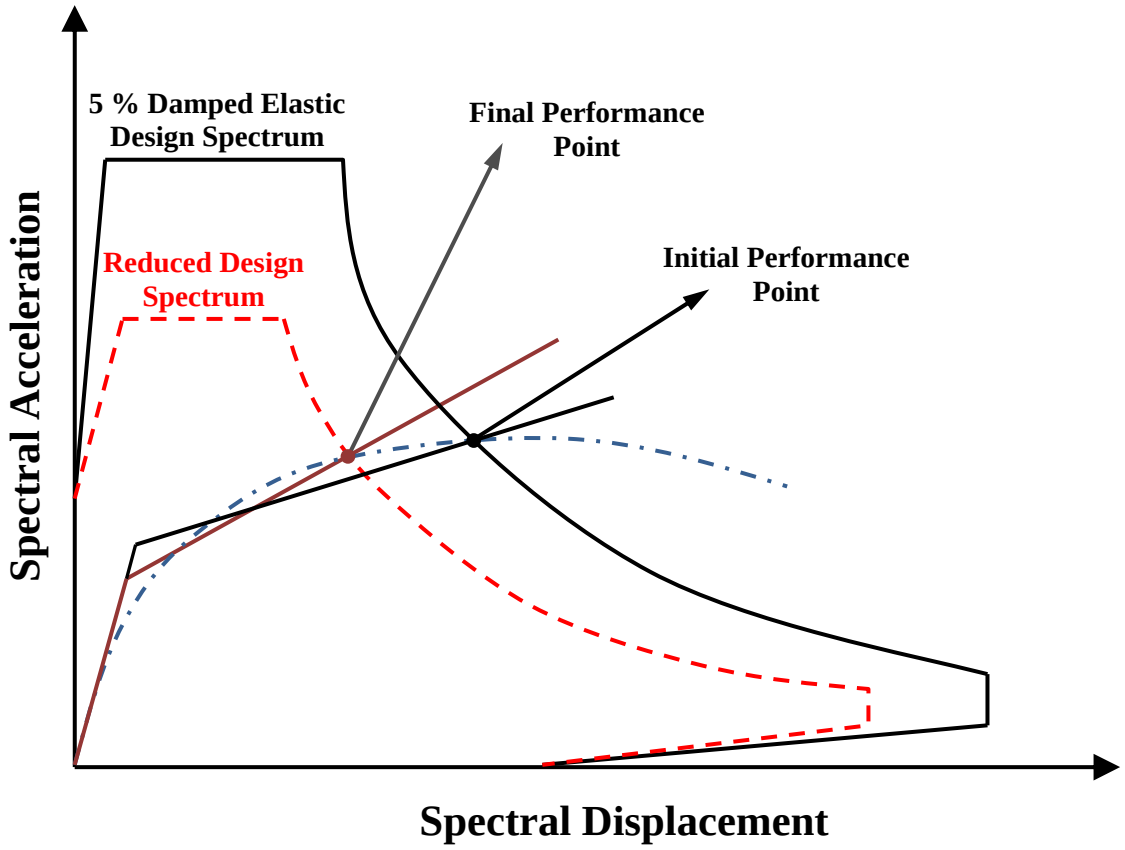

Figure B.5. Plot demand and capacity diagrams to determine the displacement demand

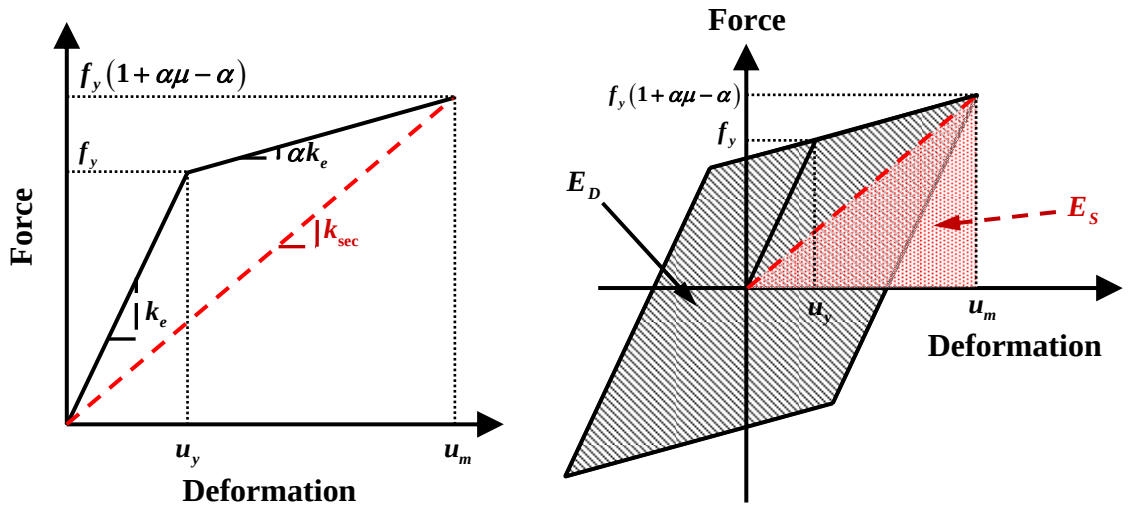

Figure B.6. *(Left):* Equivalent SDOF system based on secant stiffness; *(Right):* Equivalent viscous damping due to hysteretic energy dissipation

The ductility factor μ is determined by the performance point, indicated by deformation u_m, and the yield point of the structure, shown as (u_y, f_y) in Figure B.6, as:

$$\mu = \frac{u_m}{u_y} \tag{B.5}$$

Equivalent viscous damping here is calculated by equating the energy dissipated in a vibration cycle of the inelastic system and of the equivalent linear system (Chopra, 2000 - Section 3.9).

$$\zeta_{eq} = \frac{1}{4\pi}\frac{E_D}{E_S} \tag{B.6}$$

The energy dissipated in the inelastic system, shown as E_D in above figure, is equal to the area enclosed by the hysteresis loop. The strain energy of the elastic system is given by Eq. (B.7).

$$E_S = k_{\sec}\frac{u_m^2}{2} \tag{B.7}$$

Thus equivalent viscous damping ratio takes the form:

$$\zeta_{eq} = \frac{2}{\pi}\frac{(\mu-1)(1-\alpha)}{\mu(1+\alpha\mu-\alpha)} \tag{B.8}$$

The total (or effective) viscous damping of the equivalent linear system is obtained by adding the viscous damping ratio of the bilinear system acting within its elastic range, ζ, to the equivalent viscous damping ratio obtained through Eq. (B.8).

$$\zeta_{eff} = \zeta + \zeta_{eq} \tag{B.9}$$

ATC-40 introduces the damping modification factor, κ, in order to account for the effect of imperfect hysteresis loops, which are reduced in area when compared with the ones shown in Figure B.6 due to duration effects and poor structural ductility detailing. This term is calculated using the appropriate equation from Table B.2. Structural behavior types definitions are given in Table B.3. With this term included, the effective viscous damping ratio is given by:

$$\zeta_{eff} = \zeta + \kappa\zeta_{eq} \tag{B.10}$$

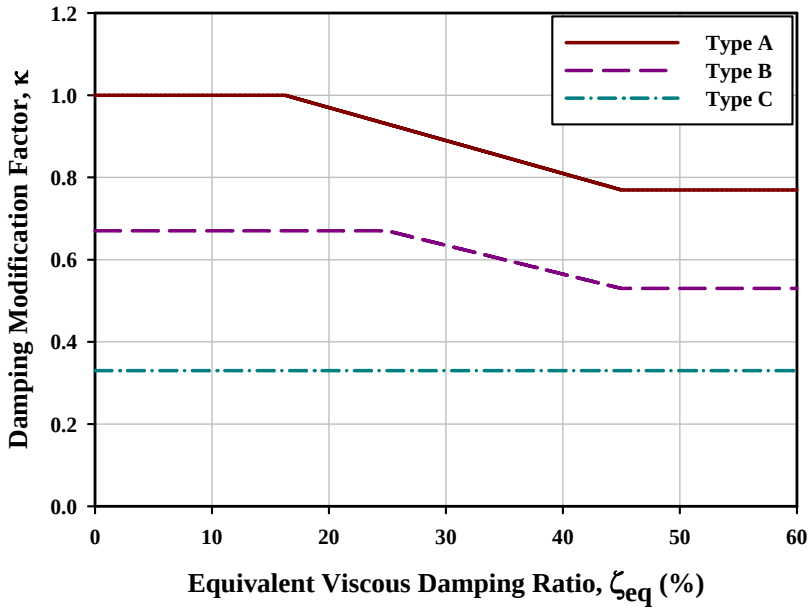

Figure B.7. Relation between the equivalent viscous damping and damping modification factor

Finally, the relation between the equivalent viscous damping and the damping modification factor is shown in Figure B.7. A maximum value of 45 percent is set for the value of allowable equivalent damping, ζ_{eq}. When multiplied with the appropriate damping modification factor from Table B.2, and added to 5 percent elastic damping, 40, 30, and 20% of maximum allowable damping is obtained for Type A, B, and C structures, respectively.

Table B.2. Equations used for calculating the damping modification factor, κ (Applied Technology Council, 1996)

Structural Behavior Type	ζ_{eq} (percent)	K
Type A	≤ 16.25	1.0
	> 16.25	$1.13 - 0.51\dfrac{(\mu-1)(1-\alpha)}{\mu(1+\alpha\mu-\alpha)}$
Type B	≤ 25	0.67
	> 25	$0.845 - 0.446\dfrac{(\mu-1)(1-\alpha)}{\mu(1+\alpha\mu-\alpha)}$
Type C	Any Value	0.33

Table B.3. Structural behavior types (Applied Technology Council, 1996)

Shaking Duration	Essentially New Building[1]	Average Existing Building[2]	Poor Existing Building[3]
Short	Type A	Type B	Type C
Long	Type B	Type C	Type C

[1] Buildings whose primary elements make up an essentially new lateral system and little strength or stiffness is contributed by non-complying elements.
[2] Buildings whose primary elements are combinations of existing and new elements, or better than average existing systems
[3] Buildings whose primary elements make up non-complying lateral force resistance systems with poor or unreliable behavior.

Once the effective damping, ζ_{eff}, is known the necessary reduction factors for the demand diagram are calculated using the Newmark and Hall relations given in Table B.1. Iterations are continued until the difference between the effective damping calculated at the trial performance point from the capacity diagram and the damping associated with demand diagram are within a predefined tolerance.

B.1.1.2. CSM with Inelastic Design Spectra

<u>Demand Reduction Factors from Newmark and Hall (1982):</u>

The demand reduction factor derived by Newmark and Hall is in the following form:

$$R_\mu = \begin{cases} 1 & T_n < T_a \\ (2\mu - 1)^{\beta/2} & T_a \le T_n < T_b \\ \sqrt{2\mu - 1} & T_b \le T_n < T_{c'} \\ \dfrac{T_n}{T_c}\mu & T_{c'} \le T_n < T_c \\ \mu & T_n \ge T_c \end{cases} \tag{B.11}$$

where:

$$\beta = \frac{\ln\left(T_n / T_a\right)}{\ln\left(T_b / T_a\right)} \tag{B.12}$$

The periods, T_a, T_b and T_c are defined in Figure B.3 and $T_{c'}$ is the period where the constant acceleration and constant velocity branches of the inelastic spectrum intersect. It can be obtained from Eq. (B.2) after appropriate reductions are made for these branches using the reduction factors calculated by Eq. (B.11).

Demand Reduction Factors from Krawinkler and Nassar (1992):

Table B.4. Constants for reduction factors from Krawinkler and Nassar (1992)

α	a	b
0.00	1.00	0.42
0.02	1.00	0.37
0.10	0.80	0.29

The demand reduction factor as proposed by Krawinkler and Nassar is in the following form:

$$R_\mu = \left[c(\mu - 1) + 1 \right]^{1/c} \tag{B.13}$$

where:

$$c(T_n, \alpha) = \frac{T_n^a}{1 + T_n^a} + \frac{b}{T_n} \tag{B.14}$$

The constants a and b can be obtained using Table B.4, depending on α, which defines the slope of the yielding branch.

Demand Reduction Factors from Vidic et al. (1994):

Vidic et al., propose the use of following reduction factor:

$$R_\mu = \begin{cases} 1.35(\mu - 1)^{0.95} \dfrac{T_n}{T_0} + 1 & T_n \le T_0 \\ 1.35(\mu - 1)^{0.95} + 1 & T_n > T_0 \end{cases} \tag{B.15}$$

where:

$$T_0 = 0.75 \mu^{0.2} T_c, \qquad T_0 \le T_c \tag{B.16}$$

Demand Reduction Factors from Miranda and Bertero (1994):

The reduction factors developed by Miranda and Bertero are in the following form:

$$R_\mu = \frac{\mu - 1}{\Phi} + 1 \qquad \geq 1 \tag{B.17}$$

where Φ is a function of μ, T_n and the soil conditions at the site, and is given by the equations provided in Table B.5:

Table B.5. Φ as function of period, ductility and soil conditions

Rock Sites	$\Phi = 1 + \frac{1}{10(T_n - \mu)} - \frac{1}{2T}\exp\left[-1.5\left(\ln T_n - 0.6\right)^2\right]$
Alluvium Sites	$\Phi = 1 + \frac{1}{12(T_n - \mu)} - \frac{2}{5T}\exp\left[-2\left(\ln T_n - 0.2\right)^2\right]$
Soft Soil Sites*	$\Phi = 1 + \frac{T_g}{3T_n} - \frac{3T_g}{4T_n}\exp\left[-3\left(\ln\frac{T_n}{T_g} - 0.25\right)^2\right]$

***** T_g is the predominant period of the ground motion, defined as the period at which maximum relative velocity of the 5% damped linear elastic system is maximum throughout the whole period range

Comparison of Different Demand Reduction Factors:

If necessary, it is also possible to write the ductility factor, μ, in terms of the reduction factor, R_μ. However, since the latter is directly used for reducing the demand spectrum, it is not included here. It is also important to note that the reduction factor R_μ is not equal to response modification factor that can be found in some seismic codes, which include over-strength in addition to inelastic energy dissipation.

In addition to the ones provided in this section, a good review of similar studies on demand reduction factors can be found in Miranda and Bertero (1994).

In order to illustrate the differences between these three studies, reduction factors are plotted for different values of ductility (Figure B.8). In addition, as an example, an elastic design spectrum of a ground motion with the parameters $PGA = 1\ g$, $PGV = 48\ in/sec$, and $PGD = 36\ in$, for a mean earthquake is reduced using the four different reduction

factors described above for a ductility ratio of $\mu = 4$. The results are shown in Figure B.9 together with the spectrum predicted by ATC-40 according to the effective damping ratio obtained from the ductility factor.

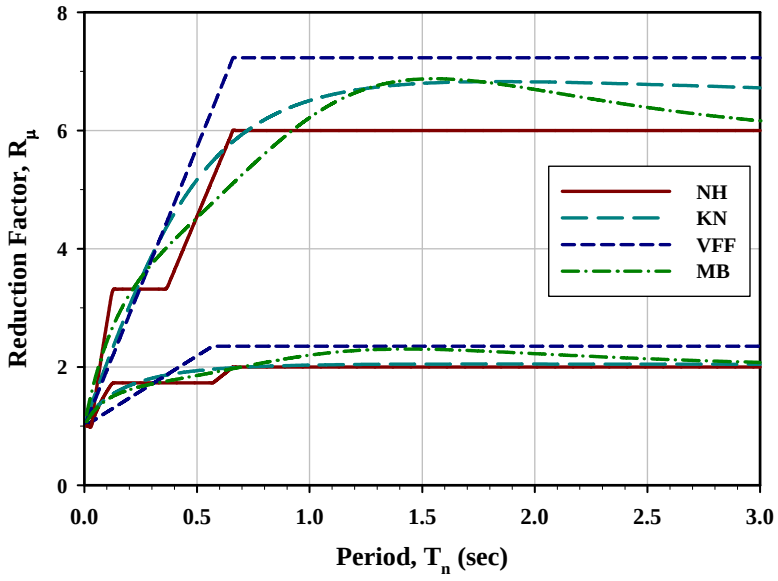

Figure B.8. Comparison of reduction factors from different studies; NH: Newmark and Hall (1982); KN: Krawinkler and Nassar (1992); VFF: Vidic et al. (1994); MB: Miranda and Bertero (1994)

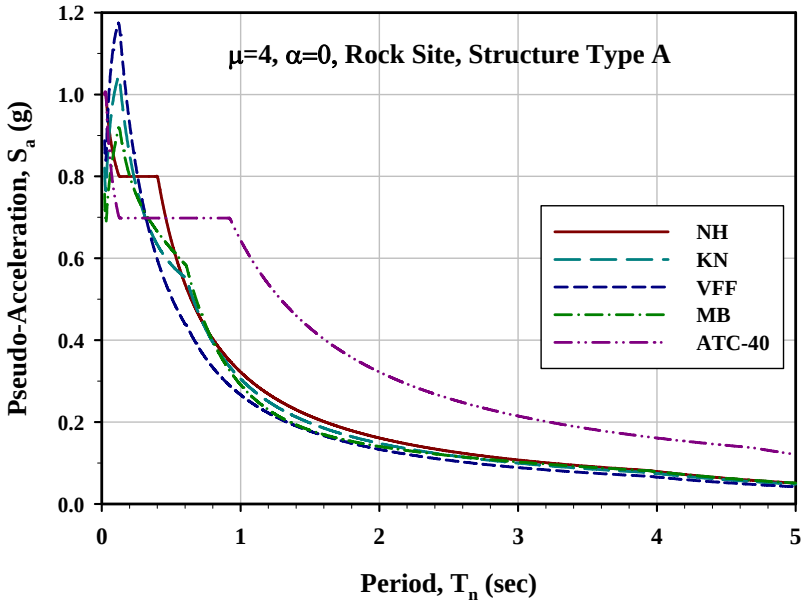

Figure B.9. Inelastic design spectra calculated using different demand reduction factors; NH: Newmark and Hall (1982); KN: Krawinkler and Nassar (1992); VFF: Vidic et al. (1994); MB: Miranda and Bertero (1994); ATC-40 (Applied Technology Council, 1996)

As can be observed from Figure B.9, there is a significant discrepancy between the inelastic design spectra obtained using the ATC-40 procedure with effective damping and from other studies. Other studies proved to be more accurate.

B.1.1.3. CSM with Equivalent Elastic Spectra from Damping Models

In addition to the ductility damping relationship given in ATC-40, Eq. (B.8), other ductility damping relationships are provided in this section, namely those by Iwan and Gates (1979), Priestley et al. (1996), WJE (1996), and Kowalsky et al. (1994b).

Iwan and Gates (1979) – According to Average Stiffness and Energy (ASE) Method:

Among many other methods considered by Iwan and Gates (1979), average stiffness and energy is found to give the least overall error. Therefore the ductility damping relationship from this method is presented here.

The effective damping ratio is given by:

$$\zeta_{eff} = \frac{3}{2\pi\mu^2}\frac{2(1-\alpha)(\mu-1)^2 + \pi\zeta\left[(1-\alpha)\left(\mu^2 - \frac{1}{3}\right) + \frac{2}{3}\alpha\mu^3\right]}{(1-\alpha)(1+\ln\mu) + \alpha\mu} \quad \text{(B.18)}$$

Priestley et al. (1996):

This damping model is based on the Takeda hysteresis model (Takeda et al., 1970).

The effective damping ratio is given by:

$$\zeta_{eff} = \zeta + \frac{1}{\pi}\left[1 - \mu^n\left(\frac{1-\alpha}{\mu} + \alpha\right)\right] \quad \text{(B.19)}$$

where the stiffness degradation factor, n, is suggested as zero for steel structures and 0.5 for reinforced concrete structures.

WJE (1996):

The WJE (1996) damping model is based on the maximum displacement determined from the elastic response spectrum being equal to that obtained from inelastic response spectrum.

Table B.6 gives the effective damping ratio depending on the ductility ratio. The study covers ductility ratios up to 4.

Table B.6. Effective damping ratio based on WJE damping model (WJE, 1996)

μ	1.0	1.25	1.5	2.0	3.0	4.0
ζ_{eff} (%) **(Based on Median + 1 Standard-Deviation Spectrum)**	5	7.5	10	14	21	26
ζ_{eff} (%) **(Based on Median Spectrum)**	5	8.5	12	16	26	35

Kowalsky et al. (1994b):

The damping model used by Kowalsky et al. (1994b) is based on the laboratory test results and curve fitting.

The effective damping ratio is given by:

$$\zeta_{eff} = \zeta + 0.39372\left[1 - \frac{1}{\sqrt{\mu}}\right] \tag{B.20}$$

B.1.1.4. Displacement Coefficient Method (DCM)

Displacement coefficient method (FEMA 273 - Federal Emergency Management Agency, 1997), is similar to CSM, and the aim is to calculate the performance point (referred to as target displacement in FEMA 273) using a procedure that takes into account the effects of nonlinear response on displacement amplitude. Similar to use of inelastic design spectra in CSM, displacement demand is determined from inelastic displacement spectra which are obtained from the elastic displacement spectra by using a number of correction factors based on statistical analysis.

The application of DCM is described below.

i. Obtain the pushover curve:

Guidelines to obtain the pushover curve of the structure are provided in FEMA 273, but results of any convenient pushover analysis can be used.

ii. Determine the elastic period of the structure:

The notation of FEMA 273 (1997) is followed here.

First construct a bilinear representation of the pushover curve (with reference to Figure B.10):

i. Draw the post-elastic stiffness, $K_S = \alpha K_e$, by judgment to represent an average stiffness in the range in which the structure strength has leveled off.

ii. Draw the effective stiffness, K_e, by constructing a secant line passing through the point on the capacity curve corresponding to a base shear of $0.6V_y$, where V_y is defined by the intersection of the K_e and K_S lines.

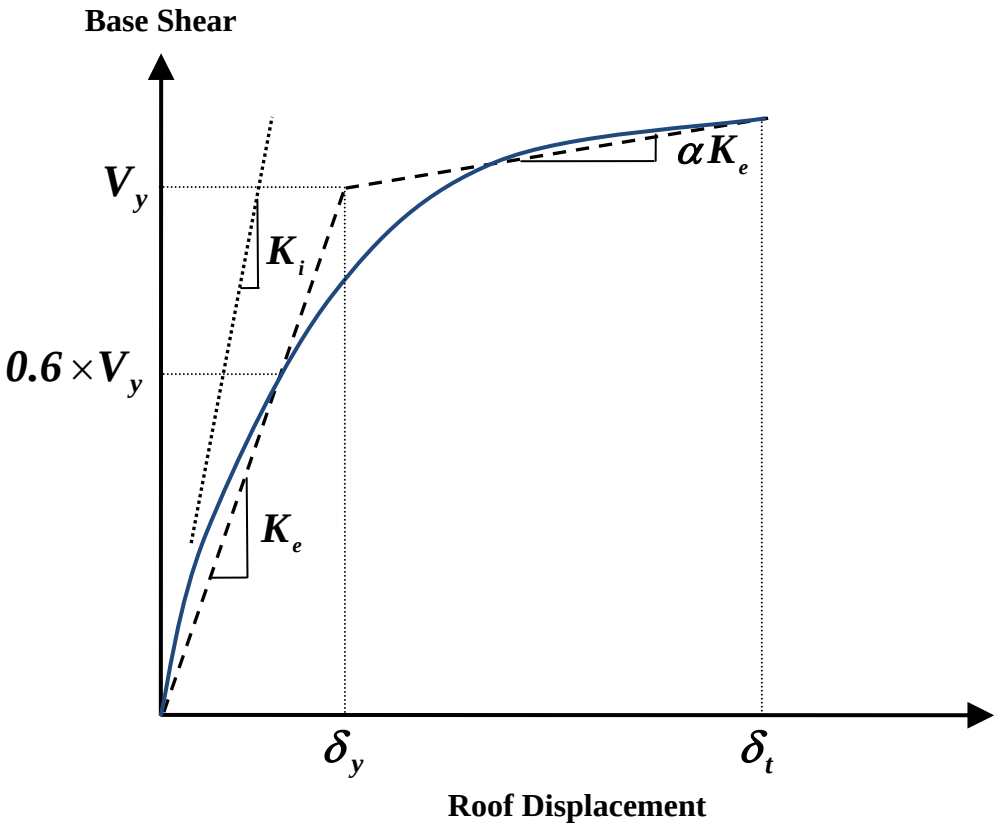

Figure B.10. Determination of the elastic period, reproduced from FEMA 273 (1997)

Note that this procedure requires some trial and error since the value V_y is not known until the K_e line is drawn.

Calculate the effective fundamental period, T_{eff}, using the following equation:

$$T_{eff} = T_i \sqrt{\frac{K_i}{K_e}} \tag{B.21}$$

where, T_i is the elastic fundamental period (in seconds), K_i is the elastic lateral stiffness of the building, and K_e is the effective lateral stiffness of the building.

iii. Calculate the Target Displacement:

The target displacement of the structure, δ_t, can be calculated using Eq. (B.22).

$$\delta_t = C_0 C_1 C_2 C_3 S_a \frac{T_{eff}^2}{4\pi^2} g \tag{B.22}$$

where:

C_0 is the modification factor to relate the spectral displacement and the likely building roof displacement. The modal participation (or transformation) factor given by Eq. (3.10) can be used for this purpose, or alternatively the table below provided in FEMA 273 can be used.

Table B.7. Values for modification factor C_0 (Federal Emergency Management Agency, 1997)

Number of Stories	Modification Factor*
1	1.0
2	1.2
3	1.3
5	1.4
10+	1.5

* Linear interpolation shall be used to calculate the intermediate values

C_1 is the modification factor to relate the expected maximum inelastic displacements to displacements calculated for linear elastic response. This factor has the same effect as reductions given by Equations (B.11), (B.13), (B.15), and (B.15). C_1 can be calculated using the Eq. (B.23). C_1 cannot exceed 1.5 for $T_{eff} < 0.1$, and cannot be taken as less than 1.0 in any case.

$$C_1 = \begin{cases} 1.0 & T_e \geq T_0 \\ \dfrac{\left[1 + (R-1)\,T_0 / T_{eff}\right]}{R} & T_e < T_0 \end{cases} \tag{B.23}$$

where, T_0 is the characteristic period of the spectrum, defined as the period associated with the transition from the constant acceleration segment of the spectrum to the constant

velocity segment, equivalent to T_c in section B.1.1. R is the ratio of inelastic strength demand to the calculated yield strength coefficient and is given by the Eq. (B.24).

$$R = \frac{S_a}{V_y / W} \frac{1}{C_0} \tag{B.24}$$

where, S_a is the response spectrum acceleration at the effective fundamental period of the building and W is the total dead and anticipated live load of the building.

C_2 is the modification factor to represent the effect of hysteresis shape on the maximum displacement response. It takes into account the increase in displacement demand if hysteresis loops exhibit considerable pinching, the same effect as κ in ATC-40 formulation (Table B.2). Values of C_2 for different framing systems and performance levels are listed in Table B.8.

Table B.8. Values for the modification factor C_2

	$T_{eff} = 0.1$		$T_{eff} \geq T_0$	
Structural Performance Level	**Framing Type 1***	**Framing Type 2****	**Framing Type 1***	**Framing Type 2****
Immediate Occupancy	1.0	1.0	1.0	1.0
Life Safety	1.3	1.0	1.1	1.0
Collapse Prevention	1.5	1.0	1.2	1.0

* Structures in which more than 30% of the shear at any level is resisted by components or elements whose strength and stiffness may deteriorate during the design earthquake. Such elements include: ordinary moment-resisting frames, concentrically-braced-frames, frames with partially restrained connections, tension-only braced frames, unreinforced masonry walls, shear-critical walls and piers, or any combination of the above.

** All frames not assigned to Framing Type 1.

C_3 is the modification factor to represent increased displacements due to second-order effects. While moderate strain hardening does not have a significant influence on the displacement demand, strain softening can considerably increase this coefficient. Therefore for buildings with positive post-yield stiffness, C_3 shall be set equal to 1.0. For buildings with negative post-yield stiffness, C_3 shall be calculated using the Eq. (B.25).

$$C_3 = 1 + \frac{|\alpha|(R-1)^{3/2}}{T_{eff}} \tag{B.25}$$

B.1.2. Results from Available Capacity Spectrum Methods

B.1.2.1. CSM with Inelastic Design Spectra

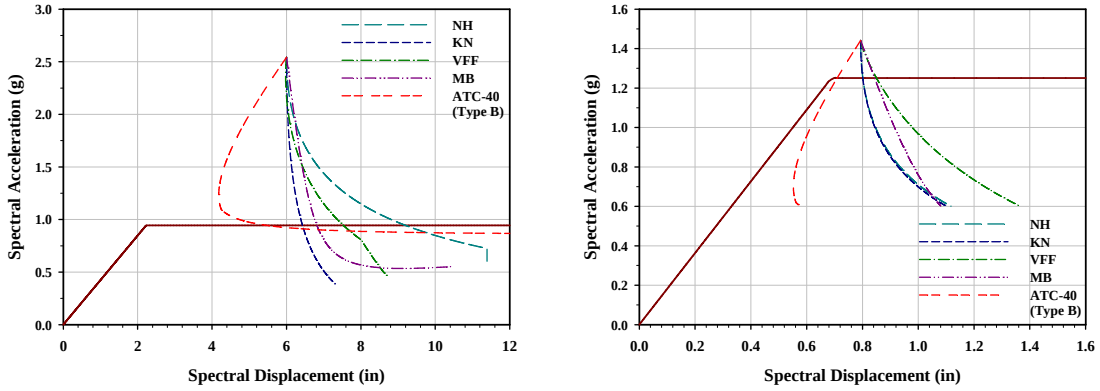

Figure B.11. Results for CSM with inelastic design spectra for the cases *(Left):* Phase 9 under Rinaldi Park record; *(Right):* Phase 10 under Canoga Park record

B.1.2.2. Displacement Coefficient Method

Calculations regarding the evaluation of the example woodframe structure using the displacement coefficient method are provided in this section.

The elasto-plastic representations, whose properties are given in Figure 4.6, developed for the purposes of CSM with inelastic design spectra, are also utilized for DCM.

For Phase 9 and Phase 10 variations of the woodframe structure the effective fundamental period T_e is calculated in Eq. (B.26) and Eq. (B.27) respectively:

$$T_{eff} = T_i\sqrt{\frac{K_i}{K_e}} = 0.332\sqrt{\frac{0.926}{0.424}} = 0.491 \text{ sec} \quad \text{(B.26)}$$

$$T_{eff} = T_i\sqrt{\frac{K_i}{K_e}} = 0.149\sqrt{\frac{4.638}{1.816}} = 0.238 \text{ sec} \quad \text{(B.27)}$$

From Table B.7, C_0 is taken as 1.2 for the two story woodframe structure.

From Figure 4.3 - *(Left)*, T_0 is obtained as 0.132 and 0.133 sec for Canoga and Rinaldi Park records, respectively. Since T_{eff} for both variations of the structure is greater than these values, C_1 is taken as one.

Phase 9 & 10 structures should be considered as Framing Type 2, therefore, from Table B.8, C_2 should be taken as one.

For elasto-plastic representations of the capacity diagrams, from Eq. (B.25), C_3 is calculated as one.

S_a can be obtained from Figure 4.3 - *(Left)* as 1.44 and 2.39 g for both of the structures in the Canoga Park and Rinaldi Park records respectively.

Finally, Table B.9 provides the results of calculating the displacement demand imposed on the variants of the woodframe structure from Eq. (B.22).

Table B.9. Structural response predictions using Displacement Coefficient Method

	Structural Response (in)	
Structural Variation	**Canoga Park Record**	**Rinaldi Park Record**
Phase 9	4.076	6.764
Phase 10	0.958	1.589

APPENDIX C

C.1. HAZUS CAPACITY DIAGRAMS

Limit state threshold values for HAZUS capacity diagrams are tabulated in this section. They are taken from HAZUS Technical Manual Chapter 5, Table 5.9a through Table 5.9d. They are calculated by multiplying the modal height values with the drift ratios, which are provided in Table A.21 through Table A.24.

Table C.1. Limit state threshold values for capacity diagrams based on HAZUS (B. T.: Building Type; S: Slight; M: Moderate; E: Extensive; C: Complete - in terms of spectral displacement)

	Damage State Threshold Value (inches)															
	Pre-Code				Low Code				Moderate Code				High Code			
B. T.	**S**	**M**	**E**	**C**	**S**	**M**	**E**	**C**	**S**	**M**	**E**	**C**	**S**	**M**	**E**	**C**
W1	0.40	1.00	3.09	7.56	0.50	1.25	3.86	9.45	0.50	1.25	3.86	9.45	0.50	1.51	5.04	12.60
W2	0.69	1.71	5.29	12.96	0.86	2.14	6.62	16.20	0.86	2.14	6.62	16.20	0.86	2.59	8.64	21.60
S1L	1.04	1.65	3.50	8.64	1.30	2.07	4.38	10.80	1.30	2.24	5.08	12.96	1.30	2.59	6.48	17.28
S1M	1.73	2.76	5.84	14.40	2.16	3.44	7.30	18.00	2.16	3.74	8.46	21.60	2.16	4.32	10.80	28.80
S1H	2.70	4.30	9.11	22.46	3.37	5.37	11.38	28.08	3.37	5.83	13.21	33.70	3.37	6.74	16.85	44.93
S2L	0.86	1.38	3.46	8.64	1.08	1.73	4.32	10.80	1.08	1.87	5.04	12.96	1.08	2.16	6.48	17.28
S2M	1.44	2.30	5.76	14.40	1.80	2.88	7.20	18.00	1.80	3.12	8.40	21.60	1.80	3.60	10.80	28.80
S2H	2.25	3.59	8.99	22.46	2.81	4.49	11.23	28.08	2.81	4.87	13.10	33.70	2.81	5.62	16.85	44.93
S3	0.43	0.69	1.73	4.73	0.54	0.87	2.17	5.91	0.54	0.94	2.52	7.09	0.54	1.08	3.24	9.45
S4L	0.69	1.11	2.77	7.56	0.86	1.38	3.47	9.45	0.86	1.50	4.04	11.34	0.86	1.73	5.18	15.12
S4M	1.15	1.85	4.62	12.60	1.44	2.31	5.78	15.75	1.44	2.50	6.73	18.90	1.44	2.88	8.64	25.20
S4H	1.80	2.88	7.21	19.66	2.25	3.60	9.01	24.57	2.25	3.90	10.50	29.48	2.25	4.49	13.48	39.31
S5L	0.52	1.04	2.59	6.05	0.65	1.30	3.24	7.56	0	0	0	0	0	0	0	0
S5M	0.86	1.73	4.32	10.08	1.08	2.16	5.40	12.60	0	0	0	0	0	0	0	0
S5H	1.35	2.70	6.74	15.72	1.68	3.37	8.42	19.66	0	0	0	0	0	0	0	0
C1L	0.72	1.15	2.88	7.20	0.90	1.44	3.60	9.00	0.90	1.56	4.20	10.80	0.90	1.80	5.40	14.40
C1M	1.20	1.92	4.80	12.00	1.50	2.40	6.00	15.00	1.50	2.60	7.00	18.00	1.50	3.00	9.00	24.00
C1H	1.73	2.76	6.91	17.28	2.16	3.46	8.64	21.60	2.16	3.74	10.08	25.92	2.16	4.32	12.96	34.56
C2L	0.58	1.10	2.84	7.20	0.72	1.37	3.55	9.00	0.72	1.52	4.17	10.80	0.72	1.80	5.40	14.40
C2M	0.96	1.83	4.74	12.00	1.20	2.29	5.92	15.00	1.20	2.53	6.95	18.00	1.20	3.00	9.00	24.00
C2H	1.38	2.64	6.82	17.28	1.73	3.30	8.53	21.60	1.73	3.64	10.00	25.92	1.73	4.32	12.96	34.56
C3L	0.43	0.86	2.16	5.04	0.54	1.08	2.70	6.30	0	0	0	0	0	0	0	0
C3M	0.72	1.44	3.60	8.40	0.90	1.80	4.50	10.50	0	0	0	0	0	0	0	0
C3H	1.04	2.07	5.18	12.10	1.30	2.59	6.48	15.12	0	0	0	0	0	0	0	0
PC1	0.43	0.69	1.73	4.73	0.54	0.87	2.17	5.91	0.54	0.94	2.52	7.09	0.54	1.08	3.24	9.45

Table C.1. (Continued)

	Damage State Threshold Value (inches)															
	Pre-Code				Low Code				Moderate Code				High Code			
B. T.	**S**	**M**	**E**	**C**	**S**	**M**	**E**	**C**	**S**	**M**	**E**	**C**	**S**	**M**	**E**	**C**
PC2L	0.58	0.92	2.31	6.30	0.72	1.15	2.89	7.88	0.72	1.25	3.37	9.45	0.72	1.44	4.32	12.60
PC2M	0.96	1.54	3.85	10.50	1.20	1.92	4.81	13.12	1.20	2.08	5.61	15.75	1.20	2.40	7.20	21.00
PC2H	1.38	2.21	5.55	15.12	1.73	2.77	6.93	18.90	1.73	3.00	8.08	22.68	1.73	3.46	10.37	30.24
RM1L	0.58	0.92	2.31	6.30	0.72	1.15	2.89	7.88	0.72	1.25	3.37	9.45	0.72	1.44	4.32	12.60
RM1M	0.96	1.54	3.85	10.50	1.20	1.92	4.81	13.12	1.20	2.08	5.61	15.75	1.20	2.40	7.20	21.00
RM2L	0.58	0.92	2.31	6.30	0.72	1.15	2.89	7.88	0.72	1.25	3.37	9.45	0.72	1.44	4.32	12.60
RM2M	0.96	1.54	3.85	10.50	1.20	1.92	4.81	13.12	1.20	2.08	5.61	15.75	1.20	2.40	7.20	21.00
RM2H	1.38	2.21	5.55	15.12	1.73	2.77	6.93	18.90	1.73	3.00	8.08	22.68	1.73	3.46	10.37	30.24
URML	0.32	0.65	1.62	3.78	0.41	0.81	2.03	4.73	0	0	0	0	0	0	0	0
URMM	0.50	1.01	2.52	5.88	0.63	1.26	3.15	7.35	0	0	0	0	0	0	0	0
MH	0.38	0.77	2.30	6.72	0.48	0.96	2.88	8.40	0.48	0.96	2.88	8.40	0.48	0.96	2.88	8.40

C.2. FRAGILITY PARAMETERS

In this section of Appendix C, fragility parameters, which are derived based on HAZUS capacity diagrams, are provided in both conventional and HAZUS compatible formats for the 36 building types.

C.2.1. Conventional Fragility Relationships

Table C.2 and Table C.3 provide the parameters of the conventional fragility relationships for the two soil profiles considered, i.e. lowlands and uplands.

Table C.2. Parameters of the conventional fragility relationships for lowlands soil profile (B.T.: Building Type; capacity diagrams are based on HAZUS)

	Lowlands Soil Profile											
	Pre-Code			Low Code			Moderate Code			High Code		
B.T.	$\boldsymbol{lna_1}$	$\boldsymbol{a_2}$	$\boldsymbol{\beta_{tot}}$	$\boldsymbol{lna_1}$	$\boldsymbol{a_2}$	$\boldsymbol{\beta_{tot}}$	$\boldsymbol{lna_1}$	$\boldsymbol{a_2}$	$\boldsymbol{\beta_{tot}}$	$\boldsymbol{lna_1}$	$\boldsymbol{a_2}$	$\boldsymbol{\beta_{tot}}$
W1	1.549	1.528	0.665	1.549	1.534	0.655	1.233	1.338	0.598	1.095	1.235	0.541
W2	2.292	1.663	0.655	2.295	1.668	0.649	1.800	1.517	0.656	1.367	1.248	0.560
S1L	2.596	1.551	0.635	2.605	1.562	0.631	2.217	1.479	0.645	1.839	1.273	0.593
S1M	3.260	1.311	0.631	3.273	1.309	0.630	3.041	1.253	0.640	2.781	1.046	0.593
S1H	3.669	1.084	0.517	3.680	1.087	0.519	3.612	1.058	0.512	3.506	0.926	0.505
S2L	2.426	1.670	0.647	2.436	1.676	0.642	1.973	1.605	0.664	1.469	1.321	0.600
S2M	3.064	1.416	0.620	3.079	1.420	0.618	2.754	1.309	0.637	2.429	1.039	0.576
S2H	3.511	1.114	0.597	3.520	1.115	0.600	3.378	0.977	0.601	3.336	0.878	0.557

Table C.2. (Continued)

Lowlands Soil Profile												
	Pre-Code			Low Code			Moderate Code			High Code		
B.T.	lna_1	a_2	β_{tot}	lna_1	a_2	β_{tot}	lna_1	a_2	β_{tot}	lna_1	a_2	β_{tot}
S3	2.426	1.670	0.647	2.436	1.676	0.642	1.973	1.605	0.664	1.469	1.321	0.600
S4L	2.412	1.714	0.646	2.420	1.719	0.641	1.967	1.716	0.666	1.404	1.450	0.632
S4M	2.910	1.480	0.629	2.923	1.487	0.624	2.583	1.417	0.661	2.225	1.213	0.617
S4H	3.384	1.237	0.611	3.398	1.233	0.607	3.199	1.150	0.628	3.025	0.999	0.603
S5L	2.365	1.732	0.648	2.367	1.736	0.644	0	0	0	0	0	0
S5M	2.878	1.481	0.633	2.883	1.489	0.629	0	0	0	0	0	0
S5H	3.379	1.219	0.608	3.379	1.223	0.609	0	0	0	0	0	0
C1L	2.456	1.655	0.644	2.464	1.665	0.640	2.017	1.600	0.658	1.551	1.363	0.602
C1M	2.984	1.451	0.632	2.998	1.459	0.629	2.653	1.351	0.662	2.322	1.104	0.603
C1H	3.484	1.186	0.589	3.495	1.181	0.588	3.370	1.183	0.612	3.176	1.037	0.606
C2L	2.220	1.739	0.660	2.231	1.751	0.651	1.699	1.616	0.668	1.178	1.298	0.574
C2M	2.649	1.516	0.644	2.659	1.520	0.639	2.287	1.425	0.651	1.904	1.175	0.564
C2H	3.210	1.287	0.638	3.228	1.278	0.637	3.002	1.210	0.624	2.744	0.981	0.580
C3L	2.294	1.745	0.653	2.297	1.748	0.648	0	0	0	0	0	0
C3M	2.707	1.519	0.636	2.709	1.522	0.635	0	0	0	0	0	0
C3H	3.260	1.276	0.632	3.259	1.278	0.634	0	0	0	0	0	0
PC1	2.103	1.737	0.667	2.116	1.754	0.656	1.547	1.548	0.661	1.052	1.207	0.541
PC2L	2.359	1.729	0.649	2.367	1.736	0.644	1.888	1.696	0.669	1.318	1.399	0.618
PC2M	2.754	1.515	0.633	2.765	1.519	0.628	2.419	1.474	0.653	2.012	1.256	0.600
PC2H	3.278	1.283	0.630	3.292	1.272	0.628	3.092	1.242	0.630	2.808	1.038	0.592
RM1L	2.183	1.745	0.661	2.194	1.756	0.652	1.649	1.600	0.668	1.120	1.260	0.565
RM1M	2.625	1.513	0.645	2.634	1.515	0.641	2.262	1.417	0.648	1.874	1.152	0.549
RM2L	2.183	1.745	0.661	2.194	1.756	0.652	1.649	1.600	0.668	1.120	1.260	0.565
RM2M	2.625	1.513	0.645	2.634	1.515	0.641	2.262	1.417	0.648	1.874	1.152	0.549
RM2H	3.204	1.274	0.637	3.222	1.266	0.635	3.004	1.198	0.616	2.753	0.973	0.571
URML	1.895	1.701	0.676	1.899	1.707	0.668	0	0	0	0	0	0
URMM	2.534	1.575	0.635	2.536	1.579	0.632	0	0	0	0	0	0
MH	2.103	1.737	0.667	2.108	1.745	0.658	2.108	1.745	0.658	2.108	1.745	0.658

Table C.3. Parameters of the conventional fragility relationships for uplands soil profile (B.T.: Building Type; capacity diagrams are based on HAZUS)

Uplands Soil Profile												
	Pre-Code			Low Code			Moderate Code			High Code		
B.T.	lna_1	a_2	β_{tot}	lna_1	a_2	β_{tot}	lna_1	a_2	β_{tot}	lna_1	a_2	β_{tot}
W1	1.257	1.399	0.620	1.254	1.402	0.613	0.982	1.203	0.521	0.891	1.124	0.476
W2	2.050	1.683	0.632	2.053	1.691	0.622	1.490	1.411	0.620	1.103	1.101	0.490
S1L	2.403	1.656	0.578	2.416	1.669	0.573	1.867	1.414	0.596	1.488	1.122	0.520
S1M	3.273	1.464	0.572	3.293	1.471	0.573	2.954	1.400	0.573	2.575	1.115	0.511
S1H	3.765	1.163	0.563	3.782	1.170	0.559	3.681	1.190	0.613	3.511	1.078	0.567
S2L	2.227	1.718	0.614	2.240	1.727	0.607	1.682	1.519	0.643	1.191	1.166	0.516
S2M	2.919	1.540	0.573	2.938	1.549	0.567	2.473	1.319	0.576	2.132	1.004	0.491
S2H	3.628	1.282	0.590	3.649	1.293	0.586	3.390	1.163	0.590	3.196	0.977	0.513
S3	2.227	1.718	0.614	2.240	1.727	0.607	1.682	1.519	0.643	1.191	1.166	0.516
S4L	2.201	1.752	0.618	2.211	1.762	0.609	1.669	1.626	0.658	1.128	1.304	0.565
S4M	2.719	1.602	0.569	2.728	1.606	0.563	2.275	1.452	0.587	1.831	1.121	0.522
S4H	3.372	1.376	0.573	3.393	1.379	0.567	3.094	1.274	0.572	2.789	1.017	0.503
S5L	2.139	1.748	0.629	2.143	1.755	0.619	0	0	0	0	0	0
S5M	2.670	1.588	0.573	2.671	1.594	0.568	0	0	0	0	0	0
S5H	3.361	1.368	0.571	3.364	1.375	0.571	0	0	0	0	0	0
C1L	2.262	1.728	0.605	2.275	1.740	0.600	1.711	1.545	0.635	1.221	1.204	0.524
C1M	2.805	1.576	0.572	2.817	1.585	0.567	2.351	1.382	0.571	1.986	1.084	0.507
C1H	3.504	1.312	0.561	3.515	1.311	0.558	3.333	1.344	0.594	3.014	1.132	0.549
C2L	1.958	1.717	0.646	1.968	1.728	0.640	1.400	1.491	0.645	0.950	1.168	0.494
C2M	2.425	1.598	0.584	2.440	1.607	0.578	1.916	1.332	0.593	1.567	1.033	0.499
C2H	3.205	1.479	0.579	3.228	1.484	0.579	2.825	1.311	0.584	2.484	1.011	0.504
C3L	2.050	1.739	0.638	2.052	1.745	0.630	0	0	0	0	0	0
C3M	2.507	1.614	0.579	2.509	1.621	0.572	0	0	0	0	0	0
C3H	3.266	1.472	0.581	3.271	1.478	0.579	0	0	0	0	0	0
PC1	1.824	1.681	0.658	1.834	1.691	0.652	1.265	1.411	0.626	0.876	1.108	0.475
PC2L	2.130	1.747	0.628	2.143	1.755	0.619	1.590	1.593	0.661	1.059	1.253	0.545
PC2M	2.573	1.624	0.572	2.585	1.627	0.566	2.096	1.441	0.602	1.650	1.100	0.527
PC2H	3.294	1.462	0.579	3.311	1.461	0.579	2.981	1.399	0.590	2.550	1.070	0.518
RM1L	1.916	1.708	0.651	1.926	1.717	0.644	1.358	1.470	0.644	0.917	1.141	0.488
RM1M	2.391	1.577	0.590	2.406	1.585	0.583	1.888	1.300	0.594	1.563	1.013	0.496
RM2L	1.916	1.708	0.651	1.926	1.717	0.644	1.358	1.470	0.644	0.917	1.141	0.488
RM2M	2.391	1.577	0.590	2.406	1.585	0.583	1.888	1.300	0.594	1.563	1.013	0.496
RM2H	3.190	1.471	0.583	3.212	1.476	0.581	2.803	1.286	0.587	2.476	0.990	0.502

Table C.3. (Continued)

	Uplands Soil Profile											
	Pre-Code			Low Code			Moderate Code			High Code		
B.T.	lna_1	a_2	β_{tot}	lna_1	a_2	β_{tot}	lna_1	a_2	β_{tot}	lna_1	a_2	β_{tot}
URML	1.606	1.603	0.669	1.606	1.606	0.663	0	0	0	0	0	0
URMM	2.331	1.627	0.606	2.333	1.634	0.598	0	0	0	0	0	0
MH	1.824	1.681	0.658	1.822	1.683	0.651	1.822	1.683	0.651	1.822	1.683	0.651

C.2.2. HAZUS Compatible Fragility Relationships

Table C.4 and Table C.5 provide the parameters of the conventional fragility relationships for the two soil profiles considered, i.e. lowlands and uplands.

Comparison of standard deviation values can be found in Figure C.1, Figure C.2, and Figure C.3, for low, moderate, and high code seismic design levels respectively.

Table C.4. Parameters of the HAZUS compatible fragility relationships for lowlands soil profile (B.T.: Building Type; capacity diagrams are based on HAZUS)

	Lowlands Soil Profile															
	Pre-Code Design Level				Low Code Design Level				Moderate Code Design Level				High Code Design Level			
B.T.	β_{tot}^1	β_{tot}^2	β_{tot}^3	β_{tot}^4	β_{tot}^1	β_{tot}^2	β_{tot}^3	β_{tot}^4	β_{tot}^1	β_{tot}^2	β_{tot}^3	β_{tot}^4	β_{tot}^1	β_{tot}^2	β_{tot}^3	β_{tot}^4
W1	0.46	0.47	0.66	0.80	0.44	0.49	0.69	0.77	0.43	0.45	0.59	0.81	0.43	0.45	0.57	0.69
W2	0.51	0.66	0.76	0.66	0.55	0.67	0.73	0.64	0.47	0.54	0.76	0.72	0.44	0.47	0.74	0.61
S1L	0.60	0.68	0.71	0.60	0.64	0.77	0.69	0.63	0.49	0.60	0.76	0.62	0.45	0.48	0.68	0.61
S1M	0.55	0.58	0.68	0.62	0.63	0.60	0.61	0.61	0.58	0.58	0.62	0.64	0.54	0.53	0.59	0.77
S1H	0.41	0.41	0.41	0.41	0.41	0.41	0.41	0.41	0.41	0.41	0.41	0.41	0.41	0.41	0.41	0.41
S2L	0.59	0.67	0.79	0.66	0.62	0.68	0.76	0.66	0.48	0.56	0.75	0.72	0.44	0.47	0.73	0.67
S2M	0.40	0.40	0.40	0.40	0.40	0.40	0.40	0.40	0.50	0.54	0.65	0.64	0.49	0.48	0.59	0.60
S2H	0.41	0.41	0.41	0.41	0.41	0.41	0.41	0.41	0.41	0.41	0.41	0.41	0.41	0.41	0.41	0.41
S3	0.40	0.56	0.71	0.72	0.54	0.59	0.73	0.72	0.46	0.46	0.62	0.79	0.50	0.44	0.52	0.78
S4L	0.66	0.71	0.75	0.69	0.69	0.72	0.77	0.67	0.51	0.59	0.73	0.75	0.45	0.49	0.70	0.74
S4M	0.57	0.67	0.67	0.66	0.62	0.72	0.66	0.64	0.51	0.54	0.71	0.65	0.47	0.48	0.68	0.68
S4H	0.63	0.61	0.60	0.57	0.55	0.57	0.60	0.55	0.53	0.53	0.62	0.54	0.54	0.52	0.56	0.41
S5L	0.60	0.69	0.74	0.73	0.59	0.72	0.74	0.70	0	0	0	0	0	0	0	0
S5M	0.48	0.64	0.70	0.63	0.52	0.72	0.66	0.64	0	0	0	0	0	0	0	0
S5H	0.96	0.58	0.61	0.53	0.66	0.54	0.63	0.54	0	0	0	0	0	0	0	0

Table C.4. (Continued)

	Lowlands Soil Profile															
	Pre-Code Design Level				Low Code Design Level				Moderate Code Design Level				High Code Design Level			
B.T.	β_{tot}^{1}	β_{tot}^{2}	β_{tot}^{3}	β_{tot}^{4}	β_{tot}^{1}	β_{tot}^{2}	β_{tot}^{3}	β_{tot}^{4}	β_{tot}^{1}	β_{tot}^{2}	β_{tot}^{3}	β_{tot}^{4}	β_{tot}^{1}	β_{tot}^{2}	β_{tot}^{3}	β_{tot}^{4}
C1L	0.59	0.66	0.77	0.70	0.61	0.67	0.77	0.65	0.49	0.54	0.72	0.74	0.44	0.48	0.66	0.67
C1M	0.51	0.64	0.68	0.67	0.58	0.70	0.65	0.66	0.51	0.57	0.72	0.67	0.45	0.48	0.63	0.72
C1H	0.68	0.70	0.56	0.55	0.61	0.65	0.52	0.59	0.56	0.56	0.59	0.55	0.41	0.41	0.41	0.41
C2L	0.48	0.66	0.75	0.75	0.58	0.66	0.76	0.70	0.45	0.53	0.69	0.77	0.42	0.47	0.70	0.73
C2M	0.54	0.67	0.72	0.61	0.57	0.73	0.71	0.61	0.45	0.53	0.71	0.60	0.44	0.45	0.67	0.60
C2H	0.61	0.56	0.59	0.64	0.52	0.58	0.61	0.63	0.54	0.53	0.58	0.67	0.57	0.54	0.57	0.64
C3L	0.53	0.63	0.74	0.73	0.50	0.66	0.74	0.74	0	0	0	0	0	0	0	0
C3M	0.45	0.61	0.76	0.63	0.51	0.70	0.76	0.61	0	0	0	0	0	0	0	0
C3H	1.02	0.56	0.62	0.63	0.64	0.56	0.57	0.63	0	0	0	0	0	0	0	0
PC1	0.40	0.55	0.68	0.78	0.47	0.53	0.71	0.76	0.44	0.45	0.58	0.74	0.43	0.43	0.50	0.74
PC2L	0.60	0.69	0.73	0.73	0.63	0.69	0.77	0.70	0.48	0.54	0.72	0.78	0.42	0.47	0.62	0.74
PC2M	0.56	0.67	0.73	0.62	0.66	0.68	0.72	0.61	0.44	0.54	0.74	0.61	0.44	0.45	0.68	0.66
PC2H	0.63	0.59	0.60	0.64	0.53	0.58	0.62	0.60	0.54	0.49	0.58	0.65	0.58	0.54	0.54	0.69
RM1L	0.48	0.60	0.73	0.75	0.59	0.64	0.72	0.75	0.43	0.50	0.68	0.79	0.41	0.44	0.58	0.75
RM1M	0.52	0.59	0.75	0.62	0.54	0.67	0.72	0.60	0.43	0.48	0.73	0.64	0.44	0.43	0.61	0.52
RM2L	0.48	0.60	0.73	0.75	0.59	0.64	0.72	0.75	0.43	0.50	0.68	0.79	0.41	0.44	0.58	0.75
RM2M	0.52	0.59	0.75	0.62	0.54	0.67	0.72	0.60	0.43	0.48	0.73	0.64	0.44	0.43	0.61	0.52
RM2H	0.60	0.58	0.60	0.64	0.53	0.53	0.57	0.63	0.56	0.50	0.55	0.65	0.57	0.56	0.51	0.73
URML	0.40	0.46	0.63	0.72	0.40	0.47	0.65	0.71	0.00	0	0	0	0	0	0	0
URMM	0.48	0.53	0.77	0.71	0.42	0.55	0.77	0.64	0.00	0	0	0	0	0	0	0
MH	0.41	0.56	0.70	0.77	0.40	0.55	0.69	0.74	0.40	0.55	0.69	0.74	0.40	0.55	0.69	0.74

Table C.5. Parameters of the HAZUS compatible fragility relationships for uplands soil profile (B.T.: Building Type; capacity diagrams are based on HAZUS)

	Uplands Soil Profile															
	Pre-Code Design Level				Low Code Design Level				Moderate Code Design Level				High Code Design Level			
B.T.	β_{tot}^{1}	β_{tot}^{2}	β_{tot}^{3}	β_{tot}^{4}	β_{tot}^{1}	β_{tot}^{2}	β_{tot}^{3}	β_{tot}^{4}	β_{tot}^{1}	β_{tot}^{2}	β_{tot}^{3}	β_{tot}^{4}	β_{tot}^{1}	β_{tot}^{2}	β_{tot}^{3}	β_{tot}^{4}
W1	0.50	0.45	0.61	0.75	0.44	0.46	0.62	0.82	0.42	0.43	0.53	0.63	0.43	0.43	0.50	0.40
W2	0.52	0.58	0.69	0.67	0.52	0.63	0.64	0.63	0.46	0.49	0.72	0.68	0.45	0.47	0.52	0.41
S1L	0.51	0.57	0.60	0.58	0.57	0.60	0.61	0.58	0.50	0.51	0.54	0.58	0.47	0.49	0.51	0.70
S1M	0.49	0.51	0.56	0.62	0.57	0.52	0.64	0.58	0.55	0.52	0.46	0.63	0.50	0.48	0.47	0.54
S1H	0.41	0.41	0.41	0.41	0.41	0.41	0.41	0.41	0.41	0.41	0.41	0.41	0.41	0.41	0.41	0.41

Table C.5. (Continued)

	Uplands Soil Profile															
	Pre-Code Design Level				Low Code Design Level				Moderate Code Design Level				High Code Design Level			
B.T.	β_{tot}^1	β_{tot}^2	β_{tot}^3	β_{tot}^4	β_{tot}^1	β_{tot}^2	β_{tot}^3	β_{tot}^4	β_{tot}^1	β_{tot}^2	β_{tot}^3	β_{tot}^4	β_{tot}^1	β_{tot}^2	β_{tot}^3	β_{tot}^4
S2L	0.53	0.64	0.70	0.64	0.58	0.63	0.69	0.63	0.47	0.50	0.74	0.65	0.44	0.46	0.55	0.61
S2M	0.48	0.50	0.58	0.61	0.48	0.53	0.59	0.58	0.52	0.45	0.54	0.62	0.53	0.47	0.49	0.47
S2H	0.65	0.46	0.54	0.41	0.58	0.54	0.41	0.41	0.41	0.41	0.41	0.41	0.41	0.41	0.41	0.41
S3	0.44	0.53	0.66	0.68	0.40	0.55	0.71	0.66	0.47	0.47	0.55	0.73	0.51	0.44	0.48	0.59
S4L	0.61	0.72	0.70	0.65	0.65	0.71	0.67	0.66	0.48	0.55	0.73	0.64	0.43	0.46	0.65	0.88
S4M	0.58	0.40	0.40	0.40	0.53	0.40	0.40	0.40	0.49	0.50	0.56	0.60	0.45	0.48	0.50	0.51
S4H	0.51	0.51	0.58	0.57	0.47	0.48	0.58	0.58	0.49	0.47	0.51	0.56	0.55	0.48	0.47	0.50
S5L	0.44	0.66	0.73	0.65	0.58	0.68	0.69	0.62	0	0	0	0	0	0	0	0
S5M	0.47	0.58	0.58	0.59	0.57	0.61	0.56	0.60	0	0	0	0	0	0	0	0
S5H	0.66	0.49	0.56	0.58	0.57	0.52	0.53	0.56	0	0	0	0	0	0	0	0
C1L	0.52	0.57	0.68	0.64	0.54	0.66	0.68	0.63	0.49	0.49	0.67	0.64	0.46	0.48	0.51	0.71
C1M	0.53	0.52	0.54	0.68	0.51	0.50	0.54	0.64	0.47	0.48	0.53	0.60	0.51	0.47	0.48	0.53
C1H	0.59	0.51	0.61	0.65	0.48	0.60	0.64	0.61	0.50	0.49	0.57	0.63	0.54	0.46	0.50	0.56
C2L	0.48	0.58	0.74	0.63	0.49	0.66	0.69	0.62	0.44	0.48	0.68	0.77	0.41	0.44	0.51	0.53
C2M	0.54	0.55	0.65	0.57	0.51	0.59	0.65	0.54	0.45	0.50	0.60	0.57	0.44	0.46	0.49	0.46
C2H	0.53	0.53	0.58	0.64	0.49	0.55	0.59	0.60	0.47	0.51	0.49	0.63	0.50	0.48	0.48	0.45
C3L	0.40	0.59	0.73	0.66	0.46	0.62	0.71	0.62	0	0	0	0	0	0	0	0
C3M	0.49	0.57	0.66	0.60	0.53	0.58	0.65	0.53	0	0	0	0	0	0	0	0
C3H	0.66	0.53	0.54	0.64	0.57	0.55	0.56	0.62	0	0	0	0	0	0	0	0
PC1	0.40	0.48	0.68	0.69	0.43	0.50	0.74	0.65	0.43	0.43	0.55	0.79	0.42	0.42	0.47	0.44
PC2L	0.48	0.63	0.74	0.64	0.59	0.67	0.72	0.62	0.44	0.48	0.74	0.71	0.42	0.44	0.58	0.72
PC2M	0.57	0.57	0.67	0.56	0.55	0.63	0.62	0.56	0.45	0.51	0.61	0.54	0.44	0.47	0.53	0.54
PC2H	0.54	0.58	0.62	0.62	0.51	0.58	0.60	0.60	0.47	0.49	0.52	0.63	0.49	0.47	0.48	0.51
RM1L	0.48	0.54	0.77	0.64	0.48	0.61	0.76	0.64	0.43	0.45	0.66	0.82	0.41	0.43	0.52	0.48
RM1M	0.51	0.54	0.64	0.58	0.49	0.60	0.65	0.54	0.44	0.49	0.58	0.64	0.45	0.44	0.52	0.57
RM2L	0.48	0.54	0.77	0.64	0.48	0.61	0.76	0.64	0.43	0.45	0.66	0.82	0.41	0.43	0.52	0.48
RM2M	0.51	0.54	0.64	0.58	0.49	0.60	0.65	0.54	0.44	0.49	0.58	0.64	0.45	0.44	0.52	0.57
RM2H	0.54	0.52	0.54	0.64	0.48	0.54	0.56	0.61	0.48	0.50	0.51	0.63	0.50	0.48	0.48	0.46
URML	0.40	0.46	0.58	0.78	0.48	0.46	0.64	0.74	0	0	0	0	0	0	0	0
URMM	0.41	0.51	0.63	0.66	0.45	0.58	0.67	0.62	0	0	0	0	0	0	0	0
MH	0.40	0.48	0.73	0.66	0.40	0.51	0.74	0.63	0.40	0.51	0.74	0.63	0.40	0.51	0.74	0.63

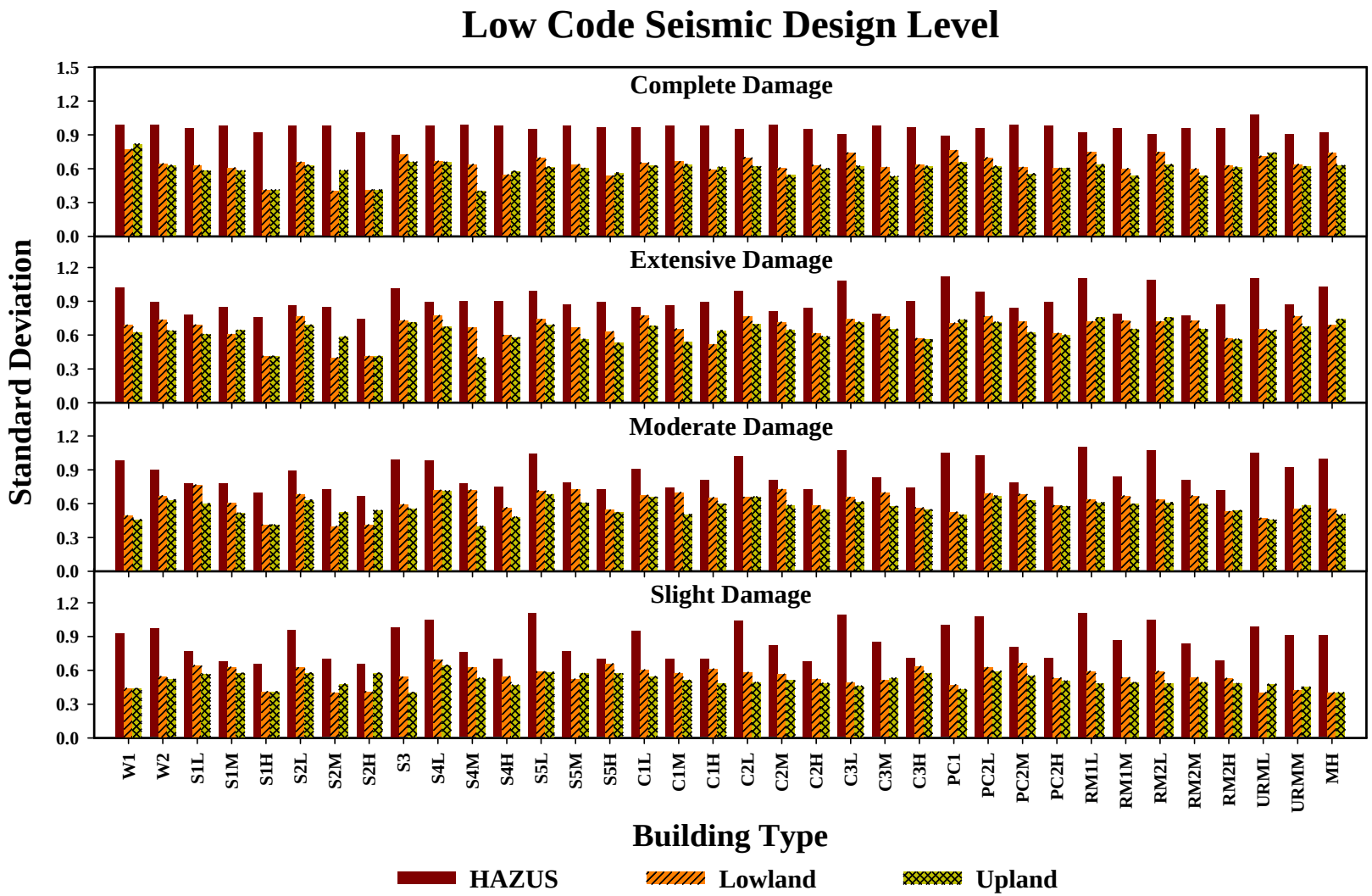

Figure C.1. Comparison of standard deviation values from HAZUS and improved fragility analysis – low code seismic design level

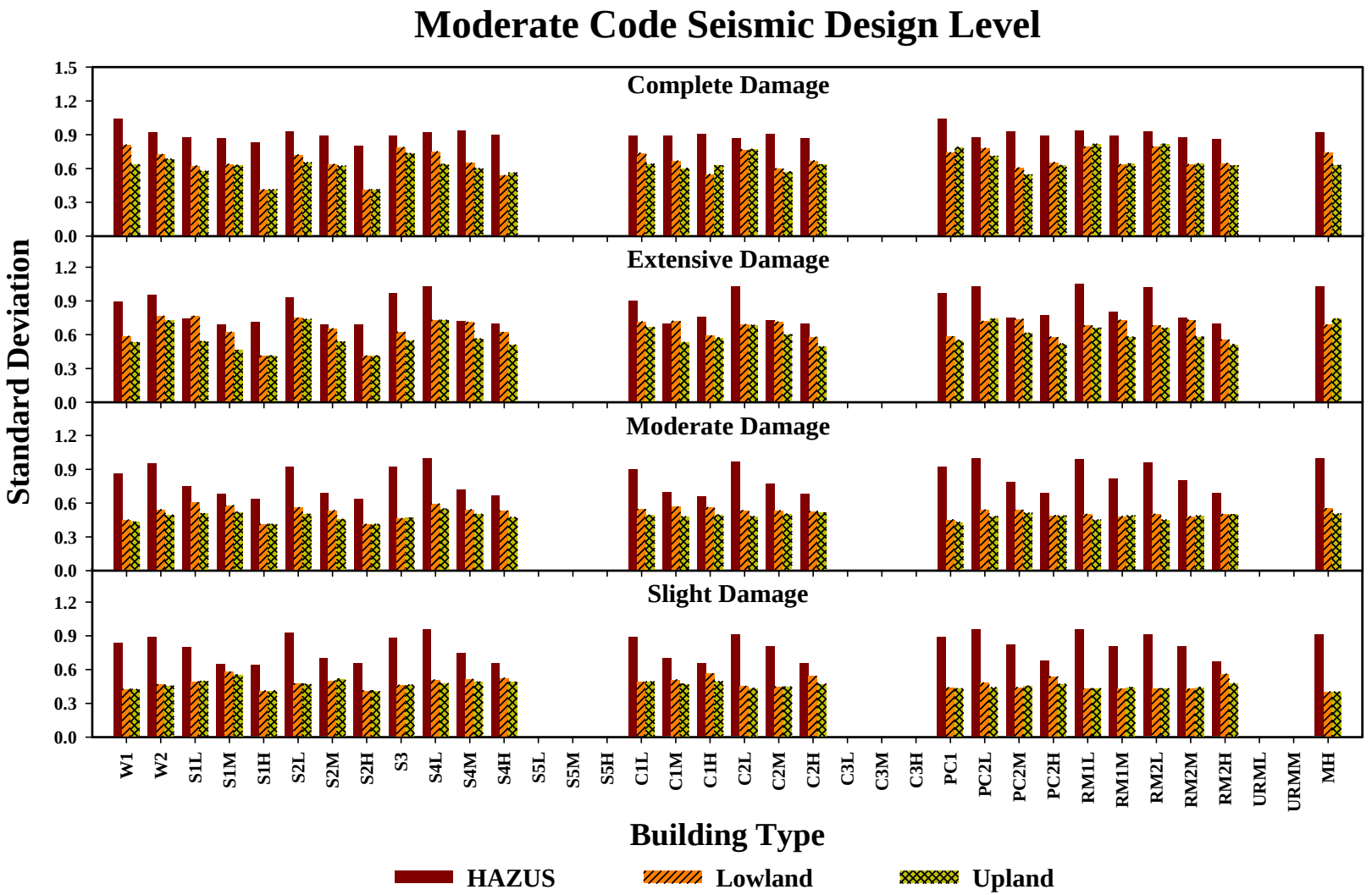

Figure C.2. Comparison of standard deviation values from HAZUS and improved fragility analysis – moderate code seismic design level

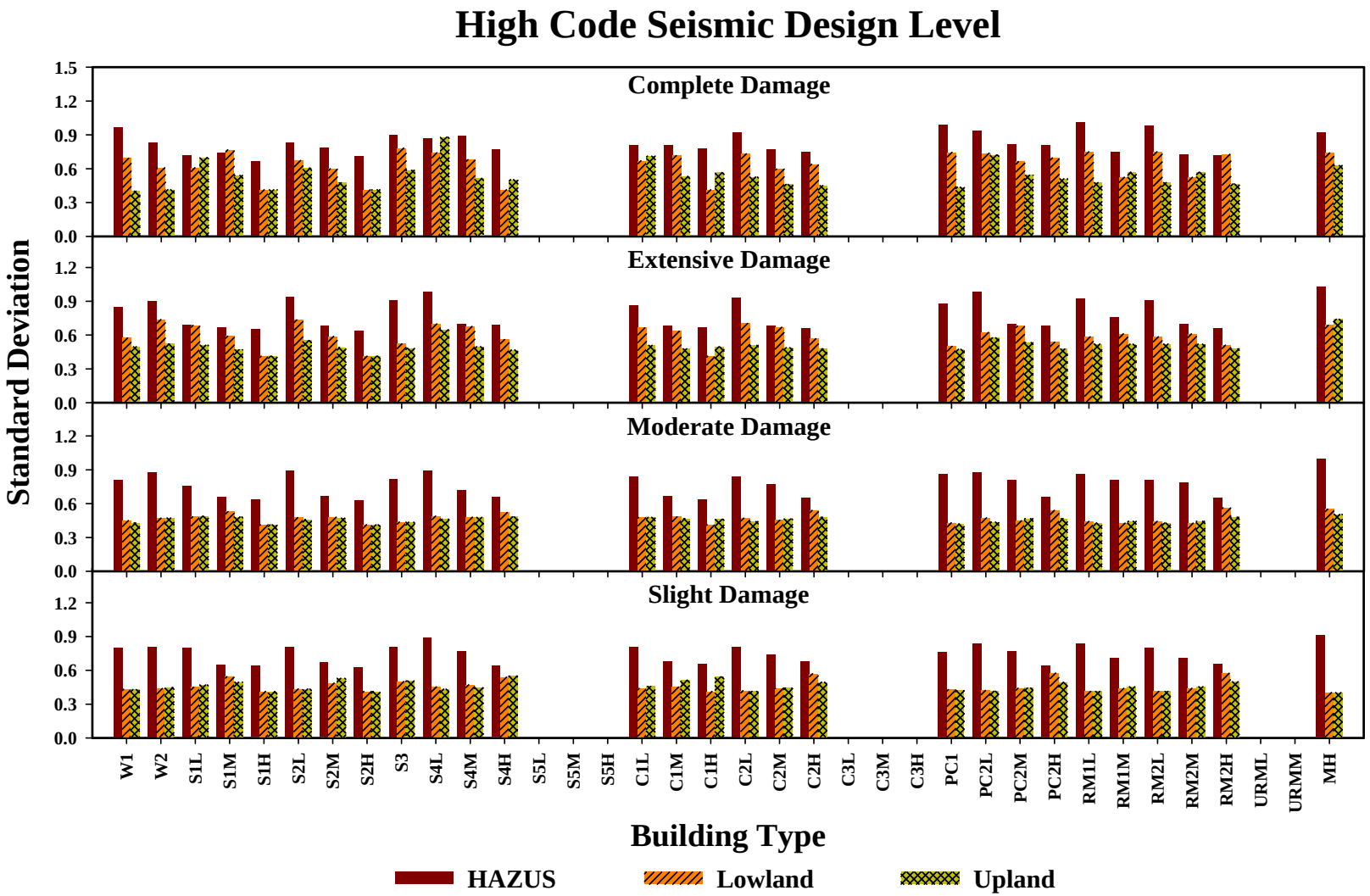

Figure C.3. Comparison of standard deviation values from HAZUS and improved fragility analysis – high code seismic design level

BIBLIOGRAPHY

American Society of Civil Engineers (2005). Minimum Design Loads for Buildings and Other Structures. Reston, Virginia.

Applied Technology Council (1985). Earthquake Damage Evaluation Data for California, Palo Alto.

Applied Technology Council (1987). Evaluating the Seismic Resistance of Existing Buildings.

Applied Technology Council (1996). Seismic Evaluation and Retrofit of Concrete Buildings.

Applied Technology Council (2007). Quantification of Building System Performance and Response Parameters.

Atkinson, G. M. and D. M. Boore (1995). Ground-motion relations for eastern North America. *Bulletin of the Seismological Society of America* **85**(1)**,** 17-30.

Ayoub, A. (2007). Seismic Analysis of Wood Building Structures. *Engineering Structures* **29**(2)**,** 213-223.

Bertero, V. V. (1977). Strength and Deformation Capacities of Buildings Under Extreme Environments. Structural Engineering and Structural Mechanics. K. S. Pister. Englewood Cliffs, New Jersey, Prentice-Hall**:** 211-215.

Bertero, V. V. (1995). Tri-service manual methods. Vision 2000, Sacramento, Structural Engineers Association of California.

Boore, D. M. (2003). Simulation of Ground Motion Using the Stochastic Method. *Pure and Applied Geophysics* **160**(3)**,** 635-676.

Borzi, B. and A. S. Elnashai (2000). Refined Force Reduction Factors for Seismic Design. *Engineering Structures* **22**(10)**,** 1244-1260.

Cao, T. and M. D. Petersen (2006). Uncertainty of Earthquake Losses due to Model Uncertainty of Input Ground Motions in the Los Angeles Area. *Bulletin of the Seismological Society of America* **96**(2)**,** 365-376.

Carr, A. J. (1998). RUAUMOKO - Inelastic Dynamic Analysis Program, Department of Civil Engineering, University of Canterbury, Christchurch, New Zealand.

Chai, Y., T. Hutchinson, et al. (2002). Seismic Behavior of Level and Stepped Cripple Walls. Richmond, California, Consortium of Universities for Research in Earthquake Engineering (CUREE).

Chopra, A. K. (2000). *Dynamics of Structures: Theory and Applications to Earthquake Engineering*. Prentice Hall, New Jersey.

Chopra, A. K. and R. K. Goel (1999). Capacity-Demand-Diagram Methods for Estimating Seismic Deformation of Inelastic Structures: SDF Systems, Pacific Earthquake Engineering Research Center, University of California, Berkeley.

Chopra, A. K. and R. K. Goel (2000). Evaluation of NSP to Estimate Seismic Deformation: SDF Systems. *Journal of Structural Engineering* **126**(4)**,** 482-490.

Cleveland, L. (2006). Seismic Loss Assessment for the New Madrid Seismic Zone. Department of Civil and Environmental Engineering. Urbana, IL, University of Illinois at Urbana-Champaign.

COLA (1995). Earthquake Hazard Reduction in Existing Reinforced Concrete Buildings and Concrete Frame Buildings with Masonry Infills. City of Los Angeles.

COLA (2001). Report of a Testing Program of Light-Framed Walls with Wood Sheated Panels. Irvine, California, Structural Engineering Association of Southern California, COLA-UCI Light Frame Test Committee, Department of Civil Engineering, University of California.

Collins, M., B. Kasal, et al. (2005a). Three-Dimensional Model of Light Frame Wood Buildings. I: Model Description. *Journal of Structural Engineering* **131**(4)**,** 676-683.

Collins, M., B. Kasal, et al. (2005b). Three-Dimensional Model of Light Frame Wood Buildings. II: Experimental Investigation and Validation of Analytical Model. *Journal of Structural Engineering* **131**(4)**,** 684-692.

Davis, J. F., J. H. Bennet, et al. (1982). *Earthquake Planning Scenario for a Magnitude 8.3 Earthquake on the San Andreas Fault in the San Francisco Bay Area*. California Dept. of Conservation, Division of Mines and Geology, Sacramento, CA.

Dina, D. A., S. Robin, et al. (1997). Earthquake Loss Estimation for Europe's Historic Town Centers. *Earthquake Spectra* **13**(4)**,** 773-793.

Dolce, M., A. Kappos, et al. (2006). Vulnerability Assessment and Earthquake Damage Scenarios of the Building Stock of Potenza (Southern Italy) Using Italian and Greek Methodologies. *Engineering Structures* **28**(3)**,** 357-371.

Ekiert, C. and J. Hong (2006). Framing-to-Sheating Connection Tests in Support of NEESWood Project. Buffalo, New York, Network of Earthquake Engineering Simulation (NEES), Host Institution: State University of New York at Buffalo.

Ellingwood, B., R., D. Rosowsky, V. , et al. (2004). Fragility Assessment of Light-Frame Wood Construction Subjected to Wind and Earthquake Hazards. *Journal of Structural Engineering* **130**(12)**,** 1921-1930.

Ellingwood, B. R., D. Rosowsky, et al. (2007). Performance of Light-Frame Wood Residential Construction Subjected to Earthquake in Regions of Moderate Seismicity. *ASCE Journal of Structural Engineering***,** (in press).

Elnashai, A. S. (2002). Do We Really Need Inelastic Dynamic Analysis? *Journal of Earthquake Engineering* **6**(1)**,** 123.

EQE International and the Governor's Office of Emergency Services (1995). The Northridge Earthquake of January 17, 1994: Data Collection and Analysis. Sacramento, CA, Office of Emergency Services.

Erberik, M. A. and A. S. Elnashai (2004). Fragility analysis of flat-slab structures. *Engineering Structures* **26**(7)**,** 937-948.

Erdik, M., N. Aydinoglu, et al. (2003). *Earthquake Risk Assessment for Istanbul Metropolitan Area*. Bogazici University Press, Istanbul.

Fah, D., F. Kind, et al. (2001). Earthquake Scenarios for the City of Basel. *Soil Dynamics and Earthquake Engineering* **21**(5)**,** 405-413.

Fajfar, P. (1999). Capacity Spectrum Method Based on Inelastic Demand Spectra. *Earthquake Engineering & Structural Dynamics* **28**(9)**,** 979-993.

Fajfar, P. (2000). A Nonlinear Analysis Method for Performance-Based Seismic Design. *Earthquake Spectra* **16**(3)**,** 573-592.

Federal Emergency Management Agency (1992). NEHRP Handbook for Seismic Evaluation of Existing Building, FEMA 178. Washington, District of Columbia, FEMA.

Federal Emergency Management Agency (1997). NEHRP Guidelines for the Seismic Rehabilitation of Buildings, FEMA 273. Washington, District of Columbia, FEMA.

Federal Emergency Management Agency (1998). NEHRP Handbook for Seismic Evaluation of Existing Building - A Prestandard, FEMA 310. Washington, District of Columbia, FEMA.

Federal Emergency Management Agency (2000). Prestandard and Commentary for the Seismic Rehabilitation of Buildings, FEMA 356. Washington, District of Columbia, FEMA.

Fernandez, A. (2007). Numerical Simulation of Earthquake Ground Motions in the Upper Mississippi Embayment. School of Civil and Environmental Engineering. Atlanta, GA, Georgia Institute of Technology. **PhD**.

Filiatrault, A. (2007). Pushover Curves for Woodframe Buildings, Applied Technology Council (ATC).

Filiatrault, A. and B. Folz (2002). Performance-Based Seismic Design of Wood Framed Buildings. *Journal of Structural Engineering* **128**(1)**,** 39-47.

Filiatrault, A., H. Isoda, et al. (2003). Hysteretic Damping of Wood Framed Buildings. *Engineering Structures* **25**(4)**,** 461-471.

Fischer, D., A. Filiatrault, et al. (2001). Shake Table Tests of a Two-Story Woodframe House. Richmond, California, Consortium of Universities for Research in Earthquake Engineering (CUREE).

Folz, B. and A. Filiatrault (2000). CASHEW-Version 1.1, A Computer Program for Cyclic Analysis of Wood Shear Walls. Richmond, California.

Folz, B. and A. Filiatrault (2001). Cyclic Analysis of Wood Shear Walls. *Journal of Structural Engineering* **127**(4)**,** 433-441.

Folz, B. and A. Filiatrault (2002). A Computer Program for Seismic Analysis of Woodframe Structures (SAWS). Richmond, California.

Folz, B. and A. Filiatrault (2004a). Seismic Analysis of Woodframe Structures. I: Model Formulation. *Journal of Structural Engineering* **130**(9)**,** 1353-1360.

Folz, B. and A. Filiatrault (2004b). Seismic Analysis of Woodframe Structures. II: Model Implementation and Verification. *Journal of Structural Engineering* **130**(9)**,** 1361-1370.

Fonseca, F., S. Rose, et al. (2002). Nail, Wood Screw, and Staple Fastener Connections. Richmond, California, Consortium of Universities for Research in Earthquake Engineering (CUREE).

Fragiacomo, M., C. Amadio, et al. (2006). Evaluation of the Structural Response under Seismic Actions Using Non-Linear Static Methods. *Earthquake Engineering & Structural Dynamics* **35**(12)**,** 1511-1531.

Frankel, A. D., C. S. Mueller, et al. (2000). USGS National Seismic Hazard Maps. *Earthquake Spectra* **16**(1)**,** 1-19.

Freeman, S. A. (1978). Prediction of Response of Concrete Buildings to Severe Earthquake Motion. *American Concrete Institute* **Publication SP-55,** 589-605.

Freeman, S. A., J. P. Nicoletti, et al. (1975). Evaluations of Existing Buildings for Seismic Risk - A Case Study of Puget Sound Naval Shipyard, Bremerton, Washington. 1st U. S. National Conference on Earthquake Engineering, Berkeley, EERI.

French, S. (2007). MAE Center Inventory Study for the City of Memphis, MAE Center.

Gupta, A. and H. Krawinkler (2000). Estimation of Seismic Drift Demands for Frame Structures. *Earthquake Engineering & Structural Dynamics* **29**(9)**,** 1287-1305.

International Conference of Building Officials (1994). Uniform Building Code.

Isoda, H., B. Folz, et al. (2002). Seismic Modeling of Index Woodframe Buildings. Richmond, California, Consortium of Universities for Research in Earthquake Engineering (CUREE).

Iwan, W. D. and N. C. Gates (1979). Estimating Earthquake Response of Simple Hysteretic Structures. *Journal of the Engineering Mechanics Division, ASCE* **105**(EM3)**,** 391-405.

Jennings, P. C. (1968). Equivalent Viscous Damping for Yielding Structures. *Journal of the Engineering Mechanics Division* **94**(1)**,** 103-116.

Jeong, S.-H. and A. S. Elnashai (2007). Probabilistic Fragility Analysis Parameterized by Fundamental Response Quantities. *Engineering Structures* **29**(6)**,** 1238-1251.

Kasal, B., R. J. Leichti, et al. (1994). Nonlinear Finite-Element Model of Complete Light-Frame Wood Structures. *Journal of Structural Engineering* **120**(1)**,** 100-119.

Kim, H., K.-W. Min, et al. (2005). Evaluation of Capacity Spectrum Method for Estimating the Peak Inelastic Responses. *Journal of Earthquake Engineering* **9**(5)**,** 695-718.

Kim, J. H. and D. Rosowsky, V. (2005). Fragility Analysis for Performance-Based Seismic Design of Engineered Wood Shearwalls. *Journal of Structural Engineering* **131**(11)**,** 1764-1773.

Kircher, C. A., A. A. Nassar, et al. (1997a). Development of Building Damage Functions for Earthquake Loss Estimation. *Earthquake Spectra* **13**(4)**,** 663-682.

Kircher, C. A., R. K. Reitherman, et al. (1997b). Estimation of earthquake losses to buildings. *Earthquake spectra* **13**(4)**,** 703-720.

Kohara, K. and K. Miyazawa (1998). Full-Scale Shaking Table Test of Two Story Wooden Houses. 5th World Conf. on Timber Engineering, Swiss Federal Institute of Technology, Lausanne, Switzerland, Presses Polytechniques et Universitaires Romandes.

Kowalsky, M., M. J. N. Priestley, et al. (1994a). Displacement-Based Design of RC Bridge Columns. 2nd International Workshop on the Seismic Design of Bridges, Queenstown, New Zealand.

Kowalsky, M. J., M. J. N. Priestley, et al. (1994b). Displacement-Based Design, a Methodology for Seismic Design Applied to SDOF Reinforced Concrete Structures. San Diego, La Jolla, California, University of California.

Krawinkler, H. and A. A. Nassar (1992). Seismic Design Based on Ductility and Cumulative Damage Demands and Capacities. Nonlinear Seismic Analysis and Design of

Reinforced Concrete Buildings. P. Fajfar and H. Krawinkler. New York, Elsevier Applied Science**:** 23-40.

Lam, F., A. Filiatrault, et al. (2002). Performance of Timber Buildings Under Seismic Load. Part 1: Experimental Studies. *Progress in Structural Engineering and Materials* **4**(3)**,** 276-285.

Lam, F., A. Filiatrault, et al. (2004). Performance of Timber Buildings Under Seismic Load. Part 2: Modeling. *Progress in Structural Engineering and Materials* **6**(2)**,** 79-83.

Lee, K. H. and D. V. Rosowsky (2006). Fragility Analysis of Woodframe Buildings Considering Combined Snow and Earthquake Loading. *Structural Safety* **28**(3)**,** 289-303.

Lin, Y.-Y. and K.-C. Chang (2003). An Improved Capacity Spectrum Method for ATC-40. *Earthquake Engineering & Structural Dynamics* **32**(13)**,** 2013-2025.

Lin, Y.-Y., K.-C. Chang, et al. (2004a). Comparison of Displacement Coefficient Method and Capacity Spectrum Method with Experimental Results of RC Columns. *Earthquake Engineering & Structural Dynamics* **33**(1)**,** 35-48.

Lin, Y.-Y., T.-F. Chuang, et al. (2004b). A Mathematical Basis for the Convergence of the Capacity Spectrum Method. *Earthquake Engineering & Structural Dynamics* **33**(9)**,** 1059-1066.

Lin, Y.-Y. and E. Miranda (2004). Non-Iterative Capacity Spectrum Method Based on Equivalent Linearization for Estimating Inelastic Deformation Demands of Buildings. *Structural Engineering/Earthquake Engineering* **21**(2)**,** 113-119.

Luco, N. and C. A. Cornell (2007). Structure-Specific Scalar Intensity Measures for Near-Source and Ordinary Earthquake Ground Motions. *Earthquake Spectra* **23**(2)**,** 357-392.

Mahaney, J. A., T. F. Paret, et al. (1993). Capacity Spectrum Method for Evaluating Structural Response During the Loma Prieta Earthquake. National Earthquake Conference, Memphis, USA.

Malik, A. (1995). Estimating Building Stocks for Earthquake Mitigation and Recovery Planning. Cornell Institute for Social and Economic Research.

Miranda, E. and V. Bertero, V. (1994). Evaluation of Strength Reduction Factors for Earthquake-Resistant Design. *Earthquake Spectra* **10**(2)**,** 357-379.

Nassar, A. A. and H. Krawinkler (1991). Seismic Demands for SDOF and MDOF Systems. Stanford, California, The John A. Blume Earthquake Engineering Center, Stanford University.

National Institute of Building Sciences, N. (2003). Multi-Hazard Loss Estimation Methodology, Earthquake Model. Washington, D.C., Federal Emergency Management Agency (FEMA). **Technical and User's Manual**.

Newmark, N. M. and W. J. Hall (1982). *Earthquake Spectra and Design*. Earthquake Engineering Research Institute, EERI, Berkeley, California.

Ohashi, Y., I. Sakamoto, et al. (1998). Shaking Table Tests of a Real Scale Wooden House Subjected to Kobe Earthquake. 5th World Conf. on Timber Engineering, Swiss Federal Institute of Technology, Lausanne, Switzerland, Presses Polytechniques et Universitaires Romandes.

Orsini, G. (1999). A Model for Buildings' Vulnerability Assessment Using the Parameterless Scale of Seismic Intensity (PSI). *Earthquake Spectra* **15**(3)**,** 463-483.

Paevere, P. J. (2002). Full-scale Testing, Modeling and Analysis of Light-frame Structures Under Lateral Loading. Department of Civil and Environmental Engineering. Melbourne, Australia, The University of Melbourne.

Papanikolaou, V. K. and A. S. Elnashai (2005). Evaluation of Conventional and Adaptive Pushover Analysis I: Methodology. *Journal of Earthquake Engineering* **9**(6)**,** 923-941.

Papanikolaou, V. K., A. S. Elnashai, et al. (2006). Evaluation of Conventional and Adaptive Pushover Analysis II: Comparative Results. *Journal of Earthquake Engineering* **10**(1)**,** 127-151.

Pardoen, G., A. Waltman, et al. (2003). Testing and Analysis of One-Storey and Two-Storey Shear Walls Under Cyclic Loading. Richmond, California, Consortium of Universities for Research in Earthquake Engineering (CUREE).

Park, R. (1988). Ductility Evaluation from Laboratory and Analytical Testing. 9th World Conference on Earthquake Engineering, Tokyo-Kyoto, Japan.

Park, Y. and A. H. Ang (1985). Mechanistic Seismic Damage Model for Reinforced Concrete. *Journal of Structural Engineering* **111**(4)**,** 722-739.

Park, Y. J., A. H. S. Ang, et al. (1987). Damage-Limiting Aseismic Design of Buildings. *Earthquake Spectra* **3**(1)**,** 1-26.

Perkins, J. B., J. Boatwright, et al. (1998). Housing Damage and Resulting Shelter Needs: Model Testing and Refinement Using Northridge Data. NEHRP Conference and Workshop on Research on the Northridge, California Earthquake of January 17, 1994, California Universities for Research in Earthquake Engineering, Richmond, California.

Porter, K. A., J. L. Beck, et al. (2002). Improving Loss Estimation for Woodframe Buildings. Richmond, California, Consortium of Universities for Research in Earthquake Engineering (CUREE).

Priestley, M. J. N., M. J. Kowalsky, et al. (1996). Preliminary Development of Direct Displacement-Based Design for Multi-Degree of Freedom Systems. Proceedings of 65th Annual SEAOC Convention, Maui, Hawaii, USA, SEAOC.

Rahnama, M. and H. Krawinkler (1993). Effects of Soft Soil and Hysteresis Model on Seismic Demands. Stanford, California, The John A. Blume Earthquake Engineering Center, Stanford University.

Ramos, L. F. and P. B. Lourenco (2004). Modeling and Vulnerability of Historical City Centers in Seismic Areas: A Case Study in Lisbon. *Engineering Structures* **26**(9)**,** 1295-1310.

Reinhorn, A. M. (1997). Inelastic Analysis Techniques in Seismic Evaluations. Seismic Design Methodologies for the Next Generation of Codes. P. Fajfar and H. Krawinkler. Balkema, Rotterdam**:** 277-287.

Reitherman, R. (1998). Overview of the Northridge Earthquake. NEHRP Conference and Workshop on Research on the Northridge, California Earthquake of January 17, 1994, California Universities for Research in Earthquake Engineering, Richmond, California.

Reitherman, R. and K. Cobeen (2003). Design Documentation of Woodframe Project Index Buildings. Richmond, California, Consortium of Universities for Research in Earthquake Engineering (CUREE).

Rix, G. and A. Fernandez (2006). Soil Attenuation Relationships and Seismic Hazard Analyses in the Upper Mississippi Embayment. Eight U.S. National Conference on Earthquake Engineering 8NCEE, San Francisco, California, EERI.

Rix, G. and A. Fernandez. (2007). "Probabilistic Ground Motions for Selected Cities in the Upper Mississippi Embayment." from http://geosystems.ce.gatech.edu/soil_dynamics/research/groundmotionsembay/.

Rosowsky, D. and P. WeiChiang (2007). Pushover Curves for Woodframe Buildings.

Rosowsky, D. V. and B. Ellingwood, R. (2002). Performance-Based Engineering of Wood Frame Housing: Fragility Analysis Methodology. *Journal of Structural Engineering* **128**(1)**,** 32-38.

Rossetto, T. and A. Elnashai (2005). A New Analytical Procedure for the Derivation of Displacement-Based Vulnerability Curves for Populations of RC Structures. *Engineering Structures* **27**(3)**,** 397-409.

Shinozuka, M., M. Q. Feng, et al. (2000). Nonlinear Static Procedure for Fragility Curve Development. *Journal of Engineering Mechanics* **126**(12)**,** 1287-1295.

Silva, W., N. Gregor, et al. (2003). Development of Regional Hard Rock Attenuation Relations for Central and Eastern North America, Mid-Continent and Gulf Coast Areas. El Cerrito, California, Pacific Engineering and Analysis.

Singhal, A. and A. S. Kiremidjian (1997). A Method for Earthquake Motion-Damage Relationships with Application to Reinforced Concrete Frames. Buffalo, New York, State University of New York at Buffalo: National Center for Earthquake Engineering Research. **200**.

Somerville, P., N. Smith, et al. (1997). Development of Ground Motion Time Histories for Phase 2 of the FEMA/SAC Steel Project, SAC Joint Venture.

Spence, R. J. S., A. W. Coburn, et al. (1992). Correlation of Ground Motion with Building Damage: the Definition of a New Damage-Based Seismic Intensity Scale. 10th World Conference on Earthquake Engineering, Rotterdam, AA Balkema.

Steinbrugge, K. V., H. J. Degenkolb, et al. (1987). *Earthquake planning scenario for a magnitude 7.5 earthquake on the Hayward Fault in the San Francisco Bay area*. California Dept. of Conservation, Division of Mines and Geology, Sacramento, CA.

Stewart, W. G. (1987). The Seismic Design of Plywood Sheated Shear Walls. Department of Civil Engineering. Christchurch, University of Canterbury.

Takeda, T., M. A. Sozen, et al. (1970). Reinforced Concrete Response to Simulated Earthquakes. *Journal of Structural Division, ASCE* **96**(ST12)**,** 2557-2573.

Tanaka, Y., Y. Ohasi, et al. (1998). Shaking Table Test of Full-Scale Wood-Framed House. 10th Earthquake Engineering Symposium, Yokohama.

Tantala, M., G. Nordenson, et al. (1999-2003). Earthquake Risks and Mitigation in the New York, New Jersey and Connecticut Region, The New York City Area Consortium for Earthquake Loss Mitigation.

Tarabia, A. M. and R. Y. Itani (1997). Static and Dynamic Modeling of Light-Frame Wood Buildings. *Computers and Structures* **63**(2)**,** 319-334.

URS Corporation, Durham Technologies, Inc., et al. (2001). Comprehensive Seismic Risk and Vulnerability Study for the State of South Carolina, South Carolina Emergency Preparedness Division, SC.

Van De Lindt, J. W. and M. A. Walz (2003). Development and Application of Wood Shear Wall Reliability Model. *Journal of Structural Engineering, ASCE* **129**(3)**,** 405-413.

Vidic, T., P. Fajfar, et al. (1994). Consistent Inelastic Design Spectra: Strength and Displacement. *Earthquake Engineering and Structural Dynamics* **23,** 507-521.

Washington Military Department, Emergency Management Division (2005). Scenario for a Magnitude 6.7 Earthquake on the Seattle Fault, Earthquake Engineering Research Institute (EERI).

Wen, Y. K., B. R. Ellingwood, et al. (2004a). Vulnerability Function Framework for Consequence-Based Engineering. Urbana, IL, Mid-America Earthquake (MAE) Center.

Wen, Y. K., B. R. Ellingwood, et al. (2004b). Vulnerability Functions. Urbana, IL, Mid-America Earthquake (MAE) Center.

Whitman, R. V., T. Anagnos, et al. (1997). Development of a National Earthquake Loss Estimation Methodology. *Earthquake Spectra* **13**(4)**,** 643-661.

WJE (1996). Seismic Dynamic Analysis for Building. Final Manuscript Prepared for U. S. Army Engineering Division by Wiss, Janney, Elnster Associates, Inc. Emeryville, California.

Xue, Q. (2001). Assessing the Accuracy of the Damping Models Used in Displacement-Based Seismic Demand Evaluation and Design of Inelastic Structures. *Earthquake Engineering and Engineering Seismology* **3**(2)**,** 37-45.

Yokel, F. Y., G. Hsi, et al. (1973). Full Scale Test on a Two-story House Subjected to Lateral Load. *Building Science Series, National Bureau of Standards, U.S. Dept. of Commerce* **Vol. 44**.